PMEL Tsunami Forecast Series: Vol. 13
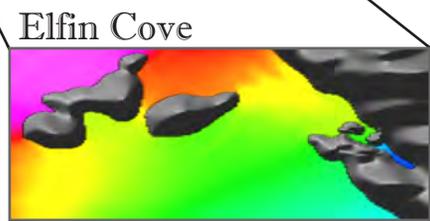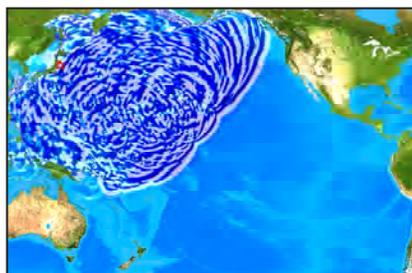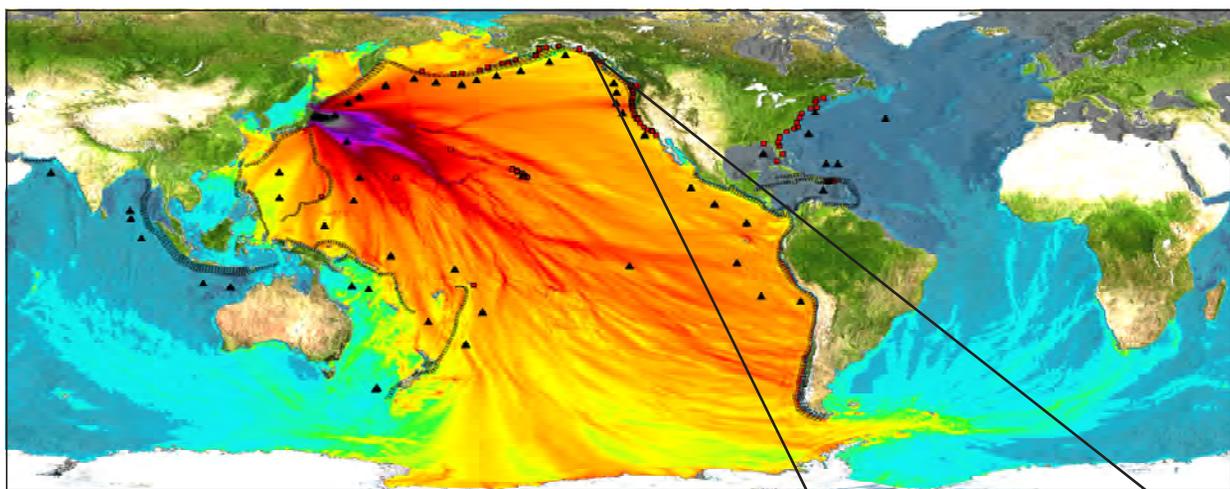# A Tsunami Forecast Model for Elfin Cove, Alaska

Michael C. Spillane

Elfin Cove

NOAA Center for Tsunami Research (NCTR)
Pacific Marine Environmental Laboratory

Front cover image: Overview of NOAA tsunami forecast system. Top frame illustrates components of the tsunami forecast using the 11 March 2011 Tohoku tsunami as an example: DART systems (black triangles), precomputed tsunami source function database (unfilled black rectangles) and high-resolution forecast models in the Pacific, Atlantic, and Indian oceans (red squares). Colors show computed maximum tsunami amplitudes of the offshore forecast. Black contour lines indicate tsunami travel times in hours. Lower panels show the forecast process sequence left to right: tsunami detection with the DART system (third generation DART ETD is shown); model propagation forecast based on DART observations; coastal forecast with high-resolution tsunami inundation model.

PMEL Tsunami Forecast Series: Vol. 13
A Tsunami Forecast Model for Elfin Cove, Alaska

M.C. Spillane[1,2]

1   Joint Institute for the Study of the Atmosphere and Ocean (JISAO), University of Washington, Seattle, WA
2   NOAA/Pacific Marine Environmental Laboratory (PMEL), Seattle, WA

September 2015

Contents

List of Figures

List of Tables

Foreword

Tsunamis have been recognized as a potential hazard to United States coastal communities since the mid-twentieth century, when multiple destructive tsunamis caused damage to the states of Hawaii, Alaska, California, Oregon, and Washington. In response to these events, the United States, under the auspices of the National Oceanic and Atmospheric Administration (NOAA), established the Pacific and National Tsunami Warning Centers, dedicated to protecting United States interests from the threat posed by tsunamis. NOAA also created a tsunami research program at the Pacific Marine Environmental Laboratory (PMEL) to develop improved warning products.

The scale of destruction and unprecedented loss of life following the December 2004 Sumatra tsunami served as the catalyst to refocus efforts in the United States on reducing tsunami vulnerability of coastal communities, and on 20 December 2006, the United States Congress passed the "Tsunami Warning and Education Act" under which education and warning activities were thereafter specified and mandated. A "tsunami forecasting capability based on models and measurements, including tsunami inundation models and maps" is a central component for the protection of United States coastlines from the threat posed by tsunamis. The forecasting capability for each community described in the PMEL Tsunami Forecast Series is the result of collaboration between the National Oceanic and Atmospheric Administration office of Oceanic and Atmospheric Research, National Weather Service, National Ocean Service, National Environmental Satellite, Data, and Information Service, the University of Washington's Joint Institute for the Study of the Atmosphere and Ocean, National Science Foundation, and United States Geological Survey.

NOAA Center for Tsunami Research

PMEL Tsunami Forecast Series: Vol. 13
A Tsunami Forecast Model for Elfin Cove, Alaska

M.C. Spillane[1,2]

Abstract. Operational tsunami forecasting by NOAA's Tsunami Warning Centers relies on the detection of tsunami wave trains in the open ocean, inversion of these data (transmitted via satellite) to quantify their source characteristics, and real-time modeling of the impact on threatened coastal communities. The latter phase of the process involves, for each such community, a pre-tested forecast model capable of predicting the impact, in terms of inundation and dangerous inshore currents, with sufficient resolution and within the time constraints appropriate to an emergency response. To achieve this goal, considerable advance effort is required to tune each forecast model to the specific bathymetry and topography, both natural and manmade, of the impact area, and to validate its performance with a broad set of tsunami sources. Where possible, the validation runs should replicate observed responses to historical events, but the sparse instrumental record of these rare but occasionally devastating occurrences dictates that comprehensive testing also include a suite of synthetic scenarios that represent potential extreme events.

During the forecast model design phase, and in research mode outside the pressures of an emergency situation, more detailed and slower-running models can be investigated. These models, referred to as reference models, represent the most credible numerical representation of tsunami response for a study region, using the most detailed bathymetry available and without the run-time constraint of operational use. Once a reference model has been developed, the process of forecast model design is to determine where efficiencies can be gained, by reducing the grid resolution and increasing the model time step, while still adequately representing the salient features of the full solution.

This report addresses the tsunami aspects of the natural hazard spectrum, documenting the reference and forecast model development for Elfin Cove, Alaska, and its vicinity. Though sparsely populated, the region is traversed by several segments of the Alaska Marine Highway and features important marine resources, including commercial and recreational fishing and the potential for tidal power extraction. Additionally, Glacier Bay is a popular venue for cruise ships and other tourist activity. The forecast model performs satisfactorily in hindcasts of major historical tsunamis and its stability in tests of large synthetic events around the Pacific basin has been demonstrated. However, it should be noted that forecast model amplitudes consistently underestimate those produced in reference model runs. The disparity is generally only a few percent in the early phases of the tsunami wave train but may be significantly larger for later waves. It is suggested that a safety factor of the order of 10% be applied in operational use of forecast model projections. During testing, the forecast model simulated 4 hr of real time in 12.92 min. While this exceeds the 10 min target for this metric, the modest increase is justified by the regional coverage provided by the intentionally enlarged model domain.

---

1 Joint Institute for the Study of the Atmosphere and Ocean (JISAO), University of Washington, Seattle, WA
2 NOAA/Pacific Marine Environmental Laboratory (PMEL), Seattle, WA

1. Background and Objectives

1.1 The setting

The "Panhandle" of southeast Alaska (see **Figures 1–3**) extends from Yakutat to the U.S./Canada border and is a region incised with deep channels and complex topography. The mainland is exposed to the open ocean north of Cross Sound, while to the south the islands of the Alexander Archipelago provide a screen. The deep waters of Chatham Strait provide a passage for tsunami waves deep into the interior: to Skagway and Haines via Lynn Canal, to the state capital Juneau, and to several of the larger communities. Cross Sound is linked to Chatham Strait via Icy Strait, along which Glacier Bay and its associated National Park is a major tourist destination.

Tsunami models are being developed for several communities of southeast Alaska in recognition of the threat they face from both local and remote sources. For most of these communities, tide gauge records, or in some cases verbal reports of observed historical events, provide ground truth with which to assess and validate model predictions. One such tide gauge is located in Elfin Cove, approximately midway between Sitka and Yakutat and the subject of this report and tsunami modeling effort. The small community (2010 population: 20; U.S. Census Bureau, 2010), accessible only by water or seaplane, is a census-designated place on the Inian Peninsula of Chichagof Island, and is well-described in the Elfin Cove Community Plan (2007). Although the fifth largest island in the U.S., the entire population of Chichagof Island in 2000 was only 1342 and has declined since. The Inian Peninsula and a cluster of islands of the same name partially block Icy Strait, while to the west several islands screen Elfin Cove from the open Pacific Ocean. The Alaska Marine Highway passes between Elfin Cove and the Inian Islands, with ferry service to Hoonah (2010 population: 760; U.S. Census Bureau, 2010) at the mouth of Port Frederic inlet, Pelican (2010 population: 88; U.S. Census Bureau, 2010) on Lisianski Inlet, and northward to Yakutat and Anchorage. During the summer months there is a significant though transient population increase. Commercial fishing vessels transiting to the Bering Sea or engaged in local recreational fishing swell the population of Elfin Cove to 170 or so, and the community is occasionally visited by tour vessels with up to 100 passengers that can tax its limited infrastructure. Power is generated locally, potable water comes from a spring, and there are no regularly scheduled modes of transportation. Elfin Cove has no roads but is served by a network of boardwalks. Medical services are volunteer-provided; all in all, the community is self-sustaining but at risk if an emergency were to arise.

As the most northerly access to the Inland Passage, Cross Sound and Icy Strait are heavily traversed year-round by ferry, cargo, and cruise ship traffic. In summer, cruise ship traffic to Glacier Bay is particularly intense, with two vessels, each carrying up to 3000 passengers and crew arriving each day. Tidal currents through the narrow North and South Inian passes and other naviga-

tional channels are very strong and it is important that the tsunami model being designed here should address the impact of tsunami-driven currents in addition to the potential for inundation. While the forecast model is named for Elfin Cove, its choice is largely dictated by the presence of a tide gauge for use in model validation and in operations; the scope of the model must be more regional than is usual. By contrast, models created for the closest communities to the north and south (Yakutat and Sitka, respectively, with greater population and infrastructure) have a more local focus.

Lisianski Strait separates Chichagof Island from the smaller Yakobi Island to the west. Farther south, Peril Strait provides another, albeit far more constricted, connection between the Pacific Ocean and Chatham Strait, allowing ferry service to Sitka (2010 population: 8881; U.S. Census Bureau, 2010) on Baranof Island. At the south end of Baranof Island, just inside the entrance to Chatham Strait, is Port Alexander (2010 population: 52; U.S. Census Bureau, 2010), whose selection as a forecast model site also reflects its strategically located tide gauge.

Though far from the open ocean, Skagway and Juneau have reported substantial tsunami waves, particularly from the major Alaskan earthquake of 1964, but also from more remote events such as 1960 Chile and 2011 Tohoku. The domain of the Elfin Cove model, which must allow for the possibility of waves arriving from the east via Chatham and Icy Straits, will be large enough to permit estimates for Juneau, Skagway, and other communities in its vicinity.

1.2 Tsunami and other coastal hazards

In an extensive compilation of tsunami knowledge for Alaska since the earliest records in the 1700s, Lander (1996) distinguishes between the several categories of tsunami to which the region is prone. Together with the National Geophysical Data Center's (NGDC) online hazard database (Dunbar, 2007; see `www.ngdc.noaa.gov/hazard/`), a wide set of historical cases are available with which to exercise a forecast model. Observations suited to model validation are, however, quite limited. Tide gauge records from Elfin Cove itself are only available after August 2005; reports and observations from other sites in the vicinity (primarily Sitka) will be employed to validate the model for earlier events.

The instrumental record is too short, in the geologic context, to provide samples of the range of tsunami events that may occur at future times within the Pacific basin. Thus, once developed and validated, the model will be exercised with a comprehensive suite of synthetic scenarios. The benefits of this are twofold: 1) to check that the model is robust and unlikely to fail in an operational setting, and; 2) as a byproduct, to identify tsunami source regions to which southeast Alaska is particularly susceptible. It should be noted that, currently, the model is applicable only to tsunamis generated by direct seismic forcing. Lander (1996) discusses other mechanisms related to volcanic activity or landslides, perhaps triggered by seismic action, that are manifested in the observational record. Notorious among the latter is the 1958 event in Lituya Bay, just north of Cross Sound, where the collapse of a steep mountainside caused a surge of over 500 m at the other side of

the bay. Though dramatic, such events are generally quite localized, but it should be stressed that in its current form the tsunami model employed in the forecast system does not cover landslide-generated tsunamis.

Earthquake, landslide, and flooding damage can result even without the medium of tsunami waves. Nonetheless, history has shown that death, injury, and property damage associated with tsunamis, both local and remote, have been significant, so the modeling effort and operational forecast capability provide important benefits to the State of Alaska. Equally, since tsunamis generated off southeast Alaska can potentially impact the entire Pacific basin, the degree of success of the Elfin Cove model in a local event can lend credence to the forecast systems projections for more remote and larger communities of the United States and other nations.

An inset to **Figure 4**, taken from the USGS seismic hazard analysis for Alaska (Wesson *et al.,* 2007), shows the major fault ruptures that have occurred in the region since the 1930s. Several are local to the Alaska Panhandle region, though none have caused major tsunami impacts since 1964. The main panel of **Figure 4** shows (in green) several of the faults, together with the unit source rectangles employed to represent them in the NCTR (NOAA Center for Tsunami Research) propagation database. The Fairweather Fault, extending northward from Haida Gwaii, generated the Queen Charlotte event of 1949, the 1958 earthquake associated with the Lituya Bay tsunami, and one near Sitka in 1972 (Doser and Lomas, 2000). It is primarily a strike-slip fault, as is the Transition Zone Fault which angles off to the northwest. The junction near Cross Sound was the site of a series of a cluster of small earthquakes in 1973. Between these faults is the Yakutat Terrane (Worthington *et al.*, 2012) or Yakutat Block (whose submarine portion is crosshatched in **Figure 4**).

The rectangular outlines of the 100 × 50 km unit sources of the NCTR propagation database are shown in **Figure 4**. Those drawn in black are combined for the ACSZ 40–49 mega-tsunami source described later in this report. Representing a Mw 9.3 event, this synthetic source is likely far in excess of any probable occurrence, but should serve as an extreme test of model stability. At the northern end of the Yakutat Block the potential for a larger event becomes more realistic as it subducts beneath the North American Plate in the vicinity of the Chugach–St. Elias Mountains. Major earthquakes occurred near Yakutat in 1899, for which the 1979 event shown in **Figure 4** is considered an aftershock. The rupture zone of the 1964 Alaska earthquake did not extend into the region (Shennan *et al.*, 2009). Often referred to as the "Yakataga Gap," this is a potential site for future large earthquakes in Alaska seismic hazard mapping (Wesson *et al.*, 2007) and Alaska Earthquake Center (AEC) charts (www.aeic.alaska.edu).

1.3 Tsunami warning and risk assessment

The forecast model development described here will permit Elfin Cove to be incorporated into the tsunami forecasting system, developed at NCTR and now in operational use at the U.S. Tsunami Warning Centers (TWCs). The system has had considerable success in accurately forecasting the impact of both moderate and severe tsunami events in recent years (Titov, 2009; Tang *et al.*, 2012), and is likely to improve as new detection sites, closer to the source line, are added (Bernard *et al.*, 2014). In the following section, the methodology that permits such forecasts is discussed as prelude to a description of development of the forecast model for Elfin Cove. With the model in hand, validated with historical events and with its stability verified by extensive testing against extreme scenarios, real-time forecasts will be available to inform local emergency response. Additionally, the synthetic scenarios investigated during model development and reported here provide an initial tsunami risk assessment, as described in Section 4.

2. Forecast Methodology

2.1 The tsunami model

A tsunami forecast model is used to extend a precomputed deep-water solution into the shallows, and onshore as inundation, if appropriate. The model consists of a set of three nested grids, of increasingly fine resolution that, in a real-time application of the MOST (Method of Splitting Tsunami) model (Titov and González, 1997; Titov and Synolakis, 1998) permits forecasts at spatial scales (as small as a few tens of meters) relevant to local emergency management. The utility of the MOST model applied in this manner, and the operational effectiveness of the forecast system built around it, has been demonstrated during unplanned tests triggered by several mild to moderate tsunami events in the years since the 2004 Indian Ocean disaster (Wei *et al.*, 2008). Successful hindcasting of observed historic events (Titov, 2009; Tang *et al.*, 2012; Bernard *et al.*, 2014), even mild ones, during forecast model development lends credence to the ability to accurately forecast the impact of future events. Such validation of tsunami modeling procedures is documented in other volumes of the series. Before proceeding to a description of the forecast model development for Elfin Cove, it is useful to describe the steps in the overall process.

2.2 NOAA's tsunami forecast system

Operational tsunami forecasts are generated at TWCs, staffed continuously around the clock in Alaska and Hawaii, using the SIFT (Short-term Inundation Forecasting for Tsunamis) tool developed at NCTR. The semi-automated process facilitates the steps by which TWC operators assimilate data from an appropriate subset of DART (Deep-ocean Assessment and Reporting of Tsunamis) sensors, "invert" the data to determine the linear combination of precomputed propagation solutions that best match the observations, then initiate a set of forecast model runs if coastal communities are threatened, or, if warranted, cancel the warning. Steps in the process are as follows:

- When a submarine earthquake occurs, the global network of seismometers registers it. Based on the epicenter, the unit sources in the propagation database (Gica *et al.*, 2008) that are most likely to be involved in the event and the DART array elements (Spillane *et al.*, 2008) best placed to detect the waves' passage are identified. TWC operators can trigger DARTs into rapid sampling mode in the event that this did not occur automatically in response to the seismic signal.

- There is now a delay while the tsunami waves are in transit to the DARTs. At least a quarter of a cycle of the first wave in the train must be sampled before moving to the "inversion" step. In the interim, the tsunami forecast

system allows the operator to request a "seismic solution," based on the location and reported magnitude of the earthquake. This solution, however, may only poorly represent the tsunami; magnitude estimates may be substantially revised as more seismic data accumulate. Only when sea level fluctuations are detected can the reality and scale of the waves be determined.

- When sufficient data have accumulated at one or more DARTs, the observed time series are compared with the model series from the candidate unit sources. Since the latter are precomputed (using the MOST code), and the dynamics of tsunami waves in deep water are linear, a least squares approach can quickly identify the unit sources (and the appropriate scale factors for each) that best fit the observations. The inversion methodology is described by Percival *et al.* (2011).

- Drawing again on the propagation database, the scale factors are applied to produce a composite basin-wide solution with which to identify the coastal regions most threatened by the radiating waves.

- It is at this point that one or more forecast models are run. The composite propagation solution is employed as the boundary condition to the outermost (A-grid) domain of a nested set of three real-time MOST model grids that telescope with increasingly fine scale to the community of concern. A-grid results provide boundary conditions to the B grid, which, in turn, forces the innermost C grid. Nonlinear processes, including inundation, are modeled so that, relying on the validation procedures during model development, credible forecasts of the current event are available.

- Each forecast model provides quantitative and graphic forecast products with which to inform the emergency response or to serve as the basis for canceling or reducing the warnings. Unless the tsunami source is local, the forecast is generally available before the waves arrive. Even when lead time cannot be provided, the several hour duration of a significant event (in which the first wave may not be the most damaging) gives added value to the multi-hour forecasts provided.

Because multiple communities may be at risk, it may be necessary to run, simultaneously or in a prioritized manner, multiple forecast models. Each must be optimized to run efficiently in as little time as possible. The current standard is that an operational forecast model should be capable of simulating 4 hr of real time within about 10 min of CPU time on a fast workstation computer.

3. Model Development

3.1 Digital elevation models

Water depth determines local tsunami wave speed, and subaerial topography determines the extent to which tsunami waves inundate the land. Thus, a prerequisite for credible tsunami modeling is the availability of accurate gridded bathymetric and topographic datasets, termed digital elevation models, or DEMs. Given their expertise in this area and the number of coastal communities needing tsunami forecast capability, NCTR relies heavily on the NGDC to provide the DEMs needed. An extract from the South Alaska DEM was used as background in **Figure 1** and the outlines of the more finely resolved southeast Alaska and Elfin Cove DEMs are indicated. In the case of Elfin Cove, a customized high-resolution DEM, a composite of multiple data sources for the region between Cross Sound and the mouth of Glacier Bay, was provided by NGDC. To create this, various datasets were merged and converted to a common datum of Mean High Water (MHW). The main features of the both DEMs are summarized in **Table 1**. The procedures employed by NGDC in their creation are documented by Caldwell *et al.* (2012; southeast Alaska) and by Love *et al.* (2011; Elfin Cove). Relying to a large extent on data from NASA's SRTM (Shuttle Radar Topography Mission) and ASTER (Advanced Spaceborne Thermal Emission and Reflection Radiometer) projects, NGDC quotes the horizontal and vertical accuracies for topography as 20–30 m and 16–20 m, respectively. Bathymetric features are resolved to only a few hundred meters horizontally in deep water but are closer to the topographic resolution in the shallows. Vertical accuracy for bathymetry varies from 0.1 m to 5 percent of water depth. The oblique views of these DEMs, produced by NGDC, are reproduced in **Figure 3** and assist in visualizing the complexity of the terrain and its multiple waterways. All of the DEMs employed were verified for consistency with charts, satellite imagery, and other datasets during the course of MOST grid development.

The use of MHW as the "zero level" is standard in forecast models. The version of MOST currently employed does not explicitly include tidal fluctuations, and, since a tsunami may arrive at any stage of the tide, it is best to employ a "worst-case" approach by assuming high tide when forecasting inundation. For some forecast models, grounding of vessels and the strong and rapidly varying currents often associated with even mild tsunamis are of concern. Even under normal circumstances the tidal currents in North and South Inian passes are very strong. NOAA Chart 17302, a portion of which appears in **Figure 5a**, alerts mariners to currents of 8–10 knots. In light of the importance of cruise ship and ferry traffic, the extent to which these might be accentuated during a tsunami will be assessed. For Elfin Cove itself, there are piers, floating docks, and refueling facilities associated with seaplane and both commercial and recreational fishing activity, as shown in the NOAA chart reproduced as **Figure 5b**. **Figure 6** shows the character of the inner cove of this small community—in particular, the reliance on piers and floating docks that do not substantially impede the circulation.

Table 1: The main features of the Elfin Cove and southeast Alaska digital elevation models, whose development is described by Love *et al.* (2011) and Caldwell *et al.* (2012). Values from the southeast Alaska dataset were adjusted from MHHW to the MHW reference level of the Elfin Cove grids.

Grid Area	Elfin Cove, Alaska
Coverage Area	137.27° to 135.97°W; 57.53° to 58.67°N
Coordinate System	Geographical decimal degrees
Horizontal Datum	World Geodetic System 1984 (WGS84)
Vertical Datum	Mean High Water (MHW)
Vertical Units	Meters
Horizontal Accuracy	Topography: 20–30 m Bathymetry: 20–30 m shallow, 300 m deep
Vertical Accuracy	Topography: 16–20 m Bathymetry: 0.1 m to 5% of water depth
Cell Size	1/3 arc sec
Grid Format	ESRI Arc ASCII grid
Version Employed	Update of 31 March 2011

Grid Area	Southeast Alaska
Coverage Area	138.21° to 129.19°W; 54.19° to 60.01°N
Coordinate System	Geographical decimal degrees
Horizontal Datum	World Geodetic System 1984 (WGS84)
Vertical Datum	Mean Higher High Water (MHHW)
Vertical Units	Meters
Horizontal Accuracy	Topography: 20–30 m Bathymetry: 20–30 m shallow, 300 m deep
Vertical Accuracy	Topography: 16–20 m Bathymetry: 0.1 m to 5% of water depth
Cell Size	8 arc sec
Grid Format	NetCDF file
Version Employed	Produced September 2010

Two different resolutions are available for the Southeast Alaska DEM: eight-thirds of an arc sec, and 8 arc sec. The coverage encompasses the region from Skagway in the north to the Haida Gwaii (Queen Charlotte) Islands in British Columbia, Canada. These DEM datasets, together with the Elfin Cove DEM, are employed in the construction of the three nested grids for the Elfin Cove model with an appropriate adjustment of their original MHHW (mean higher high water) vertical datums to the MHW used in the Elfin Cove grids. As noted earlier, the scope of the outer Elfin Cove grid was chosen to permit estimates of tsunami signals at Skagway and Juneau. However, the coarse resolution of the outer grid, required to attain acceptable operational run times, limits the quality of estimates based on the Elfin Cove model compared to what might be attained in models dedicated to these communities.

The elevations and depths used in the development of this forecast model were based on the digital elevation model provided by the NGDC, and the author considers it to be a good representation of the local topography and bathymetry. As new digital elevation models become available, forecast models will be updated, and report updates will be posted at nctr.pmel.noaa.gov/forecast_reports/.

3.2 Tides and sea level variation

The history of tidal observation at Elfin Cove dates back to 1938, though the earlier records are not readily available. Some marigrams are stored in microfiche format at NGDC, and a project to digitize the full collection is underway. The present installation of NOAA's National Ocean Service tide gauge (NOS 9452634) at Elfin Cove was in August 2005 with quality controlled 6 min, and preliminary 1 min records available online.

The tide gauge is located off the seaplane-fueling pier in the outer cove (see **Figure 5b**). The outer cove is screened by an unnamed nearby island; several other islands to the west (George and Three Hill islands) and north (the Inian Islands) further limit its exposure. A narrow channel leads to an inner cove in a steep-sided valley where the remainder of the sea level infrastructure of the community is located (see **Figure 6**). There are no roads; a network of boardwalks links the various structures and facilities.

Station characteristics for NOS 9452634 are provided in **Table 2**, based on the wealth of online tidal information available at NOAA's CO-OPS (Center for Operational Oceanographic Products and Services) website (`tidesandcurrents.noaa.gov`). Note the sizeable mean diurnal range of over 2.6 m, and that (based on the records at Sitka and Yakutat) there is a significant long-term sea level trend as expected for this tectonically active area of glacial rebound. Seasonal and inter-annual variability are also substantial, as are episodic short-term changes associated with meteorology that are reflected in the extremes listed.

Another feature of the local tidal regime, noted earlier, is the strength of the tidal currents, particularly in the North and South Inian passes that lie between Chichagof Island and the mainland. There is the potential for tidal power generation in these passes and in Icy Strait to the east. If it comes to fruition, electricity generation could positively impact the local economy and supply both southeast Alaska and nearby British Columbia (Polagye and Bedard, 2006). From the perspective of tsunami hazard, however, the bathymetric features that accentuate tidal currents and their spatial variability may pose a significant risk to commercial and recreational marine traffic in the area, including the large cruise vessels that ply the region during the summer months. An unrelated NOAA project, investigating the Cross Sound and Icy Strait region, includes current meter observations from recent years. These have been made available (P. Stabeno, NOAA/PMEL, 2012, personal communication) but do not, unfortunately, cover the recent tsunami events. They do, however, provide a baseline for a discussion of the strength of the additional rapidly varying currents that might arise in a major tsunami event.

3.3 Signal-to-noise considerations for the Elfin Cove tide gauge

Unlike the U.S. West Coast, where the Kuril event of November 2006 is a useful test case for model validation, runup reports in the NGDC catalog for the Gulf of Alaska are much weaker (~ 12 cm for Sitka and Yakutat and unreported for Elfin Cove). Other events among the mild tsunamis of recent years were only weakly felt in the region. The number of test cases for model validation at Elfin Cove is further

Table 2: Characteristics of the Elfin Cove tide gauge.

Elfin Cove, Alaska: NOS[1] Station 9452634 (58°11.6´N, 136°20.8´W)
Present installation: 11 Aug 2005

Tidal Datum and Range Values (Epoch 1983–2001)

MHHW (Mean Higher High Water)	6.250 m		
MHW (Mean High Water)	5.977 m	Great Diurnal Range 3.367 m	
MSL (Mean Sea Level)	4.637 m		Mean Range 2.648 m
MLW (Mean Low Water)	3.329 m		
MLLW (Mean Lower Low Water)	2.883 m		

Sea Level Trend (1924–2006) and Cycles from Sitka, Alaska[2], NOS Station 9451600

Long-term Sea Level Trend	Decreasing 2.05 ± 0.32 mm/yr
Seasonal Cycle Range	Min. –106 mm (Jul); Max. 131 mm (Dec)
Interannual Variation (from 1980)	Min. –20 mm (1989); Max. +21 mm (1998)

Extremes to Date (June 2012)

Maximum	7.435 m on 31 Dec 1985
Minimum	1.449 m on 14 Dec 2008

[1] NOAA's National Ocean Service, whose CO-OPS Program Office disseminates tide gauge information and data.
[2] At Yakutat, Alaska (NOS Station 9453220), the long-term trend is –11.54 ± 1.39 mm/yr.

reduced by weather and wave-related noise background at the tide gauges, particularly during the winter months. In addition to sea level itself, the validated 6 min tide data from CO-OPS provides the standard deviation of the 1 sec subsamples used to form each reported value. In the upper panel of **Figure 7** the standard deviation is plotted for the month during which the 2011 Tohoku event occurred (March). The increased high-frequency activity (periods less than 6 min) at the gauge associated with the tsunami's arrival on 11 March is evident in the sharp rise in subsample variability, as well as in the detided 1 min gauge record (highlighted in red). There is, however, another period of high variability (highlighted in blue), of similar duration though of smaller amplitude, which we refer to as a "noise burst." Such bursts are not rare; referring to **Figure 8** where an entire year of the subsample standard deviation is employed as a measure of high-frequency variability, the sole tsunami event does not stand out from the numerous bursts that occur, particularly during the winter months.

The detided 1 min record for one day extracts are contrasted in **Figure 7**, both in the time domain and through a spectral analysis. The spectrum is presented in "energy-preserving" format in the lower panel. Here, the area beneath the curves indicates the partition of energy with wave period. With the exception of a broad peak near 100 min and another near 8 min, the energy of the noise burst is concentrated near the shortest periods detectable. By contrast, during the Tohoku event, the bulk of the energy is in a tsunami band with periods between 10 and 60 min. The 100 min and 8 min peaks are present together with some other "lines" that may represent resonances associated with the topography.

Figure 9 illustrates a similar analysis to that shown in **Figure 7** but for the month of February 2010 when the 2010 Chile tsunami occurred. One-day subsamples, representing the tsunami (red) and a noise burst (blue), are extracted from the Kalman-filtered 1 min record. Longer period energy again dominates the tsunami subset, while the noise burst is dominated by high-frequency energy. There is, however, more energy in the "tsunami band" than was the case during March 2011. **Figure 10** exposes the limitations of the Elfin Cove tide gauge in discriminating weak tsunami signals in the presence of noise. The first wave peak of the 2006 Kuril event is barely visible and later waves are lost in the high-frequency noise. In the energy-preserving spectra, in the lower panel of **Figure 10**, the tsunami band is barely visible.

The detiding, referred to above and used throughout this report, was achieved using the same procedure applied to tide removal in the DART records (Percival *et al.*, 2011) with an R-code script (D. Percival, University of Washington APL, 2012 personal communication). Based on the spectra presented in **Figures 7**, **9**, and **10**, subsequent smoothing of the residuals seems best achieved with a low-pass filter with a cutoff near 10 min. This is applied with a Butterworth filter implemented in Matlab and provided by E. Tolkova (NCTR, 2009, personal communication).

3.4 The CFL condition and other considerations for grid design

Water depth-dependent wave speed, in conjunction with the spacing of the spatial grid representation, places an upper limit on the time step permissible for stable numerical solutions employing an explicit scheme. This is the CFL (Courant-Friedrichs-Levy) limit, which requires careful consideration when the grids employed for a reference or forecast model are being designed. Finer-scale spatial grids or greater water depths require shorter time steps, thereby increasing the amount of computation required to simulate a specific real-time interval.

The shortening that the wave train encounters in moving from deep water onto the shelf needs to be handled carefully when gridded numerical solutions are applied to the tsunami wave problem. In deep water, a grid spacing of 4 arc min (of latitude and longitude, corresponding to ~7 km) is normally used to represent propagating wave trains with a typical wavelength of the order of a few hundred kilometers (Gica *et al.*, 2008; Titov and Gonzalez, 1997). The stored results of such propagation model runs are typically decimated by a factor of 4, resulting in a database of ~30 km spacing (and 1 min temporal sampling) with which to generate the boundary conditions for the outermost (A grid) of the nested grids in a model solution. The extraction of the boundary conditions (of wave height and the two horizontal velocity components) is achieved by linear interpolation in space and time. To provide realistic interpolated values, the stored fields for these variables must be smoothly varying and have adequate sampling in space and time to resolve their structure. This necessitates the placement of the outer boundary of the forecast model domain well offshore.

3.5 Specifics of the model grids

After several rounds of experimentation, the extents and resolutions of the nested grids for the reference and forecast models were chosen; these are illustrated in **Figures 11** and **12** and details are provided in **Table 3**. The outermost A grid encompasses the same northern and western limits in both the reference and forecast model versions. The reference A grid extends about two degrees farther east and south to permit confirmation that the multiple passages there can be safely excluded from the operational model. The expanded domain includes the Canadian tide gauge sites of Prince Rupert and Henslung Cove (on Haida Gwaii, see **Figure 11**) for validation purposes. For the B grid, the forecast model domain was somewhat curtailed from its reference model equivalent in order to improve operational run times while retaining sufficient resolution to reasonably represent the Inian Passes. The initial choice for the reference model B grid (**Figure 11**) included more of Dundas Bay to the north, but the broad tidal flats, barely submerged with the MHW datum, caused numerous minor local instabilities that, in longer runs, impacted areas farther afield. Finally, for the innermost C grid domains, the same resolution was employed for both the reference and forecast model versions in order to reasonably represent inner Elfin Cove and its entrance. The reference model version covers a larger region, as seen in **Figure 11**, extending south into the Port Althorp inlet (see **Figure 5a**) where a strong response to tsunami waves is felt. For all of the grids, both in the reference and forecast versions, the convergence of the meridians at this northerly latitude allows a reduction of a factor of about two in the eastwest direction, achieving almost square grid cells in distance units and a considerable saving in computational effort.

Table 3: Specifics of the reference and forecast model grids employed for Elfin Cove, Alaska. For the paired values in the resolution and grid points columns, the zonal (east to west) value is listed first, followed by the meridional (north to south).

Reference Model for Elfin Cove, Alaska

Minimum offshore depth: 2.5 m; Water depth for dry land: 0.1 m; Friction coefficient (n^2): 0.0009; CPU time for a 4-hr simulation: 6.94 hr

Grid	Zonal Extent		Meridional Extent		Resolution	Grid Points
A	138.203°W	129.750°W	54.190°N	59.610°N	48" × 24"	635 × 814
B	137.310°W	135.409°W	57.830°N	59.110°N	5.333" × 2.667"	1284 × 1729
C	136.430°W	136.260°W	58.090°N	58.330°N	4/3" × 2/3"	460 × 1297

Forecast Model for Elfin Cove, Alaska

Minimum offshore depth: 2.5 m; Water depth for dry land: 0.1 m; Friction coefficient (n^2): 0.0009; CPU time for a 4-hr simulation: 12.92 min

Grid	Zonal Extent		Meridional Extent		Resolution	Grid Points
A	138.210°W	132.210°W	56.010°N	59.610°N	120" × 72"	181 × 181
B	136.630°W	136.050°W	57.840°N	58.390°N	8" × 4"	262 × 496
C	136.410°W	136.337°W	58.18°N	58.210°N	4/3" × 2/3"	199 × 163

CPU times for a 4-hr simulation are based on use of a single Intel® Xeon® E5670 2.93GHz processor.

Both C grids for Elfin Cove lie entirely within the NGDC-provided DEM; A and B grids include bathymetry and topography from other DEM datasets available at NCTR. Some smoothing and editing were necessary to eliminate grid features that tend to cause model instability. For example, "point" islands, where an isolated grid cell stands above water, are eliminated, as are narrow channels or inlets one grid-unit wide; these tend to resonate in the numerical solution. Large depth changes between adjacent grid cells can also cause numerical problems; customized tools are available to correct many of these grid defects. An additional contraint on the bathymetry (E. Tolkova, NCTR, 2009, personal communication) limits excessive depth changes in the discrete representation.

Table 4 lists the maximum depth, the CFL time step requirement that must not be exceeded, and the actual time steps chosen for the reference and forecast model runs. Since the numerical solutions in the three grids proceed simultaneously in the current version of MOST employed by SIFT, there is a requirement that the A- and B-grid time steps be integer multiples of the (innermost) C-grid time step, in addition to satisfying the appropriate CFL requirement. For both reference and forecast models, the CFL requirement of the C grid was the most stringent. The values chosen are shown in the fifth column of **Table 4**, and are such that an integer multiple of each time step is exactly 30 sec, the chosen output time interval for both models. When run on an Intel® Xeon® E5670 2.93 GHz processor, the Elfin Cove forecast model simulates 4 hr in 12.92 min, exceeding the desired 10 min value for this metric. This is somewhat compensated for by the narrow continental shelf, which reduces the overall simulation time requirement, but the wide range of communities included in the model domain and the need to properly model the alternate wave path via Chatham and Icy Straits is the main argument against curtailment of the grids to achieve shorter run times.

3.6 Model run input and output files

In addition to listing the bathymetry file names, the appropriate time step, and A and B grid multiples as provided in **Table 4**, it is necessary to provide a number of additional parameters in an input file. These include the Manning friction coefficient (n), a depth threshold to determine when a grid point becomes inundated, and the threshold amplitude at the A-grid boundary that will start the model. An upper limit on wave amplitude is specified in order to terminate the run if the waves grow beyond reasonable expectation. Standard MOST values are used: $n^2 = 0.0009$ for the friction coefficient and 0.1 m for the inundation threshold. The latter causes the inundation calculation to be avoided for insignificant water encroachments that are probably below the level of uncertainty in the topographic data. Inundation can, optionally, be ignored in the A and B grids, as is the norm in the (non-nested) MOST model runs that generate the propagation database. When A- and/or B-grid inundation is excluded, water depths less than a specified "minimum offshore depth" are assumed to be dry; in effect, a "wall" or reflective boundary condition is set at the corresponding isobath. When invoked, a value of 5 m is applied as the threshold, although A and B inundation is normally permitted as a way to gain knowledge of tsunami impact beyond the scope of the C-grid domain. Other parameter settings allow decimation of the output in space and/or time.

Table 4: Grid file names and grid-related parameters for Elfin Cove, Alaska. The time steps for the A and B grids must be integer multiples of the basic C-grid time step, as indicated in parentheses.

Grid	File Name	Maximum Depth (m)	Minimum CFL (s)	Model Time Step (s)	Water Cells
A	ElfinCoveAK_RM_A	3445	4.031	3.0 (12×)	225,975
	ElfinCoveAK_FM_A	2949	11.661	5.0 (12×)	13,142
B	ElfinCoveAK_RM_B	469.6	1.215	1.0 (4×)	743,650
	ElfinCoveAK_FM_B	347.8	2.119	1.667 (4×)	50,619
C	ElfinCoveAK_RM_C	295.1	0.383	0.25	323,566
	ElfinCoveAK_FM_C	204.2	0.461	0.41667	22,301

As previously noted, a target of 30 sec output and output at every spatial node is preferred. These choices avoid aliasing in the output fields that may be suggestive of instability (particularly in graphical output) when none, in fact, exists.

Finally, the input file (supplied in Appendix A) provides options that control the output produced. Output of the three variables—wave amplitude, zonal (positive to the east) velocity, and meridional (positive to the north) velocity—can be written (in netCDF format) for any combination of A, B, and C grids. These files can be very large. To accommodate 8 hr of 30 sec output for the Elfin Cove forecast model, 378 MB are required for the A grid, 1497 MB for the B grid, and 375 MB for the C grid. A separate file, referred to as a SIFT file, contains the time series of wave amplitude at each time step at discrete cells of a selected grid. Normally, the time series at a "reference" or warning point, typically the location of a tide gauge, is selected to permit validation in the case of future or historical events. Several additional sites of importance in the region were specified during development and included in subsequent discussion in this report. The SIFT file output also includes the distribution of the overall minimum and maximum wave amplitude and speed in each grid. By contrast with the complete space-time results of a run, the SIFT file (also netCDF) is very compact: only 2.7 MB for the Elfin Cove forecast model.

By default, two additional output files are generated. A "listing" file summarizes run specifications, progress, performance in terms of run time, and documentation of modifications to the grid files applied internally by MOST, as well as information to determine the reason, should a run not start or terminate early. A "restart" file is produced so that a run can be resumed from the time it ended, either normally or by operator intervention.

The input files described above are specific to the model itself. For an actual run, the program must be pointed toward the files that contain the boundary conditions of wave amplitude (H) and velocity components (U, V) to be imposed at the A-grid boundary. Time-varying conditions are generally extracted as a subset of a basin-wide propagation solution (either a single unit source or several, individually scaled and linearly combined) that mimics a particular event. These boundary-forcing files typically consist of 24 hr of values (beginning at the time of the earthquake), sampled at 1 min intervals and available on a 16 arc min grid. Occasionally, for more remote seismic sources or when delayed arrival of secondary waves due to reflections are a concern (as has been seen at Hawaii), the time span of the propagation run available for forcing is extended beyond one day.

4. Results and Discussion

Before proceeding to an extensive suite of model runs that explore the threat to Elfin Cove and southeast Alaska from various source regions, the stability of the model is tested in both low and extreme amplitude situations. The former we refer to as "micro-tsunami" testing, where the boundary forcing is at such a low level (but not precisely zero) that the response is expected to be negligible. With an effective magnitude of 6.17, micro-tsunamis have relevance only during model development where they may reveal localized instabilities that may result from undesirable features of the discretized bathymetry. Inlets or channels that are only one grid-cell wide may "ring" or resonate in a non-physical way in the numerical solution. An instability may not grow large enough to cause the model to fail but, in a run with typical tsunami amplitudes, may be masked by actual wave variability.

Forcing by extreme events, termed "mega-tsunami" events, is also tested. These supplement the limited historical record of tsunamis generated by "Great Earthquakes." In addition to the need to test model stability under such circumstances, there is a parameter in the input file that truncates the run if a prescribed threshold for wave height is exceeded in any of the nested grids. For operational use, the threshold must be set high enough so that an extreme event run is not unnecessarily terminated, and for Elfin Cove, where potential seismic sources are within the model domain, a threshold of 900 m is chosen. Both tests should be performed for synthetic sources whose waves enter the model domain from different directions since, although stable for one set of incoming waves, an instability may be encountered for another. The micro- and mega-tsunami testing of the forecast and reference models is reported in the following subsections; the placement of sources for these tests is illustrated in **Figure 13**. Further evidence of forecast model stability is provided by a more extensive set of scenarios described in this section and used in independent testing (see Appendix C) by other members of the NCTR team prior to the model's release for operational use.

4.1 The micro-tsunami tests

Three micro-tsunami test cases (see **Table 5**) were run representing sources in the western Aleutians, the Philippines, and south of Japan. Based on sources from the propagation database (Gica *et al.*, 2008), their amplitudes were scaled down by a factor of 100 to mimic a Mw 6.17 / Slip 0.01 m source rather than the Mw 7.5 / Slip 1 m standard. A number of grid cells in the B and C grids emerged as potential sources of instability. Generally, these were minor indentations of the coastline, barely resolved by the grids, or narrow channels. The region contains several inlets extending far inland and straits that, at a practical level of spatial resolution, proved difficult to accommodate. Minor grid corrections were made to retain features of potential importance, for example, the branch of Lisianski Strait extending westward from near the community of Pelican along the south shore

Table 5: Synthetic tsunami events employed in Elfin Cove, Alaska, model testing. The reference and forecast model solutions of those shown in bold text were intercompared extensively.

Scenario	Source Zone	Tsunami Source	α [m]
Mega-tsunami (Mw 9.3) Scenario			
KISZ 1–10	Kamchatka-Kuril-Japan-Izu-Mariana-Yap	A1–10, B1–10	25
KISZ 22–31	Kamchatka-Kuril-Japan-Izu-Mariana-Yap	A22–31, B22–31	25
KISZ 32–41	Kamchatka-Kuril-Japan-Izu-Mariana-Yap	A32–41, B32–41	25
KISZ 56–65	Kamchatka-Kuril-Japan-Izu-Mariana-Yap	A56–65, B56–65	25
ACSZ 6–15	Aleutian-Alaska-Cascadia	A6–15, B6–15	25
ACSZ 16–25	Aleutian-Alaska-Cascadia	A16–25, B16–25	25
ACSZ 22–31	Aleutian-Alaska-Cascadia	A22–31, B22–31	25
ACSZ 40–49	Aleutian-Alaska-Cascadia	A40–49, B40–49	25
ACSZ 50–59	Aleutian-Alaska-Cascadia	A50–59, B50–59	25
ACSZ 56–65	Aleutian-Alaska-Cascadia	A56–65, B56–65	25
CSSZ 1–10	Central and South America	A1–10, B1–10	25
CSSZ 37–46	Central and South America	A37–46, B37–46	25
CSSZ 89–98	Central and South America	A89–98, B89–98	25
CSSZ 102–111	Central and South America	A102–111, B102–111	25
NTSZ 30–39	New Zealand-Kermadec-Tonga	A30–39, B30–39	25
NVSZ 28–37	New Britain-Solomons-Vanuatu	A28–37, B28–37	25
MOSZ 1–10	Manus–Oceanic Convergent Boundary	A1–10, B1–10	25
NGSZ 3–12	North New Guinea	A3–12, B3–12	25
EPSZ 6–15	East Philippines	A6–15, B6–15	25
RNSZ 12–21	Ryukyu-Kyushu-Nankai	A12–21, B12–21	25
Mw 7.5 Scenario			
NTSZ B36	New Zealand-Kermadec-Tonga	B36	1
Micro-tsunami (Mw 6.5) Scenario			
EPSZ B19	East Philippines	B19	0.01
RNSZ B14	Ryukyu-Kyushu-Nankai	B14	0.01
ACSZ B6	Aleutian-Alaska-Cascadia	B6	0.01

of Yakobi Island. Also retained was Peril Strait between Chichagof and Baranof islands, which, though narrow in places, is a route for the Alaska Ferry System serving Sitka (see **Figure 2**). A limited number of grid cells in the outermost (A) grid required correction. These were generally associated with non-physical features in the topographic database, such as a track of ship-based soundings that were improperly merged with other data sources. After an iterative process of grid correction and retesting using these micro-tsunami sources, both the reference and forecast model grids were deemed satisfactory and the testing of extreme and historical events could begin. The lower panel of **Figure 14** illustrates a step in the process where a deficiency in the reference model grid generated a mild instability (in the ACSZ B06 micro-tsunami scenario—see **Table 5**), causing the reference

model time series at the reference point, initially in close agreement with the forecast model, to develop unrealistic, high-frequency oscillations. Though still generally tracking the forecast model result and not growing without bound, the feature could behave erratically in simulating real events. Modification of the reference model bathymetry eliminated the problem, as seen in the third panel of **Figure 14**, and tests involving other micro-tsunami sources (RNSZ B14 and EPSZ B19) did not reveal other issues.

4.2 The mega-tsunami tests

The record of tsunami impact on the southeast Alaskan coast, included in the comprehensive report on the region by Lander (1996; also searchable in the NGDC catalog online at www.ngdc.noaa.gov/hazard/) reveals that sources around the entire periphery of the Pacific can be felt. Indeed, the catastrophic Indian Ocean tsunami of 2004 was detected at nearby Sitka and Yakutat, though it preceded the current installation of the Elfin Cove gauge. A broad suite of 20 extreme events (so-called mega-tsunamis), whose locations are standard for testing of Pacific basin forecast models, are described in **Table 5**. The normal list is supplemented by one, ACSZ 40–49, which overlays the study area (see **Figure 4**) and is expected to generate the largest response at Elfin Cove. The locations of the full set are discussed in Section 4.4. To simulate each mega-tsunami source, ten A–B pairs of unit sources (as illustrated in **Figure 13**) are used, with an evenly distributed slip of 25 m in each. As described by Gica *et al.* (2008), each unit source represents a 100×50 km area of the fault surface with the long axis parallel to the plate boundary. Row B is shallowest, sloping from a nominal depth of 5 km (unless a depth estimate has been provided by the USGS based on the earthquake catalogs), row A is deeper, followed by rows Z, Y, X,… where appropriate. Thus, the mega-tsunami sources represent 1000 km long ruptures with a width of 100 km; the corresponding moment magnitude is Mw 9.3. Note that recent (and future) additions to the propagation database extend portions of the source domain seaward as a row C. The aim is to represent outer-rise earthquake events where they are likely to occur, such as off the Kuril Islands as evidenced by the January 2007 normal fault event.

   Discussion of the entire set of mega-tsunamis in greater detail is provided in Section 4.5, once the validity of the forecast model has been established by the modeling of historic events. Here we focus on a subset of four, highlighted in **Figure 13** and **Table 5**, to contrast the forecast model with the more highly resolved reference model. Results are presented in **Figures 15–18**, which share a common format. Panel (a) contrasts the reference and forecast model maximum amplitude fields in the sub-region of the forecast model C grid. The larger C grid of the reference model is shown at the right to broaden the scope of the result and confirm that nothing untoward happens at the smaller C grid's boundary. The lower panel compares the time series at the reference point (the Elfin Cove tide gauge); black and red curves represent the reference and forecast model, respectively. Panel (b) is similar but contrasts the maximum speed fields with the speed time series at the tide gauge in the lower panel. Finally, panel (c) for each scenario compares the speed and velocity fields for a single time step, identified by the green line in the lower panel.

It is noticeable that, in the lower panels of (a) for all four of the cases shown, the reference and forecast model are in almost perfect agreement for the amplitude of the earliest waves. Phase differences appear later, though the envelope of later wave amplitude is in essential agreement. However, there is a tendency for the largest peaks and troughs to appear in the reference model solution. This bias is reflected in the maximum wave distributions. Though the structure of the reference and forecast model maximum amplitude fields is similar, the common color bar can suggest a greater disparity.

The level of agreement for speed is less for the local event ACSZ 40–49 than was seen for its amplitude. After initially close agreement, reference model speeds can be several times larger than those of the forecast model later in the event (**Figure 15b**). For the more remote sources tested, the level of speed mismatch is far less pronounced. The velocity comparison of **Figure 15c** is for an early time in the record, as the first wave ebbs. The circulation patterns of the two model results are quite similar, though, away from Elfin Cove itself, the reference model speeds are somewhat higher.

This larger response of the reference model version quite likely reflects a physical reality: the more highly resolved bathymetry and coastline of the reference model provide greater scope for non-linear features or reflected waves to develop. This observation suggests a caveat to operational use of the forecast model. While accurate portrayal of the early history of an event is to be expected, the duration of the event and the amplitude of some later waves may be underestimated. Tide gauge data will be needed to verify this conjecture, which is pursued later in the report. It is worth noting too that, although the ACSZ 56–65 mega-tsunami event (**Figure 16**) represents a massive Cascadia tsunami, the scale of its impact to the Elfin Cove area (60 cm) is not substantially different from those caused by remote sources: CSSZ 102–111 off southern Chile (**Figure 17**) or MOSZ 01–10 near New Guinea (**Figure 18**).

The comparison time in **Figure 17c** was intentionally chosen much later in the CSSZ 102–111 mega-tsunami scenario, although still at a time where the amplitudes at the tide gauge are in good agreement. This agreement clearly extends to the velocity field throughout the C-grid domain of the forecast model. The same is true when, in the case of the MOSZ 01–10 synthetic event (**Figure 18c**), the comparison time is at the leading edge of the wave's arrival at the tide gauge. Note that in **Figure 18a** the spatial structure of maximum amplitude is consistent between the reference and forecast model solutions, though peaks in the former raise the level. In conclusion, it would appear that, while the solutions may temporarily deviate from each other, overall they maintain general agreement over several hours of simulation.

One further confirmatory test of the agreement between the reference and forecast versions of the model is usual—a mild source of Mw 7.5 at a remote location. A single unit source near Samoa (NTSZ B36) was employed for this purpose, and its representations by the reference and forecast model are compared in **Figure 19**. Such an event results in a response of less than a centimeter in Elfin Cove sea level, and there is excellent agreement between both model representations in the early portion of the record. Later, there is an onset of a high-frequency but low-level

instability in the reference model result. Since the forcing fields for NTSZ B36, drawn from the propagation database terminate at 24 hr, it appears that the forecast model more realistically represents the tapering to zero of the forcing imposed in the MOST model.

4.3 Model intercomparison using historical events

Before proceeding to illustrate the validation of model predictions with observations from tide gauges in the region, intercomparisons of the reference and forecast model simulations of four major events are presented in **Figures 20–23** using the format of **Figures 15–18**. **Figure 20** represents the Tohoku event of 11 March 2011 with a comparable level of agreement between models as was seen for the synthetic mega-tsunami events. Agreement is best for wave amplitude (**Figure 20a**), both at the Elfin Cove reference point and for the overall maximum within the C-grid domain. For wave speed (**Figure 20b**), the reference point time series shows the tendency for higher values to occur in the reference model than in the forecast model representation. A snapshot comparison of wave height and vector currents in **Figure 20c** shows that both models produce similar patterns for tsunami-induced circulation. Another recent event observed at Elfin Cove was the 2010 Chile event, whose model representations are intercompared, with satisfactory results, in **Figure 21**. More substantial impacts to the region resulted from the 1964 Alaska (**Figure 22**) and 1960 Chile (**Figure 23**) events; these, however, predate the availability of observations at the Elfin Cove reference point. Overall, the results shown in **Figures 20–23** confirm the agreement between model versions seen in the purely synthetic scenarios. We now proceed to examine how model results match regional tide gauge observations and runup reports for these and other historical events.

In **Figure 24**, the eastward progression of predicted tsunami waves from the 2011 Tohoku event across the North Pacific, as observed by the DART array, is illustrated and compared with the forecasts produced in real-time using SIFT. As described earlier, the first phase in the forecast process is to ingest observations from the closest DART(s) and determine the linear combination of unit sources from the propagation database that best matches those observations. In addition to providing the boundary conditions for the community-specific forecast models, the linearly combined propagation solution can be directly interrogated to provide forecasts for DARTs not involved in its selection. It is this set of forecasted DART time series that is compared with the observations in **Figure 24**.

There is clearly a strong agreement between the first wave of the tsunami, as detected by the DART sensors (drawn as black curves), and model predictions (drawn in red), although the observations increasingly lag the predictions, and the ratio of their amplitudes varies with location. Ultimately, on reaching DART 46410, the model "waves" are seen to be about 9 min early, a difference that is small compared to the several hours of transit time. Perhaps coincidently, the amplitude ratio for the leading wave (denoted by R in **Figure 24**) is closest to unity for the DART (46410) closest to Elfin Cove. Four DARTs between Oregon and southern California (46404, 46407, 46411, and 46412, not shown in **Figure 24**) have amplitude ratios of approximately 1.5–2.0 and time lags of about 8 min. Early

arrival is typical model behavior, and is associated with the limited resolution of the basin-wide bathymetry. Finer-scale features in the actual bathymetry, such as the Emperor Seamount chain in the western Pacific (south of ACSZ B06 in **Figure 13**), slow down the real wave trains. As part of the ongoing testing and evaluation process to determine the suitability of SIFT for operational use, the forecast procedures are applied in hindsight using accuracy metrics based on the success of a set of forecast models in replicating tide gauge observations. While such ongoing efforts may determine the "best" propagation solution, for the purpose of model validation in this report, we employ the real time source characterization defined in **Table 6**. It is one of the sources employed by Tang *et al.* (2012) in characterizing the energy released by the 2011 Tohoku event.

Figure 25 compares reference and forecast model predictions with observations at several sites within the model domain (Ketchikan falls outside the forecast model grids, though it lies within the reference model). The observed time series are 1 min tide gauge data (6 min in the case of Skagway), detided using the Kalman Filter (Percival *et al.*, 2011), and low-pass filtered. Black and red curves represent reference and forecast model predictions; the green curves are the detided and filtered observations. Runup values, from the NGDC catalog, are indicated in this and subsequent figures. At Elfin Cove itself, the focus of the innermost C grid, the result is satisfactory. The model waves arrive early and slightly underestimate the amplitude of the leading wave (but consistent with expectation based on **Figure 24**), and the later waves sustain a level consistent with the data. The other sites are in the outermost A grid, whose reduced spatial resolution has limited ability to reflect complex topography. In particular, the Gastineau Channel leading to Juneau is not resolved at all in the forecast model A grid (and only poorly in the reference model version) and forecast model results are, of necessity, drawn from a location well outside the channel. A higher-resolution DEM is available for Juneau (Caldwell *et al.*, 2012) and could be employed in a dedicated model of that region.

Nonetheless, results for these A grid sites are, in most cases, quite gratifying (Skagway and Ketchikan are underestimated by the model). For Sitka, close to the open ocean, the results are best both for the leading wave and the amplitude of the later waves. At Port Alexander, the match for the leading wave is acceptable but the excessive noise in the observed record obscures the later waves. For the remaining sites, which currently do not have dedicated forecast models, the degree of agreement suggests their utility as a significant improvement over a Green's law coastal forecast. When the forecast models specific to Sitka and Port Alexander are validated, the degree of agreement with the Elfin Cove A-grid results should be used to cast further light on this conjecture. Elfin Cove A grids are extensive by design, mainly to ensure that tsunami waves entering Cross Sound and Icy Strait from the east are appropriately represented. The relative success in replicating the observations for Juneau and Skagway suggests that this goal has been met.

4.4 Further historical simulations

Before proceeding with the discussion of the historical simulations, the contents of **Table 6** should be defined. Two specifications of source location and time are given: one based on the epicenter and reported early in the event, the other coming

later as seismic waveforms from a more widespread set of stations are assimilated. The centroid moment tensor (CMT) solution provides details of the source mechanism and moment magnitude (listed in **Table 6**). The right-hand side of **Table 6** provides the specifics of the combination of unit sources employed to represent the tsunami waves. The subduction zone in which the event occurred is given by a 4-character acronym: ACSZ, for example, refers to a line of unit sources extending from the western Aleutians to Cascadia. Individual unit sources are identified by a character-number combination. Further details on each unit source can be found in Gica *et al.* (2008) and in Appendix B of this report.

As discussed earlier, a linear combination of unit source functions provides the time varying forcing of the model that simulates a tsunami event. The coefficient applied to each source function is a weight assigned to the 100×50 km sub-fault it represents. Thus, in the final column of **Table 6**, the term "$19.7 \times B24$" in the characterization of the 1946 Unimak event implies a scaling by a factor of 19.7 of unit source B24 in the Aleutian to Cascadia subduction zone. Each unit source represents a Mw 7.5 event; by combining the coefficients, a "Tsunami Magnitude" can be produced. It should be stressed that this is not an alternate estimate of the magnitude of the seismic event. Rather, it summarizes the combined effect of the unit sources in generating tsunami waves.

Since the advent of the tsunameter array and the SIFT system to invert its observations, the "recipes" (linear combinations of unit source functions) for events are being produced in "real-time" and are classified as such in **Table 6**. The tsunamigenic description of earlier events have, in some instances, been reconstructed from tide gauge observations and reported in the literature. Others in **Table 6** are listed as "preliminary," in the sense that they have not been thoroughly studied but show some skill in representing an event. Included in **Table 6** are several sources considered "ad hoc." Generally chosen as equally weighted groupings of unit sources whose location and scaling are based on the epicenter and magnitude of an event, ad hoc sources should be considered as exploratory, providing a "reality check" on the waves that might be hindcast for the model domain. In reality, tsunami waves may be less than the magnitude of the earthquake would suggest, or exceed expectation if, for example, a submarine landslide were triggered. Therefore, the quality of the ad hoc cases will likely be poor, though the arrival time of the simulated waves may be of use for comparison with observations.

Model validation, based on a DART-derived propagation solution, is possible for the 2010 Chile event and is illustrated in **Figure 26**. The source characterization given in **Table 6** was derived in real-time as the waves were detected at DART sites in the southeast Pacific and were successfully employed to forecast impacts to Hawaii and the U.S. West Coast. With regard to timing and overall amplitude, the model predictions are satisfactory in the Gulf of Alaska, but neither the reference nor forecast model versions capture the leading trough apparent in the observed time series at Elfin Cove and Sitka. Port Alexander is again noisy, but at the remaining sites the amplitude of the response is reasonably rendered.

The 1964 earthquake in Prince William Sound and the associated tsunami has, to date, been the defining event for south and southeast Alaska. Though preceding open ocean tsunami detection, the source characteristics were elucidated though

Table 6: Source characterization for historical tsunami events employed for Elfin Cove, Alaska, model testing. Events in bold text were used to compare the reference and forecast model versions. Sources identified as "preliminary" or "ad hoc" may not be identically defined in other forecast model reports.

| Event | Earthquake / Seismic | | | Tsunami Magnitude | Subduction Zone | Model |
	USGS Date Time (UTC) Epicenter	CMT Date Time (UTC) Centroid	Magnitude Mw			Tsunami Source (Reference/Derivation)
1946 Unimak	01 Apr 12:28:56 52.75°N 163.50°W	Not Available	8.5	8.5	ACSZ	$7.5 \times B23 + 19.7 \times B24 + 3.7 \times B25$ (López and Okal, 2006)
1952 Kamchatka	04 Nov 16:58:26.0 52.76°N 160.06°E	Not Available	9.0	9.0	KISZ	$19.71 \times (A4 + Y4 + Z4 + A5 + Y5 + Z5 + A6 + Y6 + Z6)$ [ad hoc]
1957 Andreanof	09 Mar 14:22:31 51.56°N 175.39°W	Not Available	8.6	8.7	ACSZ	$31.4 \times A15 + 10.6 \times A16 + 12.2 \times A17$ [preliminary]
1960 Chile	22 May 19:11:14 38.29°S 73.05°W	Not Available	9.5	9.5	CSSZ	$125 \times (A93 + B93 + Z93 + A94 + B94 + Z94 + A95 + B95)$ (Kanamori and Cipar, 1974)
1964 Alaska	28 Mar 03:36:00 61.02°N 147.65°W	Not Available	9.2	8.9	ACSZ	$15.4 \times A34 + 18.3 \times B34 + 48.3 \times Z34 + 19.4 \times A35 + 15.1 \times B35$ (Tang *et al.* 2006, 2009)
1994 East Kuril	04 Oct 13:22:58 43.73°N 147.321°E	04 Oct 13:23:28.5 43.60°N 147.63°E	8.3	8.1	KISZ	$9.0 \times A20$ [ad hoc]
1996 Andreanof	10 Jun 04:03:35 51.56°N 175.39°W	10 Jun 04:04:03.4 51.10°N 177.410°W	7.9	7.8	ACSZ	$2.40 \times A15 + 0.80 \times B16$ [preliminary]
2001 Peru	23 Jun 20:33:14 16.265°S 73.641°W	23 Jun 20:34:23.3 17.28°S 72.71°W	8.4	8.2	CSSZ	$5.7 \times A15 + 2.9 \times B16 + 1.98 \times A16$ [preliminary]
2003 Hokkaido	25 Sep 19:50:06 41.775°N 143.904°E	25 Sep 19:50:38.2 42.21°N 143.84°E	8.3	8.3	KISZ	$3.95 \times (A22 + B22 + A23 + B23)$ [ad hoc]
2003 Rat Island	17 Nov 06:43:07 51.13°N 178.74°E	17 Nov 06:43:31.0 51.14°N 177.86°E	7.7	7.8	ACSZ	$2.81 \times B11$ [real-time]
2006 Tonga	03 May 15:26:39 20.13°S 174.161°W	03 May 15:27:03.7 20.39°S 173.47°W	8.0	8.0	NTSZ	$6.6 \times B29$ [ad hoc]
2006 Kuril	15 Nov 11:14:16 46.607°N 153.230°E	15 Nov 11:15:08 46.71°N 154.33°E	8.3	8.1	KISZ	$4.0 \times A12 + 0.5 \times B12 + 2.0 \times A13 + 1.5 \times B13$ [real-time]
2007 Kuril	13 Jan 04:23:20 46.272°N 154.455°E	13 Jan 04:23:48.1 46.17°N 154.80°E	8.1	7.9	KISZ	$-3.64 \times B13$ [real-time]
2007 Solomon	01 Apr 20:39:56 8.481°S 156.978°E	01 Apr 20:40:38.9 7.76°S 156.34°E	8.1	8.2	NVSZ	$12.0 \times B10$ [preliminary]
2007 Peru	15 Aug 23:40:57 13.354°S 76.509°W	15 Aug 23:41:57.9 13.73°S 77.04°W	8.0	8.1	CSSZ	$0.9 \times A61 + 1.25 \times B61 + 5.6 \times A62 + 6.97 \times B62 + 3.5 \times Z62$ [preliminary]

Table 6: *Continued.*

	Earthquake / Seismic				Model	
	USGS	CMT				
Event	Date Time (UTC) Epicenter	Date Time (UTC) Centroid	Magnitude Mw	Tsunami Magnitude	Subduction Zone	Tsunami Source (Reference/Derivation)
2007 Chile	14 Nov 15:40:50 22.204°S 69.869°W	14 Nov 15:41:11.2 22.64°S 70.62°W	7.7	7.6	CSSZ	$1.65 \times Z73$ [real-time]
2009 Samoa	29 Sep 17:48:10 15.509°S 172.034°W	29 Sep 17:48:26.8 15.13°S 171.97°W	8.1	8.1	NTSZ	$3.96 \times A34 + 3.96 \times B34$ [real-time]
2010 Chile	27 Feb 06:34:14 35.909°S 72.733°W	27 Feb 06:35:15.4 35.95°S 73.15°W	8.8	8.8	CSSZ	$17.24 \times A88 + 8.82 \times A90 + 11.84 \times B88 + 18.39 \times B89 + 16.75 \times B90 + 20.78 \times Z88 + 7.06 \times Z90$ [real-time]
2011 Tohoku	11 Mar 05:46:24 38.297°N 142.372°E	11 Mar 05:47:47.2 38.486°N 142.597°E	9.0	9.0	KISZ	$4.66 \times B24 + 12.23 \times B25 + 26.31 \times A26 + 21.27 \times B26 + 22.75 \times A27 + 4.98 \times B27$ (Tang et al., 2012) [real-time]

a number of studies incorporating seismic and tide gauge records. The unit source selection and slip assignments provided in **Table 6** are discussed by Tang *et al.* (2006, 2009) and used successfully in modeling the impact on Hawaii. In **Figure 27**, the predictions of the impacts at several sites in the Elfin Cove model domain are presented. Only for Sitka is an observed time series available, but several runup values are available from the NGDC catalog. The Sitka time series is based on a digitized marigram, available in the West Coast and Alaska Tsunami Warning Center (WCATWC) archives and detided and filtered using the same methods employed throughout this study. The comparison with the reported runup values at Sitka, Juneau, and Ketchikan is satisfactory. At Elfin Cove itself the model results are only about 50% of the reported runup. This was derived from the tide gauge, but the marigram is not available. The Skagway runup (eyewitness report) is also underpredicted by the model, but overall the success in replicating the character of this huge event, together with the results from the 2011 Tohoku analysis discussed earlier, strongly support the validity of the Elfin Cove models.

Two other historical events are represented by digitized marigrams for Sitka in the WCATWC archives: 1952 Kamchatka and 1960 Chile. The results for these are provided in **Figure 28**. Perhaps because these are remote events, so that the source characterizations (in **Table 6**) are less appropriate to the Gulf of Alaska, the level of success in validating the Elfin Cove model with these cases is much less than for the local 1964 Alaska tsunami. The model prediction at Sitka for the 1960 Chile event is too large by a factor of 4–5, as is that for 1952 Kamchatka. Further effort is clearly needed to more appropriately define these sources in terms of the propagation database. Then the application of the model to these historically important events should be revisited.

Next, in **Figure 29**, simulated historical events from **Table 6** (since the advent of the DART array) are presented. The results confirm a feature of the region noted earlier: Elfin Cove is less impacted by trans-basin tsunami sources than other U.S. interests in the Pacific. On a less positive note, the frequent noise bursts in recorded sea level, associated with wind and waves and illustrated in **Figure 8**, limit the suitability of Elfin Cove as a monitoring site for weak tsunami signals, thereby limiting the number of recent events available for model validation.

The modeling results for the remaining standard cases, those prior to the advent of the DART array and lacking any time series in the vicinity of Elfin Cove, are presented in **Figure 30**. The time series represent Elfin Cove, but NGDC runup values from nearby Sitka are shown when available. These model time series do little beyond demonstrating the absence of stability issues in the application of the model.

A number of other local events, not included in **Table 6** but mentioned earlier in the context of seismic hazard, deserve investigation. On 10 September 1899, a major earthquake occurred in Yakutat Bay, and was one of the earliest events measured by a seismograph. Several tsunami observations outside the immediate vicinity of Yakutat were reported (Lander, 1996), though some may have been associated with secondary generation through landslides. An icefall was reported in Glacier Bay, but no tide gauges were operational in Alaska at the time. On 24 October 1927, a magnitude 7.1 earthquake occurred that affected the Alexander

Archipelago with widespread qualitative (but no quantitative) reports. The Queen Charlotte earthquake of 22 August 1949 had reported observations in the Sitka area, but only an unreliable 8 cm measurement on the marigram. The Fairweather earthquake of 10 July 1958 is best known for the Lituya Bay landslide and tsunami it triggered. There were reports of seiching in Cross Sound, and a weak wave of about 10 cm was reported on the Sitka tide gauge. A magnitude 7.6 earthquake near Sitka on 30 July 1972 was felt over a wide area but registered only 10 cm at Juneau and 8 cm at Sitka itself. The Cross Sound sequence of earthquakes in mid-1973 have been discussed in the seismological literature (Doser and Lomas, 2000), but no reports appear in the tsunami catalogs.

None of these local events are well enough described or observed to merit a full investigation or inclusion in **Table 6** as well-documented tsunami sources. Instead, approximate (ad hoc) source definitions were adopted and run to ensure no untoward behavior of the model. The results are summarized in **Table 7** and, where observations at Sitka are reported in the catalogs, they are approximately confirmed. When sources are designated as ad hoc in **Table 6**, they may not be uniformly implemented in other forecast model reports.

One other event was noted in the runup catalog statistics for Sitka: on 29 November 1975, a magnitude 7.2 earthquake on the island of Hawaii triggered the Kalapana landslide off the southeast coast, generating waves that were seen at several sites around the Pacific. Sitka was among them, with an amplitude of about 10 cm. The marigram shown in Lander (1996) was digitized. Although the MOST model in its current form does not apply to landslide-generated tsunamis, and there are no unit sources near Hawaii, a similar modeling approach to ours was applied by Ma *et al.* (1999) to study the local impact. An ad hoc source was created (J. Newman, NCTR, 2012, personal communication), mimicking that of Ma *et al.* (1999), and applied to the Elfin Cove model. The result was of the appropriate amplitude and consistent with the reported arrival time. Given the typical noise environment of the Gulf of Alaska in November, this side exercise is not conclusive but does perhaps provide indirect support to the model.

Table 7: Ad hoc unit source representation of six local events for southeast Alaska investigated using the Elfin Cove forecast model. Sitka observations are employed where available.

Event	Mw Est.	Date	Location	Unit Sources Used	Max. Amplitude (cm)		Sitka Report (cm)
					Elfin Cove	Sitka	
Yakutat Bay	8.2	10 Sep 1899	60°N 140°W	40–42 A,B	17.4	30.5	n/a
Sitka Region	7.4	24 Oct 1927	57.7°N 136.1°W	44 B	7.4	5.5	n/a
Queen Charlotte	8.1	22 Aug 1949	53.6°N 133.3°W	47–51 B	4.1	16.4	8
Fairweather Fault	7.7	10 Jul 1958	58.3°N 136.5°W	43 A	26.8	12.2	10
Sitka Region	7.6	4 Aug 1972	56.2°N 135.3°W	46 B	6.1	33.4	8
Cross Sound	6.7	1 Jul 1973	57.8°N 137.3°W	43 B	1.2	0.9	n/a

4.5 Simulation of the remaining synthetic mega-tsunami events

We conclude this section with a summary of other model runs that were made in order to verify model stability and which provide useful information on the exposure of the Elfin Cove region to potentially hazardous future events within the Pacific. As noted earlier, the sparse instrumental record of actual events needs to be augmented with credible scenarios to permit risk assessment. While not pretending to be a full-blown risk assessment for the region, the full set of mega-tsunami events modeled during stability testing can provide some early estimates.

Mega-tsunami sources not highlighted in **Table 5** were investigated with the forecast model alone; results for the entire set of 20 are provided in **Table 8** and **Figures 31** and **32**. Each source is a composite of 20 unit sources (see **Figure 13**) from A and B rows with an evenly distributed slip representing an Mw 9.3 event. A color-coded square, drawn at the geometric center of each synthetic source, represents the impact at the Elfin Cove tide gauge predicted for that source. The measure of impact employed in **Table 8** and **Figure 31** is the maximum amplitude of the predicted time series at the reference point. Great circle distances to Elfin Cove are provided, and a vector, normal to the source line, is drawn as a crude indicator of the initial main beam orientation. The impact of the local mega-tsunami source (ACSZ 40–49) dominates all others. Moderate impacts are associated with the closer sources (ACSZ 22–31 near the Alaskan Peninsula and ACSZ 50–59 and ACSZ 56–65, representing the northern and southern portions of Cascadia) but otherwise, impacts are only loosely related to distance. Sources in the southwest Pacific (NVSZ 28–37 near the New Hebrides and MOSZ 01–10 near Manus) have almost as large an impact, but with one exception beyond the local source, the impact predicted for Elfin Cove is much less than that expected along the U.S. West Coast (see **Table 8** where Point Reyes, California, is used for comparison).

The results provided in **Table 8** and **Figures 31** and **32** are specific to the reference site: the Elfin Cove tide gauge. Based on the 20 mega-tsunami simulations, impact statistics were extracted for several communities in the region. The results are presented in **Table 9**, whose footnote identifies the site name abbreviations. Values provided for Sitka and Port Alexander would be better represented by their specific forecast models, which better resolve local bathymetry. With the exception of Elfin Cove itself, the other sites are represented by A-grid cells close to their geographic coordinates. Several of the communities are marked in **Figure 2**. Pelican, though unlabeled in **Figure 2**, is at the northwestern terminus of the Alaska ferry routes shown and can also be seen in **Figure 5a**. Bartlett Cove, north of Point Gustavus in **Figure 5a**, is offshore of the Visitor Center where cruise ships take on their National Park guides at the entrance to Glacier Bay. Auke Bay, also unlabeled in **Figure 2**, is northwest of Juneau and home to an Alaska Fisheries Science Center laboratory.

Figures produced earlier, showing the distribution of maximum current speed in the reference model C grid, confirmed the strength of tsunami-induced currents in the Inian passes north of Elfin Cove. Since these are already well known for strong tidal currents, are traversed by ferries and cruise ships plying the Alaska Marine Highway, and have potential for tidal power generation, it seems worthwhile to extract from the model results estimates of the additional rapidly varying

current speeds that might accompany a major tsunami event. A comprehensive treatment would jointly model tides and tsunamis, so the results provided in **Table 10** are incomplete. Results are given for a selection of sites, shown in **Figure 33**, instrumented by NOAA's EcoFOCI program during 2010 and 2011. The sampling interval of the Acoustic Doppler current profilers is not suited to tsunami study, and the instruments were not deployed during the 2011 Tohoku event. The final row of **Table 10** provides an estimate of the maximum current at each site, based on the 95th percentile of the depth average (only 5% of the currents exceed the tabulated value).

The strongest observed tidal currents are at the shallower locations: South Inian Pass and the mouth of Glacier Bay. Even shallower depths in the 30–40 m range are found south of the latter, marking the terminal moraine of the Glacier Bay glacier that protruded into Icy Strait in the mid-1700s at the end of the Little Ice Age. Only for the local mega-tsunami event scenario (ACSZ 40–49) do the maximum tsunami current speed predictions exceed those associated with the tides. However, with their rapid changes in direction, tsunami-induced currents are potentially of concern. In **Figure 33**, the greatest currents are to be expected near the western end of South Inian Pass, with predicted currents in excess of 10 knots for the ACSZ 40–49 scenario.

Table 8: Comparison of the response at Elfin Cove, Alaska, to that of Point Reyes, California (Spillane, 2014) for synthetic (Mw 9.3) mega-tsunami scenarios. The maximum amplitude at the reference point is used as the measure of response, which is generally far weaker at Elfin Cove than at Point Reyes. The ratio, expressed as a percentage, is tabulated below; the Elfin Cove responses are illustrated graphically in Figure 31.

Scenario	Source Region	Response (cm)		Ratio [%]
		Elfin Cove	Point Reyes	
KISZ 1–10	Kamchatka	27.6	354	7.8
KISZ 22–31	Japan Trench	42.9	251	17.1
KISZ 32–41	Bonin Trench	31.3	318	9.8
KISZ 56–65	Mariana Trench	33.9	166	20.4
ACSZ 6–15	West Aleutians	26.3	134	19.6
ACSZ 16–25	Aleutian Trench	37.9	266	14.2
ACSZ 22–31	Aleutian Trench	59.8	239	25.0
ACSZ 40–49	Cross Sound	**495.7**	n/a	n/a
ACSZ 50–59	Cascadia North	65.2	202	32.3
ACSZ 56–65	Cascadia South	59.6	159	37.5
CSSZ 1–10	Mid-America Trench	11.5	99	11.6
CSSZ 37–46	Columbia-Ecuador	43.2	42	**102.9**
CSSZ 89–98	Chile Trench	11.9	140	8.5
CSSZ 102–111	South Chile	28.0	265	10.6
NTSZ 30–39	North Tonga Trench	38.9	402	9.7
NVSZ 28–37	New Hebrides Trench	**56.4**	258	21.9
MOSZ 1–10	Manus, West Melanesia	**55.3**	460	12.0
NGSZ 3–12	New Guinea	42.6	162	26.3
EPSZ 6–15	East Philippines	34.9	246	14.2
RNSZ 12–21	Ryukyu	15.8	209	7.6

Table 9: Mega-tsunami scenario impacts, as represented by maximum amplitude (in cm) at several sites within the Elfin Cove model domain.

Scenario	ELF	PEL	GUS	BRT	HOO	TEN	JUN	SKG	HAI	PET	KAK	AUK	PTA	SIT
				Impact Sites (identified below)										
KISZ 1–10	28	29	27	33	26	27	46	36	29	16	36	39	21	135
KISZ 22–31	43	35	24	30	23	19	30	43	20	10	41	27	20	164
KISZ 32–41	31	37	19	27	19	18	32	24	18	10	39	20	20	144
KISZ 56–65	34	29	26	39	24	33	45	40	20	19	43	36	27	148
ACSZ 6–15	26	24	15	24	18	24	34	32	23	14	45	21	18	110
ACSZ 16–25	38	40	35	47	28	39	61	51	41	23	54	50	35	127
ACSZ 22–31	60	65	34	53	24	61	79	74	61	37	62	38	51	123
ACSZ 40–49	496	350	272	262	219	339	423	386	310	162	401	162	401	695
ACSZ 50–59	65	79	53	63	58	70	109	83	66	30	87	80	56	156
ACSZ 56–65	60	61	69	63	52	56	145	61	57	31	74	92	54	142
CSSZ 1–10	11	12	9	11	10	10	18	18	17	13	13	17	9	33
CSSZ 37–46	12	14	13	15	15	15	23	22	20	14	18	18	11	35
CSSZ 89–98	28	23	17	29	21	17	23	26	19	13	23	23	13	91
CSSZ 102–111	43	28	34	37	25	30	43	33	18	18	32	38	23	216
NTSZ 30–39	39	36	25	26	24	27	53	39	37	18	32	39	25	158
NVSZ 28–37	56	49	23	24	37	34	53	51	40	22	42	27	39	209
MOSZ 1–10	55	31	42	47	37	26	49	56	25	17	38	61	36	333
NGSZ 3–12	43	57	37	58	31	60	88	63	52	25	87	61	40	168
EPSZ 6–15	35	39	25	32	24	29	49	49	31	15	47	48	26	110
RNSZ 12–21	16	16	14	18	11	16	18	27	15	8	24	14	13	84

ELF—Elfin Cove; PEL—Pelican; GUS—Gustavus; BRT—Bartlett Cove; HOO—Hoonah;
TEN—Tenekee Springs; JUN—Juneau; SKG—Skagway; HAI—Haines; PET—Petersburg;
KAK—Kake; AUK—Auke Bay; PTA—Port Alexander; SIT—Sitka

Table 10: Maximum speeds at various locations from Cross Sound to Icy Strait in mega-tsunami simulations using the Elfin Cove forecast model. For rows with bold text, the forecast model value is followed by the reference model equivalent. Speeds are given in knots for ease of comparison with the NOAA chart warnings of tidal currents of 8–10 knots that are frequently encountered in North and South Inian passes. Observed maxima (and water depths) are based on NOAA EcoFOCI current meter data from 2010 and 2011.

Scenario	Cross Sound	North Inian Pass	South Inian Pass	Glacier Bay	Icy Strait
KISZ 1–10	0.10	0.26	0.58	0.17	0.22
KISZ 22–31	0.13	0.28	0.61	0.15	0.17
KISZ 32–41	0.14	0.26	0.60	0.12	0.20
KISZ 56–65	0.11	0.34	0.80	0.13	0.26
ACSZ 6–15	0.08	0.18	0.39	0.14	0.21
ACSZ 16–25	0.12	0.34	0.78	0.23	0.30
ACSZ 22–31	0.17	0.45	0.97	0.23	0.38
ACSZ 40–49	**1.39 / 1.43**	**3.52 / 3.35**	**5.63 / 6.78**	**1.93 / 1.55**	**2.33 / 2.77**
ACSZ 50–59	0.23	0.69	1.56	0.35	0.48
ACSZ 56–65	**0.19 / 0.23**	**0.71 / 0.61**	**1.40 / 1.39**	**0.29 / 0.41**	**0.29 / 0.46**
CSSZ 1–10	0.04	0.15	0.28	0.08	0.08
CSSZ 37–46	0.07	0.19	0.34	0.08	0.08
CSSZ 89–98	0.12	0.32	0.67	0.22	0.15
CSSZ 102–111	**0.18 / 0.17**	**0.42 / 0.32**	**0.87 / 0.71**	**0.24 / 0.20**	**0.23 / 0.23**
NTSZ 30–39	0.12	0.27	0.54	0.18	0.21
NVSZ 28–37	0.15	0.39	0.83	0.17	0.27
MOSZ 1–10	**0.16 / 0.23**	**0.35 / 0.35**	**0.74 / 0.95**	**0.25 / 0.18**	**0.25 / 0.18**
NGSZ 3–12	0.16	0.36	0.91	0.26	0.48
EPSZ 6–15	0.09	0.30	0.72	0.20	0.25
RNSZ 12–21	0.06	0.16	0.38	0.06	0.14
Observed maxima (kts)	**1.19** (318 m)	**2.21** (289 m)	**3.16** (72 m)	**3.49** (71 m)	**1.24** (132 m)

5. Conclusions

In conclusion, good agreement between observations and model predictions for a subset of the larger historical events, including the recent 2011 Tohoku tsunami, has been established, and the stability of the model for numerous synthetic events has been demonstrated for Elfin Cove, Alaska, and its vicinity. In particular, the reliability of the forecast model, designed to run rapidly in real-time emergency conditions, has been proven by the favorable comparison with reference model predictions, particularly during the early hours of an event. The model is included in the tsunami forecast system employed operationally at the Tsunami Warning Centers, thus adding the Cross Sound to Icy Strait region of southeast Alaska to the coastal areas for which forecast capability is available. Additionally, this model will provide a useful tool in risk assessment studies.

The tendency of the forecast model to underestimate the amplitude extremes of the reference model was noted earlier in the case of the mega-tsunami scenarios (**Figures 15–18**). During the review process it was noticed that this behavior was evident too for the historical cases employed for model intercomparison (**Figures 20–23**). The statistics of these eight cases are summarized in **Table 11**. Percent differences in both leading peak and overall maximum amplitude show consistently higher values for the reference model predictions. Leading wave arrival times, however, are in close agreement. For the leading peak amplitude, the reference model excess is a few percent at worst, with a simple average of 2.2% for the eight cases available. For the overall maximum amplitudes in 18-hour time series at Elfin Cove, the range of reference model excesses is much greater with the worst case (61.8%) associated with a mega-tsunami source scenario near New Guinea. The largest excesses occur when the overall maximum comes in the later-wave portion of the record, while those that occur in the early part of the wave train are more consistently reproduced in both models. A geometric average of the reference model excesses in overall maximum amplitude is 8.3%, so that in operational use of forecast model estimates, an underestimation of the order of 10% should be factored into forecast products.

The presence of Icy Strait, linking Cross Sound to the deep north–south channel of Chatham Strait, necessitated a more extensive outermost grid for the Elfin Cove model. While this increases model run time somewhat (to 12.92 min, some 30% above the 10 min target), it does provide the benefit of permitting forecasts for communities not presently selected for specific forecast models: Juneau and Skagway, for example. Statistics for tsunami wave amplitude were extracted during model development, and testing for other communities of southeast Alaska and maximum tsunami-induced currents were extracted for the Cross Sound–Icy Strait region where tidal currents are known to be strong.

Testing of model stability using mega-tsunami (Mw 9.3) scenarios from a selection of sites around the Pacific Rim suggest that, with the exception of sources in the vicinity of Elfin Cove, the impact there is considerably less than on the U.S.

Table 11: Intercomparison of reference (RM) and forecast model (FM) estimates of peak wave amplitudes and arrival time at Elfin Cove, Alaska. Reference model amplitudes are consistently higher, particularly for late-arriving waves, suggesting that a safety factor of the order of 10% be applied in operational use of forecast model projections. The models are very consistent in their travel time predictions.

| | Leading Peak Amplitude and Travel Time | | | | | | Maximum Amplitude | | |
Source	RM (cm)	FM (cm)	RM Excess	RM (hr)	FM (hr)	RM Excess	RM (cm)	FM (cm)	RM Excess
1960 Chile	122.5	120.4	+1.7%	18.57	18.58	-0.05%	126.3	120.4	+4.9%
1964 Alaska	99.6	97.0	+2.7%	1.550	1.558	-0.51%	99.95	96.95	+3.1%
2010 Chile	9.50	9.31	+2.1%	18.16	18.16	–	9.50	9.31	+2.1%
2011 Tohoku	5.65	5.50	+2.7%	8.25	8.25	–	17.2	13.9	+23.9%
ACSZ 40–49	367.9	364.6	+0.9%	0.267	0.267	–	503	496	+1.6%
ACSZ 56–65	52.6	50.7	+3.8%	2.88	2.83	+1.48%	68.5	59.6	+14.9%
CSSZ 102–111	27.4	26.8	+2.2%	19.54	19.55	-0.05%	52.1	43.3	+20.4%
MOSZ 1–10	44.1	43.6	+1.2%	12.08	12.08	–	89.5	55.3	+61.8%
Summary	**Average RM Excess +2.2%; Negligible Time Lag**						**Geometric Average 8.3%**		

West Coast. This, in conjunction with recurring episodes of noise at the tide gauge, substantially reduced the number of historical events in recent years available for model validation. Tsunami waves emanating from the southwest Pacific result in proportionately greater response in the Alaska Panhandle. This report does not suggest that the mega-tsunami event scenarios represent probable tsunami sources and should not be considered a thorough risk assessment study.

In addition to the scenarios run by the author and reported here, further tests have been made by other members of the group at NCTR, and will continue to be made by staff at the Tsunami Warning Centers and others, perhaps in training situations. Among the many related tools developed at NCTR is ComMIT (the Community Model Interface for Tsunamis; Titov *et al.*, 2011), which provides a highly intuitive graphical environment in which to exercise and explore forecast models for any combination of propagation database unit sources. Were any of these avenues to reveal a problem with the model, its origin (most likely in some quirk of the bathymetric files) would be located and corrected, and the revised version would then be re-installed for operational use. The development of the forecast system is a dynamic process, with new models added (and old ones revisited) from the current list of U.S. interests and globally. As algorithms and methodologies to represent meteo- or landslide-generated tsunamis become available in the coming years, the utility of current forecast models beyond purely seismic events could well expand.

6. Acknowledgments

7. References

Bernard, E., L. Tang, Y. Wei, and V. Titov (2014): Impact of near-field, deep-ocean tsunami observations on forecasting the 7 December 2012 Japanese tsunami. *Pure and Appl. Geophys., 171*(12), 3483–3491, doi:10.1007/s00024-013-0720-8.

Caldwell, R.J., L.A. Taylor, B.W. Eakins, K.S. Carignan, and S.V. Collins (2012): Digital Elevation Models of Juneau and Southeast Alaska: Procedures, Data Sources and Analysis. National Geophysical Data Center, Boulder, Colorado.

Doser, D.I., and R. Lomas (2000): The transition from strike-slip to oblique subduction in southeastern Alaska from seismological studies. *Tectonophysics, 316*, 45–65.

Dunbar, P. (2007): Increasing public awareness of natural hazards via the internet. *Nat. Hazards, 42*(3), 529–536, doi:10.1007/s11069-006-9072-3.

Elfin Cove Community Plan (2007): Community of Elfin Cove NonProfit Corporation (CECNPC), 111 pp.

Gica, E., M. Spillane, V.V. Titov, C.D. Chamberlin, and J.C. Newman (2008): Development of the forecast propagation database for NOAA's Short-term Inundation Forecast for Tsunamis (SIFT). NOAA Tech. Memo. OAR PMEL-139, NTIS: PB2008-109391, 89 pp.

Kanamori, H., and J.J. Cipar (1974): Focal process of the great Chilean earthquake, May 22, 1960. *Phys. Earth Planet. Inter., 9*, 128–136.

Lander, J.F. (1996): Tsunamis Affecting Alaska 1737–1996. KGRD No. 31. US Department of Commerce, NOAA, National Geophysical Data Center, Boulder, Colorado, 155 pp.

López, A.M., and E.A. Okal (2006): A seismological reassessment of the source of the 1946 Aleutian "tsunami" earthquake. *Geophys. J. Int., 165*(3), 835–849, doi:10.1111/j.1365- 246x.2006.02899.x.

Love, M.R., B.W. Eakins, L.A. Taylor, K.S. Carignan, D. Friday, P.R. Grothe (2011): Digital Elevation Model of Elfin Cove, Alaska: Procedures, Data Sources and Analysis. National Geophysical Data Center, Boulder, Colorado.

Ma, K-F, H. Kanamori and K. Satake (1999): Mechanism of the 1975 Kalapana, Hawaii, earthquake inferred from tsunami data. *J. Geophys. Res., 104*, 13,153-13,167.

Percival, D.B., D.W. Denbo, M.C. Eble, E. Gica, H.O. Mofjeld, M.C. Spillane, L. Tang, and V.V. Titov (2011): Extraction of tsunami source coefficients via inversion of DART® buoy data. *Nat. Hazards, 58*(1), 567–590, doi:10.1007/s11069-010-9688-1.

Polagye, B., and R Bedard (2006): Tidal In-stream Energy Assessment for Southeast Alaska. Report EPRI-TP-003 AK to the Alaska Energy Authority. `oceanenergy.epri.com/attachments/streamenergy/reports/003_TP_AK_011007.pdf`.

Shennan, I., R. Bruhn, and G. Plafker, G. (2009): Multi-segment earthquakes and tsunami potential of the Aleutian megathrust. *Quaternary Science Reviews, 28*(1), 7–13.

Spillane, M.C. (2014): A Tsunami Forecast Model for Point Reyes, California. NOAA OAR Special Report, PMEL Tsunami Forecast Series Vol. 6, 176 pp., doi:10.7289/V5W9573D.

Spillane, M.C., E. Gica, V.V. Titov, and H.O. Mofjeld (2008): Tsunameter network design for the U.S. DART® arrays in the Pacific and Atlantic oceans. NOAA Tech. Memo. OAR PMEL-143, 165 pp.

Tang, L., C. Chamberlin, E. Tolkova, M. Spillane, V.V. Titov, E.N. Bernard, and H.O. Mofjeld (2006): Assessment of potential tsunami impact for Pearl Harbor, Hawaii. NOAA Tech.Memo. OAR PMEL-131, NTIS: PB2007-100617, 36 pp.

Tang, L., V.V. Titov, and C.D. Chamberlin (2009): Development, testing, and applications of site-specific tsunami inundation models for real-time forecasting. *J. Geophys. Res., 114*, C12025, doi:10.1029/2009JC005476.

Tang, L., V.V. Titov, E. Bernard, Y. Wei, C. Chamberlin, J.C. Newman, H. Mofjeld, D. Arcas, M. Eble, C. Moore, B. Uslu, C. Pells, M.C. Spillane, L.M. Wright, and E. Gica (2012): Direct energy estimation of the 2011 Japan tsunami using deep-ocean pressure measurements. *J. Geophys. Res., 117*, C08008, doi:10.1029/2011JC007635.

Titov, V.V. (2009): Tsunami Forecasting. Chapter 12 in *The Sea, Volume 15: Tsunamis*, Harvard University Press, Cambridge, Massachusetts and London, England.

Titov, V., and F.I. González (1997): Implementation and testing of the Method of Splitting Tsunami (MOST) model. NOAA Tech. Memo. ERL PMEL-112, NTIS: PB98-122773, NOAA/Pacific Marine Environmental Laboratory, Seattle, WA, 11 pp.

Titov, V.V., and C.E. Synolakis (1998): Numerical modeling of tidal wave runup. *J. Waterw. Port Coast. Ocean Eng., 124*(4), 157–171.

Titov, V.V., C. Moore, D.J.M. Greenslade, C. Pattiaratchi, R. Badal, C.E. Synolakis, and U. Kânoğlu (2011): A new tool for inundation modeling: Community Modeling Interface for Tsunamis (ComMIT). *Pure Appl. Geophys., 168*(11), 2121–2131, doi:10.1007/s00024-011-0292-4.

U.S. Census Bureau (2010): 2010 Census Interactive Population Search. URL: `http://www.census.gov/2010census/popmap/ipmtext.php`.

Wei, Y., E. Bernard, L. Tang, R. Weiss, V. Titov, C. Moore, M. Spillane, M. Hopkins, and U. Kânoğlu (2008): Real-time experimental forecast of the Peruvian tsunami of August 2007 for U.S. coastlines. *Geophys. Res. Lett., 35*, L04609, doi:10.1029/2007GL032250.

Wesson, R.L., O.S. Boyd, C.S. Mueller, C.G. Bufe, A.D. Frankel, and M.D. Petersen (2007): Revision of time-independent probabilistic seismic hazard maps for Alaska. U.S. Geological Survey Open-File Report 2007-1043.

Worthington, L.L., H.J. Van Avendonk, S.P. Gulick, G.L. Christeson, and T.L. Pavlis (2012): Crustal structure of the Yakutat terrane and the evolution of subduction and collision in southern Alaska. *J. Geophys. Res., 117*, B01102, doi:10.1029/2011JB008493.

FIGURES
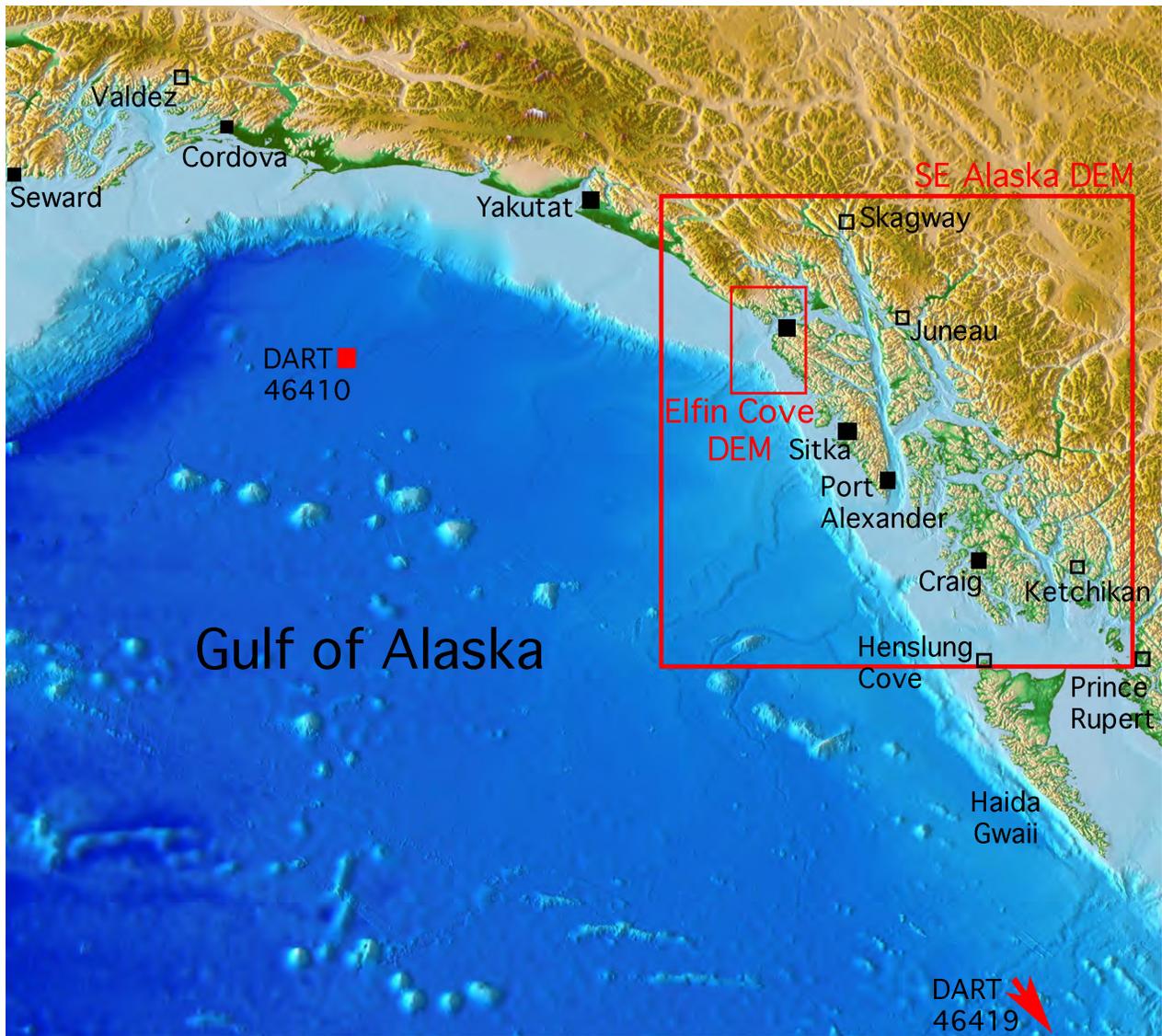
Figure 1: The northern Gulf of Alaska, showing regional digital elevation model resources, tide gauge, and DART tsunami detection assets.
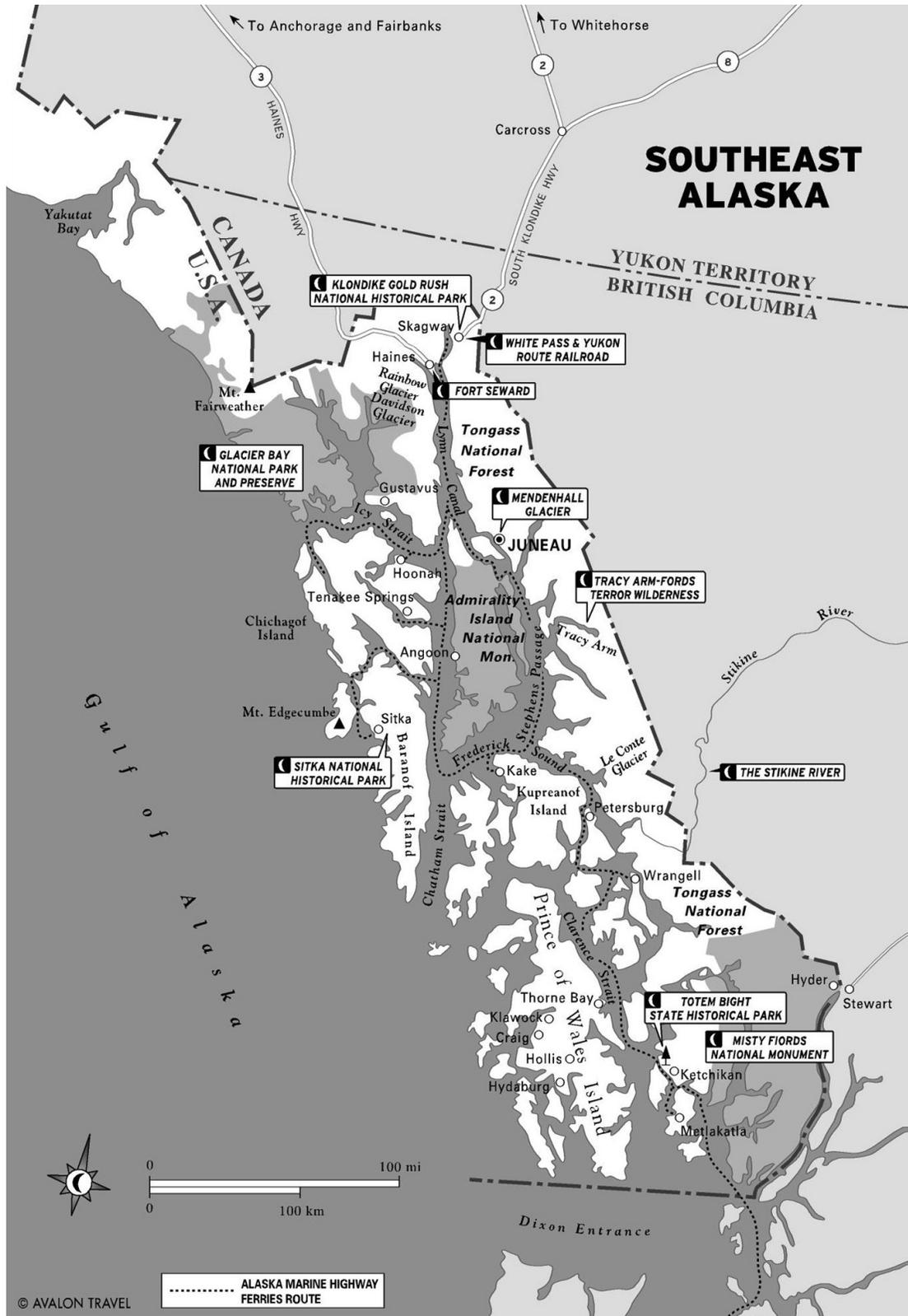
Figure 2: Southeast Alaska geographic features, communities, and the Alaska Marine Highway (reproduced with permission of the Alaska Department of Transportation and Public Facilities).
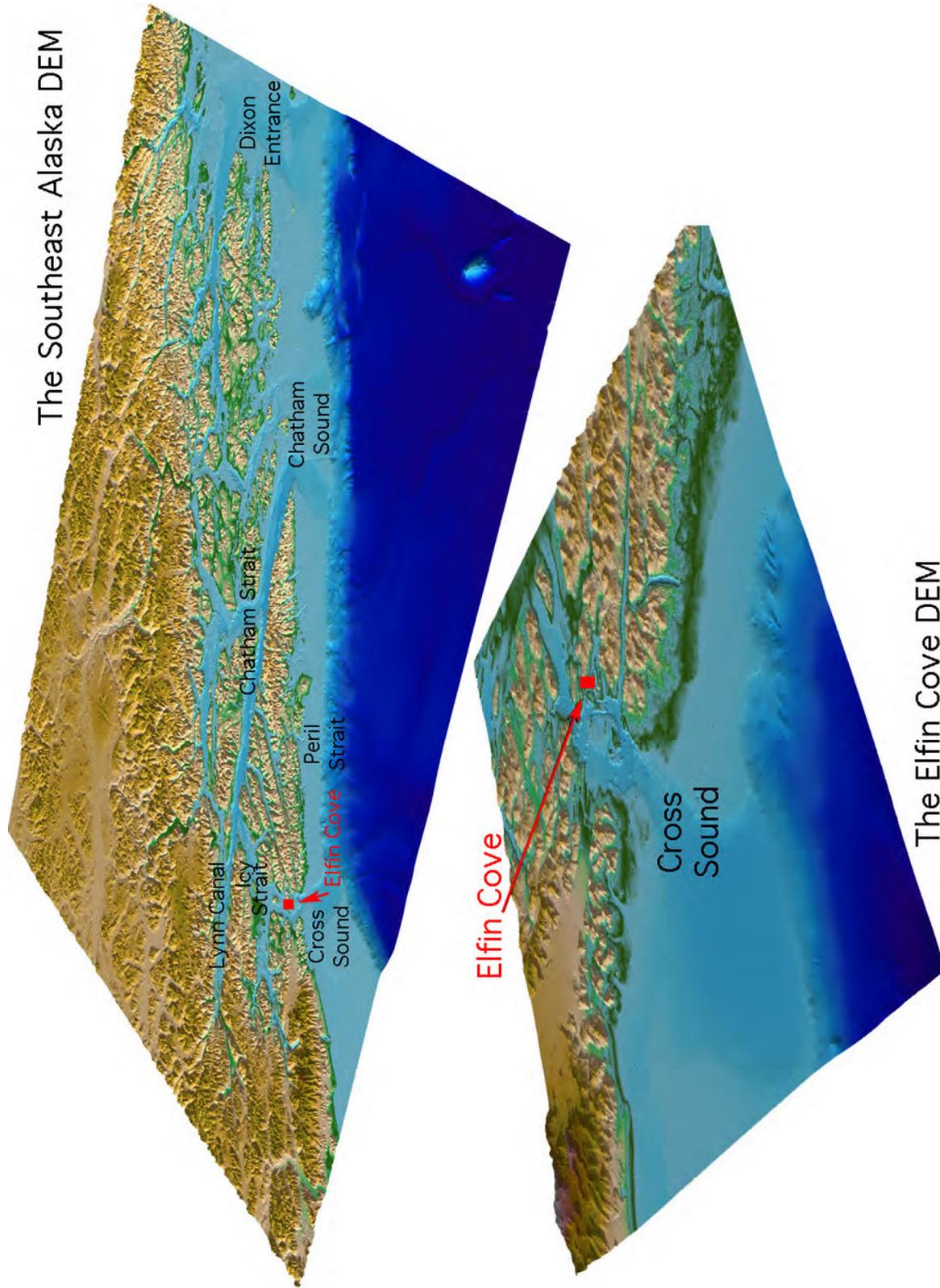
Figure 3: Oblique views of the southeast Alaska and Elfin Cove digital elevation models developed by the National Geophysical Data Center.
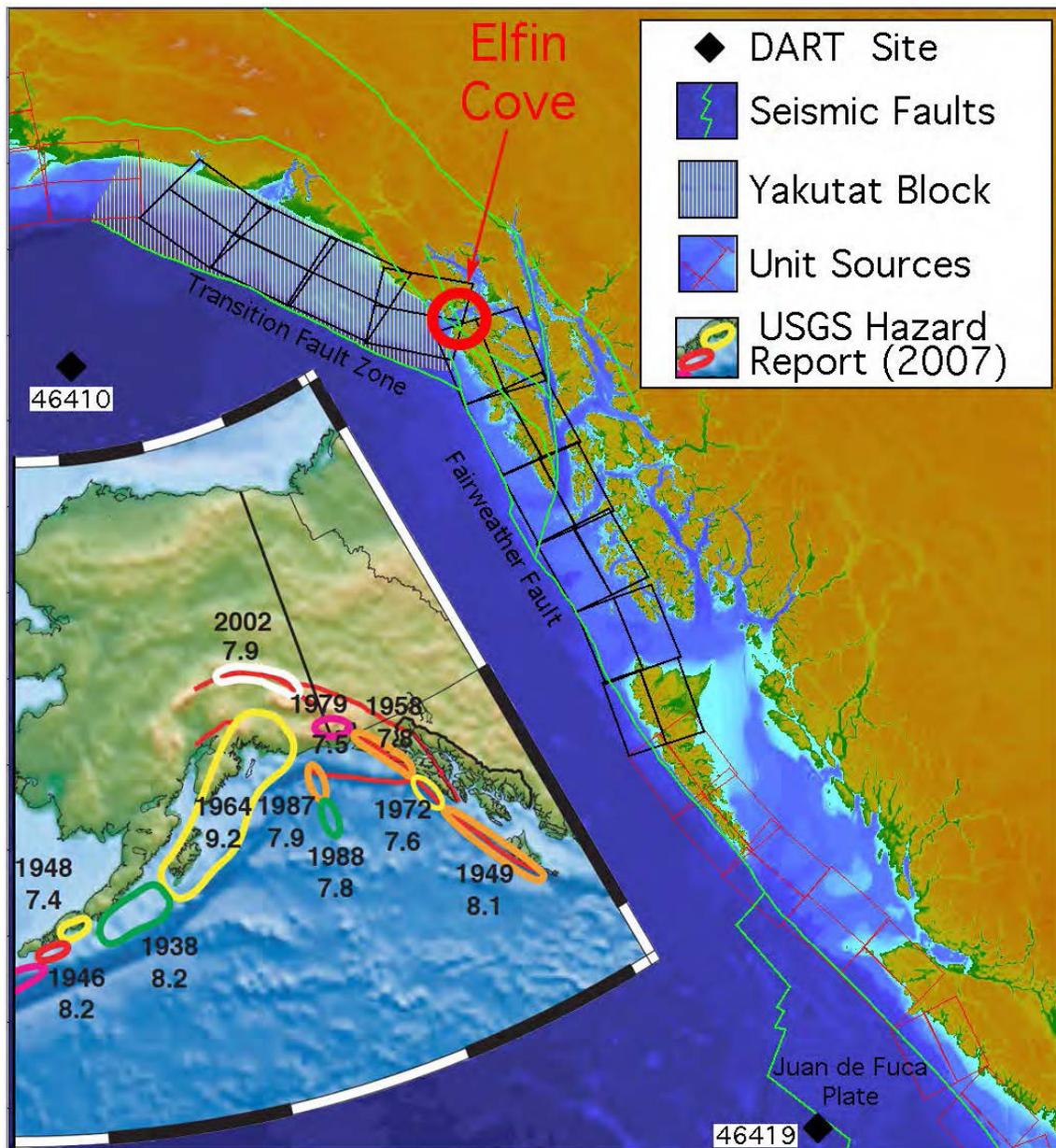
Figure 4: Regional seismic hazards and the unit sources employed to model their tsunamigenic potential. The inset panel is adapted from the USGS Seismic Hazard Maps for Alaska.
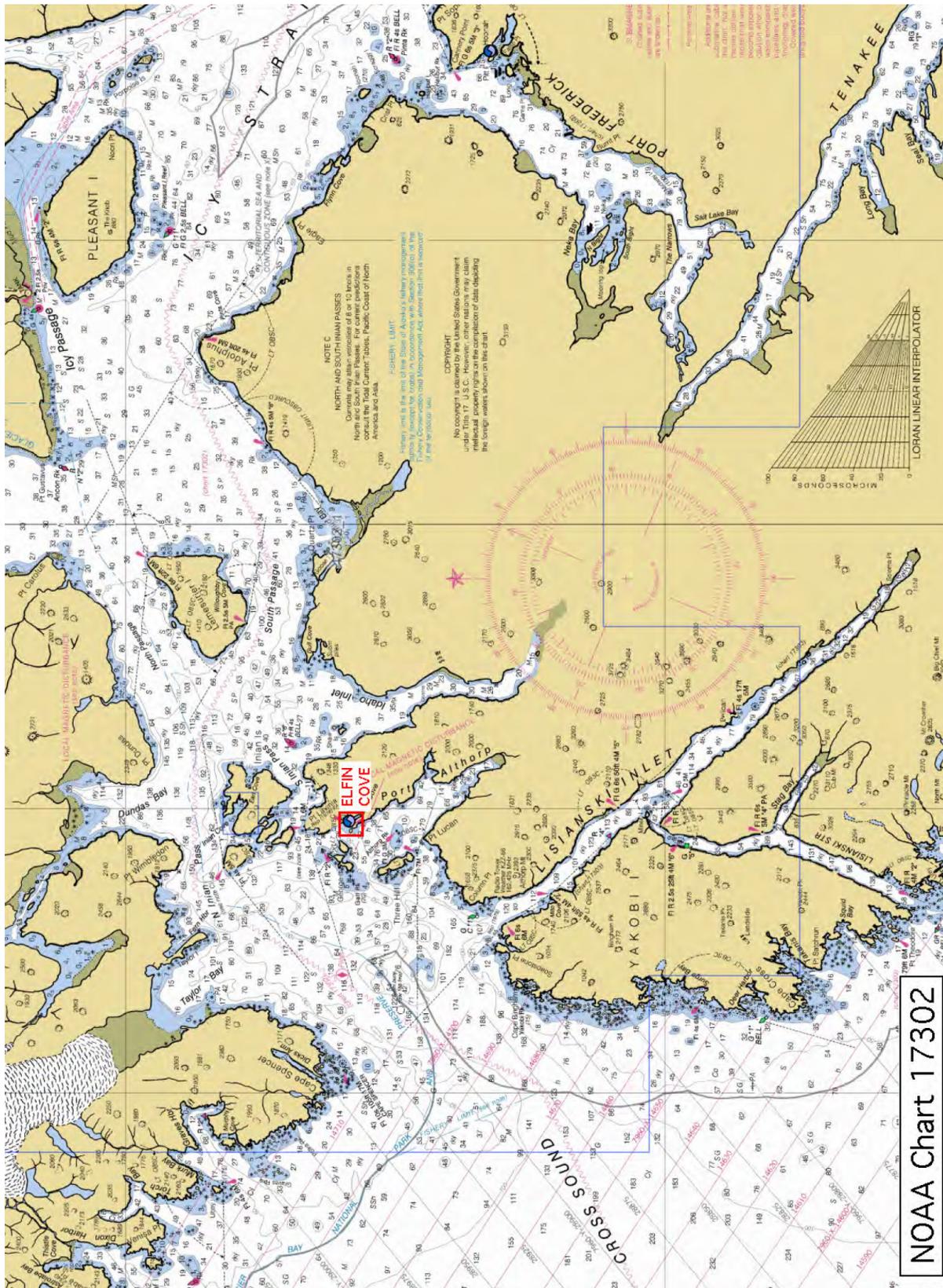
Figure 5: Extracts from NOAA Chart 17302. (a): Cross Sound to Icy Strait. *Continued on next page.*
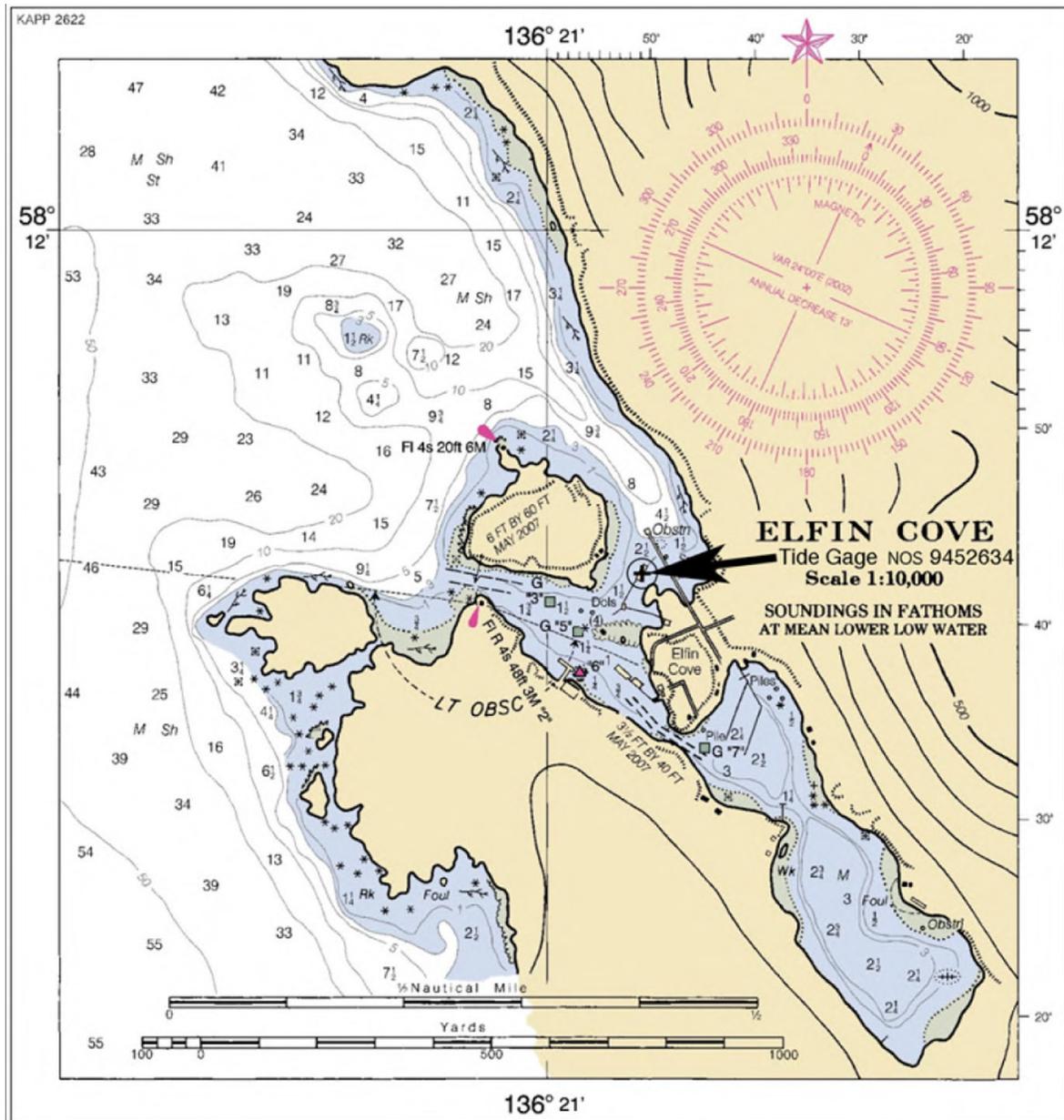
Figure 5, continued: Extracts from NOAA Chart 17302. (b) The Elfin Cove sub-chart, annotated with the NOS tide gauge location.

Figure 6: View southeast into Elfin Cove's inner cove, showing the boardwalks, finger docks, and other community facilities. (Photograph by Rick Sood, `roundezvous.comImagesAlaska2006ElfinCove.jpg`).
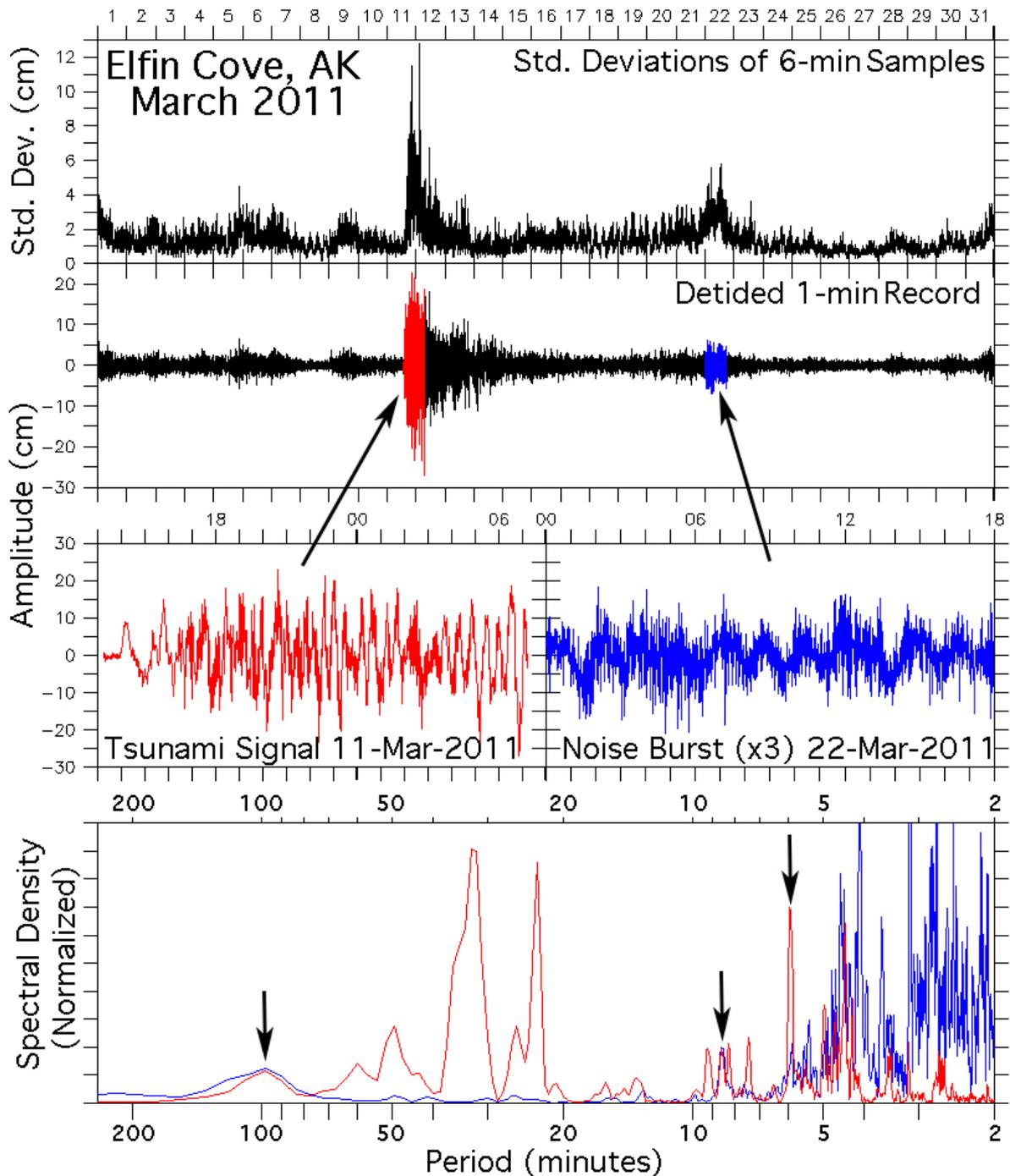
Figure 7: Elfin Cove tide gauge data from March 2011 illustrating episodes of high-frequency, non-tsunami related signals (blue) that can mask tsunami signals such as that associated with the 2011 Tohoku event (red). The upper panel shows, for the whole month, the standard deviation of the subsamples employed in computing the published 6 min data record. The central panels show the 1 min record, processed with a Kalman filter to eliminate the tidal signal. In the lower panel, the spectrum (in energy-preserving form) of two highlighted one-day segments are contrasted. Strong spectral peaks associated with the tsunami (red) are absent in the sample from a noise burst (blue).
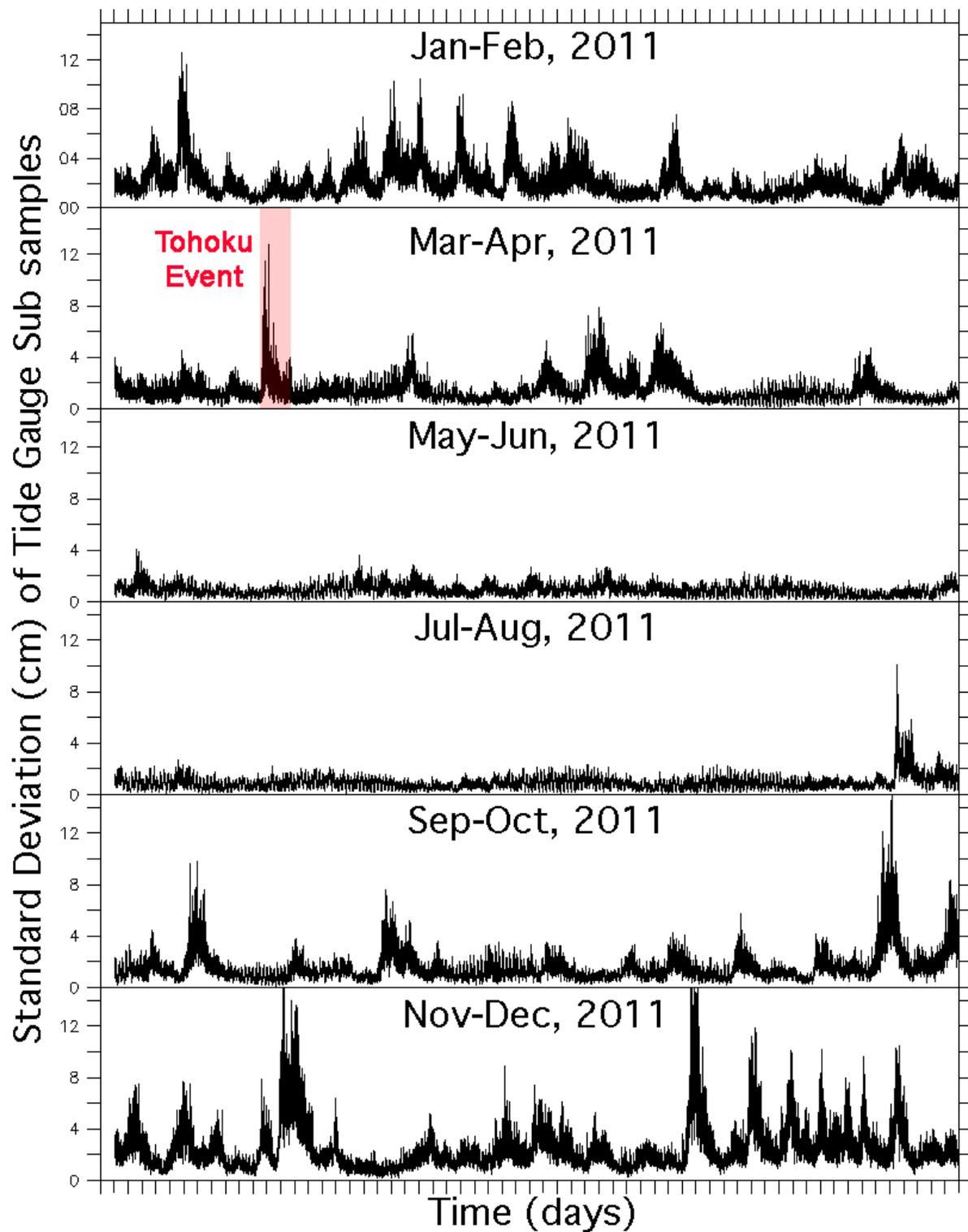
Figure 8: One year of the standard deviation measure of subsample noise that accompanies the 6 min tide gauge data from Elfin Cove (in 2-month strips with a common vertical scale). Only one tsunami event (highlighted) of significance occurred during the year, but noise "bursts" associated with winds and waves are common, particularly during winter months.
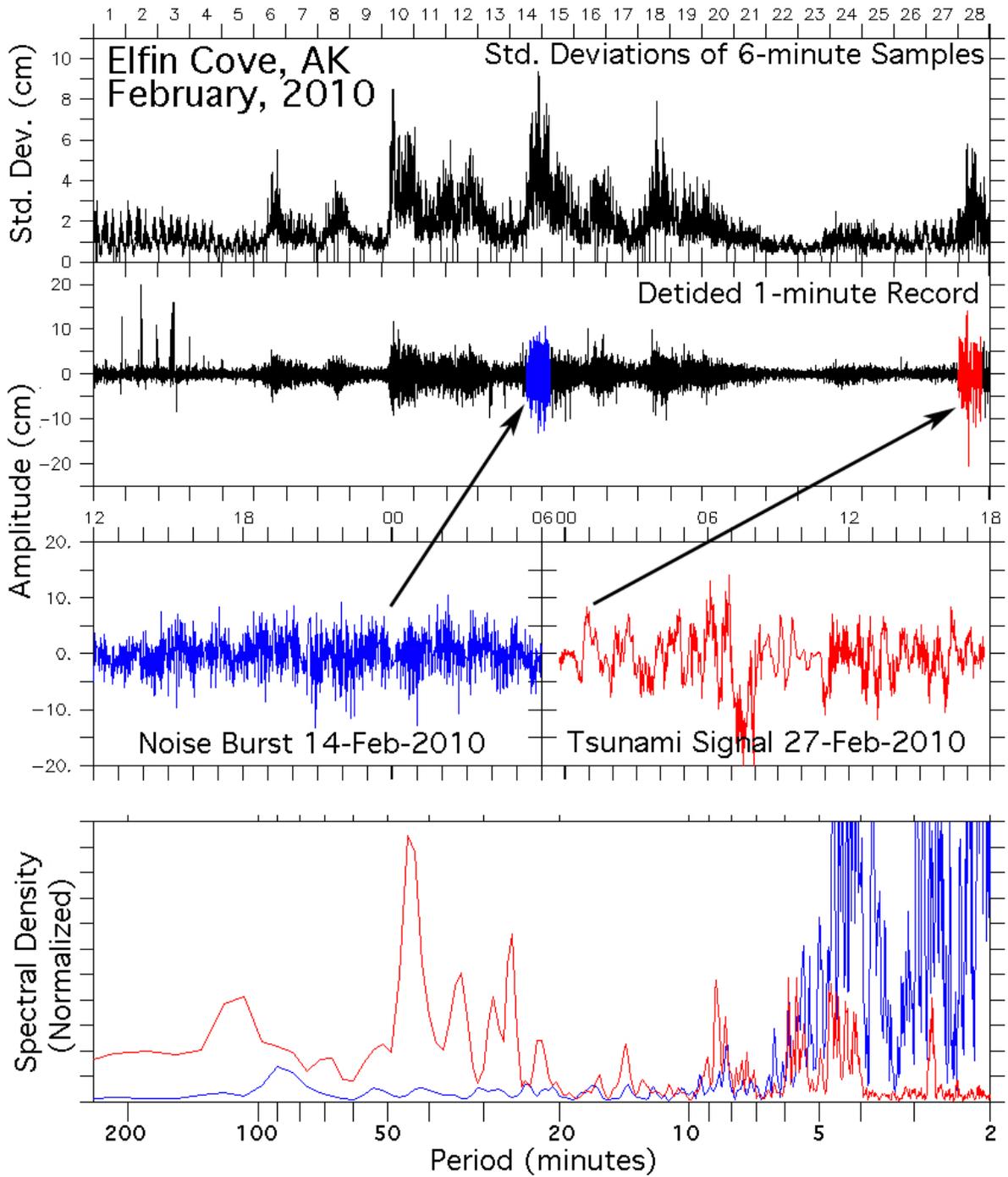
Figure 9: As in Figure 7, but for the Chile tsunami event of February 2010, whose impact in the Gulf of Alaska was comparable to that of 2011 Tohoku. The tsunami signal stands out well above the noise, making this a suitable case for model validation.
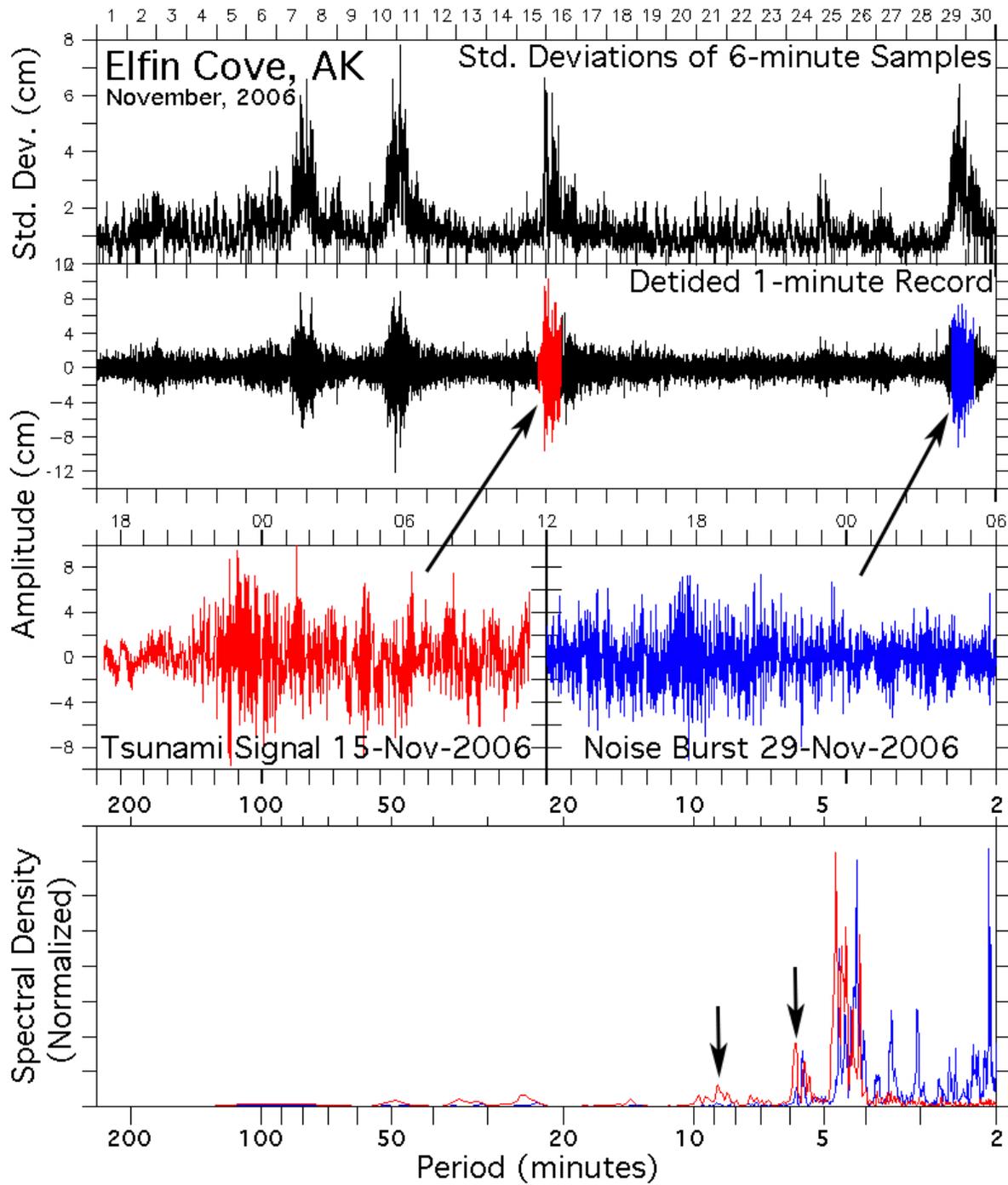
Figure 10: As in Figures 7 and 9, but illustrating the poor signal-to-noise ratio during the Kuril tsunami event of November 2006. Although a standard for validation of other Pacific basin forecast models, this event is of limited use for Elfin Cove, Alaska.
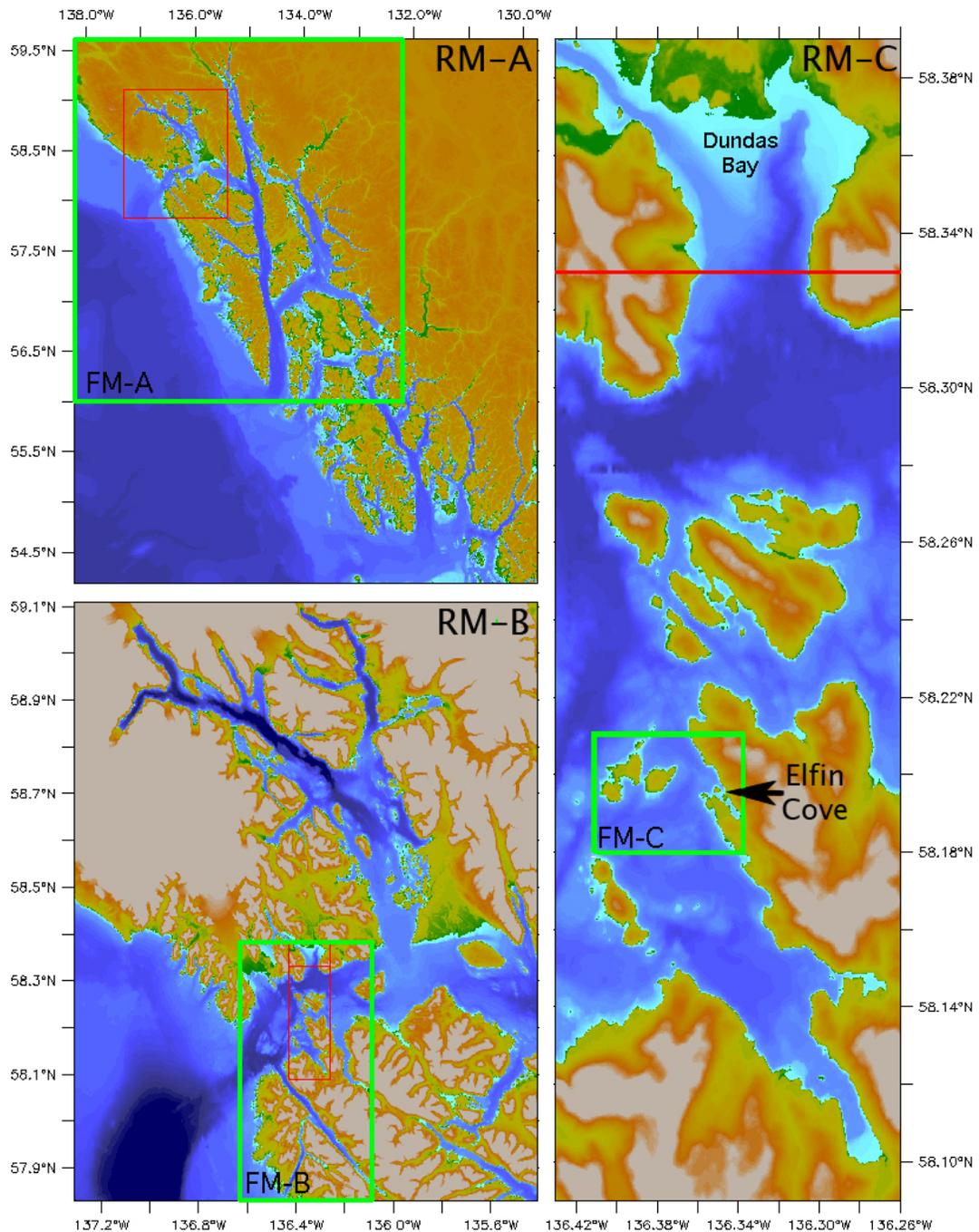
Figure 11: Nested grid representation employed in the reference (RM) version of the Elfin Cove tsunami model, progressing counterclockwise from the coarsest-resolution A grid (upper left), through the extensive, medium-resolution B grid, which includes all of Glacier Bay, to the finely resolved C grid, which includes the Inian passes (see Figure 5). Red rectangles are used to indicate the inner reference model grids. Green rectangles indicate the more limited extents of the forecast model (FM) grids shown in Figure 12. See main text for a discussion of the upper section of Dundas Bay, excluded in the final version of the reference model C grid.
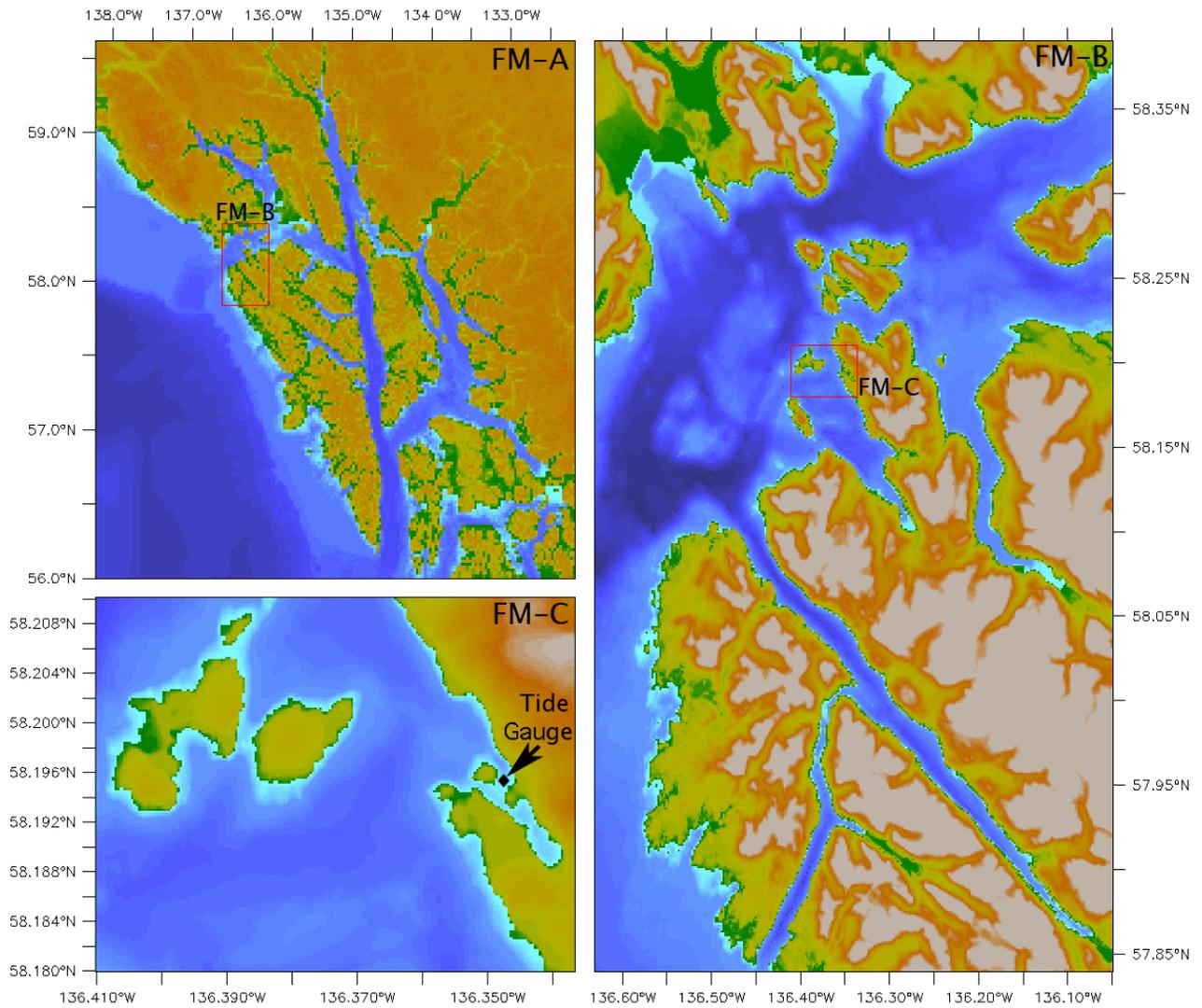
Figure 12: Nested grids employed in the forecast model (FM) version of the Elfin Cove tsunami model, progressing clockwise with the innermost C grid, which is much reduced in extent, appearing in the lower left. The Inian passes are best represented in the B grid, while Glacier Bay appears only coarsely in the outermost A grid. For the more extensive reference model grids, see Figure 11.
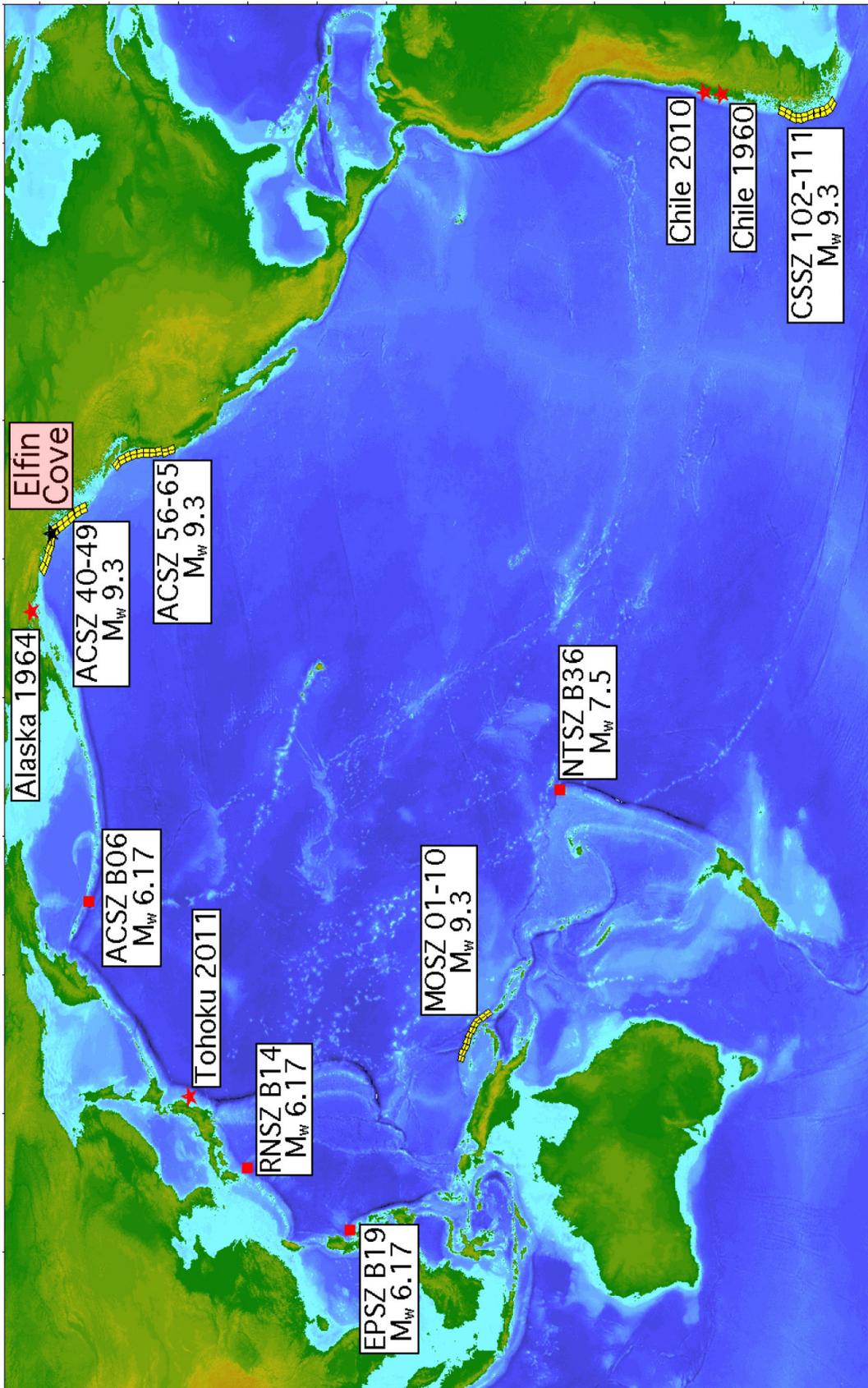
Figure 13: Synthetic and historic event scenarios employed in intercomparison of the reference and forecast versions of Elfin Cove tsunami model. Evenly distributed slip values are applied in 20 adjacent unit sources (yellow rectangles) of the propagation database to represent mega-tsunami events; single unit sources are employed, as detailed in Table 6. For the historic cases, a linear combination of unit sources is employed, as detailed in Table 6.
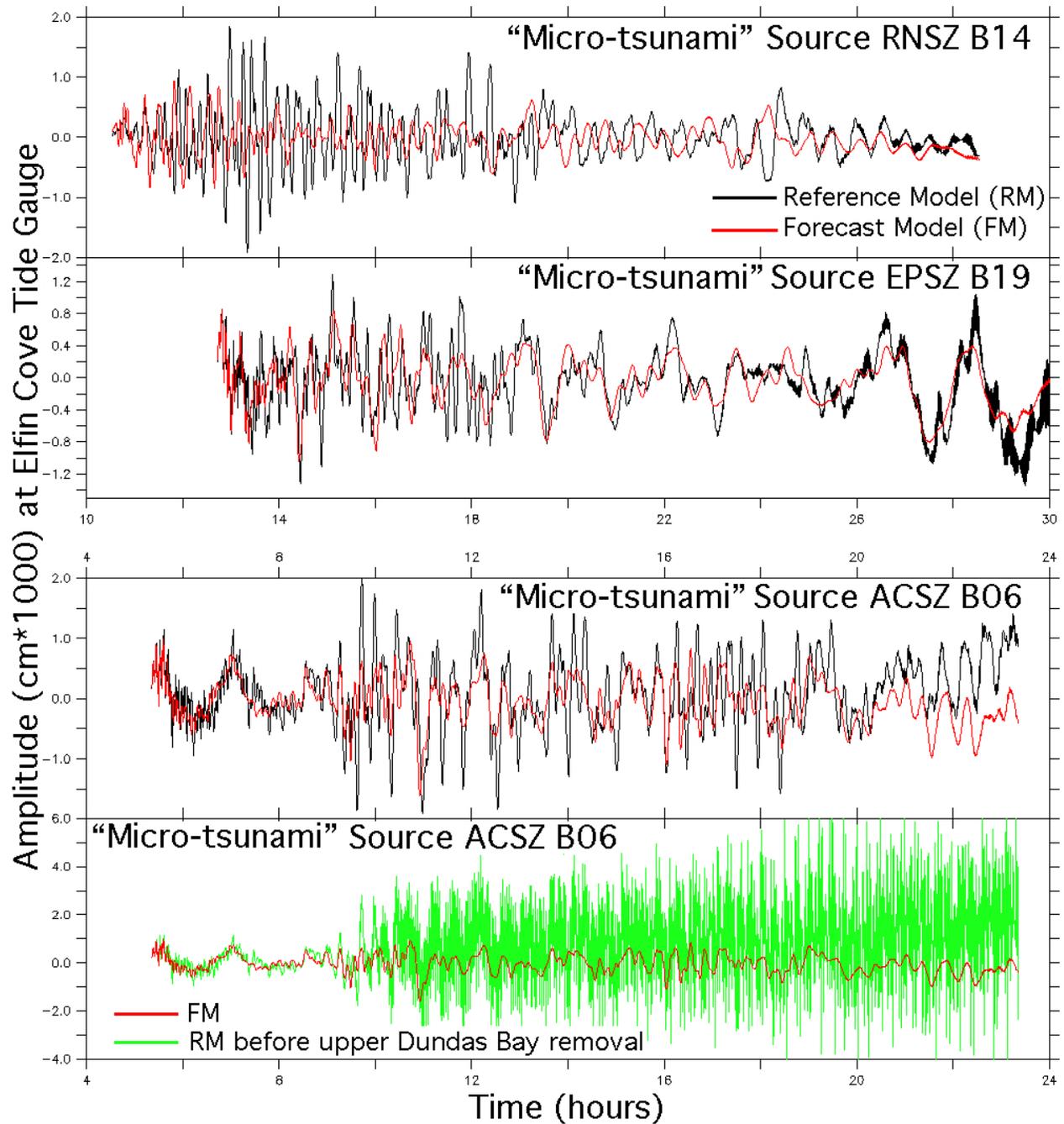
Figure 14: Comparison of reference (RM) and forecast (FM) model predictions for the Elfin Cove tide gauge site for three "micro-tsunami" (very low magnitude) sources. Such runs highlight low-level model instabilities that might be missed in modeling larger events. The lower panel shows the reference model at an early stage of development; instabilities emanating from upper Dundas Bay (see Figure 11) proved difficult to eliminate while employing reasonable time and space steps. These instabilities are essentially eliminated in the final C grid..
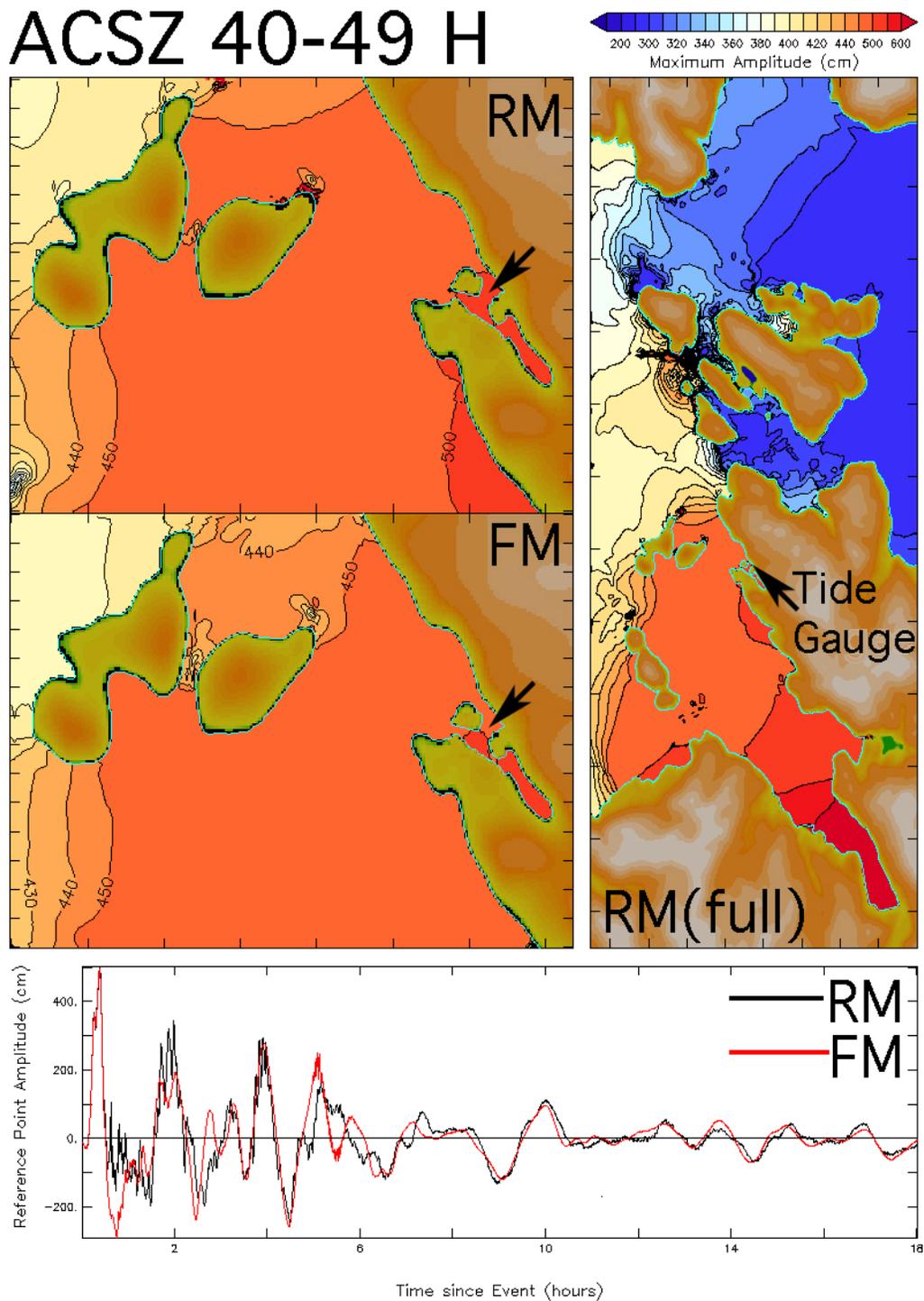
Figure 15: Comparison of reference (RM) and forecast (FM) model results for the synthetic ACSZ 40–49 mega-tsunami scenario, which is local to Elfin Cove. The left panels are for the C-grid domain of the forecast model; the right panel shows the entirety of the reference model C grid. The lower panel contrasts the reference (black) and forecast (red) model versions of the time series at the Elfin Cove tide gauge location, marked in the upper panels and in Figure 6b. (a) Distribution of maximum amplitude during the 18 hr simulation. *The comparison is continued on the following pages.*
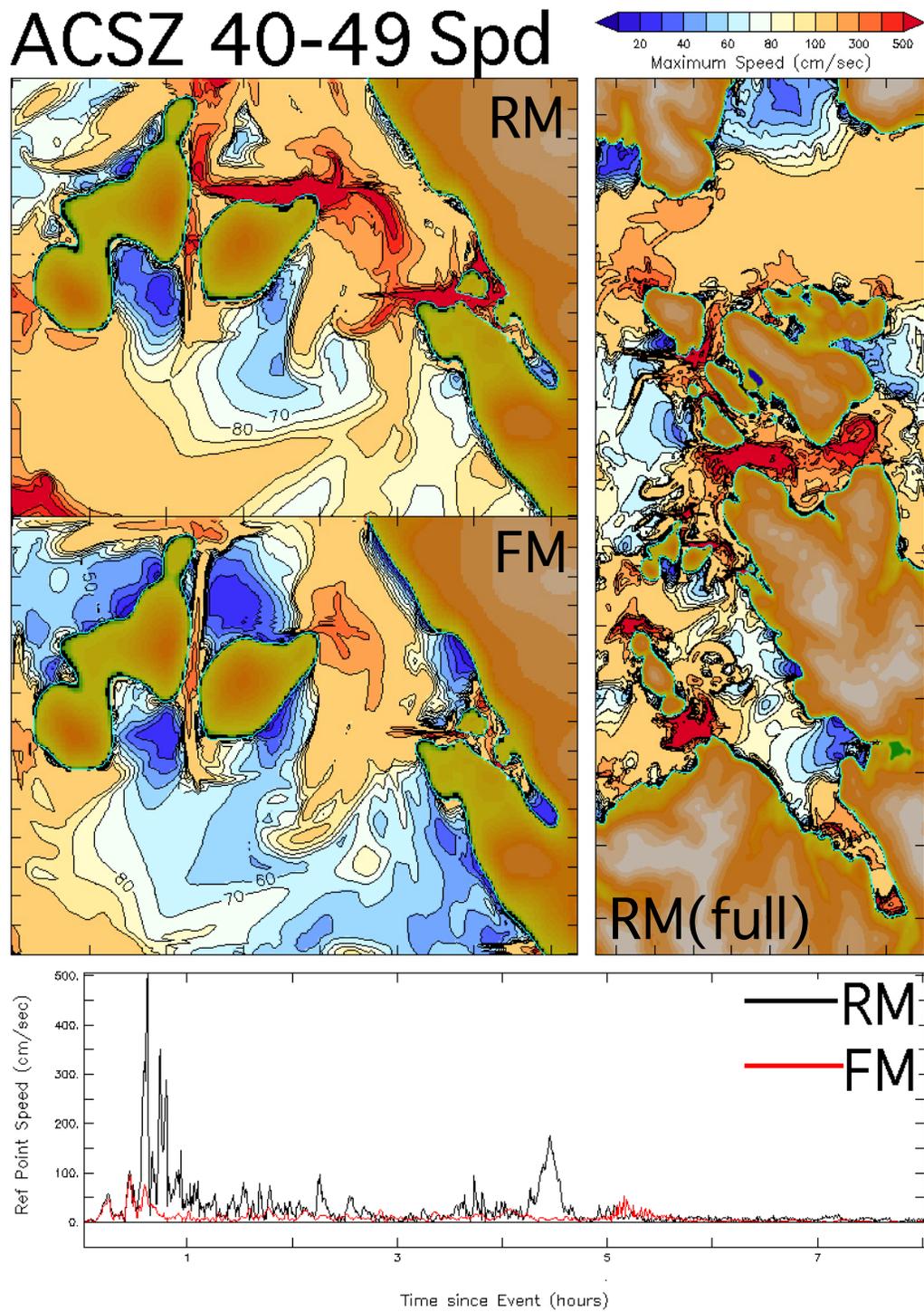
Figure 15 (continued): Comparison of reference (RM) and forecast (FM) model results for the synthetic ACSZ 40–49 mega-tsunami scenario. (b) Distribution of maximum speed.
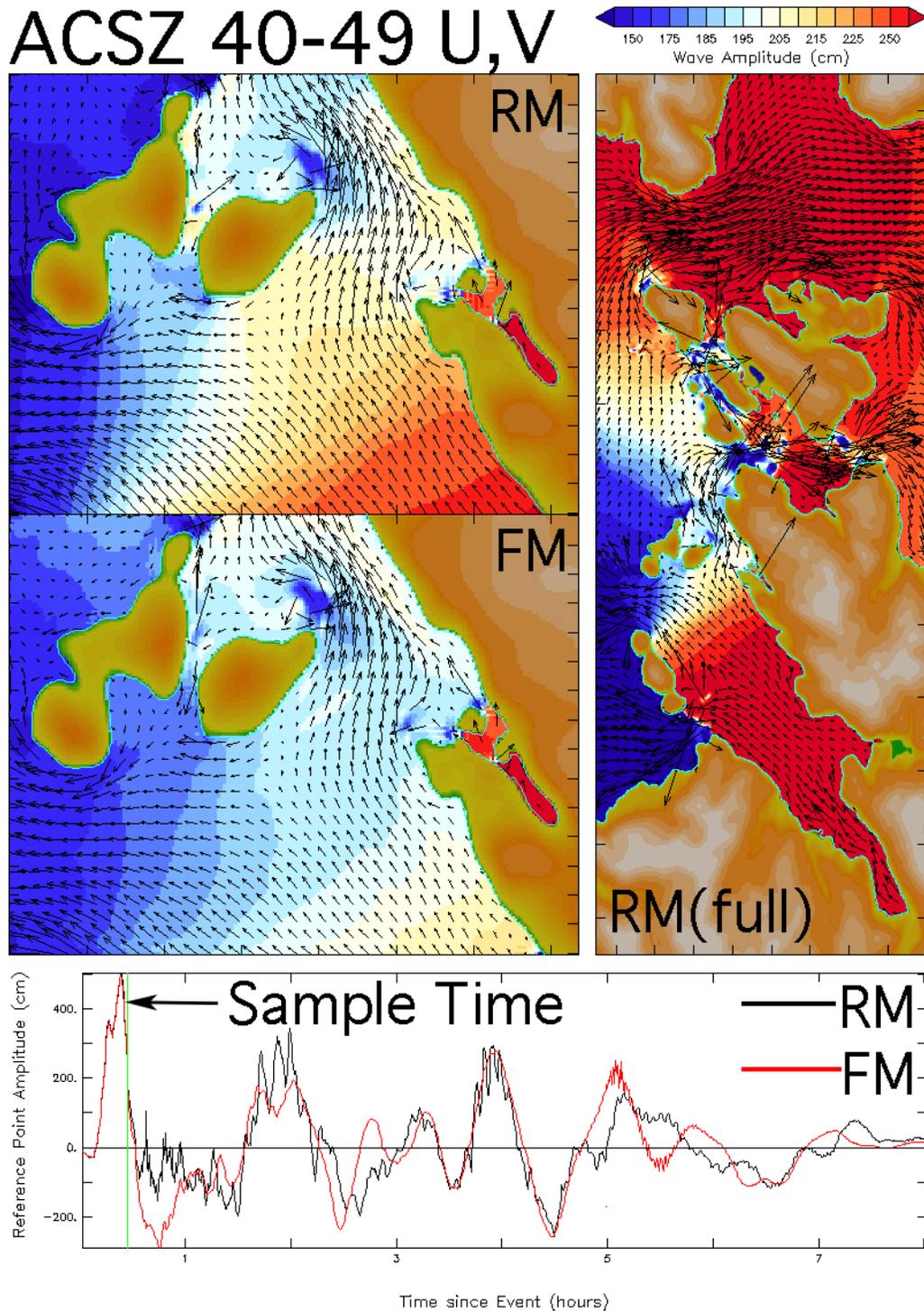
Figure 15 (continued): Comparison of reference (RM) and forecast (FM) model results for the synthetic ACSZ 40–49 mega-tsunami scenario. (c) A snapshot of the current field at the time indicated by the green line in the lower panel.
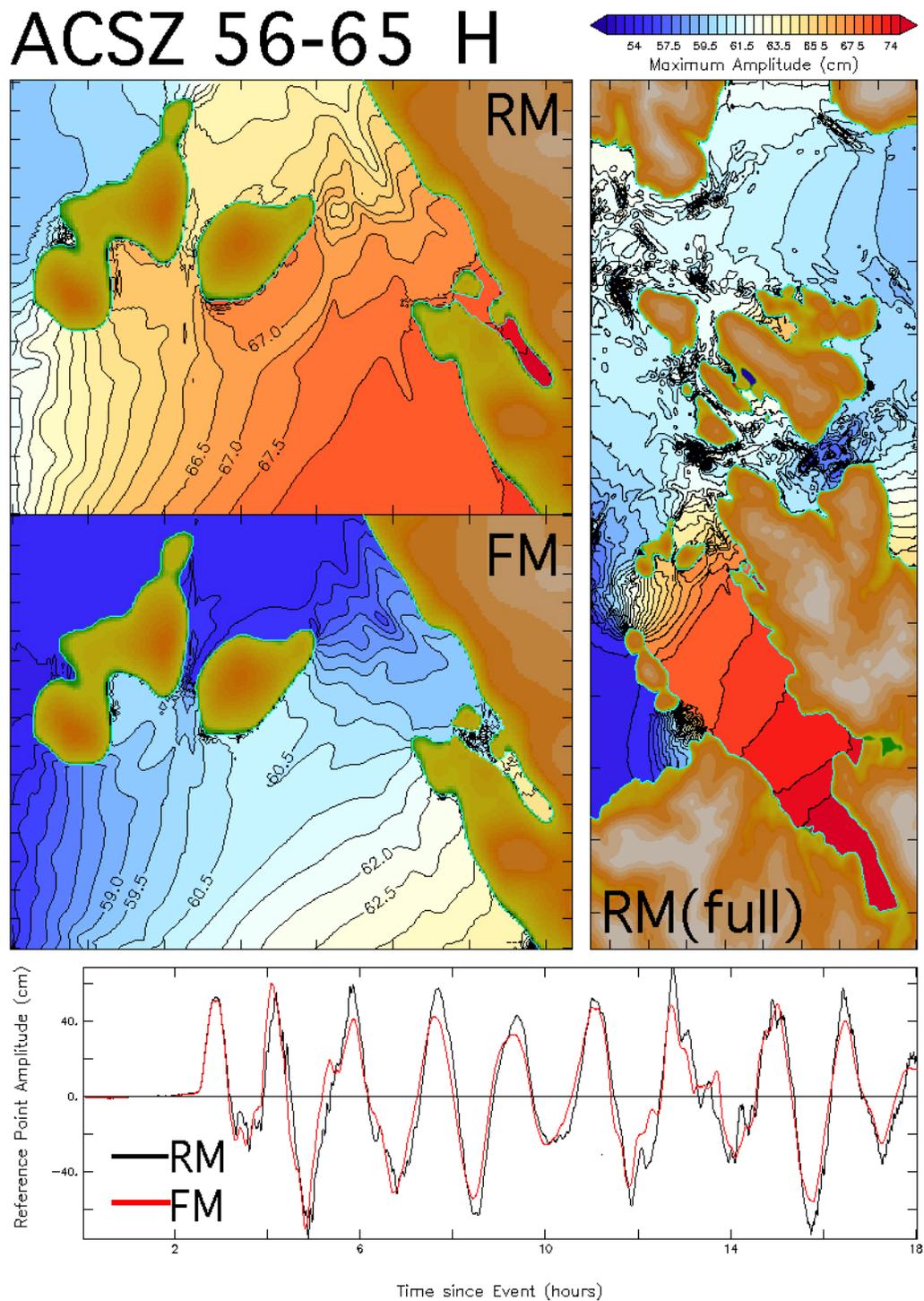
Figure 16: Comparison of reference (RM) and forecast (FM) model results, as in Figure 15 but for the ACSZ 56–65 mega-tsunami scenario, which is representative of the Cascadia Subduction Zone. (a) Distribution of maximum amplitude during the 18 hr simulation. *The comparison is continued on the following pages.*
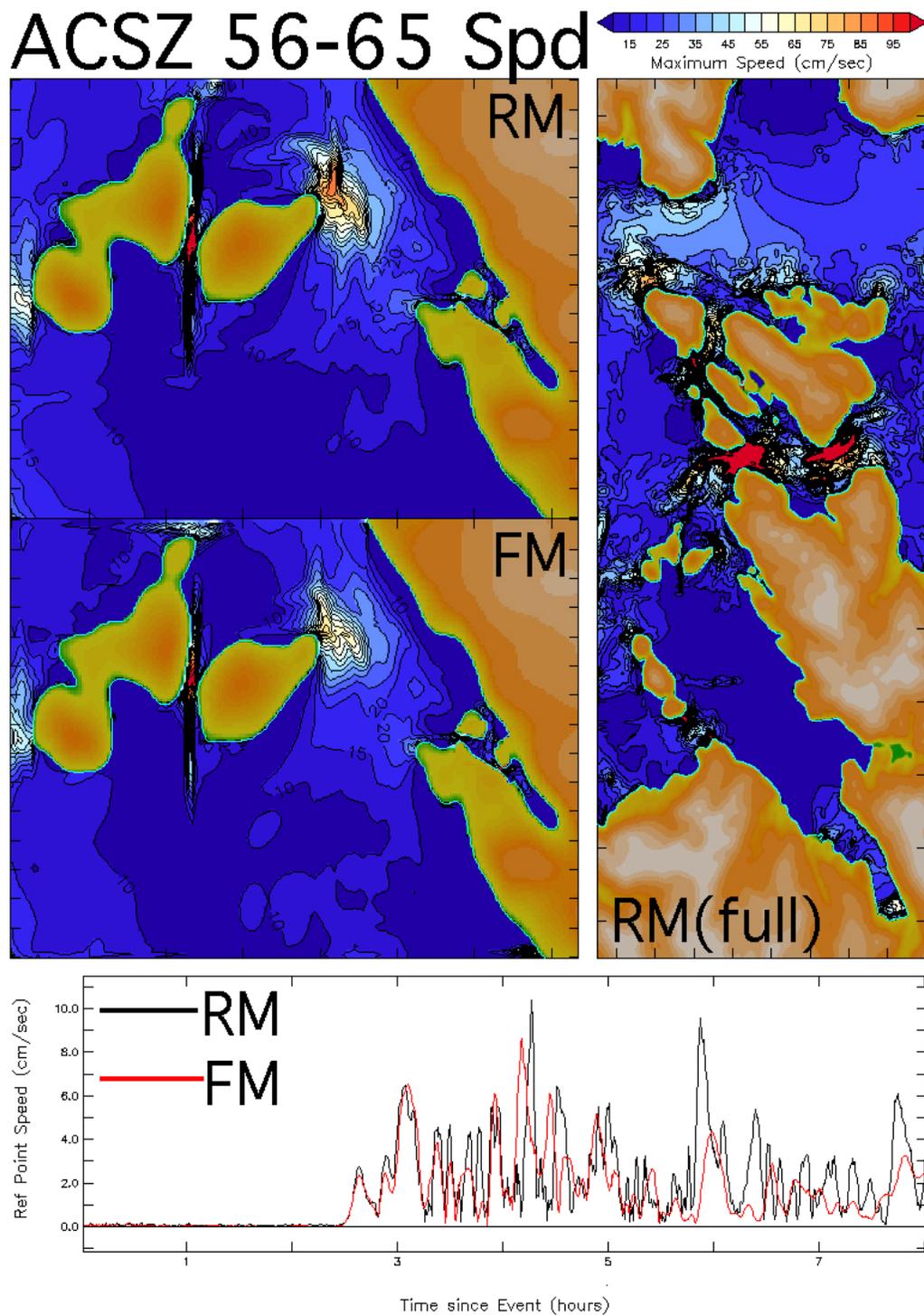
Figure 16 (continued): Comparison of reference (RM) and forecast (FM) model results for the synthetic ACSZ 56–65 mega-tsunami scenario. (b) Distribution of maximum speed.
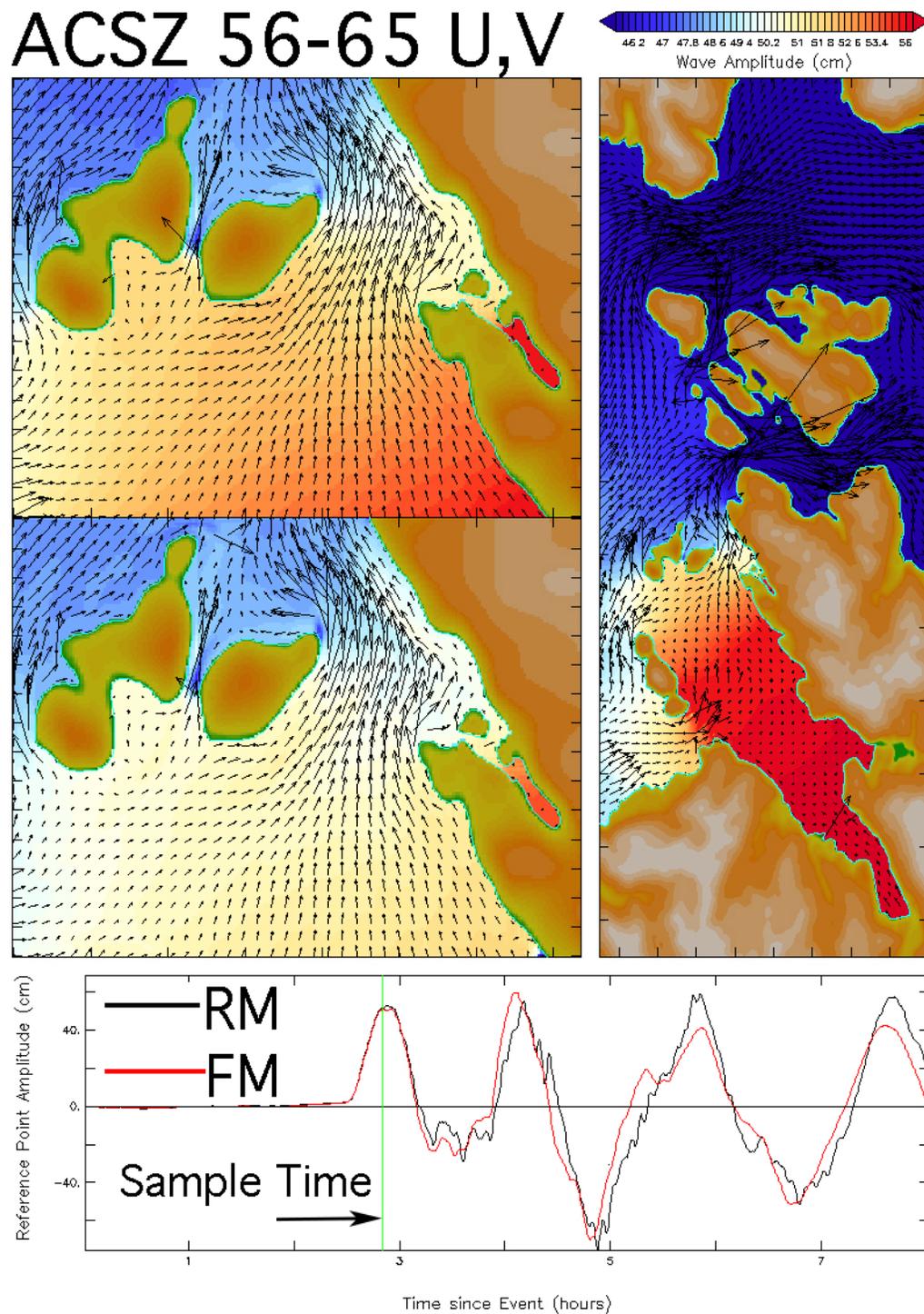
Figure 16 (continued): Comparison of reference (RM) and forecast (FM) model results for the synthetic ACSZ 56–65 mega-tsunami scenario. (c) A snapshot of the current field at the time indicated by the green line in the lower panel.
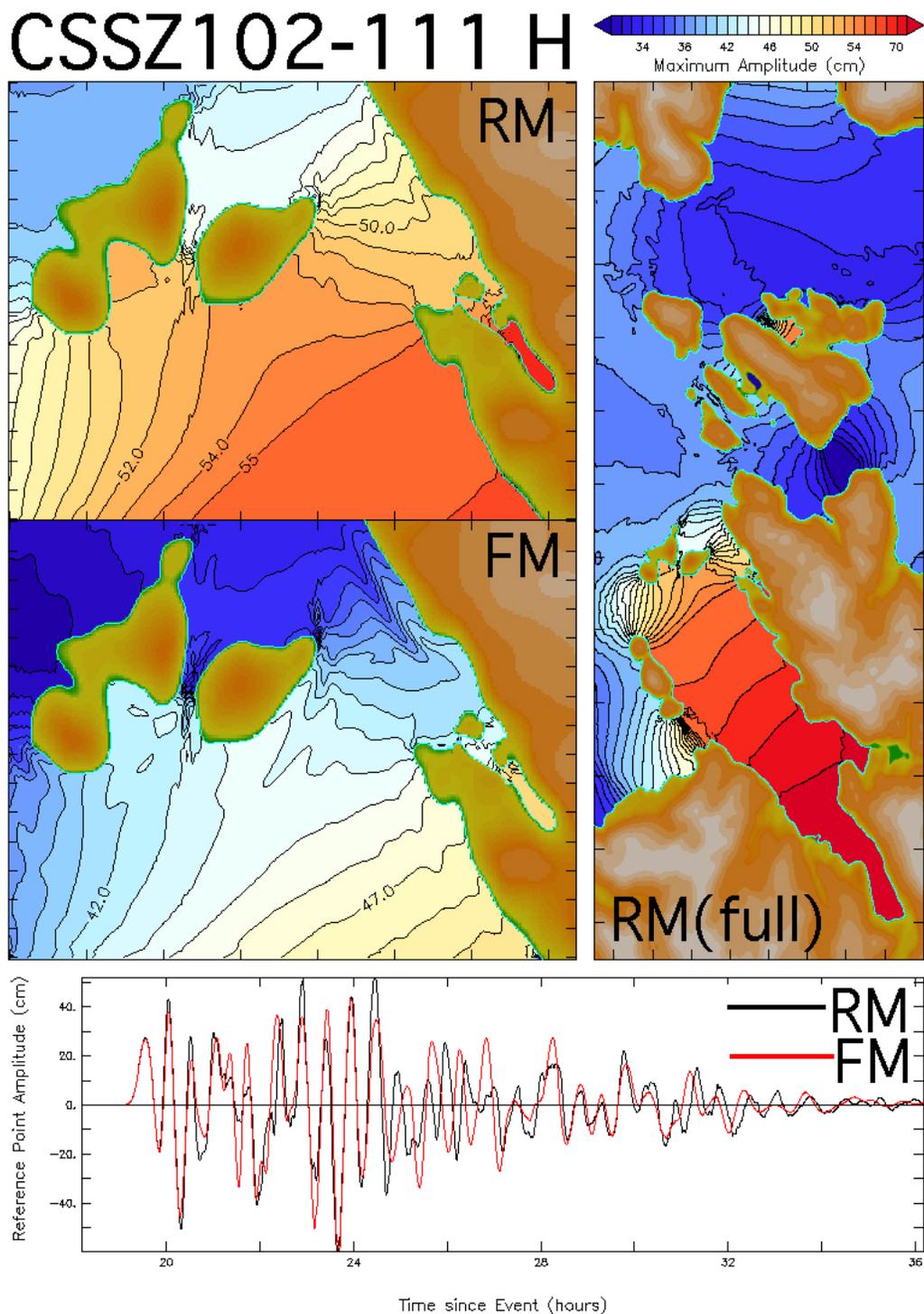
Figure 17: Comparison of reference (RM) and forecast (FM) model results, as in Figure 15 but for the CSSZ 102–111 mega-tsunami scenario, which is representative of the South American Subduction Zone. (a) Distribution of maximum amplitude during the 18 hr simulation. *The comparison is continued on the following pages.*
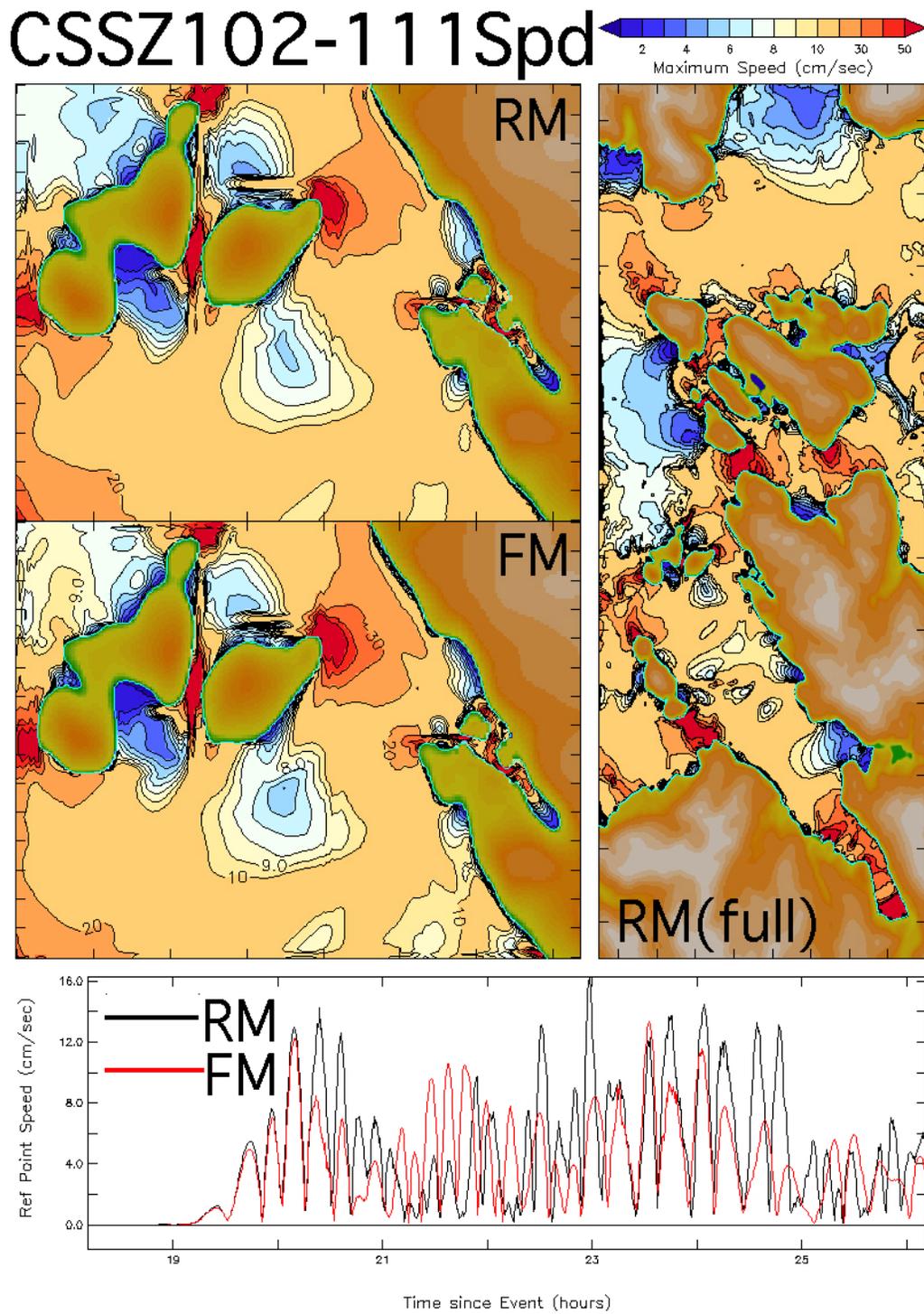
Figure 17 (continued): Comparison of reference (RM) and forecast (FM) model results for the synthetic CSSZ 102–111 mega-tsunami scenario. (b) Distribution of maximum speed.
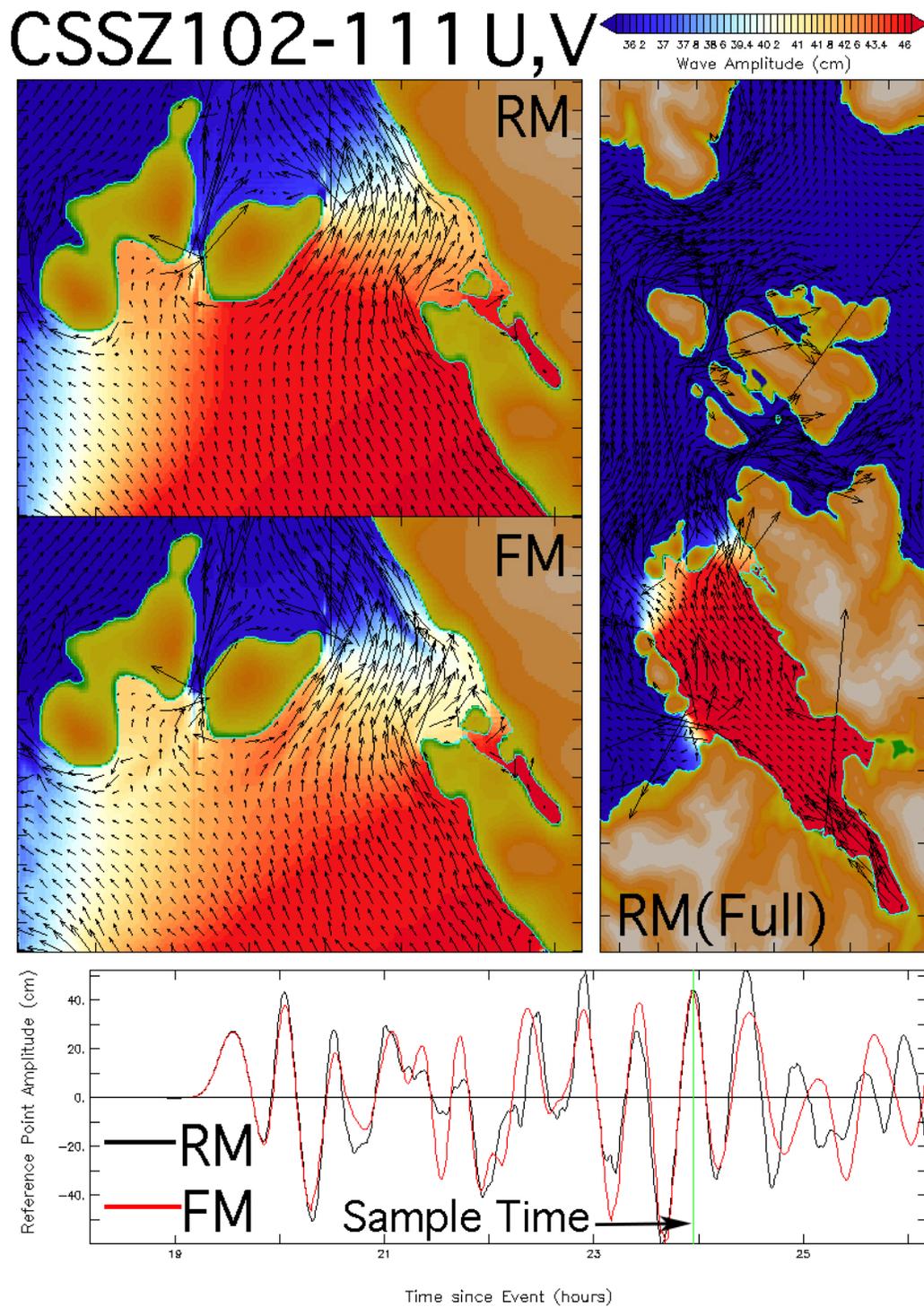
Figure 17 (continued): Comparison of reference (RM) and forecast (FM) model results for the synthetic CSSZ 102–111 mega-tsunami scenario. (c) A snapshot of the current field at the time indicated by the green line in the lower panel.
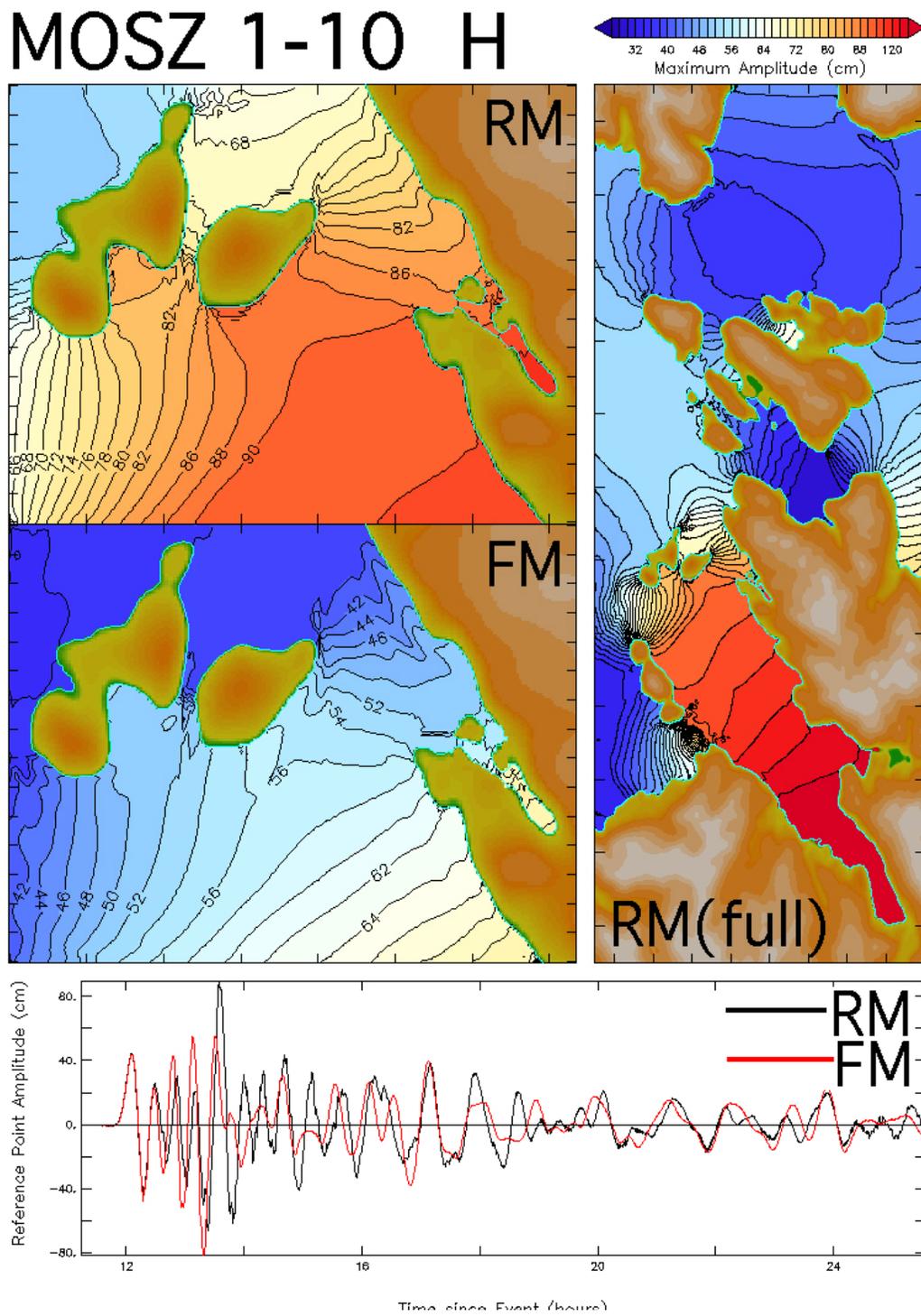
Figure 18: Comparison of reference (RM) and forecast (FM) model results, as in Figure 15 but for the MOSZ 1–10 mega-tsunami scenario, which is representative of the Manus Oceanic Convergent plate boundary in the southwest Pacific. (a) Distribution of maximum amplitude during the 18 hr simulation. *The comparison is continued on the following pages.*
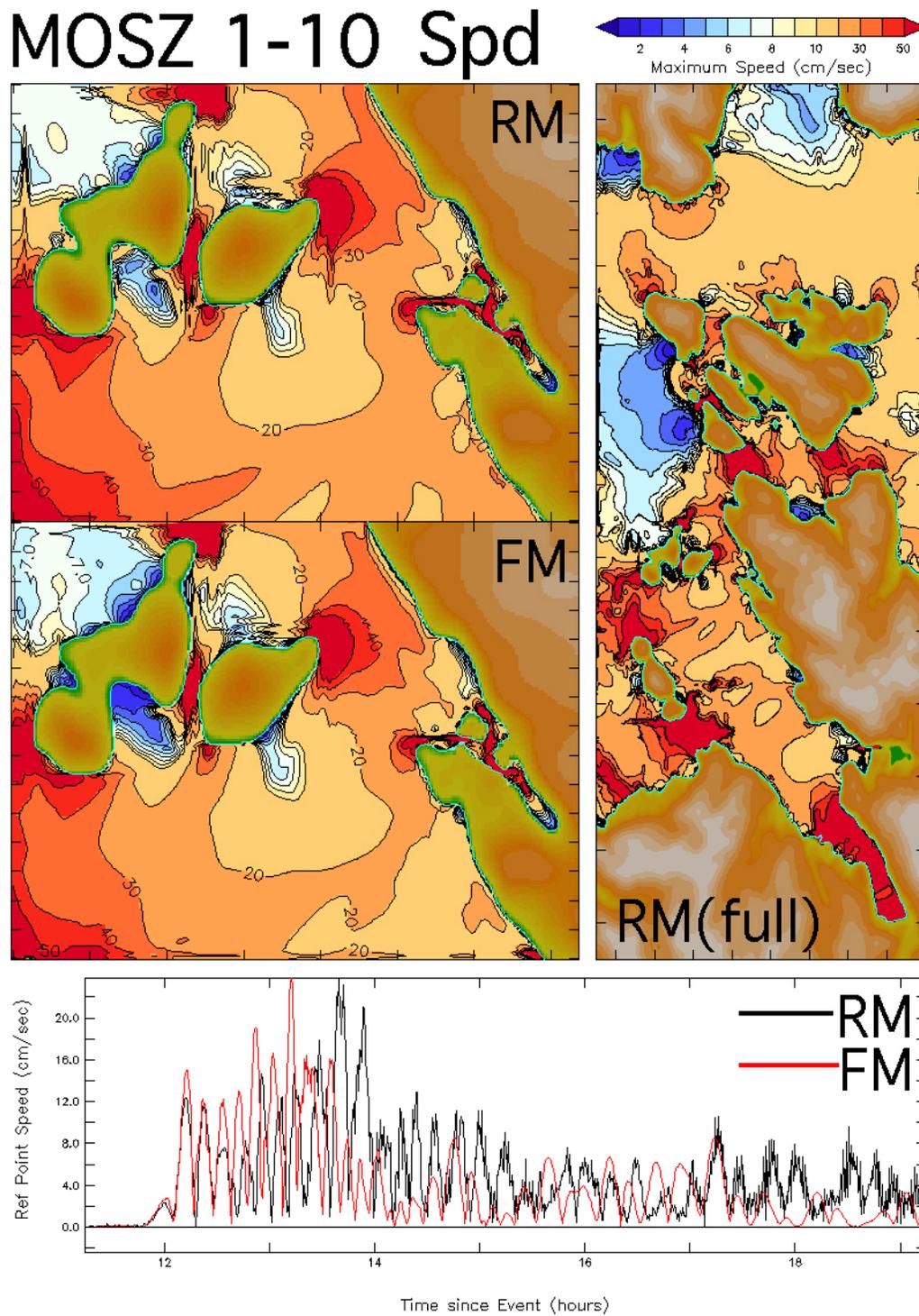
Figure 18 (continued): Comparison of reference (RM) and forecast (FM) model results for the synthetic MOSZ 1–10 mega-tsunami scenario. (b) Distribution of maximum speed.
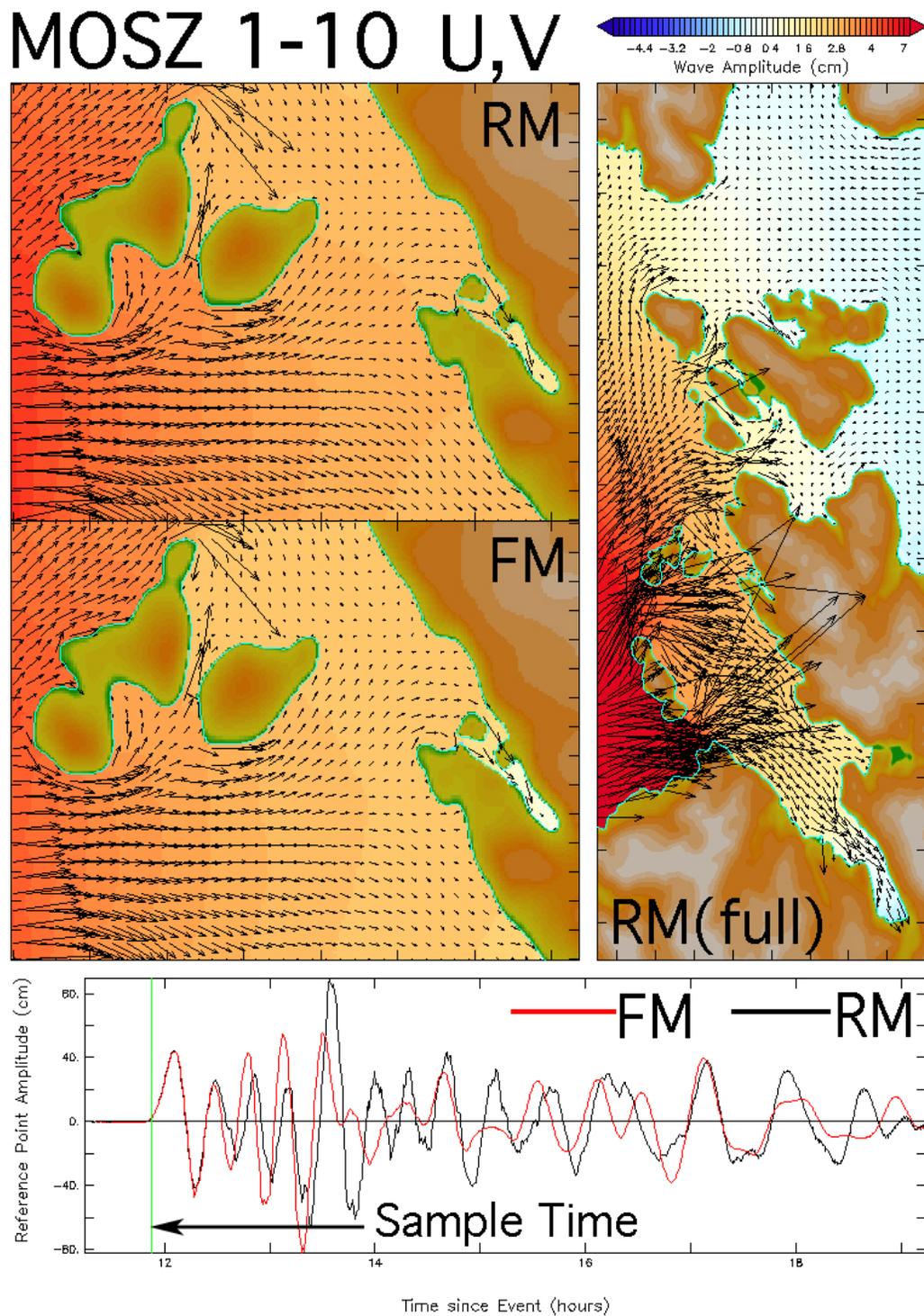
Figure 18 (continued): Comparison of reference (RM) and forecast (FM) model results for the synthetic MOSZ 1–10 mega-tsunami scenario. (c) A snapshot of the current field at the time indicated by the green line in the lower panel.
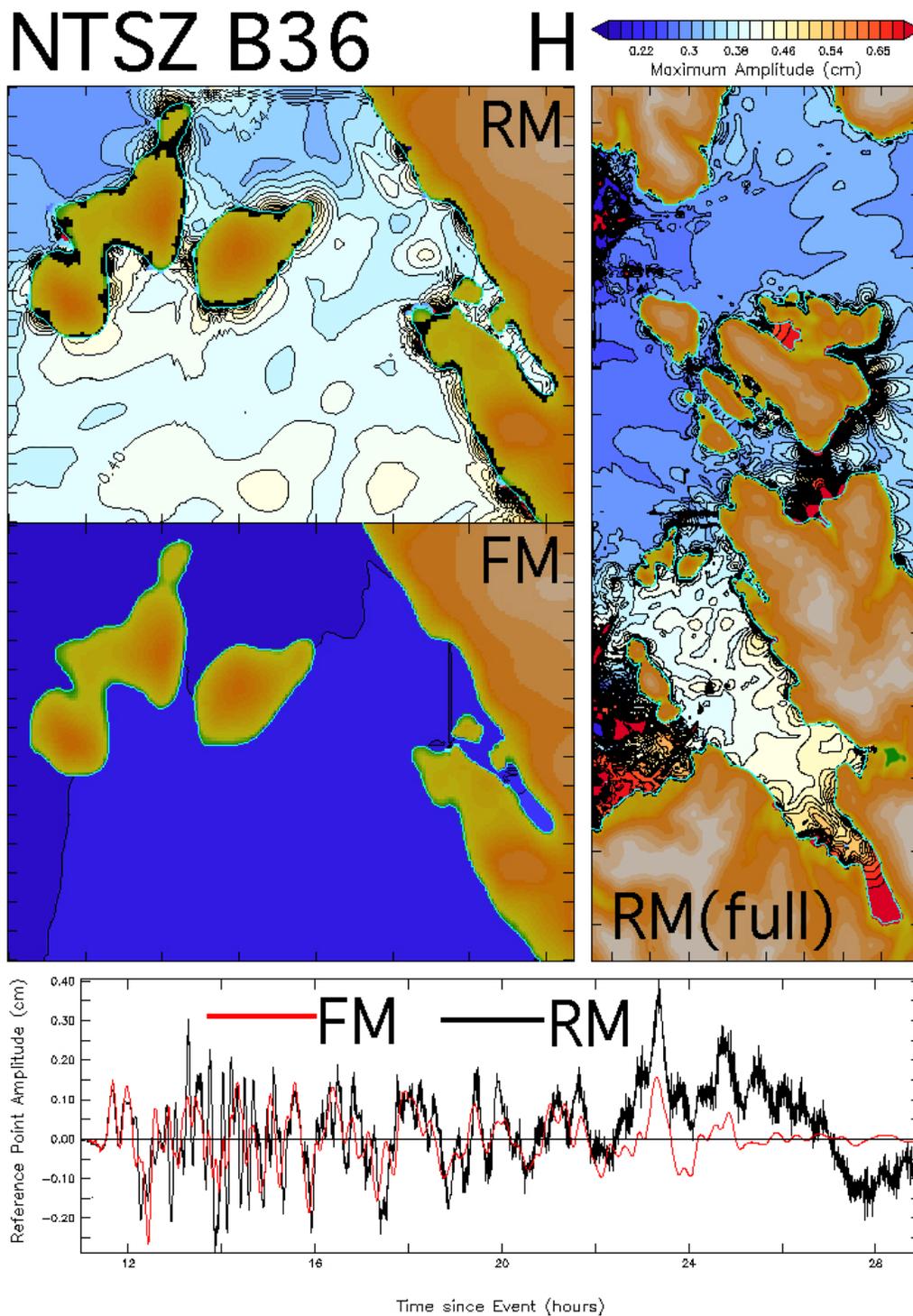
Figure 19: Comparison of reference (RM) and forecast (FM) model solutions for a mild synthetic tsunami near Samoa (the single unit source NTSZ B36.) Though tracking well for 22 hr of the simulation, the time series at the tide gauge diverge later and degrade the comparison of the maximum amplitude field.
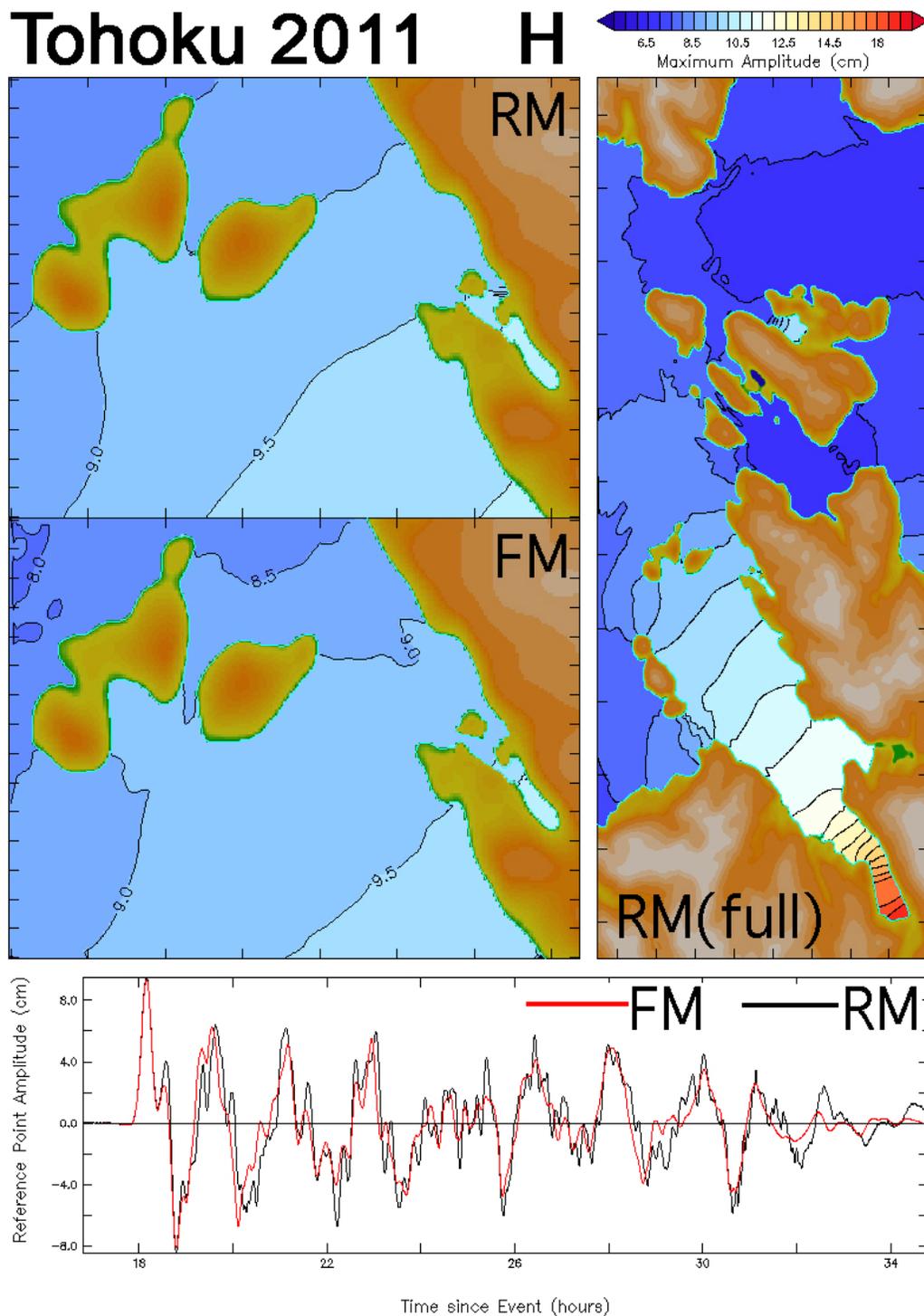
Figure 20: Comparison of reference (RM) and forecast (FM) model results, as in Figure 15 but for a hindcast of the 2011 Tohoku historic event. The model is forced by a combination of unit sources and slip values selected in real time during the event (see Table 6) using DART observations near the tsunami source. The reference (RM) and forecast (FM) model predictions are in good agreement; validation results, using data from the Elfin Cove tide gauge, are presented later. (a) Distribution of maximum amplitude during the 18 hr simulation. *The comparison is continued on the following pages.*
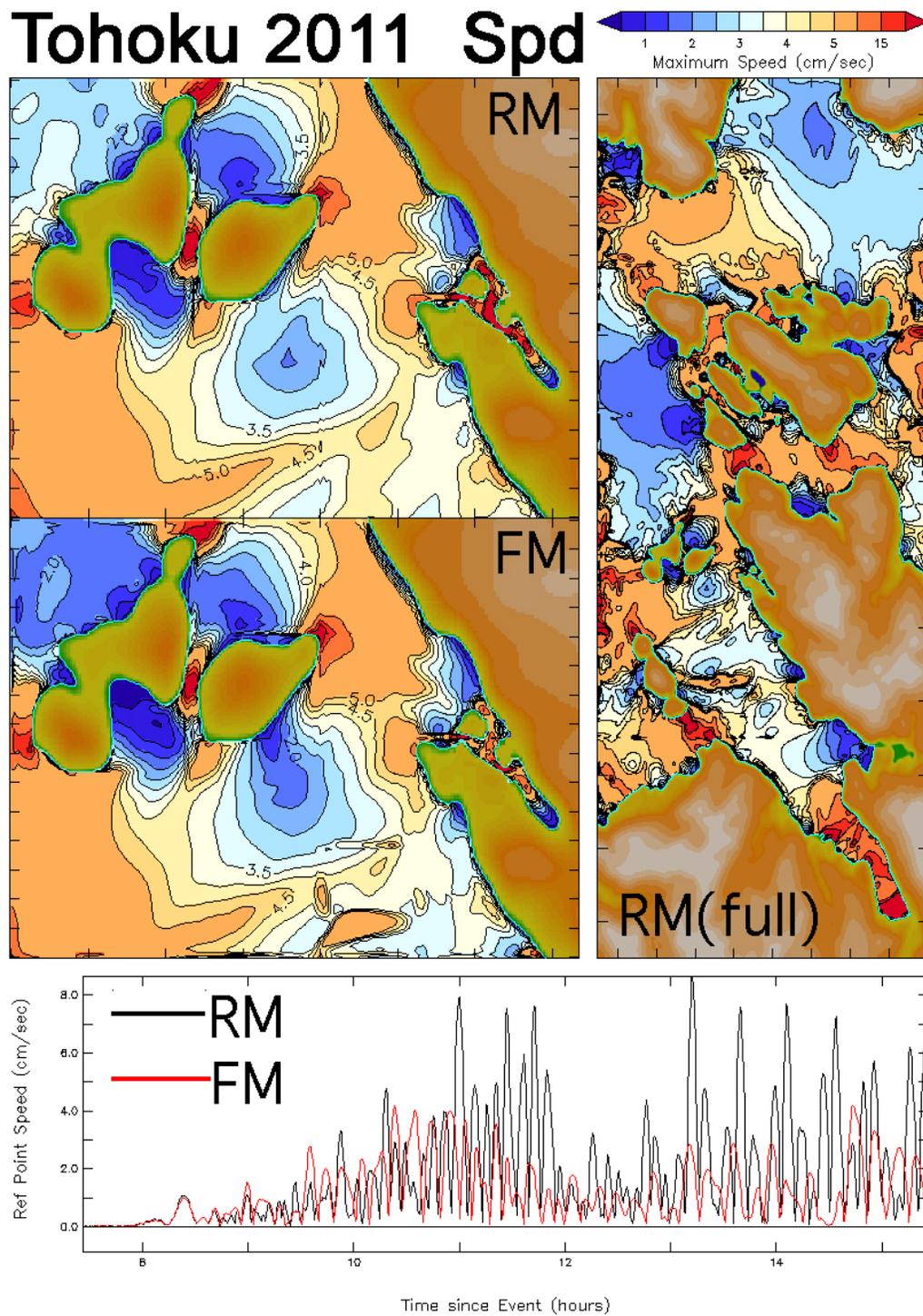
Figure 20 (continued): Comparison of reference (RM) and forecast (FM) model results for the 2011 Tohoku historic event. (b) Distribution of maximum speed.
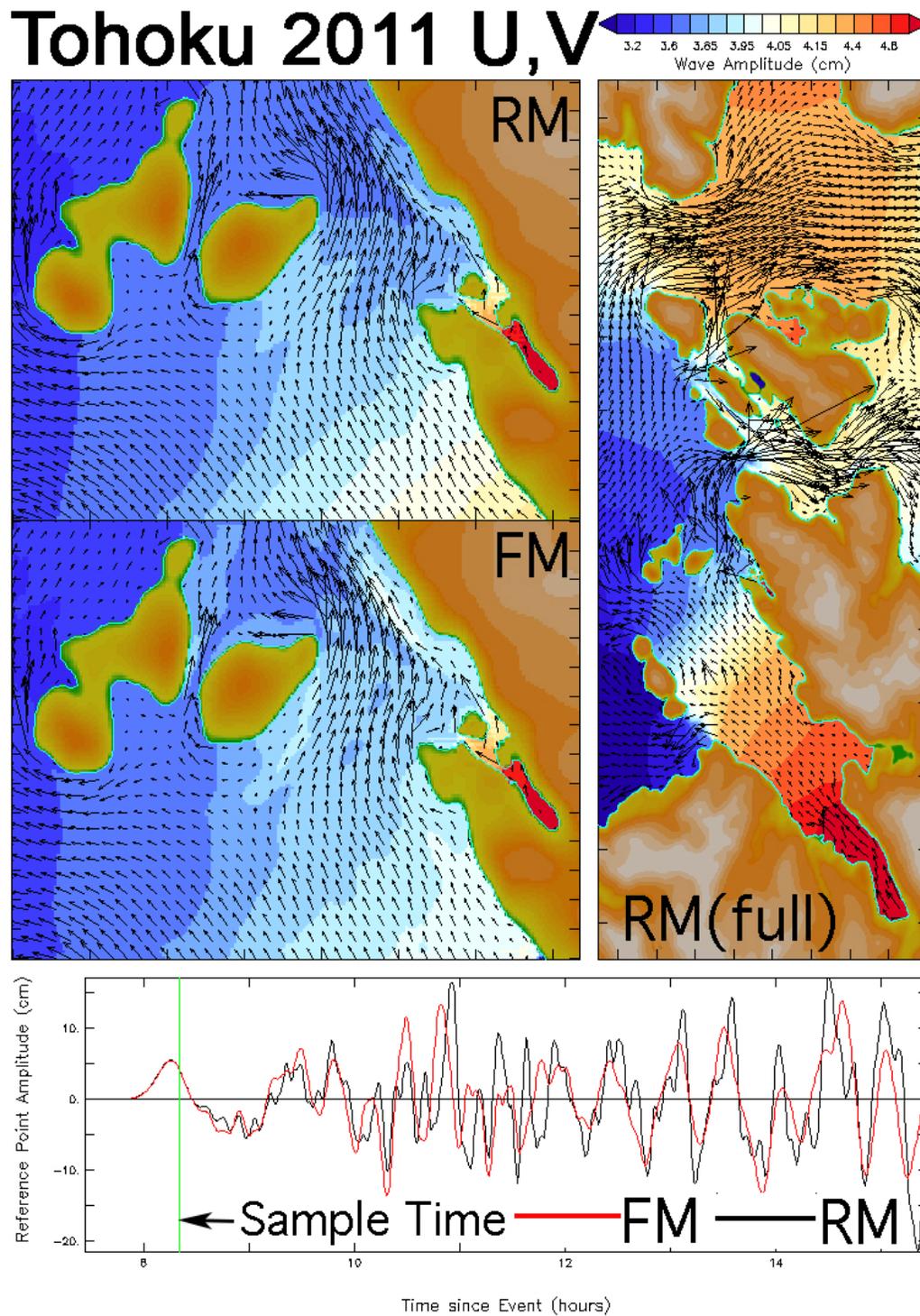
Figure 20 (continued): Comparison of reference (RM) and forecast (FM) model results for the 2011 Tohoku historic event. (c) A snapshot of the current field at the time indicated by the green line in the lower panel.
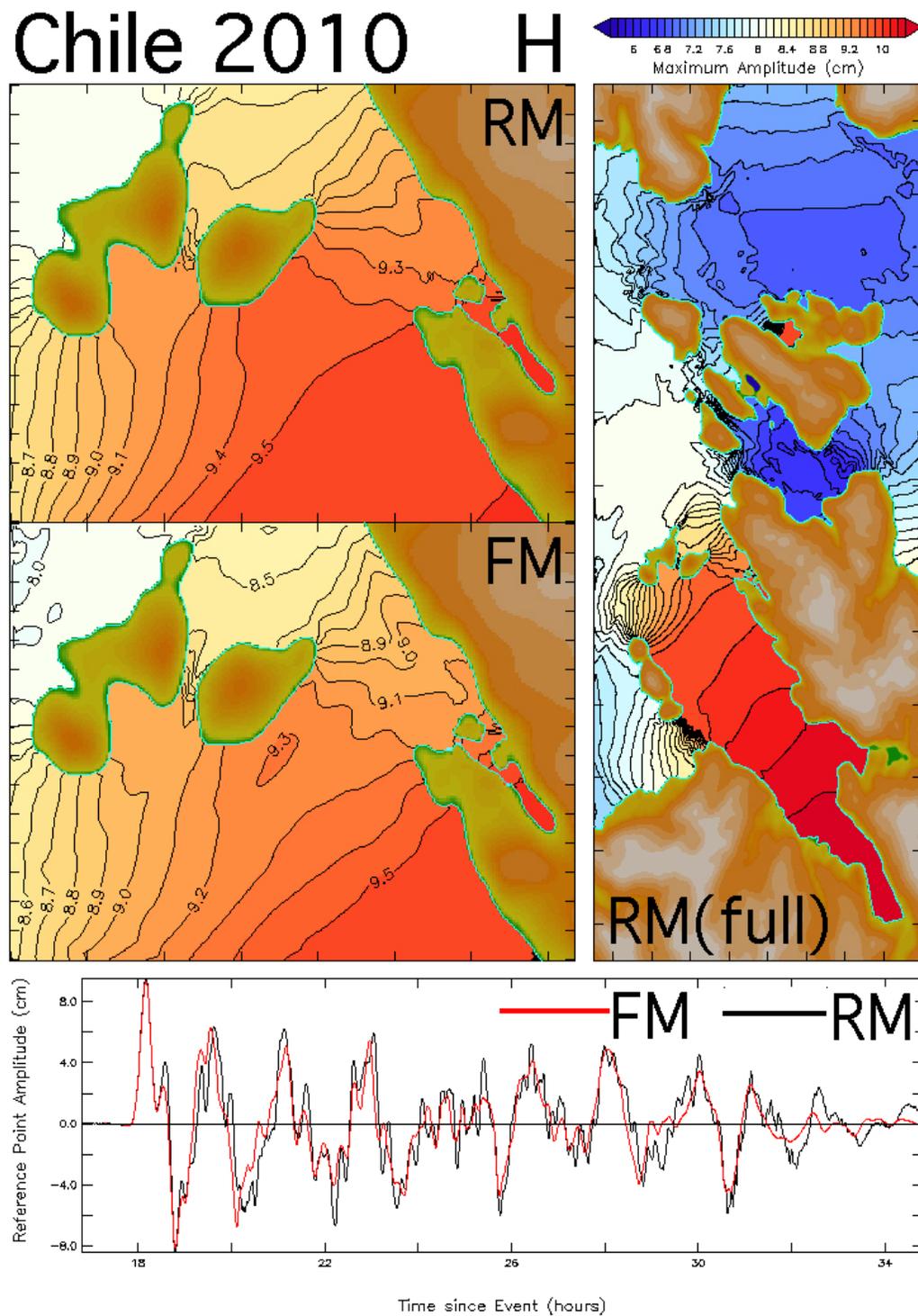
Figure 21: Comparison of reference (RM) and forecast (FM) model results, as in Figure 20 but for a hindcast of the 2010 Chile historic event. The model forcing is based on DART data collected during the event, and validation results are presented later. (a) Distribution of maximum amplitude during the 18 hr simulation. *The comparison is continued on the following pages.*
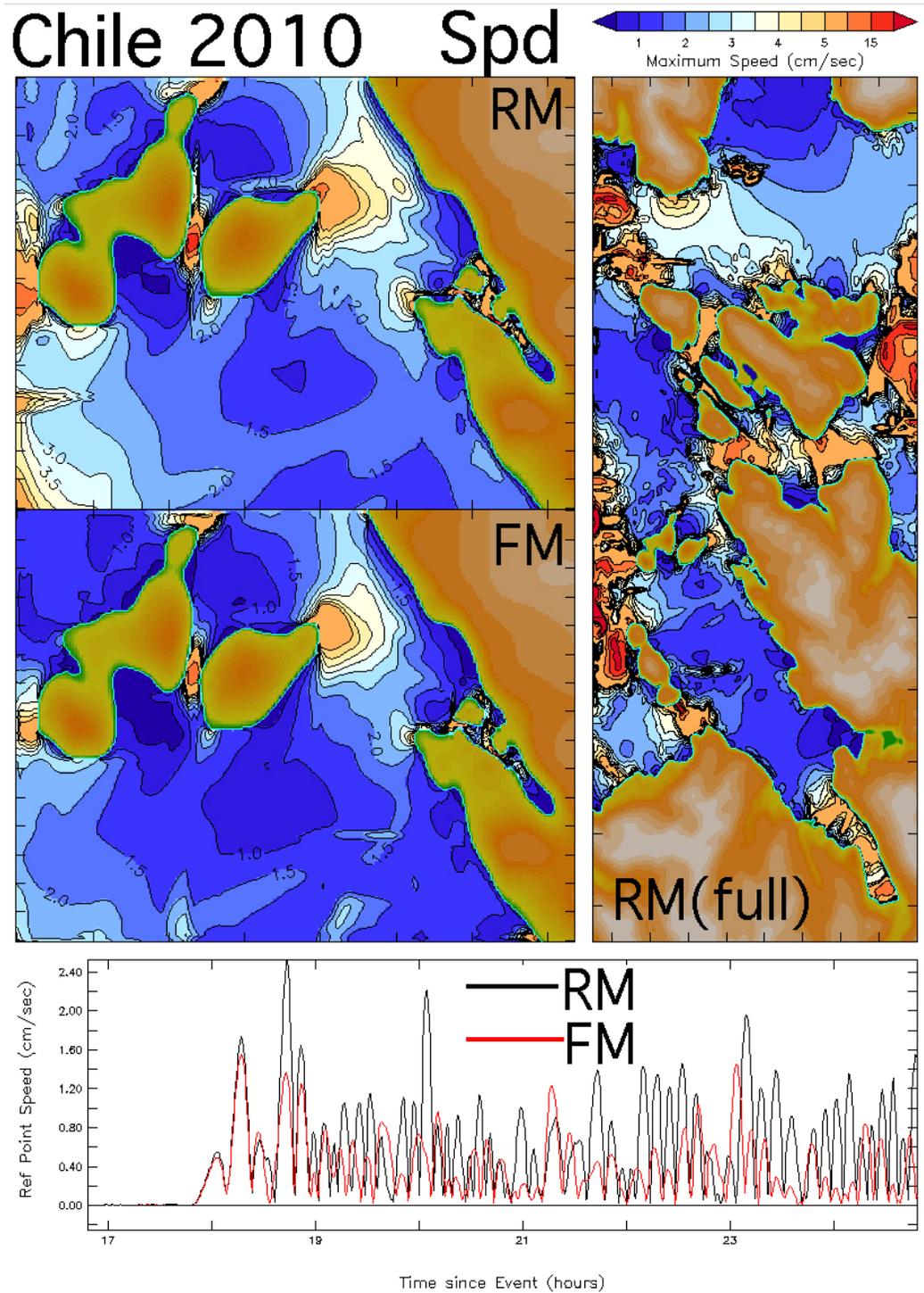
Figure 21 (continued): Comparison of reference (RM) and forecast (FM) model results for the 2010 Chile historic event. (b) Distribution of maximum speed.
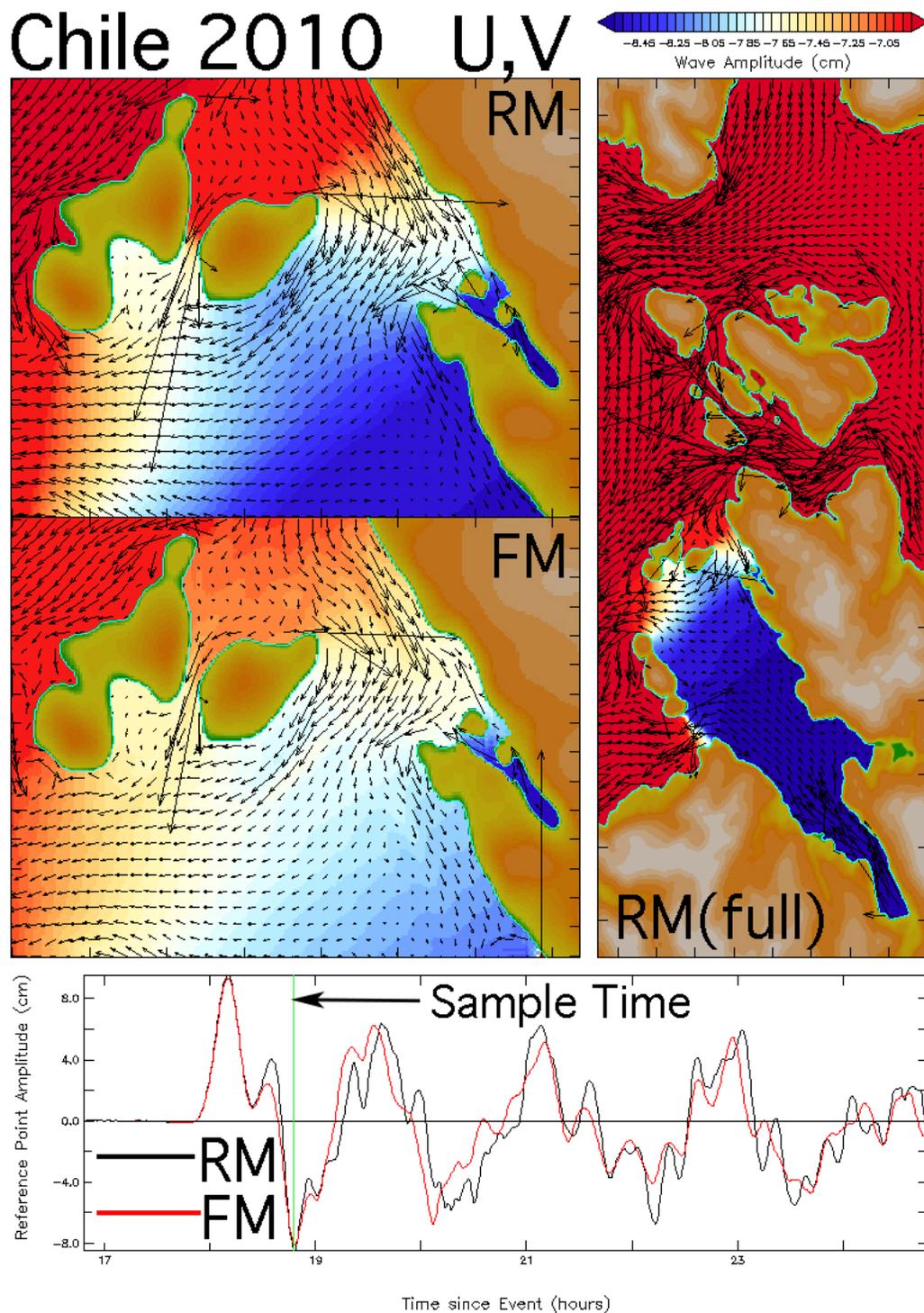
Figure 21 (continued): Comparison of reference (RM) and forecast (FM) model results for the 2010 Chile historic event. (c) A snapshot of the current field at the time indicated by the green line in the lower panel.
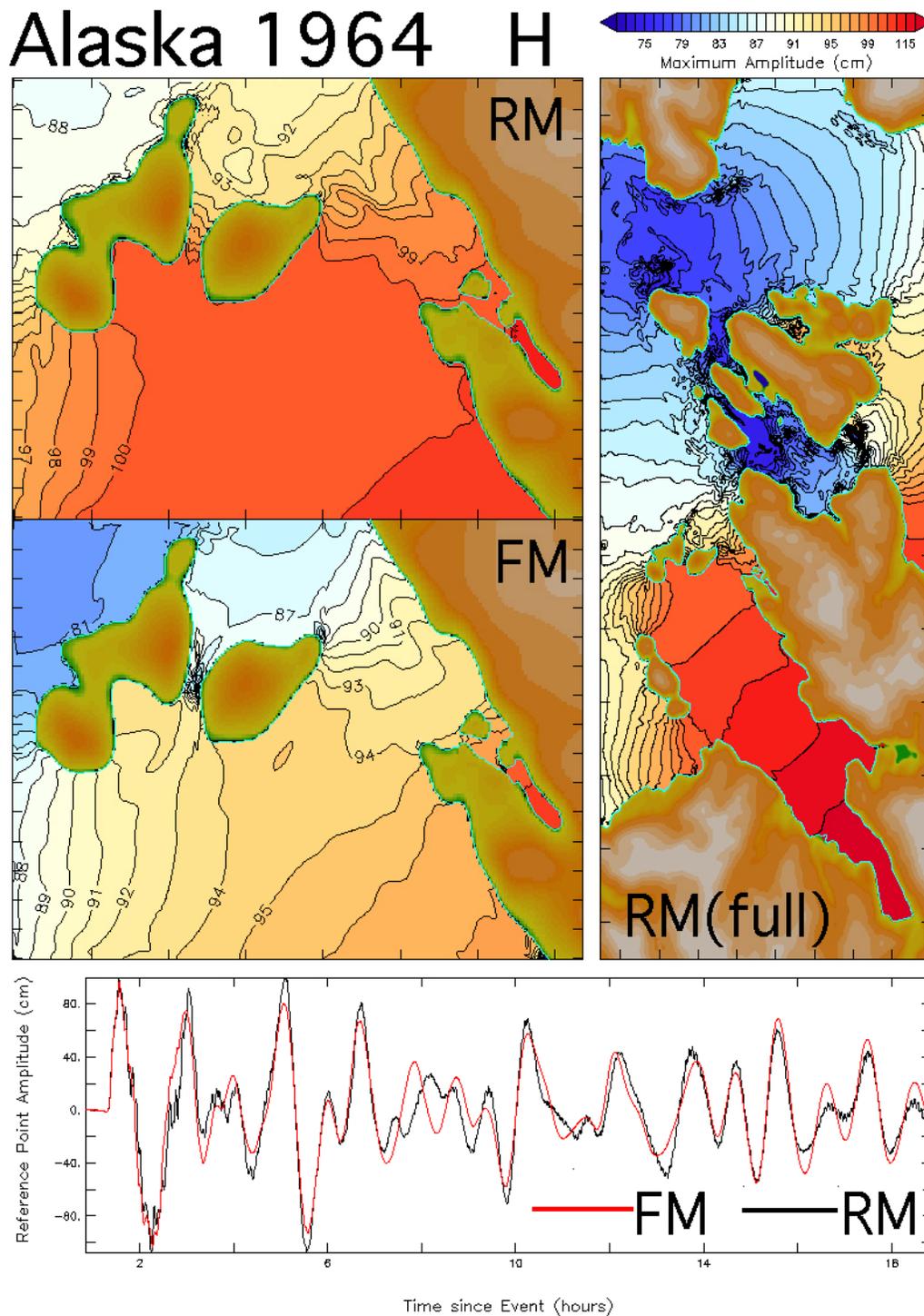
Figure 22: Comparison of reference (RM) and forecast (FM) model results, as in Figure 20 but for a hindcast of the 1964 Alaska historic event. The event predated deep ocean tsunami detection capability, so the representation of the source is based on post-event studies reported in the literature. (a) Distribution of maximum amplitude during the 18 hr simulation. *The comparison is continued on the following pages.*
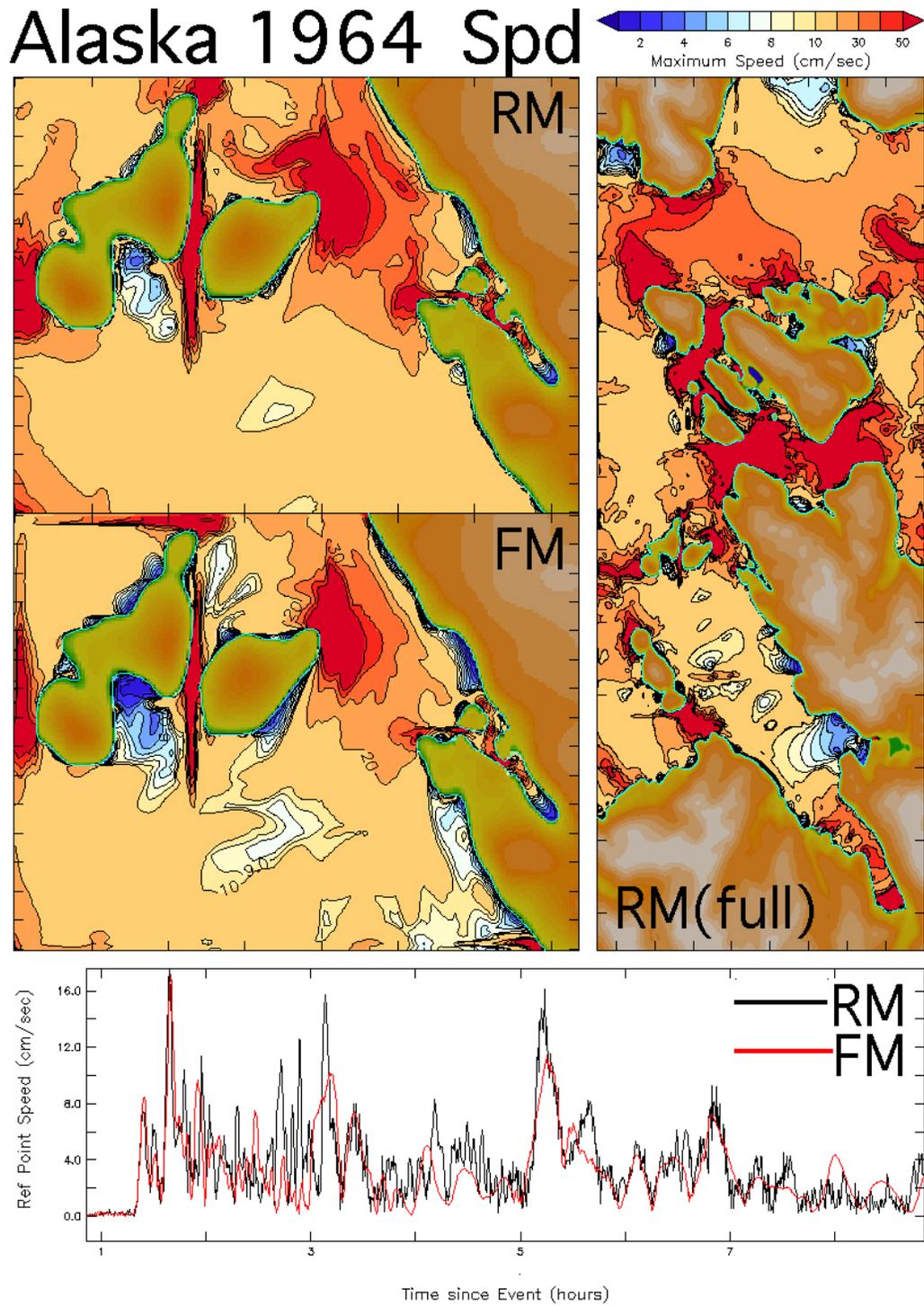
Figure 22 (continued): Comparison of reference (RM) and forecast (FM) model results for the 1964 Alaska historic event. (b) Distribution of maximum speed.
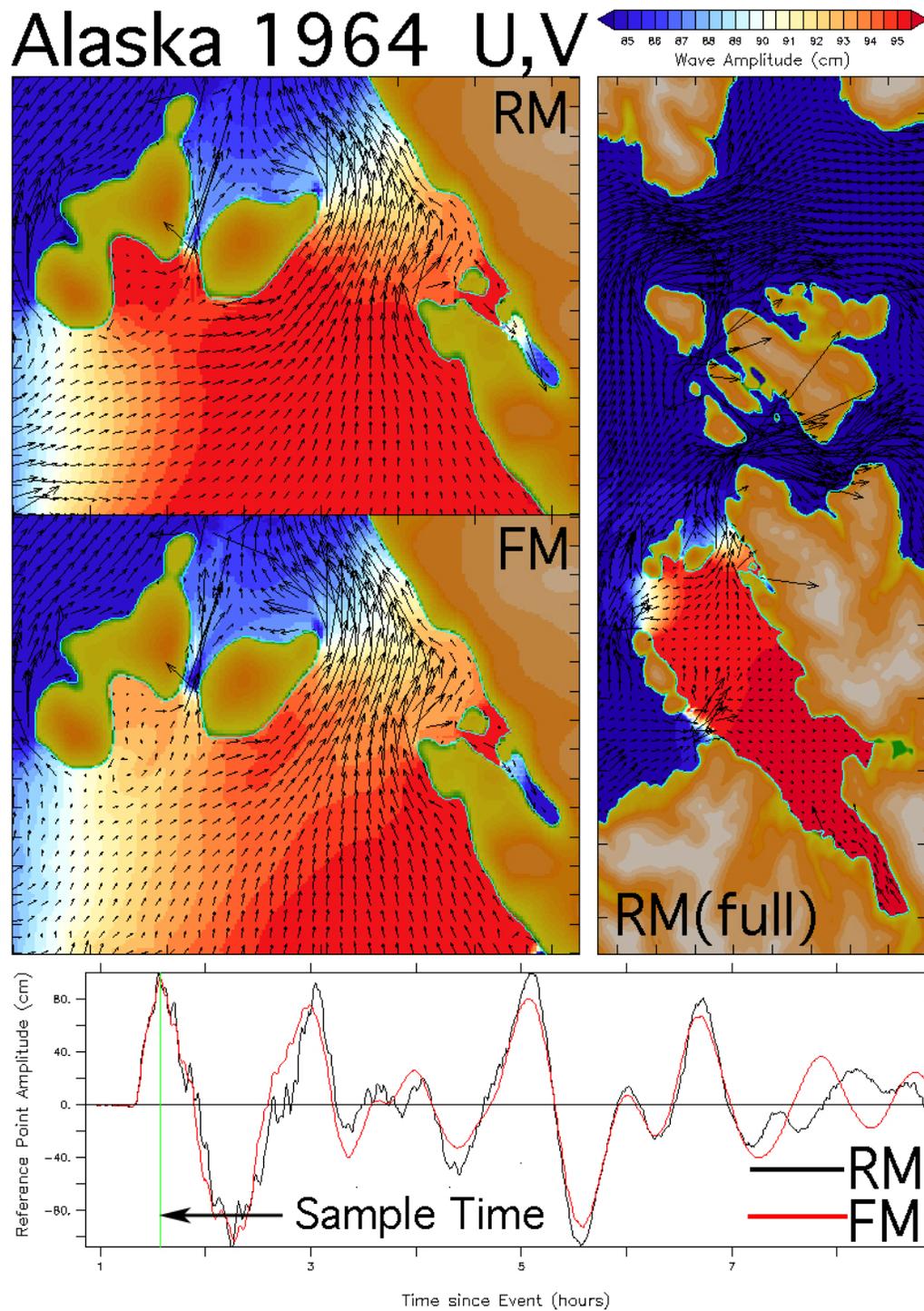
Figure 22 (continued): Comparison of reference (RM) and forecast (FM) model results for the 1964 Alaska historic event. (c) A snapshot of the current field at the time indicated by the green line in the lower panel.
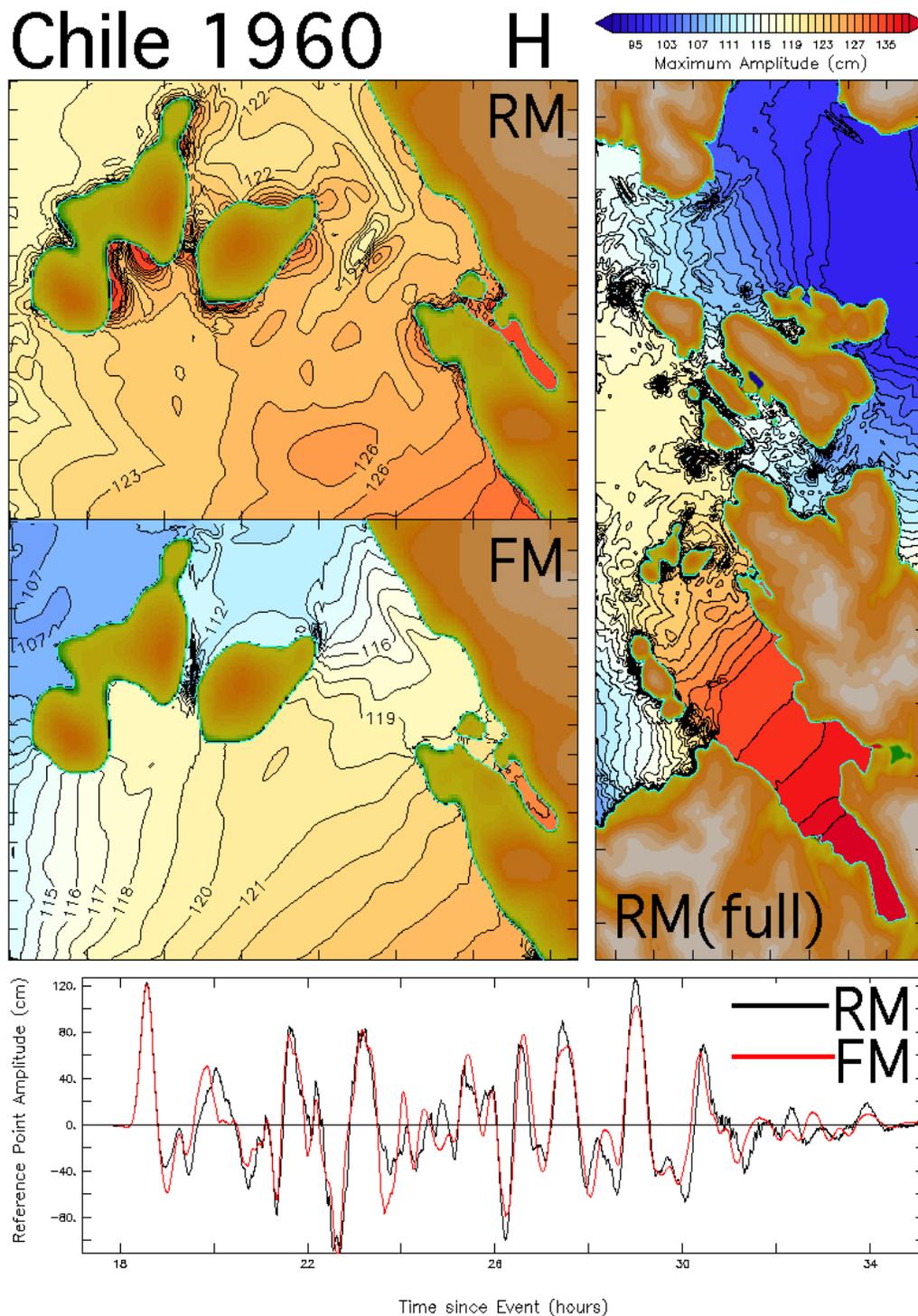
Figure 23: Comparison of reference (RM) and forecast (FM) model results, as in Figure 20 but for a hindcast of the 1960 Chile historic event. The event predated deep ocean tsunami detection capability, so the representation of the source is based on post-event studies reported in the literature. (a) Distribution of maximum amplitude during the 18 hr simulation. *The comparison is continued on the following pages.*
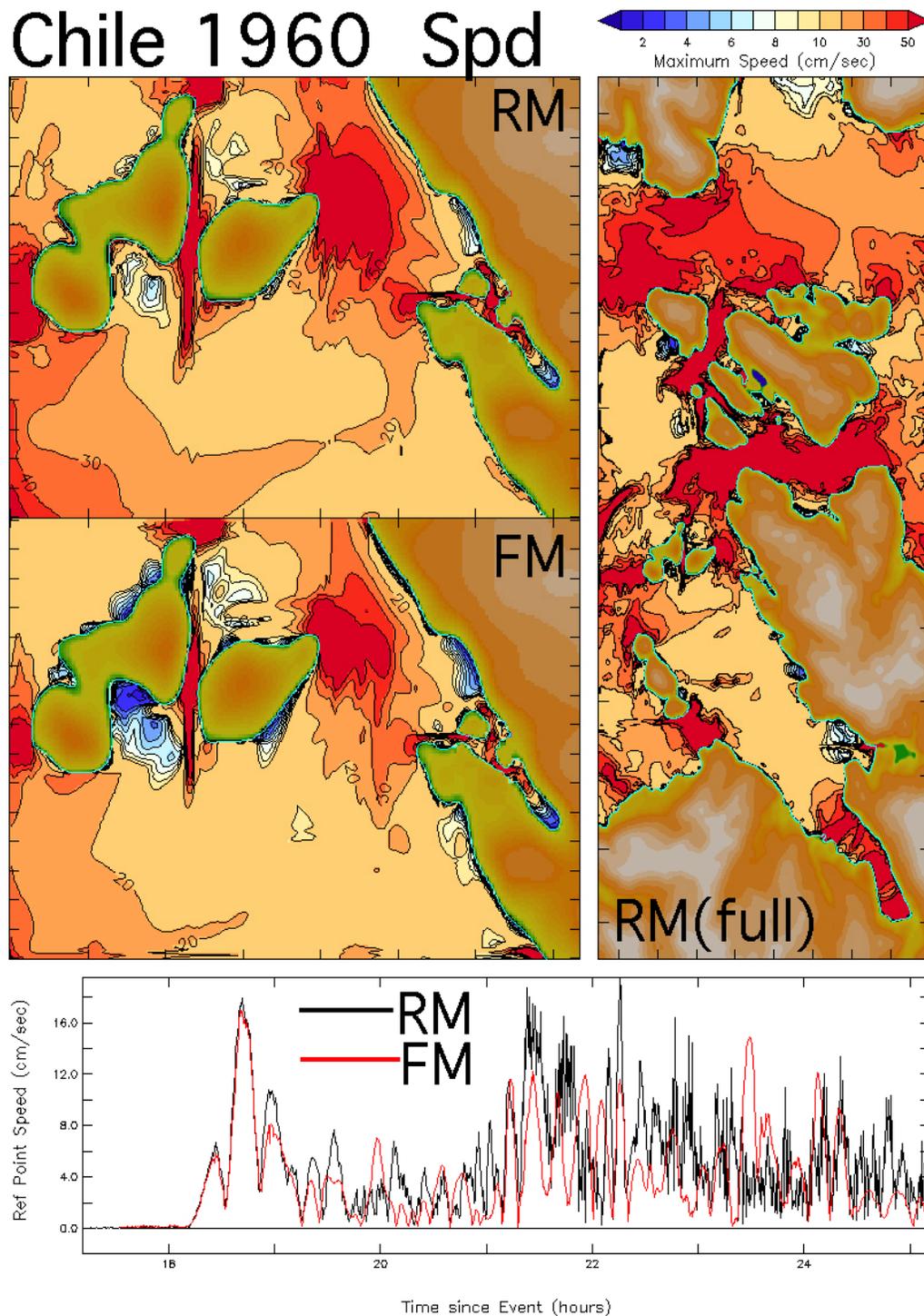
Figure 23 (continued): Comparison of reference (RM) and forecast (FM) model results for the 1960 Chile historic event. (b) Distribution of maximum speed.
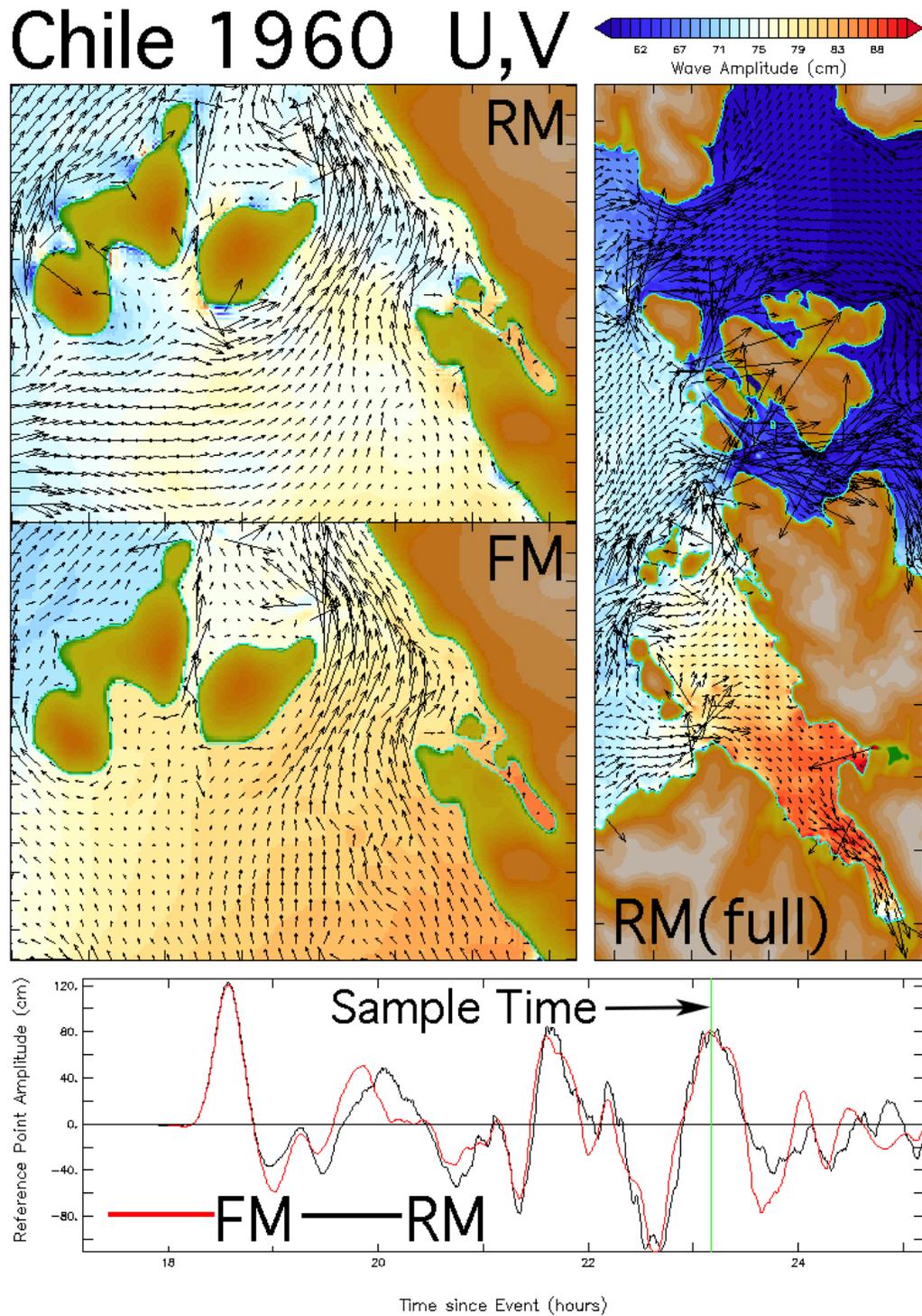
Figure 23 (continued): Comparison of reference (RM) and forecast (FM) model results for the 1960 Chile historic event. (c) A snapshot of the current field at the time indicated by the green line in the lower panel.
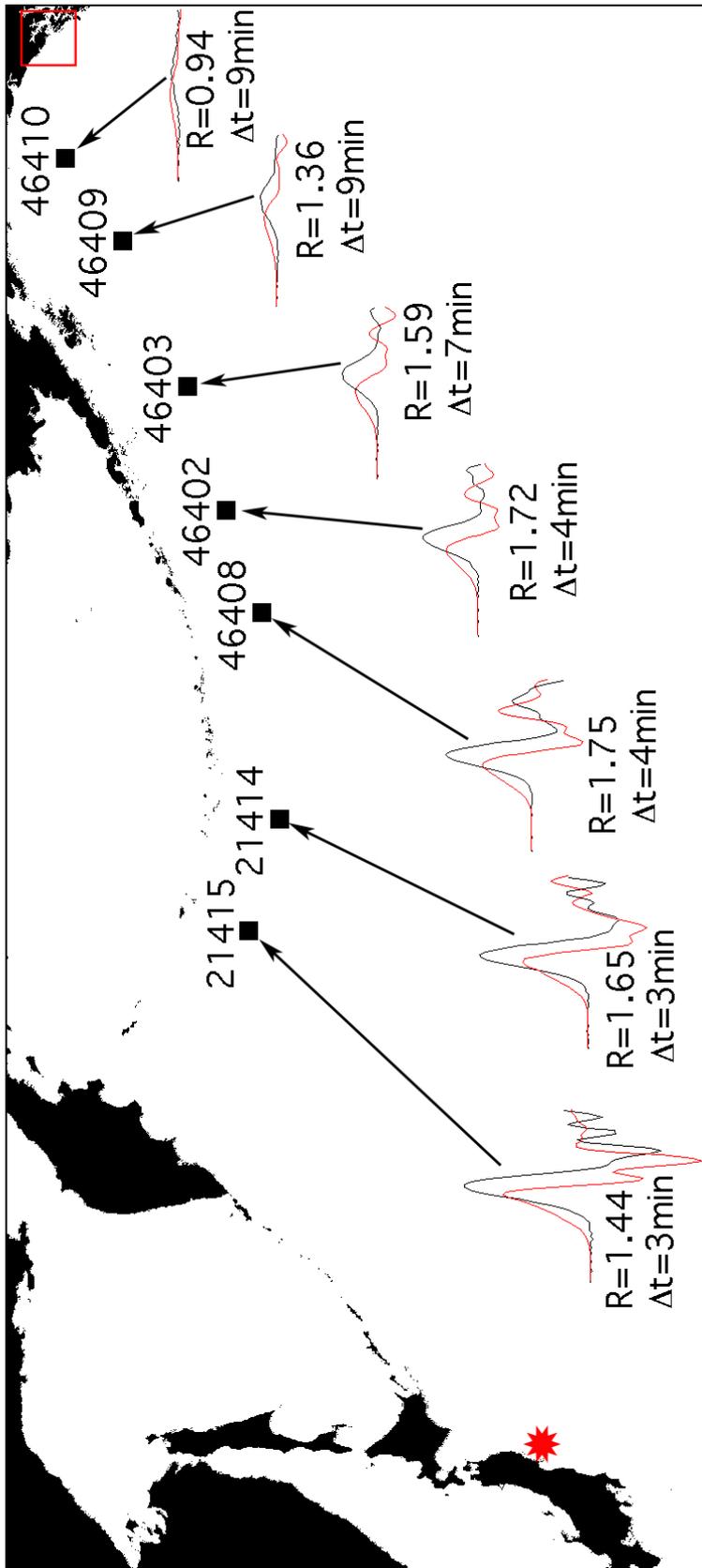
Figure 24: Propagation of the 2011 Tohoku tsunami across the North Pacific from its epicenter (red star) to the Gulf of Alaska. DART observations and model results from MOST use a common vertical and horizontal scale at all locations. The ratio of observed to model amplitude is denoted by R; Δt is the time lead of the model.
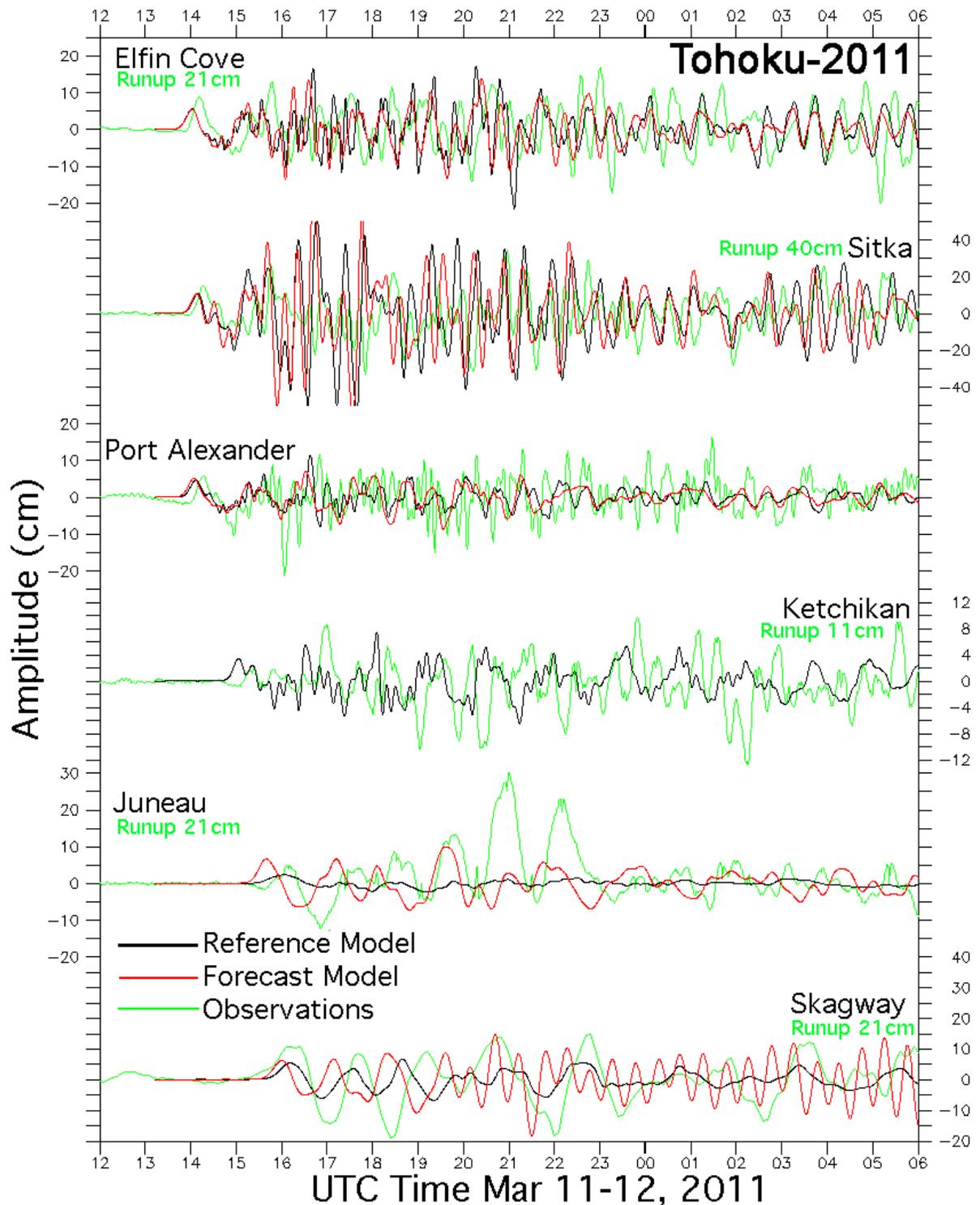
Figure 25: Model validation based on detided and low-passed observations (green) of the 2011 Tohoku tsunami at Elfin Cove model grid locations. The reference and forecast model hindcasts are shown in black and red, respectively. Model time series lead the observations, as is common for tele-tsunami events. Agreement is best for Elfin Cove (in the model C grid), Sitka (in the B grid), and Ketchikan (in the reference model A grid). Port Alexander validation is unclear due to noise in the observations. Only an approximate match is found at Juneau and Skagway, whose grid representation has low resolution.
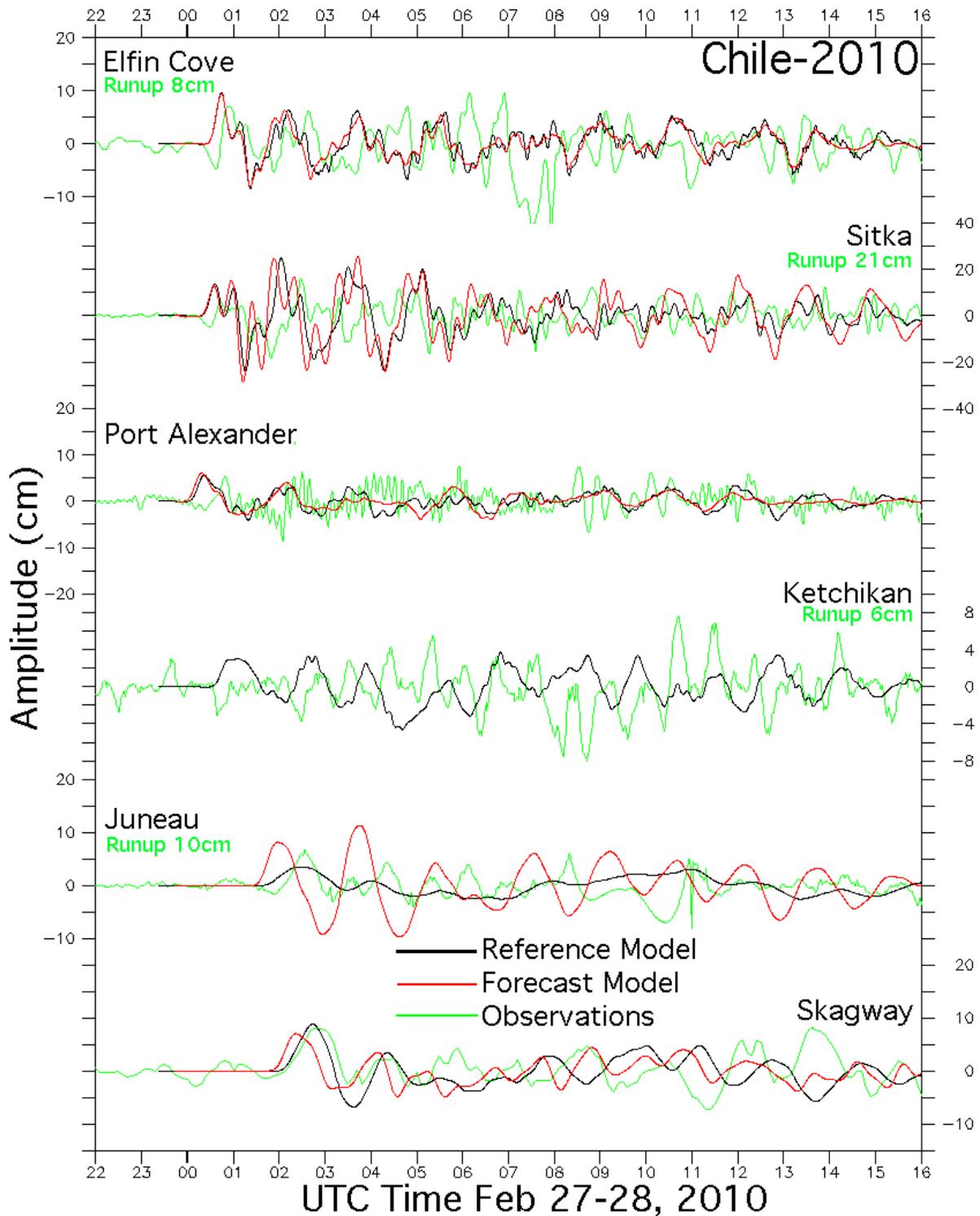
Figure 26: As in Figure 25 but for the 2010 Chile historic tsunami. The model results at the various sites are consistent for the upper three panels in overestimating the observed signal. For Juneau and Skagway, better resolution of the reference model A grid results in improved agreement with the data.
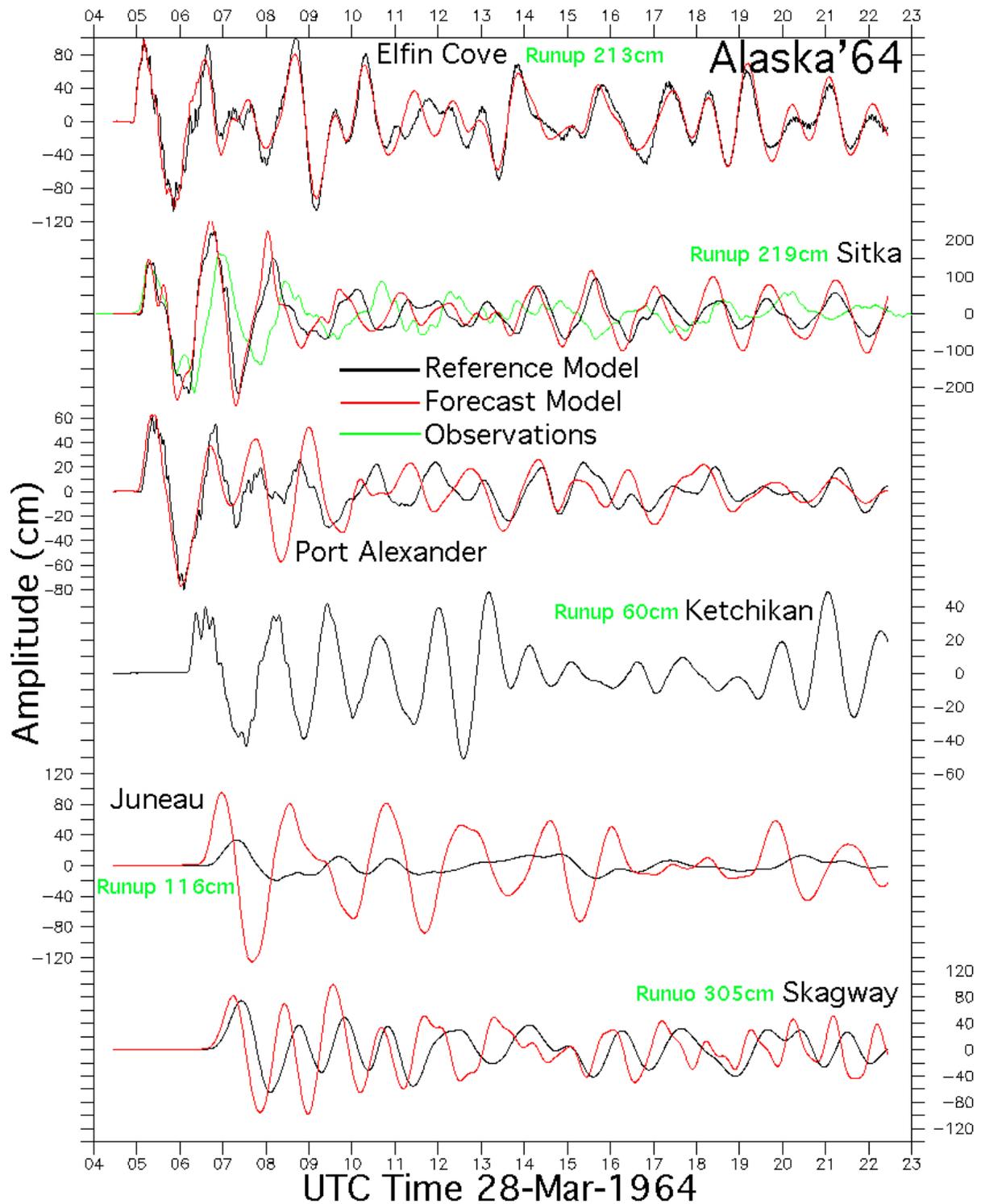
Figure 27: Model validation based on the 1964 Alaska historic tsunami. An observed time series is only available for Sitka, based on a digitized marigram in the WCATWC archives. At Elfin Cove, Port Alexander, and Skagway the agreement between the reference and forecast model hindcasts is good throughout the event. Juneau is less satisfactory, but, consistent with the 2011 Tohoku and 2010 Chile results, the forecast model values exceeds those from the reference model.
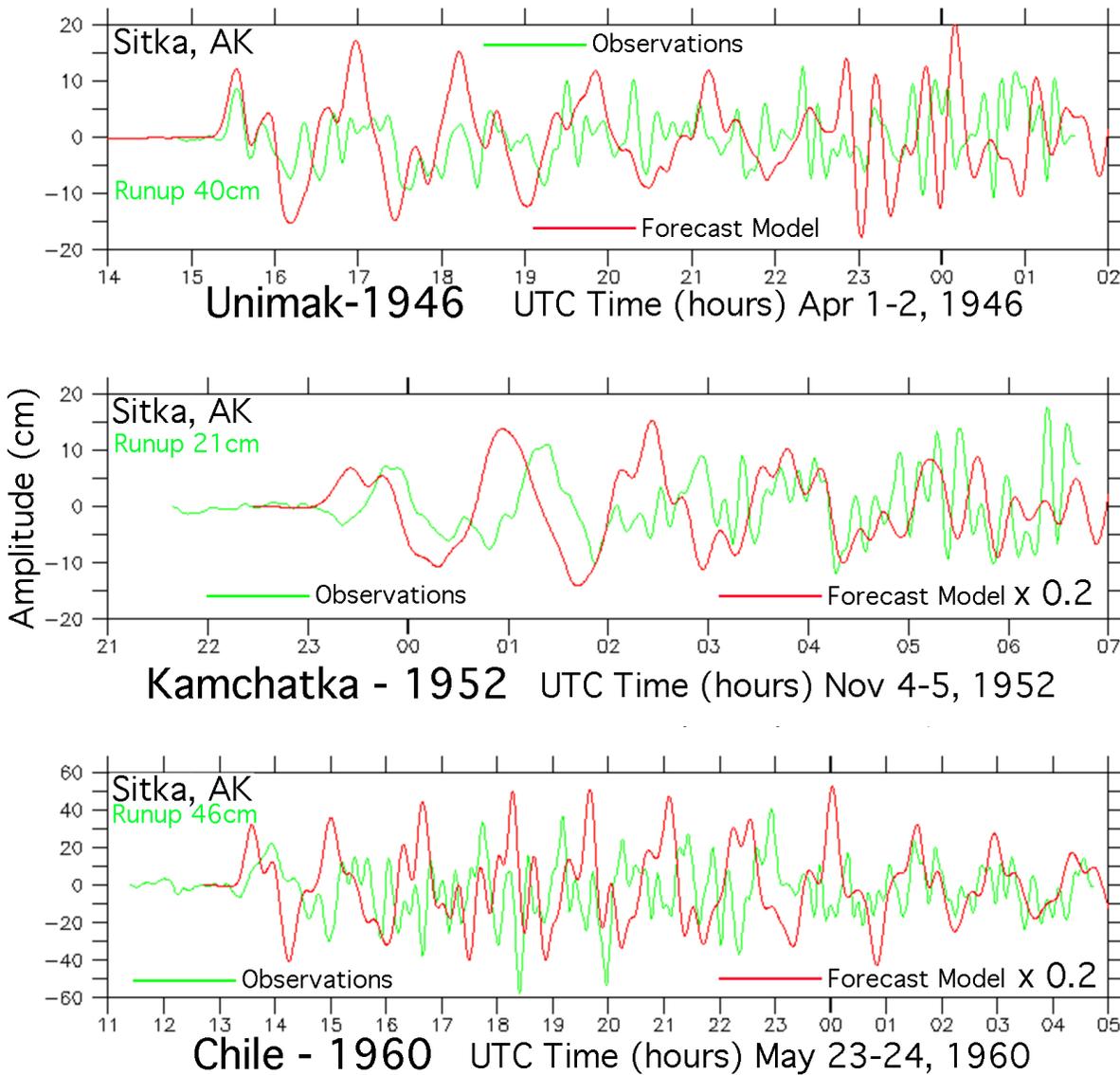
Figure 28: Attempted model validation based on digitized marigrams for Sitka associated with the 1946 Unimak, 1952 Kamchatka, and 1960 Chile tsunamis. The forecast model time series exceeded observation (probably due to an inadequate source representation) and were scaled down by a factor of one fifth to highlight the approximate match in arrival time.
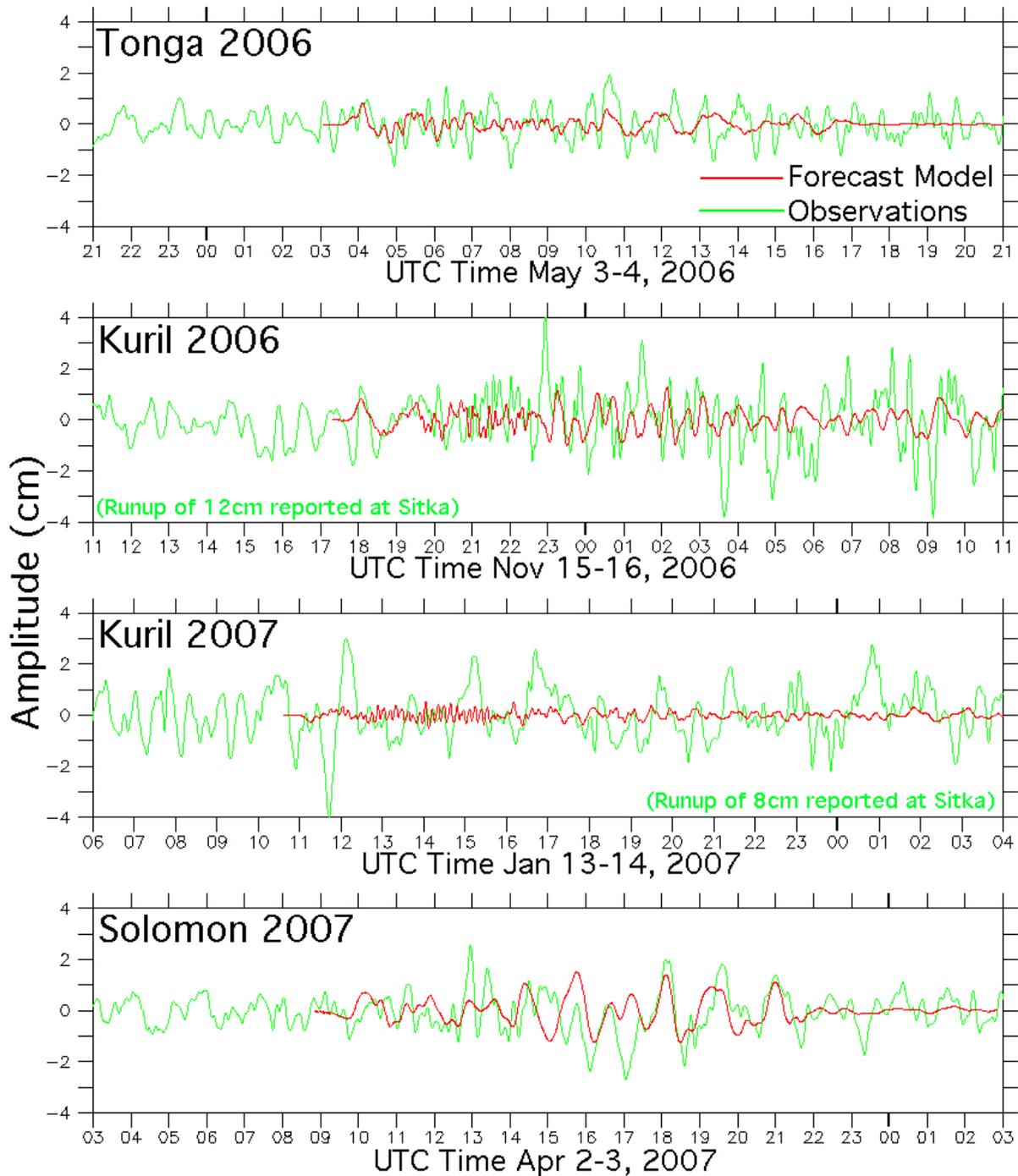
Figure 29: Comparison of forecast model hindcasts at the Elfin Cove tide gauge with observations for selection of historic events since 1 min data became available. Owing to the weak response of the Gulf of Alaska region and poor signal-to-noise ratios, none of these events were of use in model validation. (a) 2006 Tonga, 2006 Kuril, 2007 Kuril, and 2007 Solomon. *The comparisons are continued on the following page.*
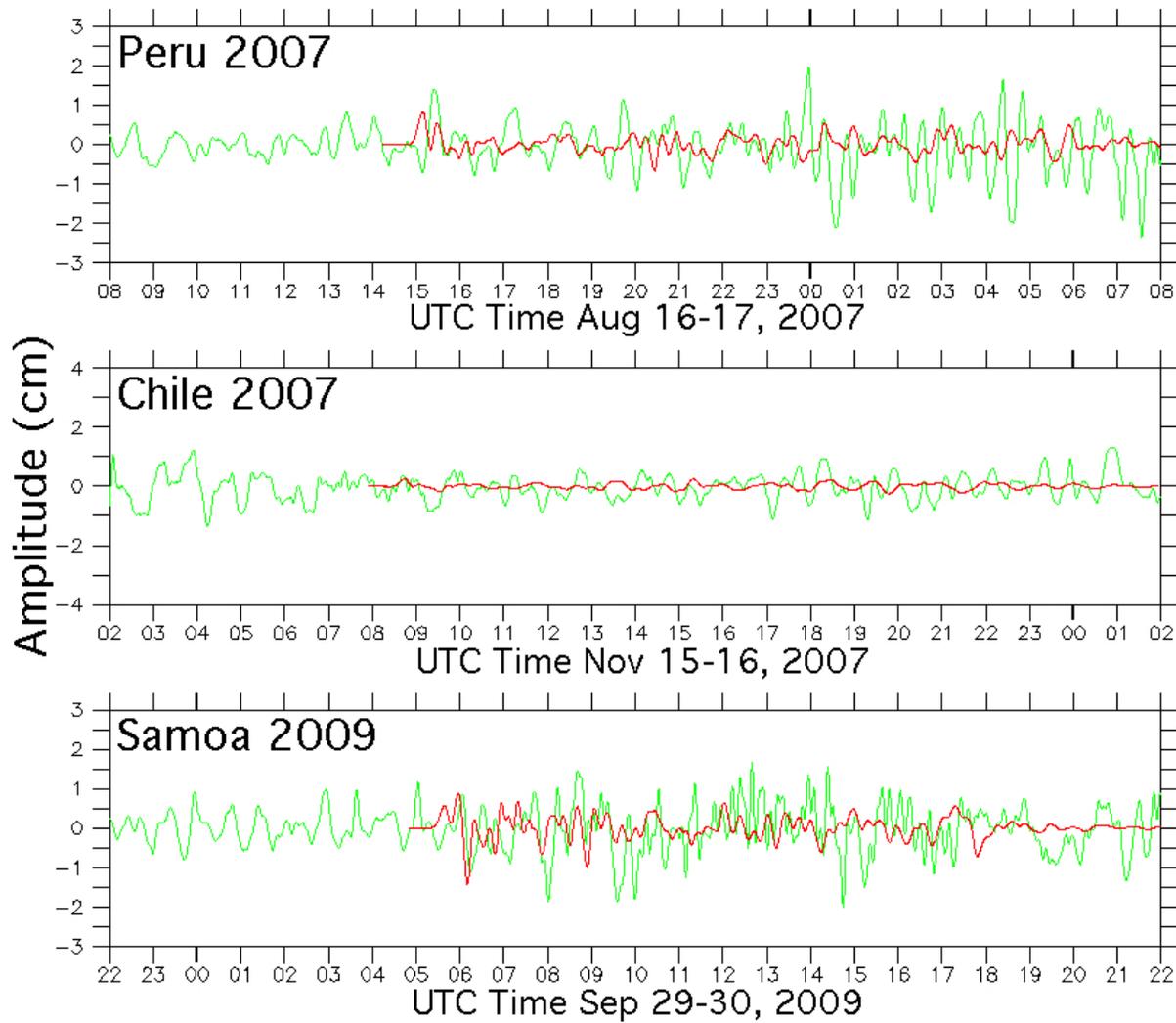
Figure 29, continued: Comparison of forecast model hindcasts at the Elfin Cove tide gauge with observations for selection of historic events since 1 min data became available. (b) hindcasts for 2007 Peru, 2007 Chile, and 2009 Samoa historical events.
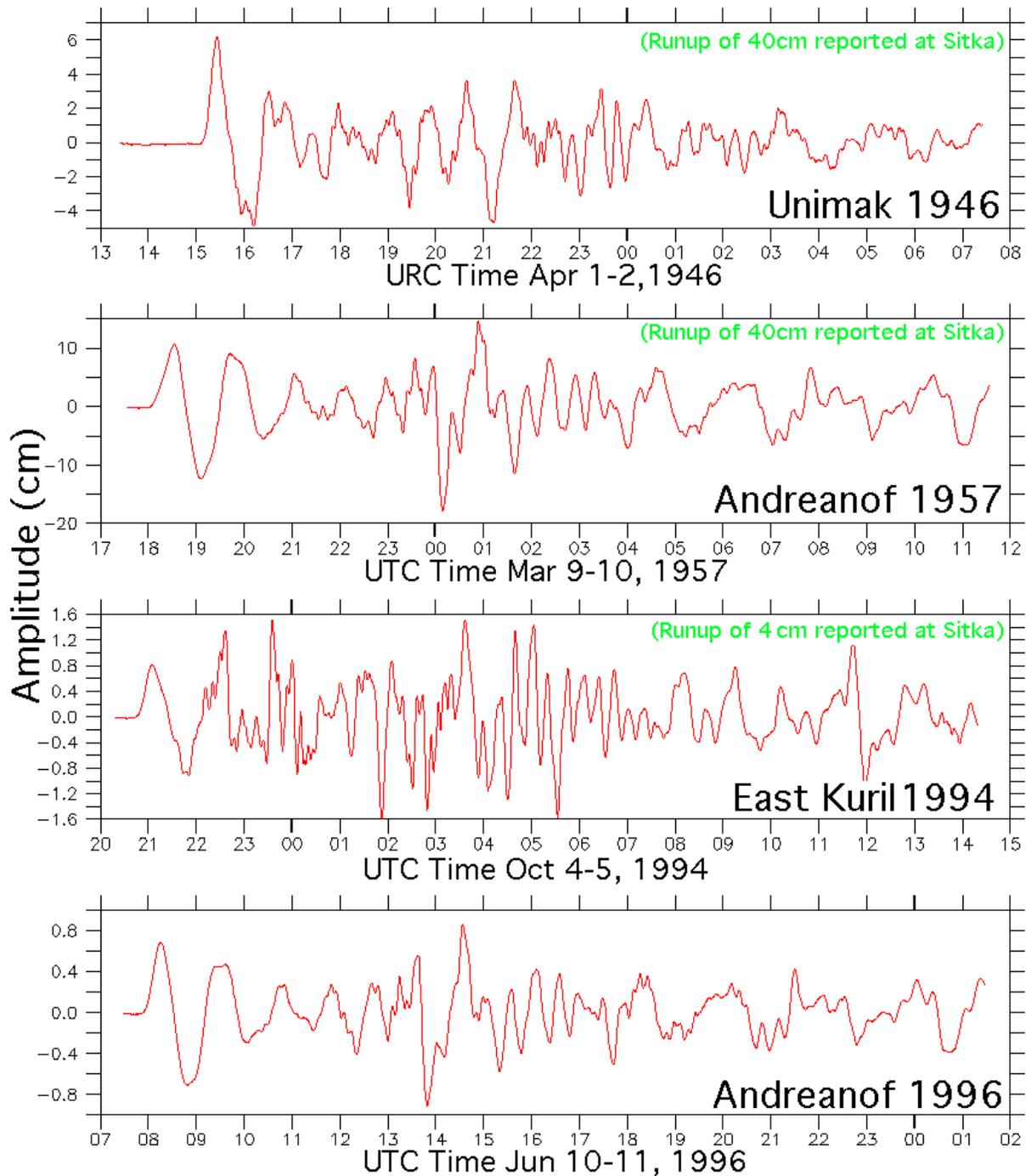
Figure 30: Forecast model hindcasts for Elfin Cove during various earlier tsunamis for which tide gauge records are unavailable. Some Sitka runup reports are given. (a) 1946 Unimak, 1957 Andreanof, 1994 East Kuril, and 1996 Andreanof. *The comparisons are continued on the following page.*
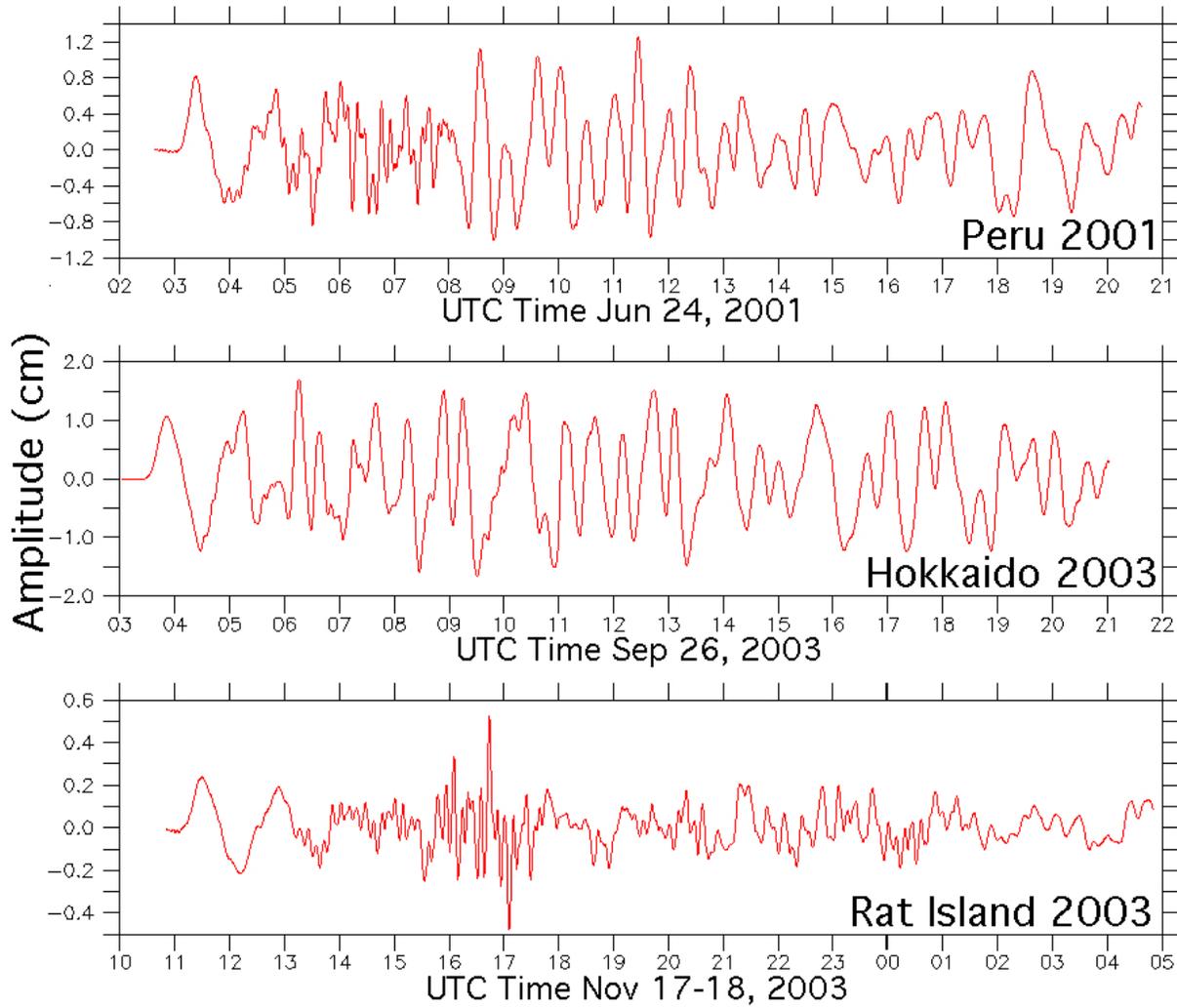
Figure 30, continued: Forecast model hindcasts for Elfin Cove during various earlier tsunamis for which tide gauge records are unavailable. (b) further hindcasts for 2001 Peru, 2003 Hokkaido, and 2003 Rat Island historical events.

Figure 31: Predicted maximum amplitude at the Elfin Cove tide gauge associated with the full suite of mega-tsunami scenarios listed in **Table 5**. Numerical values are shown, together with great circle distances to Elfin Cove and an indication of the likely main beam direction near the source.
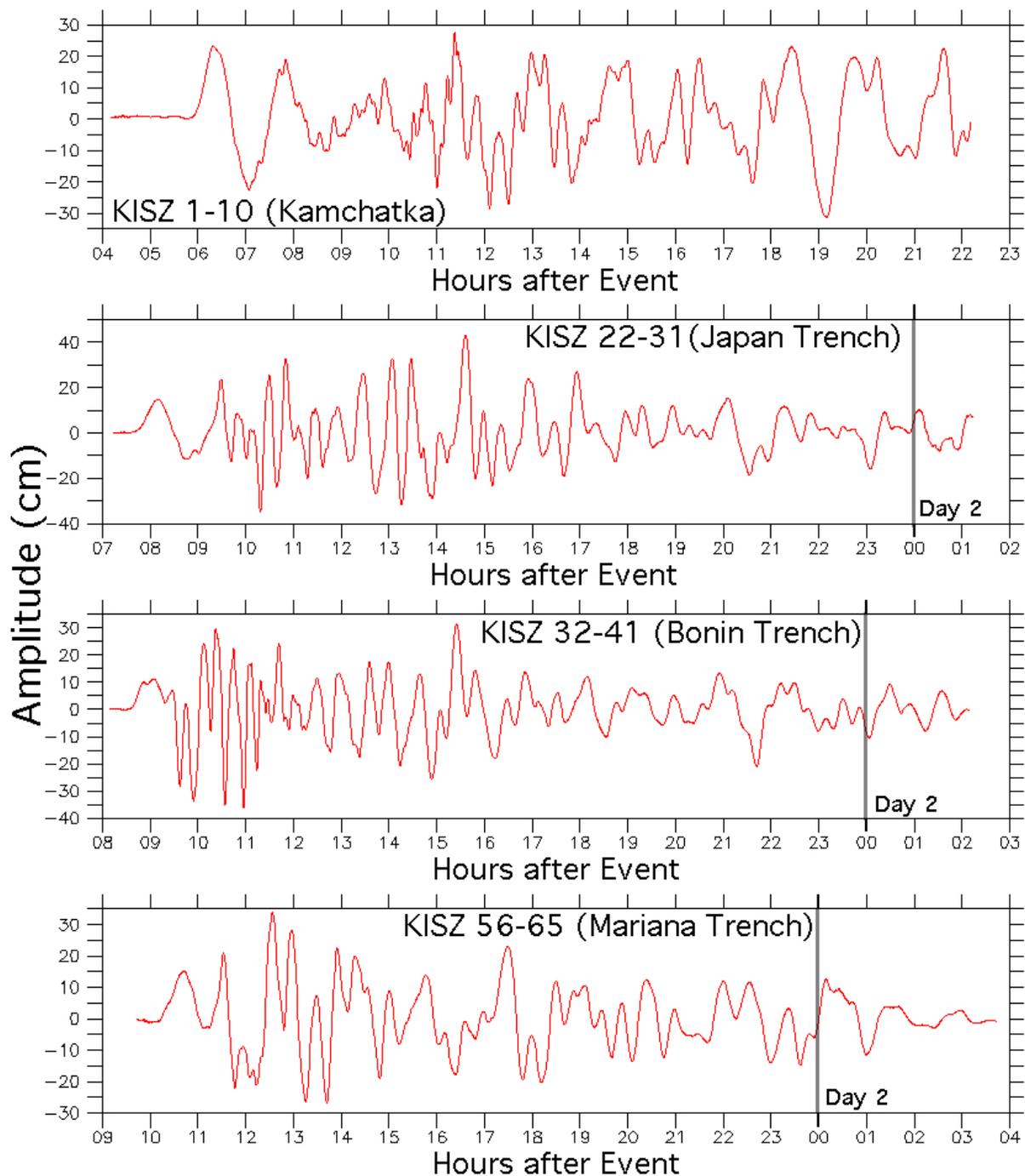
Figure 32: Complete time series of forecast model predictions at the Elfin Cove tide gauge site for each of the mega-tsunami scenarios. Time is in hours from the event, and, although each simulation is limited to 18 hr after the wave enters the model domain, some events extend into a second day after the event. (a) KISZ 1–10, KISZ 22–31, KISZ 32–41, and KISZ 56–65. *The comparisons are continued on the following pages.*
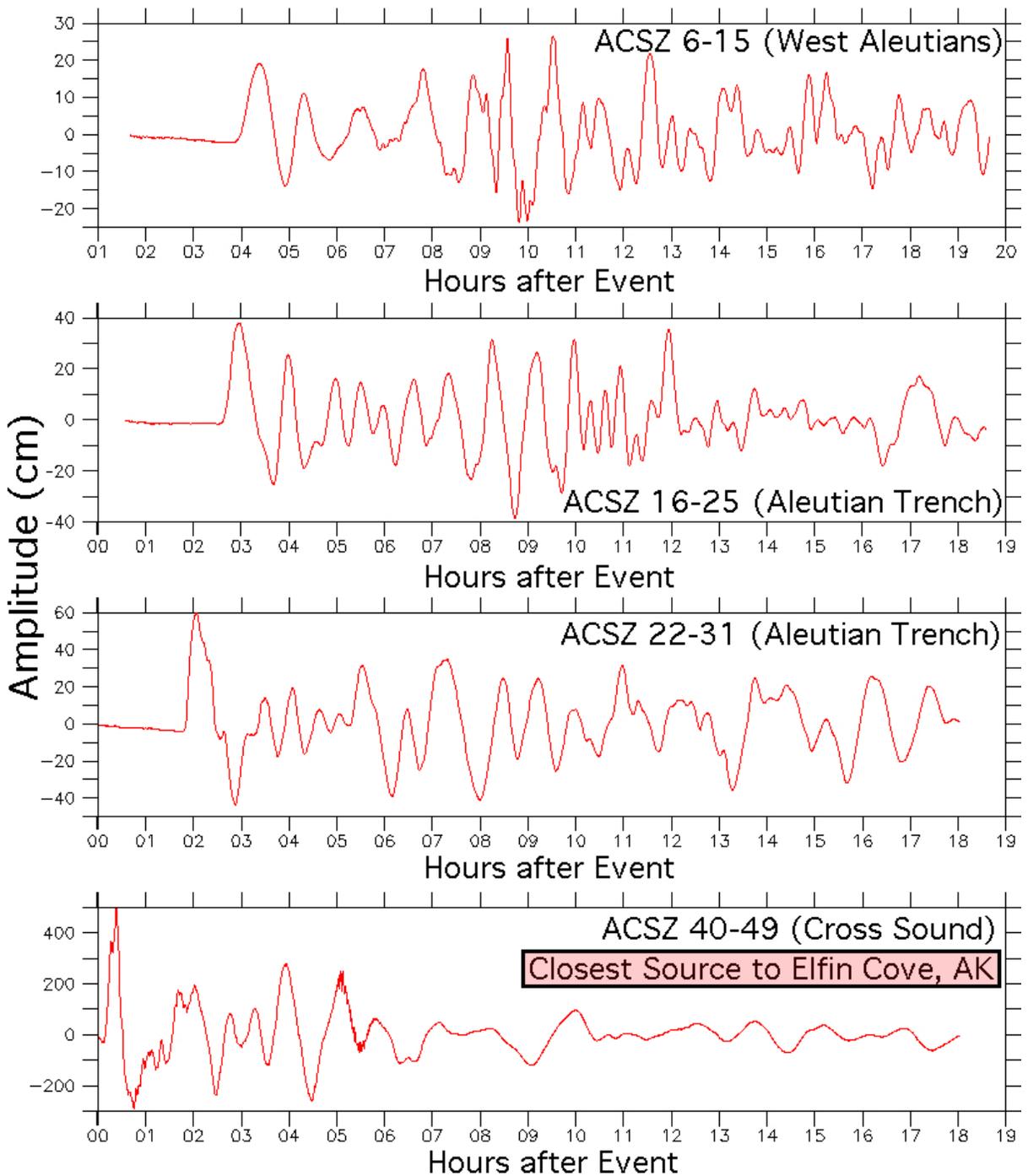
Figure 32, continued: Complete time series of forecast model predictions at the Elfin Cove tide gauge site for each of the mega-tsunami scenarios. (b) further mega-tsunami scenarios, representing ACSZ 6–15, ACSZ 16–25, ACSZ 22–31, and ACSZ 40–49.
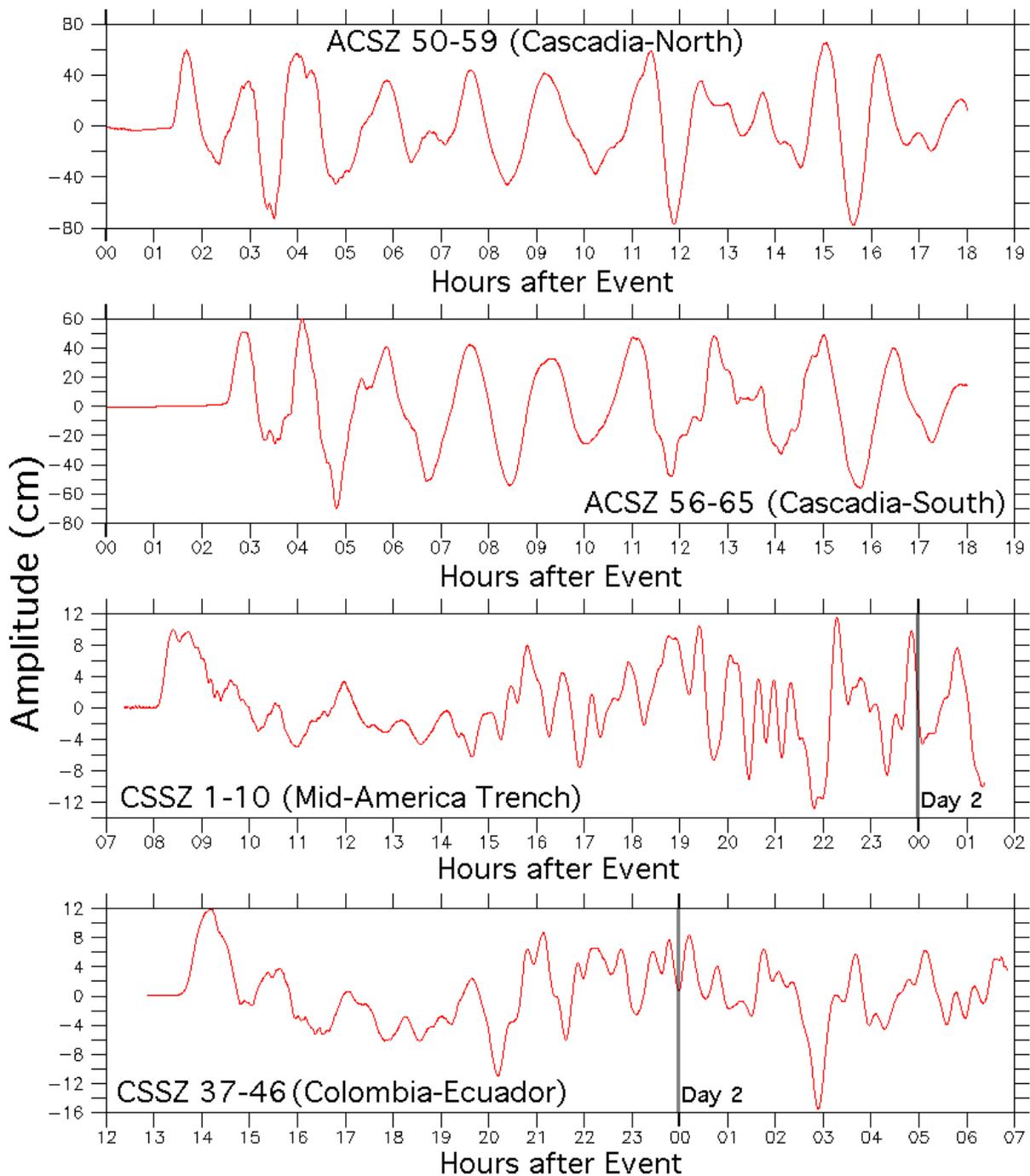
Figure 32, continued: Complete time series of forecast model predictions at the Elfin Cove tide gauge site for each of the mega-tsunami scenarios. (c) further mega-tsunami scenarios, representing ACSZ 50–59, ACSZ 56–65, CSSZ 1–10, and CSSZ 37–46.
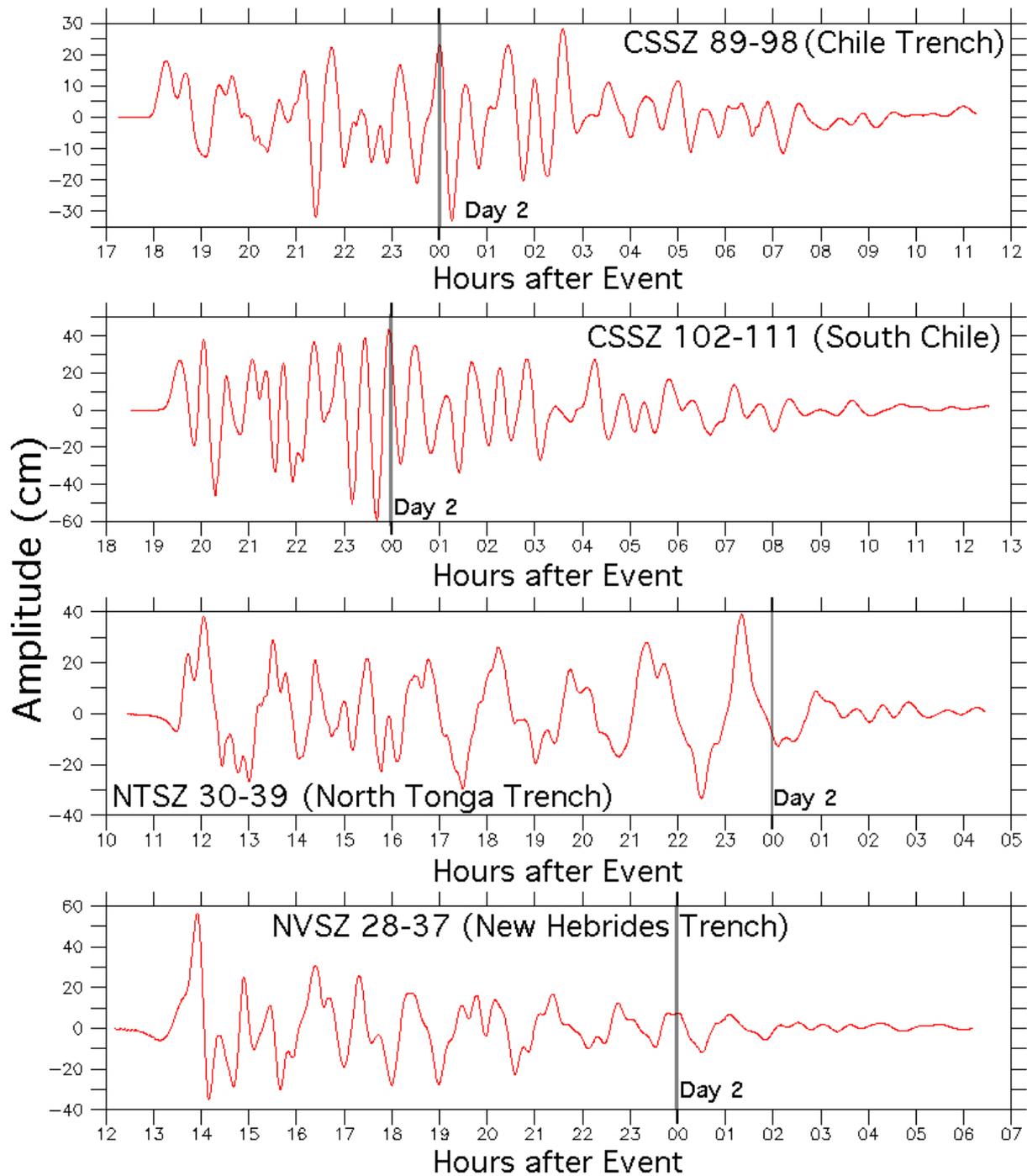
Figure 32, continued: Complete time series of forecast model predictions at the Elfin Cove tide gauge site for each of the mega-tsunami scenarios. (d) further mega-tsunami scenarios, representing CSSZ 89–98, CSSZ 102–111, NTSZ 30–39, and NVSZ 28–37.
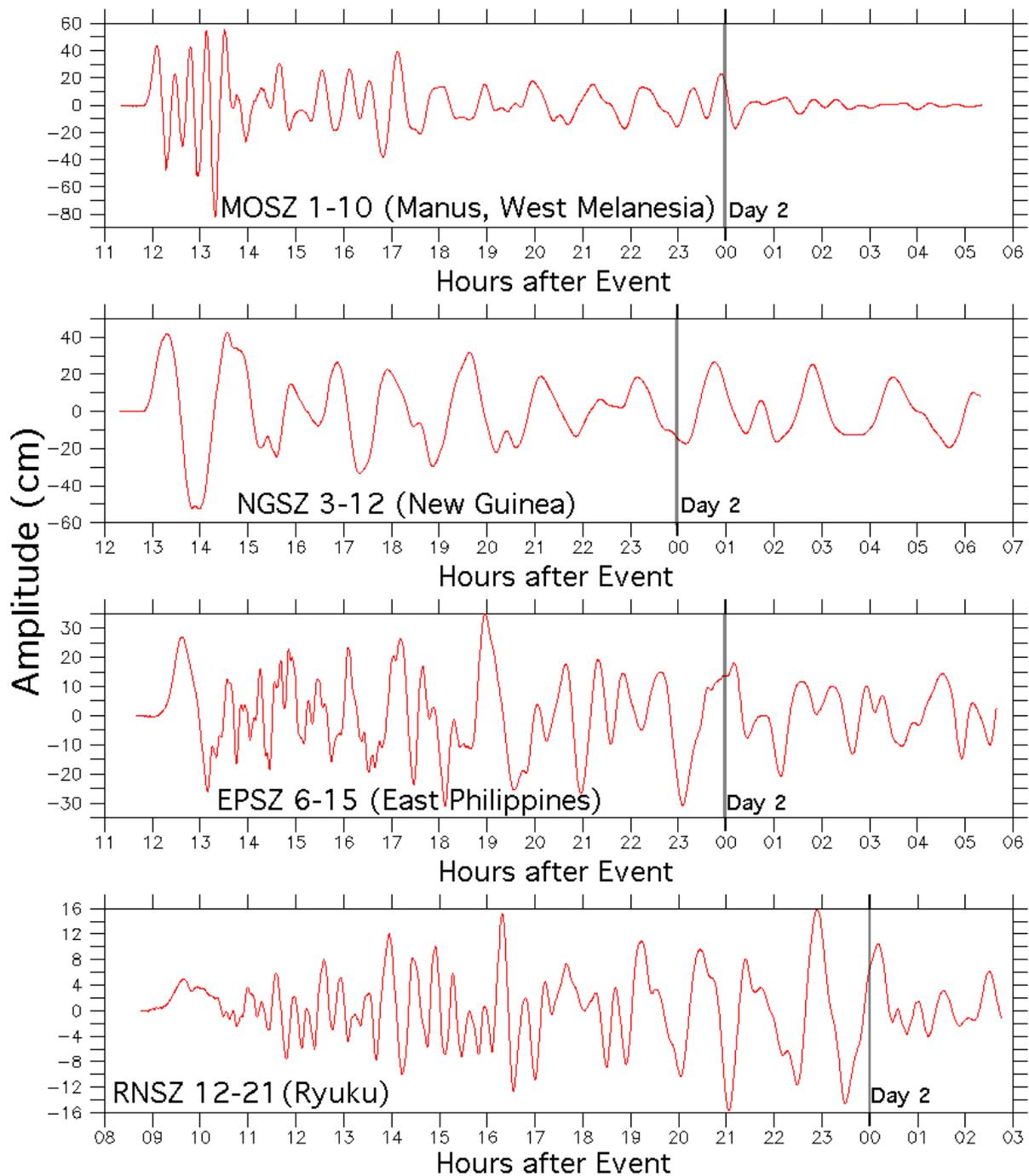
Figure 32, continued: Complete time series of forecast model predictions at the Elfin Cove tide gauge site for each of the mega-tsunami scenarios. (e) further mega-tsunami scenarios, representing MOSZ 1–10, NGSZ 3–12, EPSZ 6–15, and RNSZ 12–21.
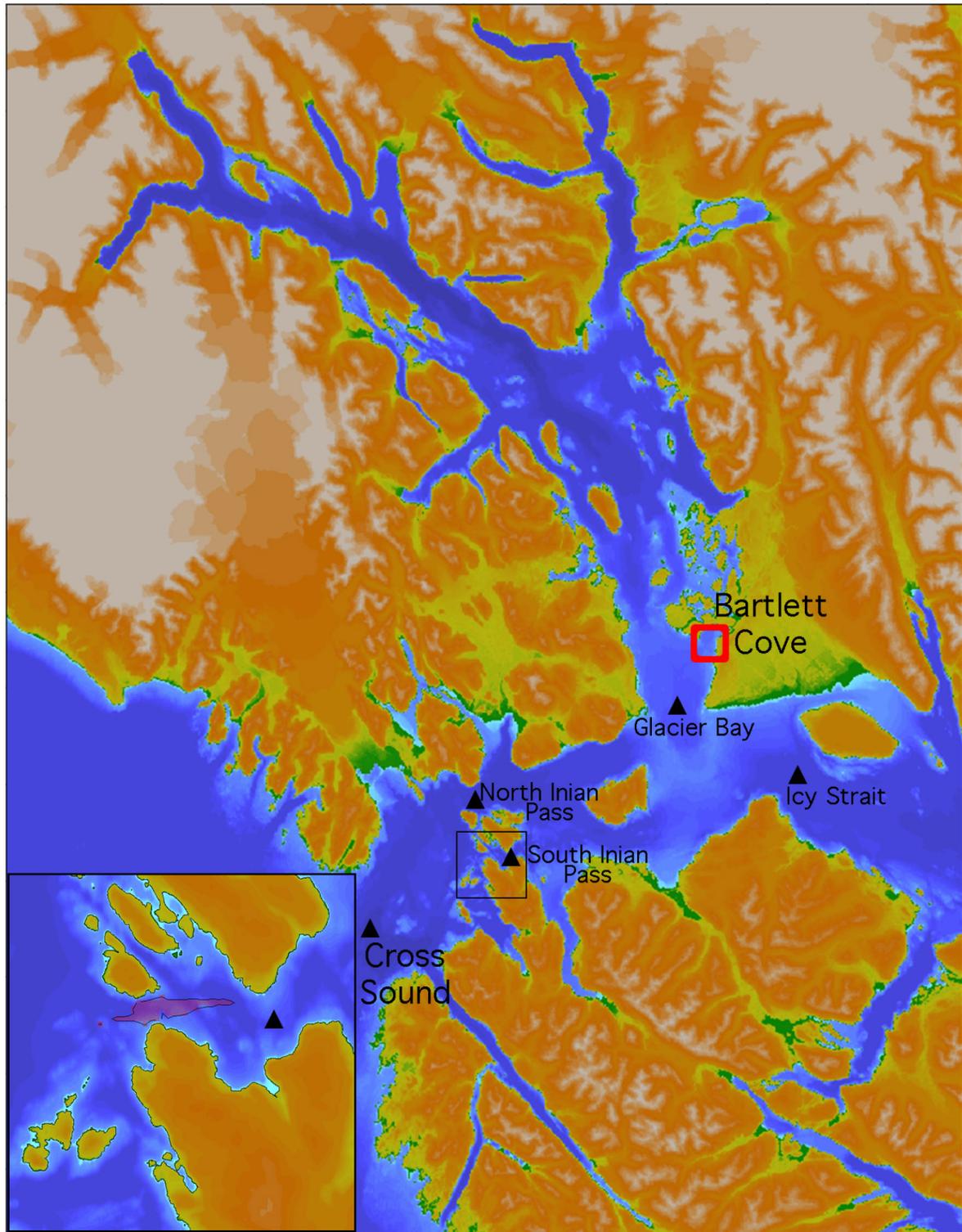
Figure 33: Current meter sites instrumented by NOAA's EcoFOCI Program (P. Stabeno, NOAA PMEL, 2012 personal communication) for which mega-tsunami event speed maxima from the Elfin Cove model were extracted (listed in Table 10). The inset panel shows the 10-knot contour for the local (ACSZ 40–49) scenario that produces the strongest currents.

Appendix A. Model input files for Elfin Cove, Alaska

As discussed in Section 3.6, input files providing model parameters, the file names of the nested grids, and the output specifications are necessary in order to run the model in either its reference or forecast mode. These files are provided below; each record contains the value(s) and an annotation of purpose.

A1. Reference model *.in file for Elfin Cove, Alaska

The following table contains the parameter and file choices used in the input file for the SIFT implementation (most3_facts_nc.in) of the reference model (RM) for Elfin Cove, Alaska. When run on an Intel® Xeon® E5670 2.93 GHz processor during development the model simulated 4 hr in 6.94 CPU hr.

```
0.001                     Minimum amplitude of input offshore wave (m)
2.5                       Minimum depth of offshore (m)
0.1                       Dry land depth of inundation (m)
0.0009                    Friction coefficient (n**2)
1                         Let A Grid and B Grid run up
900.0                     Max eta before blow-up (m)
0.25                      Time step (sec)
115200                    Total number of time steps in run
12                        Time steps between A-grid computations
4                         Time steps between B-grid computations
120                       Time steps between output steps
0                         Time steps before saving first output step
1                         Save output every n-th grid point, n=
ElfinCoveAK_RM_A.most     A-grid bathymetry file
ElfinCoveAK_RM_B.most     B-grid bathymetry file
ElfinCoveAK_RM_C.most     C-grid bathymetry file
./                        Directory of source files
./                        Directory for output files
1 1 1 1                   netCDF output for A, B, C, SIFT
1                         Number of time series locations
3 225 728                 Grid & cell indices for reference point
```

A2. Forecast model *.in file for Elfin Cove, Alaska

The following table contains the parameter and file choices used in the input file for the SIFT implementation (most3_facts_nc.in) of the optimized forecast model (FM) for Elfin Cove, Alaska. When run on an Intel® Xeon® E5670 2.93 GHz processor the model simulated 4 hr in 12.92 min, about 30% above the 10 min target for this metric.

```
0.001                   Minimum amplitude of input offshore wave (m)
2.5                     Minimum depth of offshore (m)
0.1                     Dry land depth of inundation (m)
0.0009                  Friction coefficient (n**2)
1                       Let A Grid and B Grid run up
900.0                   Max eta before blow-up (m)
0.4166667               Time step (sec)
69120                   Total number of time steps in run
12                      Time steps between A-grid computations
4                       Time steps between B-grid computations
72                      Time steps between output steps
0                       Time steps before saving first output step
1                       Save output every n-th grid point, n=
ElfinCoveAK_FM_A.most   A-grid bathymetry file
ElfinCoveAK_FM_B.most   B-grid bathymetry file
ElfinCoveAK_FM_C.most   C-grid bathymetry file
./                      Directory of source files
./                      Directory for output files
1 1 1 1                 netCDF output for A, B, C, SIFT
1                       Number of time series locations
3 171 81                Grid & cell indices
                            for 223.652963 58.1951852
```

Appendix B.   Propagation Database

Pacific Ocean Unit Sources

The NOAA propagation database presented in this section is the representation of the database as of March 2013, and may not be the most current version of the database available upon publication.
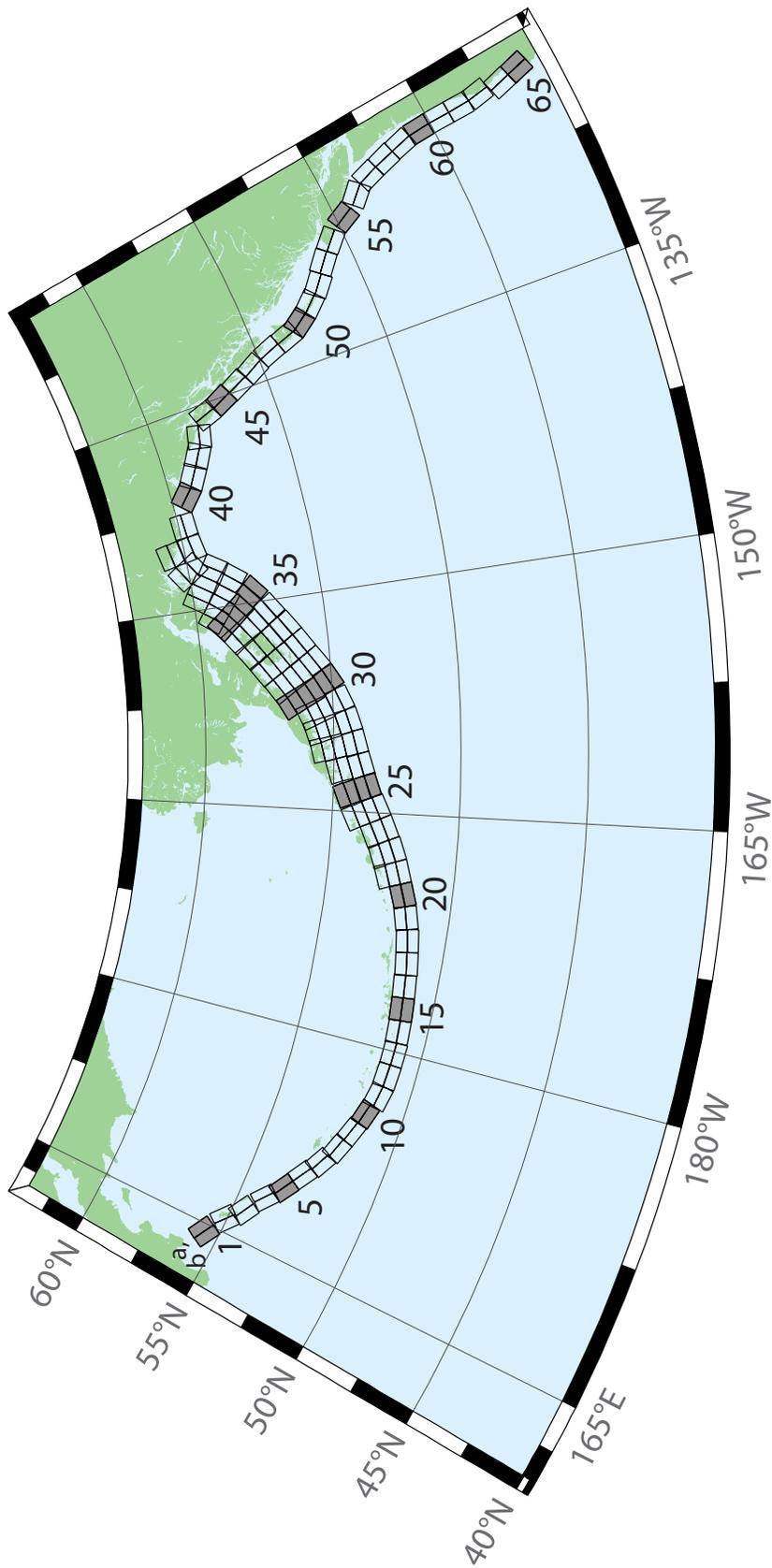
Figure B1: Aleutian–Alaska–Cascadia Subduction Zone unit sources.

Table B1: Earthquake parameters for Aleutian–Alaska–Cascadia Subduction Zone unit sources.

Segment	Description	Longitude (°E)	Latitude (°N)	Strike (°)	Dip (°)	Depth (km)
acsz-1a	Aleutian–Alaska–Cascadia	164.7994	55.9606	299	17	19.61
acsz-1b	Aleutian–Alaska–Cascadia	164.4310	55.5849	299	17	5
acsz-2a	Aleutian–Alaska–Cascadia	166.3418	55.4016	310.2	17	19.61
acsz-2b	Aleutian–Alaska–Cascadia	165.8578	55.0734	310.2	17	5
acsz-3a	Aleutian–Alaska–Cascadia	167.2939	54.8919	300.2	23.36	24.82
acsz-3b	Aleutian–Alaska–Cascadia	166.9362	54.5356	300.2	23.36	5
acsz-4a	Aleutian–Alaska–Cascadia	168.7131	54.2852	310.2	38.51	25.33
acsz-4b	Aleutian–Alaska–Cascadia	168.3269	54.0168	310.2	24	5
acsz-5a	Aleutian–Alaska–Cascadia	169.7447	53.7808	302.8	37.02	23.54
acsz-5b	Aleutian–Alaska–Cascadia	169.4185	53.4793	302.8	21.77	5
acsz-6a	Aleutian–Alaska–Cascadia	171.0144	53.3054	303.2	35.31	22.92
acsz-6b	Aleutian–Alaska–Cascadia	170.6813	52.9986	303.2	21	5
acsz-7a	Aleutian–Alaska–Cascadia	172.1500	52.8528	298.2	35.56	20.16
acsz-7b	Aleutian–Alaska–Cascadia	171.8665	52.5307	298.2	17.65	5
acsz-8a	Aleutian–Alaska–Cascadia	173.2726	52.4579	290.8	37.92	20.35
acsz-8b	Aleutian–Alaska–Cascadia	173.0681	52.1266	290.8	17.88	5
acsz-9a	Aleutian–Alaska–Cascadia	174.5866	52.1434	289	39.09	21.05
acsz-9b	Aleutian–Alaska–Cascadia	174.4027	51.8138	289	18.73	5
acsz-10a	Aleutian–Alaska–Cascadia	175.8784	51.8526	286.1	40.51	20.87
acsz-10b	Aleutian–Alaska–Cascadia	175.7265	51.5245	286.1	18.51	5
acsz-11a	Aleutian–Alaska–Cascadia	177.1140	51.6488	280	15	17.94
acsz-11b	Aleutian–Alaska–Cascadia	176.9937	51.2215	280	15	5
acsz-12a	Aleutian–Alaska–Cascadia	178.4500	51.5690	273	15	17.94
acsz-12b	Aleutian–Alaska–Cascadia	178.4130	51.1200	273	15	5
acsz-13a	Aleutian–Alaska–Cascadia	179.8550	51.5340	271	15	17.94
acsz-13b	Aleutian–Alaska–Cascadia	179.8420	51.0850	271	15	5
acsz-14a	Aleutian–Alaska–Cascadia	181.2340	51.5780	267	15	17.94
acsz-14b	Aleutian–Alaska–Cascadia	181.2720	51.1290	267	15	5
acsz-15a	Aleutian–Alaska–Cascadia	182.6380	51.6470	265	15	17.94
acsz-15b	Aleutian–Alaska–Cascadia	182.7000	51.2000	265	15	5
acsz-16a	Aleutian–Alaska–Cascadia	184.0550	51.7250	264	15	17.94
acsz-16b	Aleutian–Alaska–Cascadia	184.1280	51.2780	264	15	5
acsz-17a	Aleutian–Alaska–Cascadia	185.4560	51.8170	262	15	17.94
acsz-17b	Aleutian–Alaska–Cascadia	185.5560	51.3720	262	15	5
acsz-18a	Aleutian–Alaska–Cascadia	186.8680	51.9410	261	15	17.94
acsz-18b	Aleutian–Alaska–Cascadia	186.9810	51.4970	261	15	5
acsz-19a	Aleutian–Alaska–Cascadia	188.2430	52.1280	257	15	17.94
acsz-19b	Aleutian–Alaska–Cascadia	188.4060	51.6900	257	15	5

Table B1: (continued)

Segment	Description	Longitude (°E)	Latitude (°N)	Strike (°)	Dip (°)	Depth (km)
acsz-20a	Aleutian–Alaska–Cascadia	189.5810	52.3550	251	15	17.94
acsz-20b	Aleutian–Alaska–Cascadia	189.8180	51.9300	251	15	5
acsz-21a	Aleutian–Alaska–Cascadia	190.9570	52.6470	251	15	17.94
acsz-21b	Aleutian–Alaska–Cascadia	191.1960	52.2220	251	15	5
acsz-21z	Aleutian–Alaska–Cascadia	190.7399	53.0443	250.8	15	30.88
acsz-22a	Aleutian–Alaska–Cascadia	192.2940	52.9430	247	15	17.94
acsz-22b	Aleutian–Alaska–Cascadia	192.5820	52.5300	247	15	5
acsz-22z	Aleutian–Alaska–Cascadia	192.0074	53.3347	247.8	15	30.88
acsz-23a	Aleutian–Alaska–Cascadia	193.6270	53.3070	245	15	17.94
acsz-23b	Aleutian–Alaska–Cascadia	193.9410	52.9000	245	15	5
acsz-23z	Aleutian–Alaska–Cascadia	193.2991	53.6768	244.6	15	30.88
acsz-24a	Aleutian–Alaska–Cascadia	194.9740	53.6870	245	15	17.94
acsz-24b	Aleutian–Alaska–Cascadia	195.2910	53.2800	245	15	5
acsz-24y	Aleutian–Alaska–Cascadia	194.3645	54.4604	244.4	15	43.82
acsz-24z	Aleutian–Alaska–Cascadia	194.6793	54.0674	244.6	15	30.88
acsz-25a	Aleutian–Alaska–Cascadia	196.4340	54.0760	250	15	17.94
acsz-25b	Aleutian–Alaska–Cascadia	196.6930	53.6543	250	15	5
acsz-25y	Aleutian–Alaska–Cascadia	195.9009	54.8572	247.9	15	43.82
acsz-25z	Aleutian–Alaska–Cascadia	196.1761	54.4536	248.1	15	30.88
acsz-26a	Aleutian–Alaska–Cascadia	197.8970	54.3600	253	15	17.94
acsz-26b	Aleutian–Alaska–Cascadia	198.1200	53.9300	253	15	5
acsz-26y	Aleutian–Alaska–Cascadia	197.5498	55.1934	253.1	15	43.82
acsz-26z	Aleutian–Alaska–Cascadia	197.7620	54.7770	253.3	15	30.88
acsz-27a	Aleutian–Alaska–Cascadia	199.4340	54.5960	256	15	17.94
acsz-27b	Aleutian–Alaska–Cascadia	199.6200	54.1600	256	15	5
acsz-27x	Aleutian–Alaska–Cascadia	198.9736	55.8631	256.5	15	56.24
acsz-27y	Aleutian–Alaska–Cascadia	199.1454	55.4401	256.6	15	43.82
acsz-27z	Aleutian–Alaska–Cascadia	199.3135	55.0170	256.8	15	30.88
acsz-28a	Aleutian–Alaska–Cascadia	200.8820	54.8300	253	15	17.94
acsz-28b	Aleutian–Alaska–Cascadia	201.1080	54.4000	253	15	5
acsz-28x	Aleutian–Alaska–Cascadia	200.1929	56.0559	252.5	15	56.24
acsz-28y	Aleutian–Alaska–Cascadia	200.4167	55.6406	252.7	15	43.82
acsz-28z	Aleutian–Alaska–Cascadia	200.6360	55.2249	252.9	15	30.88
acsz-29a	Aleutian–Alaska–Cascadia	202.2610	55.1330	247	15	17.94
acsz-29b	Aleutian–Alaska–Cascadia	202.5650	54.7200	247	15	5
acsz-29x	Aleutian–Alaska–Cascadia	201.2606	56.2861	245.7	15	56.24
acsz-29y	Aleutian–Alaska–Cascadia	201.5733	55.8888	246	15	43.82
acsz-29z	Aleutian–Alaska–Cascadia	201.8797	55.4908	246.2	15	30.88

Table B1: (continued)

Segment	Description	Longitude (°E)	Latitude (°N)	Strike (°)	Dip (°)	Depth (km)
acsz-30a	Aleutian–Alaska–Cascadia	203.6040	55.5090	240	15	17.94
acsz-30b	Aleutian–Alaska–Cascadia	203.9970	55.1200	240	15	5
acsz-30w	Aleutian–Alaska–Cascadia	201.9901	56.9855	239.5	15	69.12
acsz-30x	Aleutian–Alaska–Cascadia	202.3851	56.6094	239.8	15	56.24
acsz-30y	Aleutian–Alaska–Cascadia	202.7724	56.2320	240.2	15	43.82
acsz-30z	Aleutian–Alaska–Cascadia	203.1521	55.8534	240.5	15	30.88
acsz-31a	Aleutian–Alaska–Cascadia	204.8950	55.9700	236	15	17.94
acsz-31b	Aleutian–Alaska–Cascadia	205.3400	55.5980	236	15	5
acsz-31w	Aleutian–Alaska–Cascadia	203.0825	57.3740	234.5	15	69.12
acsz-31x	Aleutian–Alaska–Cascadia	203.5408	57.0182	234.9	15	56.24
acsz-31y	Aleutian–Alaska–Cascadia	203.9904	56.6607	235.3	15	43.82
acsz-31z	Aleutian–Alaska–Cascadia	204.4315	56.3016	235.7	15	30.88
acsz-32a	Aleutian–Alaska–Cascadia	206.2080	56.4730	236	15	17.94
acsz-32b	Aleutian–Alaska–Cascadia	206.6580	56.1000	236	15	5
acsz-32w	Aleutian–Alaska–Cascadia	204.4129	57.8908	234.3	15	69.12
acsz-32x	Aleutian–Alaska–Cascadia	204.8802	57.5358	234.7	15	56.24
acsz-32y	Aleutian–Alaska–Cascadia	205.3385	57.1792	235.1	15	43.82
acsz-32z	Aleutian–Alaska–Cascadia	205.7880	56.8210	235.5	15	30.88
acsz-33a	Aleutian–Alaska–Cascadia	207.5370	56.9750	236	15	17.94
acsz-33b	Aleutian–Alaska–Cascadia	207.9930	56.6030	236	15	5
acsz-33w	Aleutian–Alaska–Cascadia	205.7126	58.3917	234.2	15	69.12
acsz-33x	Aleutian–Alaska–Cascadia	206.1873	58.0371	234.6	15	56.24
acsz-33y	Aleutian–Alaska–Cascadia	206.6527	57.6808	235	15	43.82
acsz-33z	Aleutian–Alaska–Cascadia	207.1091	57.3227	235.4	15	30.88
acsz-34a	Aleutian–Alaska–Cascadia	208.9371	57.5124	236	15	17.94
acsz-34b	Aleutian–Alaska–Cascadia	209.4000	57.1400	236	15	5
acsz-34w	Aleutian–Alaska–Cascadia	206.9772	58.8804	233.5	15	69.12
acsz-34x	Aleutian–Alaska–Cascadia	207.4677	58.5291	233.9	15	56.24
acsz-34y	Aleutian–Alaska–Cascadia	207.9485	58.1760	234.3	15	43.82
acsz-34z	Aleutian–Alaska–Cascadia	208.4198	57.8213	234.7	15	30.88
acsz-35a	Aleutian–Alaska–Cascadia	210.2597	58.0441	230	15	17.94
acsz-35b	Aleutian–Alaska–Cascadia	210.8000	57.7000	230	15	5
acsz-35w	Aleutian–Alaska–Cascadia	208.0204	59.3199	228.8	15	69.12
acsz-35x	Aleutian–Alaska–Cascadia	208.5715	58.9906	229.3	15	56.24
acsz-35y	Aleutian–Alaska–Cascadia	209.1122	58.6590	229.7	15	43.82
acsz-35z	Aleutian–Alaska–Cascadia	209.6425	58.3252	230.2	15	30.88
acsz-36a	Aleutian–Alaska–Cascadia	211.3249	58.6565	218	15	17.94
acsz-36b	Aleutian–Alaska–Cascadia	212.0000	58.3800	218	15	5

Table B1: (continued)

Segment	Description	Longitude (°E)	Latitude (°N)	Strike (°)	Dip (°)	Depth (km)
acsz-36w	Aleutian–Alaska–Cascadia	208.5003	59.5894	215.6	15	69.12
acsz-36x	Aleutian–Alaska–Cascadia	209.1909	59.3342	216.2	15	56.24
acsz-36y	Aleutian–Alaska–Cascadia	209.8711	59.0753	216.8	15	43.82
acsz-36z	Aleutian–Alaska–Cascadia	210.5412	58.8129	217.3	15	30.88
acsz-37a	Aleutian–Alaska–Cascadia	212.2505	59.2720	213.7	15	17.94
acsz-37b	Aleutian–Alaska–Cascadia	212.9519	59.0312	213.7	15	5
acsz-37x	Aleutian–Alaska–Cascadia	210.1726	60.0644	213	15	56.24
acsz-37y	Aleutian–Alaska–Cascadia	210.8955	59.8251	213.7	15	43.82
acsz-37z	Aleutian–Alaska–Cascadia	211.6079	59.5820	214.3	15	30.88
acsz-38a	Aleutian–Alaska–Cascadia	214.6555	60.1351	260.1	0	15
acsz-38b	Aleutian–Alaska–Cascadia	214.8088	59.6927	260.1	0	15
acsz-38y	Aleutian–Alaska–Cascadia	214.3737	60.9838	259	0	15
acsz-38z	Aleutian–Alaska–Cascadia	214.5362	60.5429	259	0	15
acsz-39a	Aleutian–Alaska–Cascadia	216.5607	60.2480	267	0	15
acsz-39b	Aleutian–Alaska–Cascadia	216.6068	59.7994	267	0	15
acsz-40a	Aleutian–Alaska–Cascadia	219.3069	59.7574	310.9	0	15
acsz-40b	Aleutian–Alaska–Cascadia	218.7288	59.4180	310.9	0	15
acsz-41a	Aleutian–Alaska–Cascadia	220.4832	59.3390	300.7	0	15
acsz-41b	Aleutian–Alaska–Cascadia	220.0382	58.9529	300.7	0	15
acsz-42a	Aleutian–Alaska–Cascadia	221.8835	58.9310	298.9	0	15
acsz-42b	Aleutian–Alaska–Cascadia	221.4671	58.5379	298.9	0	15
acsz-43a	Aleutian–Alaska–Cascadia	222.9711	58.6934	282.3	0	15
acsz-43b	Aleutian–Alaska–Cascadia	222.7887	58.2546	282.3	0	15
acsz-44a	Aleutian–Alaska–Cascadia	224.9379	57.9054	340.9	12	11.09
acsz-44b	Aleutian–Alaska–Cascadia	224.1596	57.7617	340.9	7	5
acsz-45a	Aleutian–Alaska–Cascadia	225.4994	57.1634	334.1	12	11.09
acsz-45b	Aleutian–Alaska–Cascadia	224.7740	56.9718	334.1	7	5
acsz-46a	Aleutian–Alaska–Cascadia	226.1459	56.3552	334.1	12	11.09
acsz-46b	Aleutian–Alaska–Cascadia	225.4358	56.1636	334.1	7	5
acsz-47a	Aleutian–Alaska–Cascadia	226.7731	55.5830	332.3	12	11.09
acsz-47b	Aleutian–Alaska–Cascadia	226.0887	55.3785	332.3	7	5
acsz-48a	Aleutian–Alaska–Cascadia	227.4799	54.6763	339.4	12	11.09
acsz-48b	Aleutian–Alaska–Cascadia	226.7713	54.5217	339.4	7	5
acsz-49a	Aleutian–Alaska–Cascadia	227.9482	53.8155	341.2	12	11.09
acsz-49b	Aleutian–Alaska–Cascadia	227.2462	53.6737	341.2	7	5
acsz-50a	Aleutian–Alaska–Cascadia	228.3970	53.2509	324.5	12	11.09
acsz-50b	Aleutian–Alaska–Cascadia	227.8027	52.9958	324.5	7	5
acsz-51a	Aleutian–Alaska–Cascadia	229.1844	52.6297	318.4	12	11.09

Table B1: (continued)

Segment	Description	Longitude (°E)	Latitude (°N)	Strike (°)	Dip (°)	Depth (km)
acsz-51b	Aleutian–Alaska–Cascadia	228.6470	52.3378	318.4	7	5
acsz-52a	Aleutian–Alaska–Cascadia	230.0306	52.0768	310.9	12	11.09
acsz-52b	Aleutian–Alaska–Cascadia	229.5665	51.7445	310.9	7	5
acsz-53a	Aleutian–Alaska–Cascadia	231.1735	51.5258	310.9	12	11.09
acsz-53b	Aleutian–Alaska–Cascadia	230.7150	51.1935	310.9	7	5
acsz-54a	Aleutian–Alaska–Cascadia	232.2453	50.8809	314.1	12	11.09
acsz-54b	Aleutian–Alaska–Cascadia	231.7639	50.5655	314.1	7	5
acsz-55a	Aleutian–Alaska–Cascadia	233.3066	49.9032	333.7	12	11.09
acsz-55b	Aleutian–Alaska–Cascadia	232.6975	49.7086	333.7	7	5
acsz-56a	Aleutian–Alaska–Cascadia	234.0588	49.1702	315	11	12.82
acsz-56b	Aleutian–Alaska–Cascadia	233.5849	48.8584	315	9	5
acsz-57a	Aleutian–Alaska–Cascadia	234.9041	48.2596	341	11	12.82
acsz-57b	Aleutian–Alaska–Cascadia	234.2797	48.1161	341	9	5
acsz-58a	Aleutian–Alaska–Cascadia	235.3021	47.3812	344	11	12.82
acsz-58b	Aleutian–Alaska–Cascadia	234.6776	47.2597	344	9	5
acsz-59a	Aleutian–Alaska–Cascadia	235.6432	46.5082	345	11	12.82
acsz-59b	Aleutian–Alaska–Cascadia	235.0257	46.3941	345	9	5
acsz-60a	Aleutian–Alaska–Cascadia	235.8640	45.5429	356	11	12.82
acsz-60b	Aleutian–Alaska–Cascadia	235.2363	45.5121	356	9	5
acsz-61a	Aleutian–Alaska–Cascadia	235.9106	44.6227	359	11	12.82
acsz-61b	Aleutian–Alaska–Cascadia	235.2913	44.6150	359	9	5
acsz-62a	Aleutian–Alaska–Cascadia	235.9229	43.7245	359	11	12.82
acsz-62b	Aleutian–Alaska–Cascadia	235.3130	43.7168	359	9	5
acsz-63a	Aleutian–Alaska–Cascadia	236.0220	42.9020	350	11	12.82
acsz-63b	Aleutian–Alaska–Cascadia	235.4300	42.8254	350	9	5
acsz-64a	Aleutian–Alaska–Cascadia	235.9638	41.9818	345	11	12.82
acsz-64b	Aleutian–Alaska–Cascadia	235.3919	41.8677	345	9	5
acsz-65a	Aleutian–Alaska–Cascadia	236.2643	41.1141	345	11	12.82
acsz-65b	Aleutian–Alaska–Cascadia	235.7000	41.0000	345	9	5
acsz-238a	Aleutian–Alaska–Cascadia	213.2878	59.8406	236.8	15	17.94
acsz-238y	Aleutian–Alaska–Cascadia	212.3424	60.5664	236.8	15	43.82
acsz-238z	Aleutian–Alaska–Cascadia	212.8119	60.2035	236.8	15	30.88
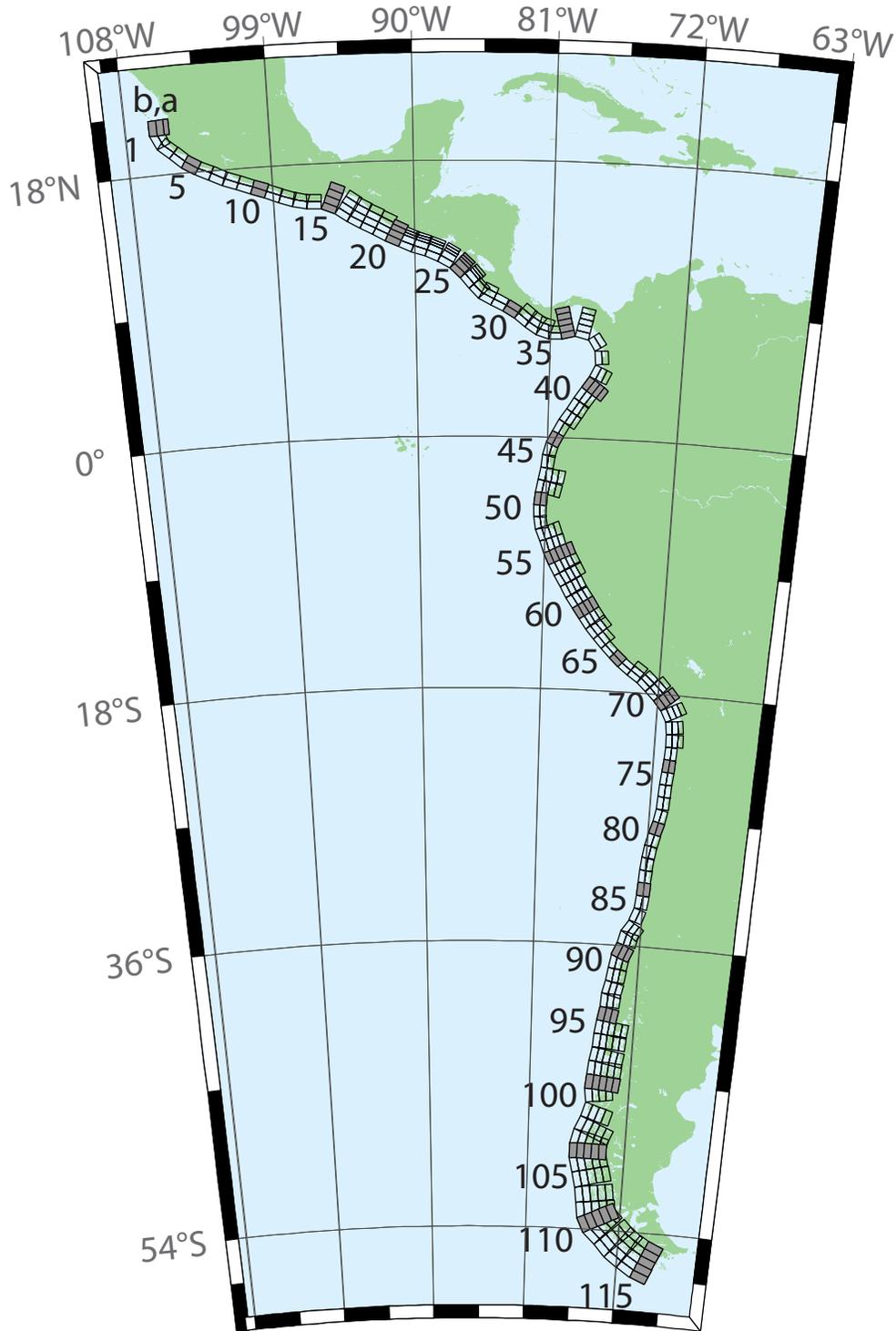
Figure B2: Central and South America Subduction Zone unit sources.

Table B2: Earthquake parameters for Central and South America Subduction Zone unit sources.

Segment	Description	Longitude (°E)	Latitude (°N)	Strike (°)	Dip (°)	Depth (km)
cssz-1a	Central and South America	254.4573	20.8170	359	19	15.4
cssz-1b	Central and South America	254.0035	20.8094	359	12	5
cssz-1z	Central and South America	254.7664	20.8222	359	50	31.67
cssz-2a	Central and South America	254.5765	20.2806	336.8	19	15.4
cssz-2b	Central and South America	254.1607	20.1130	336.8	12	5
cssz-3a	Central and South America	254.8789	19.8923	310.6	18.31	15.27
cssz-3b	Central and South America	254.5841	19.5685	310.6	11.85	5
cssz-4a	Central and South America	255.6167	19.2649	313.4	17.62	15.12
cssz-4b	Central and South America	255.3056	18.9537	313.4	11.68	5
cssz-5a	Central and South America	256.2240	18.8148	302.7	16.92	15
cssz-5b	Central and South America	255.9790	18.4532	302.7	11.54	5
cssz-6a	Central and South America	256.9425	18.4383	295.1	16.23	14.87
cssz-6b	Central and South America	256.7495	18.0479	295.1	11.38	5
cssz-7a	Central and South America	257.8137	18.0339	296.9	15.54	14.74
cssz-7b	Central and South America	257.6079	17.6480	296.9	11.23	5
cssz-8a	Central and South America	258.5779	17.7151	290.4	14.85	14.61
cssz-8b	Central and South America	258.4191	17.3082	290.4	11.08	5
cssz-9a	Central and South America	259.4578	17.4024	290.5	14.15	14.47
cssz-9b	Central and South America	259.2983	16.9944	290.5	10.92	5
cssz-10a	Central and South America	260.3385	17.0861	290.8	13.46	14.34
cssz-10b	Central and South America	260.1768	16.6776	290.8	10.77	5
cssz-11a	Central and South America	261.2255	16.7554	291.8	12.77	14.21
cssz-11b	Central and South America	261.0556	16.3487	291.8	10.62	5
cssz-12a	Central and South America	262.0561	16.4603	288.9	12.08	14.08
cssz-12b	Central and South America	261.9082	16.0447	288.9	10.46	5
cssz-13a	Central and South America	262.8638	16.2381	283.2	11.38	13.95
cssz-13b	Central and South America	262.7593	15.8094	283.2	10.31	5
cssz-14a	Central and South America	263.6066	16.1435	272.1	10.69	13.81
cssz-14b	Central and South America	263.5901	15.7024	272.1	10.15	5
cssz-15a	Central and South America	264.8259	15.8829	293	10	13.68
cssz-15b	Central and South America	264.6462	15.4758	293	10	5
cssz-15y	Central and South America	265.1865	16.6971	293	10	31.05
cssz-15z	Central and South America	265.0060	16.2900	293	10	22.36
cssz-16a	Central and South America	265.7928	15.3507	304.9	15	15.82
cssz-16b	Central and South America	265.5353	14.9951	304.9	12.5	5
cssz-16y	Central and South America	266.3092	16.0619	304.9	15	41.7
cssz-16z	Central and South America	266.0508	15.7063	304.9	15	28.76
cssz-17a	Central and South America	266.4947	14.9019	299.5	20	17.94
cssz-17b	Central and South America	266.2797	14.5346	299.5	15	5
cssz-17y	Central and South America	266.9259	15.6365	299.5	20	52.14

Table B2: (continued)

Segment	Description	Longitude (°E)	Latitude (°N)	Strike (°)	Dip (°)	Depth (km)
cssz-17z	Central and South America	266.7101	15.2692	299.5	20	35.04
cssz-18a	Central and South America	267.2827	14.4768	298	21.5	17.94
cssz-18b	Central and South America	267.0802	14.1078	298	15	5
cssz-18y	Central and South America	267.6888	15.2148	298	21.5	54.59
cssz-18z	Central and South America	267.4856	14.8458	298	21.5	36.27
cssz-19a	Central and South America	268.0919	14.0560	297.6	23	17.94
cssz-19b	Central and South America	267.8943	13.6897	297.6	15	5
cssz-19y	Central and South America	268.4880	14.7886	297.6	23	57.01
cssz-19z	Central and South America	268.2898	14.4223	297.6	23	37.48
cssz-20a	Central and South America	268.8929	13.6558	296.2	24	17.94
cssz-20b	Central and South America	268.7064	13.2877	296.2	15	5
cssz-20y	Central and South America	269.1796	14.2206	296.2	45.5	73.94
cssz-20z	Central and South America	269.0362	13.9382	296.2	45.5	38.28
cssz-21a	Central and South America	269.6797	13.3031	292.6	25	17.94
cssz-21b	Central and South America	269.5187	12.9274	292.6	15	5
cssz-21x	Central and South America	269.8797	13.7690	292.6	68	131.8
cssz-21y	Central and South America	269.8130	13.6137	292.6	68	85.43
cssz-21z	Central and South America	269.7463	13.4584	292.6	68	39.07
cssz-22a	Central and South America	270.4823	13.0079	288.6	25	17.94
cssz-22b	Central and South America	270.3492	12.6221	288.6	15	5
cssz-22x	Central and South America	270.6476	13.4864	288.6	68	131.8
cssz-22y	Central and South America	270.5925	13.3269	288.6	68	85.43
cssz-22z	Central and South America	270.5374	13.1674	288.6	68	39.07
cssz-23a	Central and South America	271.3961	12.6734	292.4	25	17.94
cssz-23b	Central and South America	271.2369	12.2972	292.4	15	5
cssz-23x	Central and South America	271.5938	13.1399	292.4	68	131.8
cssz-23y	Central and South America	271.5279	12.9844	292.4	68	85.43
cssz-23z	Central and South America	271.4620	12.8289	292.4	68	39.07
cssz-24a	Central and South America	272.3203	12.2251	300.2	25	17.94
cssz-24b	Central and South America	272.1107	11.8734	300.2	15	5
cssz-24x	Central and South America	272.5917	12.6799	300.2	67	131.1
cssz-24y	Central and South America	272.5012	12.5283	300.2	67	85.1
cssz-24z	Central and South America	272.4107	12.3767	300.2	67	39.07
cssz-25a	Central and South America	273.2075	11.5684	313.8	25	17.94
cssz-25b	Central and South America	272.9200	11.2746	313.8	15	5
cssz-25x	Central and South America	273.5950	11.9641	313.8	66	130.4
cssz-25y	Central and South America	273.4658	11.8322	313.8	66	84.75
cssz-25z	Central and South America	273.3366	11.7003	313.8	66	39.07
cssz-26a	Central and South America	273.8943	10.8402	320.4	25	17.94

Table B2: (continued)

Segment	Description	Longitude (°E)	Latitude (°N)	Strike (°)	Dip (°)	Depth (km)
cssz-26b	Central and South America	273.5750	10.5808	320.4	15	5
cssz-26x	Central and South America	274.3246	11.1894	320.4	66	130.4
cssz-26y	Central and South America	274.1811	11.0730	320.4	66	84.75
cssz-26z	Central and South America	274.0377	10.9566	320.4	66	39.07
cssz-27a	Central and South America	274.4569	10.2177	316.1	25	17.94
cssz-27b	Central and South America	274.1590	9.9354	316.1	15	5
cssz-27z	Central and South America	274.5907	10.3444	316.1	66	39.07
cssz-28a	Central and South America	274.9586	9.8695	297.1	22	14.54
cssz-28b	Central and South America	274.7661	9.4988	297.1	11	5
cssz-28z	Central and South America	275.1118	10.1643	297.1	42.5	33.27
cssz-29a	Central and South America	275.7686	9.4789	296.6	19	11.09
cssz-29b	Central and South America	275.5759	9.0992	296.6	7	5
cssz-30a	Central and South America	276.6346	8.9973	302.2	19	9.36
cssz-30b	Central and South America	276.4053	8.6381	302.2	5	5
cssz-31a	Central and South America	277.4554	8.4152	309.1	19	7.62
cssz-31b	Central and South America	277.1851	8.0854	309.1	3	5
cssz-31z	Central and South America	277.7260	8.7450	309.1	19	23.9
cssz-32a	Central and South America	278.1112	7.9425	303	18.67	8.49
cssz-32b	Central and South America	277.8775	7.5855	303	4	5
cssz-32z	Central and South America	278.3407	8.2927	303	21.67	24.49
cssz-33a	Central and South America	278.7082	7.6620	287.6	18.33	10.23
cssz-33b	Central and South America	278.5785	7.2555	287.6	6	5
cssz-33z	Central and South America	278.8328	8.0522	287.6	24.33	25.95
cssz-34a	Central and South America	279.3184	7.5592	269.5	18	17.94
cssz-34b	Central and South America	279.3223	7.1320	269.5	15	5
cssz-35a	Central and South America	280.0039	7.6543	255.9	17.67	14.54
cssz-35b	Central and South America	280.1090	7.2392	255.9	11	5
cssz-35x	Central and South America	279.7156	8.7898	255.9	29.67	79.22
cssz-35y	Central and South America	279.8118	8.4113	255.9	29.67	54.47
cssz-35z	Central and South America	279.9079	8.0328	255.9	29.67	29.72
cssz-36a	Central and South America	281.2882	7.6778	282.5	17.33	11.09
cssz-36b	Central and South America	281.1948	7.2592	282.5	7	5
cssz-36x	Central and South America	281.5368	8.7896	282.5	32.33	79.47
cssz-36y	Central and South America	281.4539	8.4190	282.5	32.33	52.73
cssz-36z	Central and South America	281.3710	8.0484	282.5	32.33	25.99
cssz-37a	Central and South America	282.5252	6.8289	326.9	17	10.23
cssz-37b	Central and South America	282.1629	6.5944	326.9	6	5
cssz-38a	Central and South America	282.9469	5.5973	355.4	17	10.23
cssz-38b	Central and South America	282.5167	5.5626	355.4	6	5

Table B2: (continued)

Segment	Description	Longitude (°E)	Latitude (°N)	Strike (°)	Dip (°)	Depth (km)
cssz-39a	Central and South America	282.7236	4.3108	24.13	17	10.23
cssz-39b	Central and South America	282.3305	4.4864	24.13	6	5
cssz-39z	Central and South America	283.0603	4.1604	24.13	35	24.85
cssz-40a	Central and South America	282.1940	3.3863	35.28	17	10.23
cssz-40b	Central and South America	281.8427	3.6344	35.28	6	5
cssz-40y	Central and South America	282.7956	2.9613	35.28	35	53.52
cssz-40z	Central and South America	282.4948	3.1738	35.28	35	24.85
cssz-41a	Central and South America	281.6890	2.6611	34.27	17	10.23
cssz-41b	Central and South America	281.3336	2.9030	34.27	6	5
cssz-41z	Central and South America	281.9933	2.4539	34.27	35	24.85
cssz-42a	Central and South America	281.2266	1.9444	31.29	17	10.23
cssz-42b	Central and South America	280.8593	2.1675	31.29	6	5
cssz-42z	Central and South America	281.5411	1.7533	31.29	35	24.85
cssz-43a	Central and South America	280.7297	1.1593	33.3	17	10.23
cssz-43b	Central and South America	280.3706	1.3951	33.3	6	5
cssz-43z	Central and South America	281.0373	0.9573	33.3	35	24.85
cssz-44a	Central and South America	280.3018	0.4491	28.8	17	10.23
cssz-44b	Central and South America	279.9254	0.6560	28.8	6	5
cssz-45a	Central and South America	279.9083	-0.3259	26.91	10	8.49
cssz-45b	Central and South America	279.5139	-0.1257	26.91	4	5
cssz-46a	Central and South America	279.6461	-0.9975	15.76	10	8.49
cssz-46b	Central and South America	279.2203	-0.8774	15.76	4	5
cssz-47a	Central and South America	279.4972	-1.7407	6.9	10	8.49
cssz-47b	Central and South America	279.0579	-1.6876	6.9	4	5
cssz-48a	Central and South America	279.3695	-2.6622	8.96	10	8.49
cssz-48b	Central and South America	278.9321	-2.5933	8.96	4	5
cssz-48y	Central and South America	280.2444	-2.8000	8.96	10	25.85
cssz-48z	Central and South America	279.8070	-2.7311	8.96	10	17.17
cssz-49a	Central and South America	279.1852	-3.6070	13.15	10	8.49
cssz-49b	Central and South America	278.7536	-3.5064	13.15	4	5
cssz-49y	Central and South America	280.0486	-3.8082	13.15	10	25.85
cssz-49z	Central and South America	279.6169	-3.7076	13.15	10	17.17
cssz-50a	Central and South America	279.0652	-4.3635	4.78	10.33	9.64
cssz-50b	Central and South America	278.6235	-4.3267	4.78	5.33	5
cssz-51a	Central and South America	279.0349	-5.1773	359.4	10.67	10.81
cssz-51b	Central and South America	278.5915	-5.1817	359.4	6.67	5
cssz-52a	Central and South America	279.1047	-5.9196	349.8	11	11.96
cssz-52b	Central and South America	278.6685	-5.9981	349.8	8	5
cssz-53a	Central and South America	279.3044	-6.6242	339.2	10.25	11.74

Table B2: (continued)

Segment	Description	Longitude (°E)	Latitude (°N)	Strike (°)	Dip (°)	Depth (km)
cssz-53b	Central and South America	278.8884	-6.7811	339.2	7.75	5
cssz-53y	Central and South America	280.1024	-6.3232	339.2	19.25	37.12
cssz-53z	Central and South America	279.7035	-6.4737	339.2	19.25	20.64
cssz-54a	Central and South America	279.6256	-7.4907	340.8	9.5	11.53
cssz-54b	Central and South America	279.2036	-7.6365	340.8	7.5	5
cssz-54y	Central and South America	280.4267	-7.2137	340.8	20.5	37.29
cssz-54z	Central and South America	280.0262	-7.3522	340.8	20.5	19.78
cssz-55a	Central and South America	279.9348	-8.2452	335.4	8.75	11.74
cssz-55b	Central and South America	279.5269	-8.4301	335.4	7.75	5
cssz-55x	Central and South America	281.0837	-7.7238	335.4	21.75	56.4
cssz-55y	Central and South America	280.7009	-7.8976	335.4	21.75	37.88
cssz-55z	Central and South America	280.3180	-8.0714	335.4	21.75	19.35
cssz-56a	Central and South America	280.3172	-8.9958	331.6	8	11.09
cssz-56b	Central and South America	279.9209	-9.2072	331.6	7	5
cssz-56x	Central and South America	281.4212	-8.4063	331.6	23	57.13
cssz-56y	Central and South America	281.0534	-8.6028	331.6	23	37.59
cssz-56z	Central and South America	280.6854	-8.7993	331.6	23	18.05
cssz-57a	Central and South America	280.7492	-9.7356	328.7	8.6	10.75
cssz-57b	Central and South America	280.3640	-9.9663	328.7	6.6	5
cssz-57x	Central and South America	281.8205	-9.0933	328.7	23.4	57.94
cssz-57y	Central and South America	281.4636	-9.3074	328.7	23.4	38.08
cssz-57z	Central and South America	281.1065	-9.5215	328.7	23.4	18.22
cssz-58a	Central and South America	281.2275	-10.5350	330.5	9.2	10.4
cssz-58b	Central and South America	280.8348	-10.7532	330.5	6.2	5
cssz-58y	Central and South America	281.9548	-10.1306	330.5	23.8	38.57
cssz-58z	Central and South America	281.5913	-10.3328	330.5	23.8	18.39
cssz-59a	Central and South America	281.6735	-11.2430	326.2	9.8	10.05
cssz-59b	Central and South America	281.2982	-11.4890	326.2	5.8	5
cssz-59y	Central and South America	282.3675	-10.7876	326.2	24.2	39.06
cssz-59z	Central and South America	282.0206	-11.0153	326.2	24.2	18.56
cssz-60a	Central and South America	282.1864	-11.9946	326.5	10.4	9.71
cssz-60b	Central and South America	281.8096	-12.2384	326.5	5.4	5
cssz-60y	Central and South America	282.8821	-11.5438	326.5	24.6	39.55
cssz-60z	Central and South America	282.5344	-11.7692	326.5	24.6	18.73
cssz-61a	Central and South America	282.6944	-12.7263	325.5	11	9.36
cssz-61b	Central and South America	282.3218	-12.9762	325.5	5	5
cssz-61y	Central and South America	283.3814	-12.2649	325.5	25	40.03
cssz-61z	Central and South America	283.0381	-12.4956	325.5	25	18.9
cssz-62a	Central and South America	283.1980	-13.3556	319	11	9.79

Table B2: (continued)

Segment	Description	Longitude (°E)	Latitude (°N)	Strike (°)	Dip (°)	Depth (km)
cssz-62b	Central and South America	282.8560	-13.6451	319	5.5	5
cssz-62y	Central and South America	283.8178	-12.8300	319	27	42.03
cssz-62z	Central and South America	283.5081	-13.0928	319	27	19.33
cssz-63a	Central and South America	283.8032	-14.0147	317.9	11	10.23
cssz-63b	Central and South America	283.4661	-14.3106	317.9	6	5
cssz-63z	Central and South America	284.1032	-13.7511	317.9	29	19.77
cssz-64a	Central and South America	284.4144	-14.6482	315.7	13	11.96
cssz-64b	Central and South America	284.0905	-14.9540	315.7	8	5
cssz-65a	Central and South America	285.0493	-15.2554	313.2	15	13.68
cssz-65b	Central and South America	284.7411	-15.5715	313.2	10	5
cssz-66a	Central and South America	285.6954	-15.7816	307.7	14.5	13.68
cssz-66b	Central and South America	285.4190	-16.1258	307.7	10	5
cssz-67a	Central and South America	286.4127	-16.2781	304.3	14	13.68
cssz-67b	Central and South America	286.1566	-16.6381	304.3	10	5
cssz-67z	Central and South America	286.6552	-15.9365	304.3	23	25.78
cssz-68a	Central and South America	287.2481	-16.9016	311.8	14	13.68
cssz-68b	Central and South America	286.9442	-17.2264	311.8	10	5
cssz-68z	Central and South America	287.5291	-16.6007	311.8	26	25.78
cssz-69a	Central and South America	287.9724	-17.5502	314.9	14	13.68
cssz-69b	Central and South America	287.6496	-17.8590	314.9	10	5
cssz-69y	Central and South America	288.5530	-16.9934	314.9	29	50.02
cssz-69z	Central and South America	288.2629	-17.2718	314.9	29	25.78
cssz-70a	Central and South America	288.6731	-18.2747	320.4	14	13.25
cssz-70b	Central and South America	288.3193	-18.5527	320.4	9.5	5
cssz-70y	Central and South America	289.3032	-17.7785	320.4	30	50.35
cssz-70z	Central and South America	288.9884	-18.0266	320.4	30	25.35
cssz-71a	Central and South America	289.3089	-19.1854	333.2	14	12.82
cssz-71b	Central and South America	288.8968	-19.3820	333.2	9	5
cssz-71y	Central and South America	290.0357	-18.8382	333.2	31	50.67
cssz-71z	Central and South America	289.6725	-19.0118	333.2	31	24.92
cssz-72a	Central and South America	289.6857	-20.3117	352.4	14	12.54
cssz-72b	Central and South America	289.2250	-20.3694	352.4	8.67	5
cssz-72z	Central and South America	290.0882	-20.2613	352.4	32	24.63
cssz-73a	Central and South America	289.7731	-21.3061	358.9	14	12.24
cssz-73b	Central and South America	289.3053	-21.3142	358.9	8.33	5
cssz-73z	Central and South America	290.1768	-21.2991	358.9	33	24.34
cssz-74a	Central and South America	289.7610	-22.2671	3.06	14	11.96
cssz-74b	Central and South America	289.2909	-22.2438	3.06	8	5

Table B2: (continued)

Segment	Description	Longitude (°E)	Latitude (°N)	Strike (°)	Dip (°)	Depth (km)
cssz-75a	Central and South America	289.6982	-23.1903	4.83	14.09	11.96
cssz-75b	Central and South America	289.2261	-23.1536	4.83	8	5
cssz-76a	Central and South America	289.6237	-24.0831	4.67	14.18	11.96
cssz-76b	Central and South America	289.1484	-24.0476	4.67	8	5
cssz-77a	Central and South America	289.5538	-24.9729	4.3	14.27	11.96
cssz-77b	Central and South America	289.0750	-24.9403	4.3	8	5
cssz-78a	Central and South America	289.4904	-25.8621	3.86	14.36	11.96
cssz-78b	Central and South America	289.0081	-25.8328	3.86	8	5
cssz-79a	Central and South America	289.3491	-26.8644	11.34	14.45	11.96
cssz-79b	Central and South America	288.8712	-26.7789	11.34	8	5
cssz-80a	Central and South America	289.1231	-27.7826	14.16	14.54	11.96
cssz-80b	Central and South America	288.6469	-27.6762	14.16	8	5
cssz-81a	Central and South America	288.8943	-28.6409	13.19	14.63	11.96
cssz-81b	Central and South America	288.4124	-28.5417	13.19	8	5
cssz-82a	Central and South America	288.7113	-29.4680	9.68	14.72	11.96
cssz-82b	Central and South America	288.2196	-29.3950	9.68	8	5
cssz-83a	Central and South America	288.5944	-30.2923	5.36	14.81	11.96
cssz-83b	Central and South America	288.0938	-30.2517	5.36	8	5
cssz-84a	Central and South America	288.5223	-31.1639	3.8	14.9	11.96
cssz-84b	Central and South America	288.0163	-31.1351	3.8	8	5
cssz-85a	Central and South America	288.4748	-32.0416	2.55	15	11.96
cssz-85b	Central and South America	287.9635	-32.0223	2.55	8	5
cssz-86a	Central and South America	288.3901	-33.0041	7.01	15	11.96
cssz-86b	Central and South America	287.8768	-32.9512	7.01	8	5
cssz-87a	Central and South America	288.1050	-34.0583	19.4	15	11.96
cssz-87b	Central and South America	287.6115	-33.9142	19.4	8	5
cssz-88a	Central and South America	287.5309	-35.0437	32.81	15	11.96
cssz-88b	Central and South America	287.0862	-34.8086	32.81	8	5
cssz-88z	Central and South America	287.9308	-35.2545	32.81	30	24.9
cssz-89a	Central and South America	287.2380	-35.5993	14.52	16.67	11.96
cssz-89b	Central and South America	286.7261	-35.4914	14.52	8	5
cssz-89z	Central and South America	287.7014	-35.6968	14.52	30	26.3
cssz-90a	Central and South America	286.8442	-36.5645	22.64	18.33	11.96
cssz-90b	Central and South America	286.3548	-36.4004	22.64	8	5
cssz-90z	Central and South America	287.2916	-36.7142	22.64	30	27.68
cssz-91a	Central and South America	286.5925	-37.2488	10.9	20	11.96
cssz-91b	Central and South America	286.0721	-37.1690	10.9	8	5
cssz-91z	Central and South America	287.0726	-37.3224	10.9	30	29.06

Table B2: (continued)

Segment	Description	Longitude (°E)	Latitude (°N)	Strike (°)	Dip (°)	Depth (km)
cssz-92a	Central and South America	286.4254	-38.0945	8.23	20	11.96
cssz-92b	Central and South America	285.8948	-38.0341	8.23	8	5
cssz-92z	Central and South America	286.9303	-38.1520	8.23	26.67	29.06
cssz-93a	Central and South America	286.2047	-39.0535	13.46	20	11.96
cssz-93b	Central and South America	285.6765	-38.9553	13.46	8	5
cssz-93z	Central and South America	286.7216	-39.1495	13.46	23.33	29.06
cssz-94a	Central and South America	286.0772	-39.7883	3.4	20	11.96
cssz-94b	Central and South America	285.5290	-39.7633	3.4	8	5
cssz-94z	Central and South America	286.6255	-39.8133	3.4	20	29.06
cssz-95a	Central and South America	285.9426	-40.7760	9.84	20	11.96
cssz-95b	Central and South America	285.3937	-40.7039	9.84	8	5
cssz-95z	Central and South America	286.4921	-40.8481	9.84	20	29.06
cssz-96a	Central and South America	285.7839	-41.6303	7.6	20	11.96
cssz-96b	Central and South America	285.2245	-41.5745	7.6	8	5
cssz-96x	Central and South America	287.4652	-41.7977	7.6	20	63.26
cssz-96y	Central and South America	286.9043	-41.7419	7.6	20	46.16
cssz-96z	Central and South America	286.3439	-41.6861	7.6	20	29.06
cssz-97a	Central and South America	285.6695	-42.4882	5.3	20	11.96
cssz-97b	Central and South America	285.0998	-42.4492	5.3	8	5
cssz-97x	Central and South America	287.3809	-42.6052	5.3	20	63.26
cssz-97y	Central and South America	286.8101	-42.5662	5.3	20	46.16
cssz-97z	Central and South America	286.2396	-42.5272	5.3	20	29.06
cssz-98a	Central and South America	285.5035	-43.4553	10.53	20	11.96
cssz-98b	Central and South America	284.9322	-43.3782	10.53	8	5
cssz-98x	Central and South America	287.2218	-43.6866	10.53	20	63.26
cssz-98y	Central and South America	286.6483	-43.6095	10.53	20	46.16
cssz-98z	Central and South America	286.0755	-43.5324	10.53	20	29.06
cssz-99a	Central and South America	285.3700	-44.2595	4.86	20	11.96
cssz-99b	Central and South America	284.7830	-44.2237	4.86	8	5
cssz-99x	Central and South America	287.1332	-44.3669	4.86	20	63.26
cssz-99y	Central and South America	286.5451	-44.3311	4.86	20	46.16
cssz-99z	Central and South America	285.9574	-44.2953	4.86	20	29.06
cssz-100a	Central and South America	285.2713	-45.1664	5.68	20	11.96
cssz-100b	Central and South America	284.6758	-45.1246	5.68	8	5
cssz-100x	Central and South America	287.0603	-45.2918	5.68	20	63.26
cssz-100y	Central and South America	286.4635	-45.2500	5.68	20	46.16
cssz-100z	Central and South America	285.8672	-45.2082	5.68	20	29.06
cssz-101a	Central and South America	285.3080	-45.8607	352.6	20	9.36

Table B2: (continued)

Segment	Description	Longitude (°E)	Latitude (°N)	Strike (°)	Dip (°)	Depth (km)
cssz-101b	Central and South America	284.7067	-45.9152	352.6	5	5
cssz-101y	Central and South America	286.5089	-45.7517	352.6	20	43.56
cssz-101z	Central and South America	285.9088	-45.8062	352.6	20	26.46
cssz-102a	Central and South America	285.2028	-47.1185	17.72	5	9.36
cssz-102b	Central and South America	284.5772	-46.9823	17.72	5	5
cssz-102y	Central and South America	286.4588	-47.3909	17.72	5	18.07
cssz-102z	Central and South America	285.8300	-47.2547	17.72	5	13.72
cssz-103a	Central and South America	284.7075	-48.0396	23.37	7.5	11.53
cssz-103b	Central and South America	284.0972	-47.8630	23.37	7.5	5
cssz-103x	Central and South America	286.5511	-48.5694	23.37	7.5	31.11
cssz-103y	Central and South America	285.9344	-48.3928	23.37	7.5	24.58
cssz-103z	Central and South America	285.3199	-48.2162	23.37	7.5	18.05
cssz-104a	Central and South America	284.3440	-48.7597	14.87	10	13.68
cssz-104b	Central and South America	283.6962	-48.6462	14.87	10	5
cssz-104x	Central and South America	286.2962	-49.1002	14.87	10	39.73
cssz-104y	Central and South America	285.6440	-48.9867	14.87	10	31.05
cssz-104z	Central and South America	284.9933	-48.8732	14.87	10	22.36
cssz-105a	Central and South America	284.2312	-49.4198	0.25	9.67	13.4
cssz-105b	Central and South America	283.5518	-49.4179	0.25	9.67	5
cssz-105x	Central and South America	286.2718	-49.4255	0.25	9.67	38.59
cssz-105y	Central and South America	285.5908	-49.4236	0.25	9.67	30.2
cssz-105z	Central and South America	284.9114	-49.4217	0.25	9.67	21.8
cssz-106a	Central and South America	284.3730	-50.1117	347.5	9.25	13.04
cssz-106b	Central and South America	283.6974	-50.2077	347.5	9.25	5
cssz-106x	Central and South America	286.3916	-49.8238	347.5	9.25	37.15
cssz-106y	Central and South America	285.7201	-49.9198	347.5	9.25	29.11
cssz-106z	Central and South America	285.0472	-50.0157	347.5	9.25	21.07
cssz-107a	Central and South America	284.7130	-50.9714	346.5	9	12.82
cssz-107b	Central and South America	284.0273	-51.0751	346.5	9	5
cssz-107x	Central and South America	286.7611	-50.6603	346.5	9	36.29
cssz-107y	Central and South America	286.0799	-50.7640	346.5	9	28.47
cssz-107z	Central and South America	285.3972	-50.8677	346.5	9	20.64
cssz-108a	Central and South America	285.0378	-51.9370	352	8.67	12.54
cssz-108b	Central and South America	284.3241	-51.9987	352	8.67	5
cssz-108x	Central and South America	287.1729	-51.7519	352	8.67	35.15
cssz-108y	Central and South America	286.4622	-51.8136	352	8.67	27.61
cssz-108z	Central and South America	285.7505	-51.8753	352	8.67	20.07
cssz-109a	Central and South America	285.2635	-52.8439	353.1	8.33	12.24
cssz-109b	Central and South America	284.5326	-52.8974	353.1	8.33	5

Table B2: (continued)

Segment	Description	Longitude (°E)	Latitude (°N)	Strike (°)	Dip (°)	Depth (km)
cssz-109x	Central and South America	287.4508	-52.6834	353.1	8.33	33.97
cssz-109y	Central and South America	286.7226	-52.7369	353.1	8.33	26.73
cssz-109z	Central and South America	285.9935	-52.7904	353.1	8.33	19.49
cssz-110a	Central and South America	285.5705	-53.4139	334.2	8	11.96
cssz-110b	Central and South America	284.8972	-53.6076	334.2	8	5
cssz-110x	Central and South America	287.5724	-52.8328	334.2	8	32.83
cssz-110y	Central and South America	286.9081	-53.0265	334.2	8	25.88
cssz-110z	Central and South America	286.2408	-53.2202	334.2	8	18.92
cssz-111a	Central and South America	286.1627	-53.8749	313.8	8	11.96
cssz-111b	Central and South America	285.6382	-54.1958	313.8	8	5
cssz-111x	Central and South America	287.7124	-52.9122	313.8	8	32.83
cssz-111y	Central and South America	287.1997	-53.2331	313.8	8	25.88
cssz-111z	Central and South America	286.6832	-53.5540	313.8	8	18.92
cssz-112a	Central and South America	287.3287	-54.5394	316.4	8	11.96
cssz-112b	Central and South America	286.7715	-54.8462	316.4	8	5
cssz-112x	Central and South America	288.9756	-53.6190	316.4	8	32.83
cssz-112y	Central and South America	288.4307	-53.9258	316.4	8	25.88
cssz-112z	Central and South America	287.8817	-54.2326	316.4	8	18.92
cssz-113a	Central and South America	288.3409	-55.0480	307.6	8	11.96
cssz-113b	Central and South America	287.8647	-55.4002	307.6	8	5
cssz-113x	Central and South America	289.7450	-53.9914	307.6	8	32.83
cssz-113y	Central and South America	289.2810	-54.3436	307.6	8	25.88
cssz-113z	Central and South America	288.8130	-54.6958	307.6	8	18.92
cssz-114a	Central and South America	289.5342	-55.5026	301.5	8	11.96
cssz-114b	Central and South America	289.1221	-55.8819	301.5	8	5
cssz-114x	Central and South America	290.7472	-54.3647	301.5	8	32.83
cssz-114y	Central and South America	290.3467	-54.7440	301.5	8	25.88
cssz-114z	Central and South America	289.9424	-55.1233	301.5	8	18.92
cssz-115a	Central and South America	290.7682	-55.8485	292.7	8	11.96
cssz-115b	Central and South America	290.4608	-56.2588	292.7	8	5
cssz-115x	Central and South America	291.6714	-54.6176	292.7	8	32.83
cssz-115y	Central and South America	291.3734	-55.0279	292.7	8	25.88
cssz-115z	Central and South America	291.0724	-55.4382	292.7	8	18.92
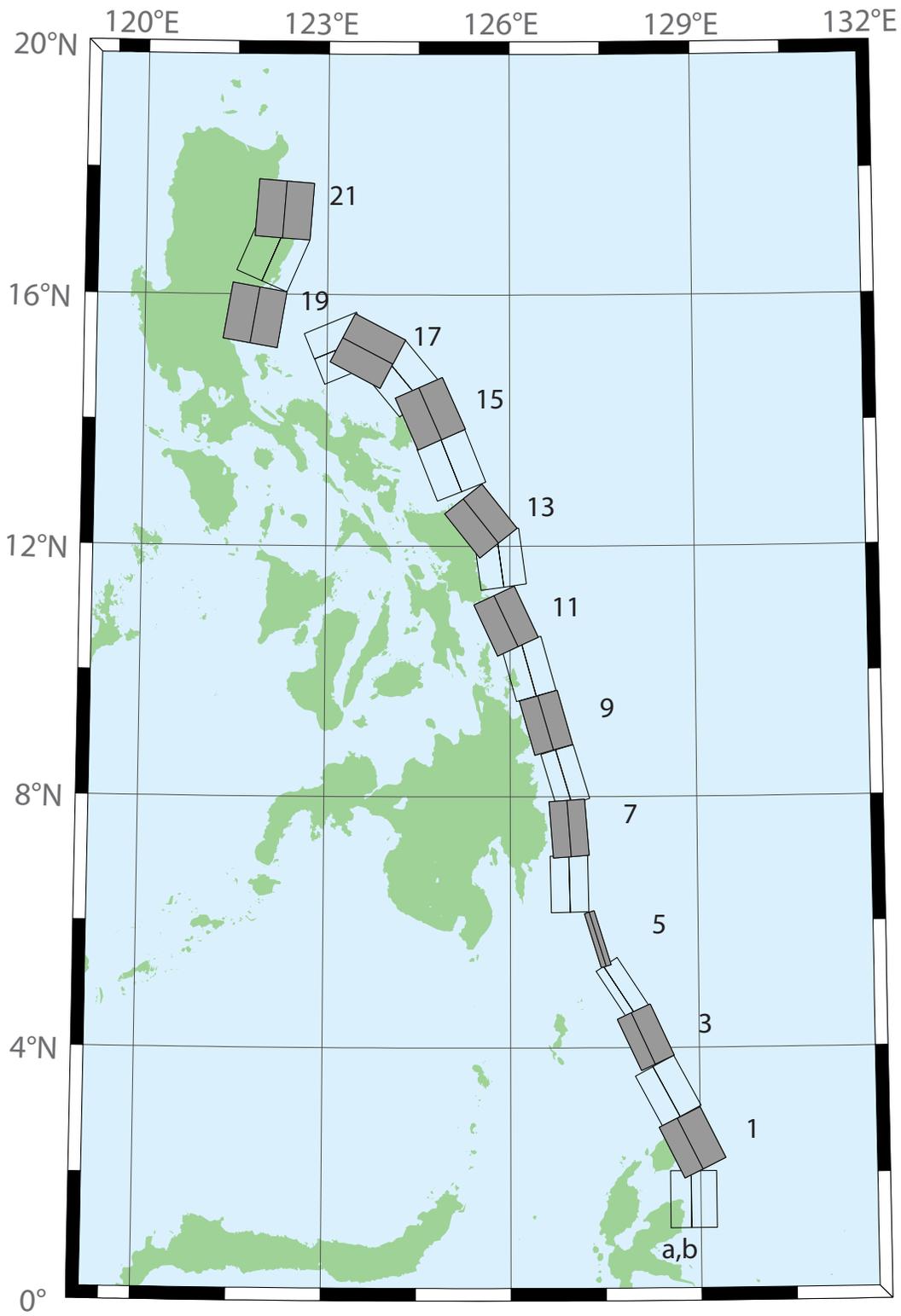
Figure B3: Eastern Philippines Subduction Zone unit sources.

Table B3: Earthquake parameters for Eastern Philippines Subduction Zone unit sources.

Segment	Description	Longitude (°E)	Latitude (°N)	Strike (°)	Dip (°)	Depth (km)
epsz-0a	Eastern Philippines	128.5264	1.5930	180	44	26.92
epsz-0b	Eastern Philippines	128.8496	1.5930	180	26	5
epsz-1a	Eastern Philippines	128.5521	2.3289	153.6	44.2	27.62
epsz-1b	Eastern Philippines	128.8408	2.4720	153.6	26.9	5
epsz-2a	Eastern Philippines	128.1943	3.1508	151.9	45.9	32.44
epsz-2b	Eastern Philippines	128.4706	3.2979	151.9	32.8	5.35
epsz-3a	Eastern Philippines	127.8899	4.0428	155.2	57.3	40.22
epsz-3b	Eastern Philippines	128.1108	4.1445	155.2	42.7	6.31
epsz-4a	Eastern Philippines	127.6120	4.8371	146.8	71.4	48.25
epsz-4b	Eastern Philippines	127.7324	4.9155	146.8	54.8	7.39
epsz-5a	Eastern Philippines	127.3173	5.7040	162.9	79.9	57.4
epsz-5b	Eastern Philippines	127.3930	5.7272	162.9	79.4	8.25
epsz-6a	Eastern Philippines	126.6488	6.6027	178.9	48.6	45.09
epsz-6b	Eastern Philippines	126.9478	6.6085	178.9	48.6	7.58
epsz-7a	Eastern Philippines	126.6578	7.4711	175.8	50.7	45.52
epsz-7b	Eastern Philippines	126.9439	7.4921	175.8	50.7	6.83
epsz-8a	Eastern Philippines	126.6227	8.2456	163.3	56.7	45.6
epsz-8b	Eastern Philippines	126.8614	8.3164	163.3	48.9	7.92
epsz-9a	Eastern Philippines	126.2751	9.0961	164.1	47	43.59
epsz-9b	Eastern Philippines	126.5735	9.1801	164.1	44.9	8.3
epsz-10a	Eastern Philippines	125.9798	9.9559	164.5	43.1	42.25
epsz-10b	Eastern Philippines	126.3007	10.0438	164.5	43.1	8.09
epsz-11a	Eastern Philippines	125.6079	10.6557	155	37.8	38.29
epsz-11b	Eastern Philippines	125.9353	10.8059	155	37.8	7.64
epsz-12a	Eastern Philippines	125.4697	11.7452	172.1	36	37.01
epsz-12b	Eastern Philippines	125.8374	11.7949	172.1	36	7.62
epsz-13a	Eastern Philippines	125.2238	12.1670	141.5	32.4	33.87
epsz-13b	Eastern Philippines	125.5278	12.4029	141.5	32.4	7.08
epsz-14a	Eastern Philippines	124.6476	13.1365	158.2	23	25.92
epsz-14b	Eastern Philippines	125.0421	13.2898	158.2	23	6.38
epsz-15a	Eastern Philippines	124.3107	13.9453	156.1	24.1	26.51
epsz-15b	Eastern Philippines	124.6973	14.1113	156.1	24.1	6.09
epsz-16a	Eastern Philippines	123.8998	14.4025	140.3	19.5	21.69
epsz-16b	Eastern Philippines	124.2366	14.6728	140.3	19.5	5
epsz-17a	Eastern Philippines	123.4604	14.7222	117.6	15.3	18.19
epsz-17b	Eastern Philippines	123.6682	15.1062	117.6	15.3	5
epsz-18a	Eastern Philippines	123.3946	14.7462	67.4	15	17.94
epsz-18b	Eastern Philippines	123.2219	15.1467	67.4	15	5
epsz-19a	Eastern Philippines	121.3638	15.7400	189.6	15	17.94
epsz-19b	Eastern Philippines	121.8082	15.6674	189.6	15	5
epsz-20a	Eastern Philippines	121.6833	16.7930	203.3	15	17.94
epsz-20b	Eastern Philippines	122.0994	16.6216	203.3	15	5
epsz-21a	Eastern Philippines	121.8279	17.3742	184.2	15	17.94
epsz-21b	Eastern Philippines	122.2814	17.3425	184.2	15	5
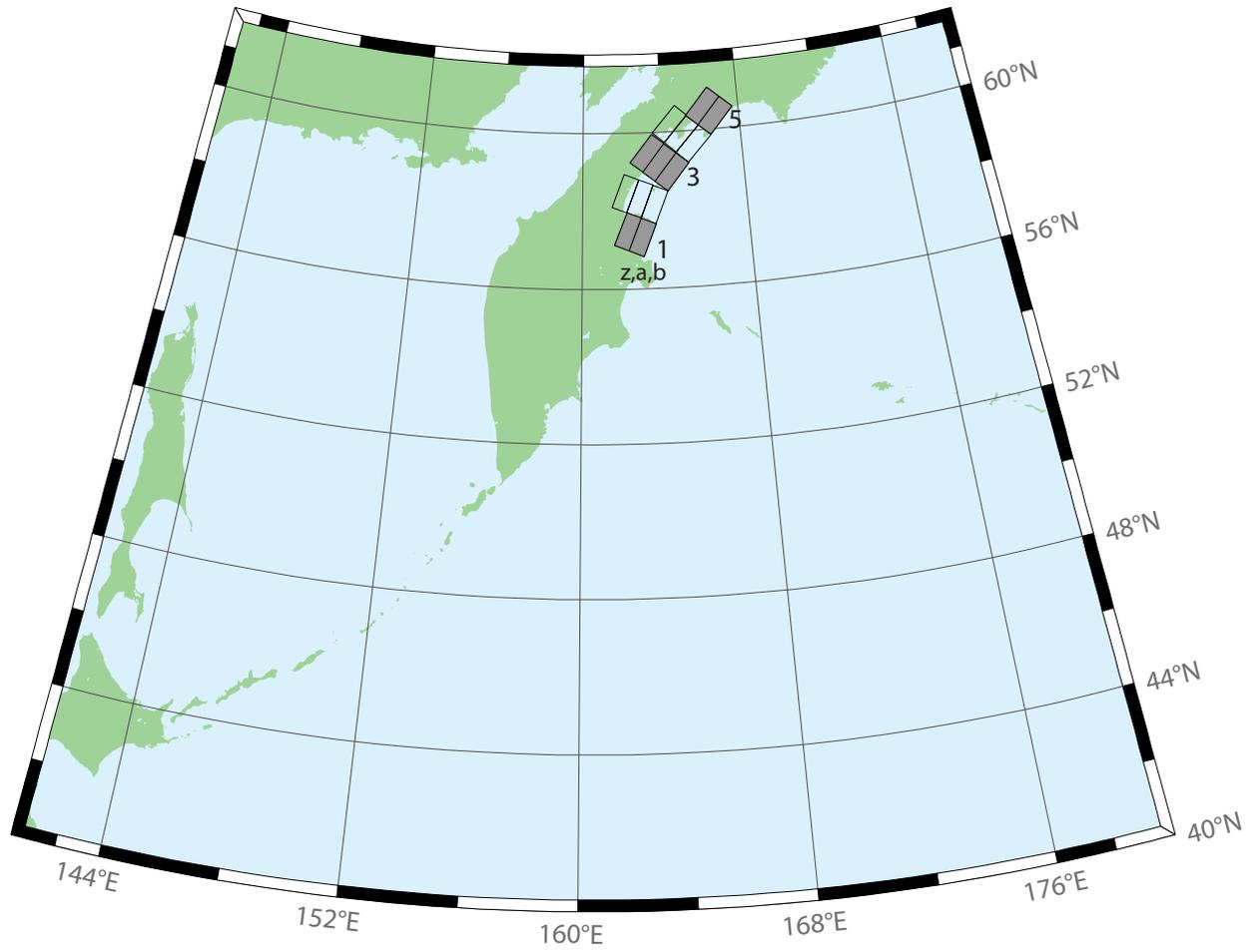
Figure B4: Kamchatka–Bering Subduction Zone unit sources.

Table B4: Earthquake parameters for Kamchatka–Bering Subduction Zone unit sources.

Segment	Description	Longitude (°E)	Latitude (°N)	Strike (°)	Dip (°)	Depth (km)
kbsz-1a	Kamchatka-Bering	161.8374	57.5485	201.5	29	26.13
kbsz-1b	Kamchatka-Bering	162.5162	57.4030	202.1	25	5
kbsz-2a	Kamchatka-Bering	162.4410	58.3816	201.7	29	26.13
kbsz-2b	Kamchatka-Bering	163.1344	58.2343	202.3	25	5
kbsz-2z	Kamchatka-Bering	161.7418	58.5249	201.1	29	50.37
kbsz-3a	Kamchatka-Bering	163.5174	59.3493	218.9	29	26.13
kbsz-3b	Kamchatka-Bering	164.1109	59.1001	219.4	25	5
kbsz-3z	Kamchatka-Bering	162.9150	59.5958	218.4	29	50.37
kbsz-4a	Kamchatka-Bering	164.7070	60.0632	222.2	29	26.13
kbsz-4b	Kamchatka-Bering	165.2833	59.7968	222.7	25	5
kbsz-4z	Kamchatka-Bering	164.1212	60.3270	221.7	29	50.37
kbsz-5a	Kamchatka-Bering	165.8652	60.7261	220.5	29	26.13
kbsz-5b	Kamchatka-Bering	166.4692	60.4683	221	25	5
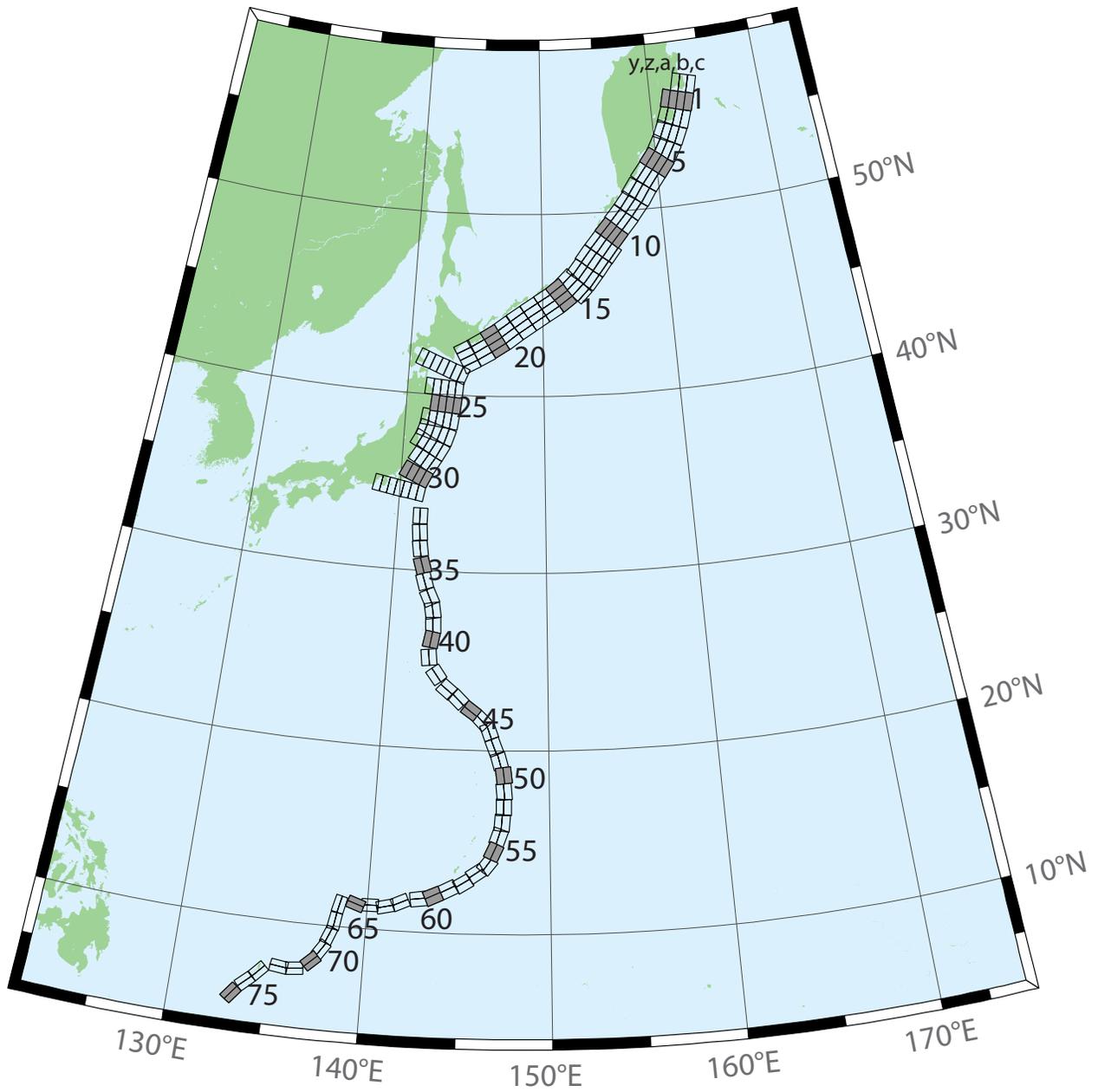
Figure B5: Kamchatka–Kuril–Japan–Izu–Mariana–Yap Subduction Zone unit sources.

Table B5: Earthquake parameters for Kamchatka-Kuril-Japan-Izu-Mariana-Yap Subduction Zone unit sources.

Segment	Description	Longitude (°E)	Latitude (°N)	Strike (°)	Dip (°)	Depth (km)
kisz-0a	Kamchatka-Kuril-Japan-Izu-Mariana-Yap	162.8200	56.3667	194.4	29	26.13
kisz-0b	Kamchatka-Kuril-Japan-Izu-Mariana-Yap	163.5057	56.2677	195	25	5
kisz-0z	Kamchatka-Kuril-Japan-Izu-Mariana-Yap	162.1309	56.4618	193.8	29	50.37
kisz-1a	Kamchatka-Kuril-Japan-Izu-Mariana-Yap	162.4318	55.5017	195	29	26.13
kisz-1b	Kamchatka-Kuril-Japan-Izu-Mariana-Yap	163.1000	55.4000	195	25	5
kisz-1y	Kamchatka-Kuril-Japan-Izu-Mariana-Yap	161.0884	55.7050	195	29	74.61
kisz-1z	Kamchatka-Kuril-Japan-Izu-Mariana-Yap	161.7610	55.6033	195	29	50.37
kisz-2a	Kamchatka-Kuril-Japan-Izu-Mariana-Yap	161.9883	54.6784	200	29	26.13
kisz-2b	Kamchatka-Kuril-Japan-Izu-Mariana-Yap	162.6247	54.5440	200	25	5
kisz-2y	Kamchatka-Kuril-Japan-Izu-Mariana-Yap	160.7072	54.9471	200	29	74.61
kisz-2z	Kamchatka-Kuril-Japan-Izu-Mariana-Yap	161.3488	54.8127	200	29	50.37
kisz-3a	Kamchatka-Kuril-Japan-Izu-Mariana-Yap	161.4385	53.8714	204	29	26.13
kisz-3b	Kamchatka-Kuril-Japan-Izu-Mariana-Yap	162.0449	53.7116	204	25	5
kisz-3y	Kamchatka-Kuril-Japan-Izu-Mariana-Yap	160.2164	54.1910	204	29	74.61
kisz-3z	Kamchatka-Kuril-Japan-Izu-Mariana-Yap	160.8286	54.0312	204	29	50.37
kisz-4a	Kamchatka-Kuril-Japan-Izu-Mariana-Yap	160.7926	53.1087	210	29	26.13
kisz-4b	Kamchatka-Kuril-Japan-Izu-Mariana-Yap	161.3568	52.9123	210	25	5
kisz-4y	Kamchatka-Kuril-Japan-Izu-Mariana-Yap	159.6539	53.5015	210	29	74.61
kisz-4z	Kamchatka-Kuril-Japan-Izu-Mariana-Yap	160.2246	53.3051	210	29	50.37
kisz-5a	Kamchatka-Kuril-Japan-Izu-Mariana-Yap	160.0211	52.4113	218	29	26.13
kisz-5b	Kamchatka-Kuril-Japan-Izu-Mariana-Yap	160.5258	52.1694	218	25	5
kisz-5y	Kamchatka-Kuril-Japan-Izu-Mariana-Yap	159.0005	52.8950	218	29	74.61
kisz-5z	Kamchatka-Kuril-Japan-Izu-Mariana-Yap	159.5122	52.6531	218	29	50.37
kisz-6a	Kamchatka-Kuril-Japan-Izu-Mariana-Yap	159.1272	51.7034	218	29	26.13
kisz-6b	Kamchatka-Kuril-Japan-Izu-Mariana-Yap	159.6241	51.4615	218	25	5
kisz-6y	Kamchatka-Kuril-Japan-Izu-Mariana-Yap	158.1228	52.1871	218	29	74.61
kisz-6z	Kamchatka-Kuril-Japan-Izu-Mariana-Yap	158.6263	51.9452	218	29	50.37
kisz-7a	Kamchatka-Kuril-Japan-Izu-Mariana-Yap	158.2625	50.9549	214	29	26.13
kisz-7b	Kamchatka-Kuril-Japan-Izu-Mariana-Yap	158.7771	50.7352	214	25	5
kisz-7y	Kamchatka-Kuril-Japan-Izu-Mariana-Yap	157.2236	51.3942	214	29	74.61
kisz-7z	Kamchatka-Kuril-Japan-Izu-Mariana-Yap	157.7443	51.1745	214	29	50.37
kisz-8a	Kamchatka-Kuril-Japan-Izu-Mariana-Yap	157.4712	50.2459	218	31	27.7
kisz-8b	Kamchatka-Kuril-Japan-Izu-Mariana-Yap	157.9433	50.0089	218	27	5
kisz-8y	Kamchatka-Kuril-Japan-Izu-Mariana-Yap	156.5176	50.7199	218	31	79.2
kisz-8z	Kamchatka-Kuril-Japan-Izu-Mariana-Yap	156.9956	50.4829	218	31	53.45
kisz-9a	Kamchatka-Kuril-Japan-Izu-Mariana-Yap	156.6114	49.5583	220	31	27.7
kisz-9b	Kamchatka-Kuril-Japan-Izu-Mariana-Yap	157.0638	49.3109	220	27	5
kisz-9y	Kamchatka-Kuril-Japan-Izu-Mariana-Yap	155.6974	50.0533	220	31	79.2
kisz-9z	Kamchatka-Kuril-Japan-Izu-Mariana-Yap	156.1556	49.8058	220	31	53.45

Table B5: (continued)

Segment	Description	Longitude (°E)	Latitude (°N)	Strike (°)	Dip (°)	Depth (km)
kisz-10a	Kamchatka-Kuril-Japan-Izu-Mariana-Yap	155.7294	48.8804	221	31	27.7
kisz-10b	Kamchatka-Kuril-Japan-Izu-Mariana-Yap	156.1690	48.6278	221	27	5
kisz-10y	Kamchatka-Kuril-Japan-Izu-Mariana-Yap	154.8413	49.3856	221	31	79.2
kisz-10z	Kamchatka-Kuril-Japan-Izu-Mariana-Yap	155.2865	49.1330	221	31	53.45
kisz-11a	Kamchatka-Kuril-Japan-Izu-Mariana-Yap	154.8489	48.1821	219	31	27.7
kisz-11b	Kamchatka-Kuril-Japan-Izu-Mariana-Yap	155.2955	47.9398	219	27	5
kisz-11y	Kamchatka-Kuril-Japan-Izu-Mariana-Yap	153.9472	48.6667	219	31	79.2
kisz-11z	Kamchatka-Kuril-Japan-Izu-Mariana-Yap	154.3991	48.4244	219	31	53.45
kisz-11c	Kamchatka-Kuril-Japan-Izu-Mariana-Yap	156.0358	47.5374	39	57.89	4.602
kisz-12a	Kamchatka-Kuril-Japan-Izu-Mariana-Yap	153.9994	47.4729	217	31	27.7
kisz-12b	Kamchatka-Kuril-Japan-Izu-Mariana-Yap	154.4701	47.2320	217	27	5
kisz-12y	Kamchatka-Kuril-Japan-Izu-Mariana-Yap	153.0856	47.9363	217	31	79.2
kisz-12z	Kamchatka-Kuril-Japan-Izu-Mariana-Yap	153.5435	47.7046	217	31	53.45
kisz-12c	Kamchatka-Kuril-Japan-Izu-Mariana-Yap	155.2208	46.8473	37	57.89	4.602
kisz-13a	Kamchatka-Kuril-Japan-Izu-Mariana-Yap	153.2239	46.7564	218	31	27.7
kisz-13b	Kamchatka-Kuril-Japan-Izu-Mariana-Yap	153.6648	46.5194	218	27	5
kisz-13y	Kamchatka-Kuril-Japan-Izu-Mariana-Yap	152.3343	47.2304	218	31	79.2
kisz-13z	Kamchatka-Kuril-Japan-Izu-Mariana-Yap	152.7801	46.9934	218	31	53.45
kisz-13c	Kamchatka-Kuril-Japan-Izu-Mariana-Yap	154.3957	46.1257	38	57.89	4.602
kisz-14a	Kamchatka-Kuril-Japan-Izu-Mariana-Yap	152.3657	46.1514	225	23	24.54
kisz-14b	Kamchatka-Kuril-Japan-Izu-Mariana-Yap	152.7855	45.8591	225	23	5
kisz-14y	Kamchatka-Kuril-Japan-Izu-Mariana-Yap	151.5172	46.7362	225	23	63.62
kisz-14z	Kamchatka-Kuril-Japan-Izu-Mariana-Yap	151.9426	46.4438	225	23	44.08
kisz-14c	Kamchatka-Kuril-Japan-Izu-Mariana-Yap	153.4468	45.3976	45	57.89	4.602
kisz-15a	Kamchatka-Kuril-Japan-Izu-Mariana-Yap	151.4663	45.5963	233	25	23.73
kisz-15b	Kamchatka-Kuril-Japan-Izu-Mariana-Yap	151.8144	45.2712	233	22	5
kisz-15y	Kamchatka-Kuril-Japan-Izu-Mariana-Yap	150.7619	46.2465	233	25	65.99
kisz-15z	Kamchatka-Kuril-Japan-Izu-Mariana-Yap	151.1151	45.9214	233	25	44.86
kisz-16a	Kamchatka-Kuril-Japan-Izu-Mariana-Yap	150.4572	45.0977	237	25	23.73
kisz-16b	Kamchatka-Kuril-Japan-Izu-Mariana-Yap	150.7694	44.7563	237	22	5
kisz-16y	Kamchatka-Kuril-Japan-Izu-Mariana-Yap	149.8253	45.7804	237	25	65.99
kisz-16z	Kamchatka-Kuril-Japan-Izu-Mariana-Yap	150.1422	45.4390	237	25	44.86
kisz-17a	Kamchatka-Kuril-Japan-Izu-Mariana-Yap	149.3989	44.6084	237	25	23.73
kisz-17b	Kamchatka-Kuril-Japan-Izu-Mariana-Yap	149.7085	44.2670	237	22	5
kisz-17y	Kamchatka-Kuril-Japan-Izu-Mariana-Yap	148.7723	45.2912	237	25	65.99
kisz-17z	Kamchatka-Kuril-Japan-Izu-Mariana-Yap	149.0865	44.9498	237	25	44.86
kisz-18a	Kamchatka-Kuril-Japan-Izu-Mariana-Yap	148.3454	44.0982	235	25	23.73
kisz-18b	Kamchatka-Kuril-Japan-Izu-Mariana-Yap	148.6687	43.7647	235	22	5
kisz-18y	Kamchatka-Kuril-Japan-Izu-Mariana-Yap	147.6915	44.7651	235	25	65.99

Table B5: (continued)

Segment	Description	Longitude (°E)	Latitude (°N)	Strike (°)	Dip (°)	Depth (km)
kisz-18z	Kamchatka-Kuril-Japan-Izu-Mariana-Yap	148.0194	44.4316	235	25	44.86
kisz-19a	Kamchatka-Kuril-Japan-Izu-Mariana-Yap	147.3262	43.5619	233	25	23.73
kisz-19b	Kamchatka-Kuril-Japan-Izu-Mariana-Yap	147.6625	43.2368	233	22	5
kisz-19y	Kamchatka-Kuril-Japan-Izu-Mariana-Yap	146.6463	44.2121	233	25	65.99
kisz-19z	Kamchatka-Kuril-Japan-Izu-Mariana-Yap	146.9872	43.8870	233	25	44.86
kisz-20a	Kamchatka-Kuril-Japan-Izu-Mariana-Yap	146.3513	43.0633	237	25	23.73
kisz-20b	Kamchatka-Kuril-Japan-Izu-Mariana-Yap	146.6531	42.7219	237	22	5
kisz-20y	Kamchatka-Kuril-Japan-Izu-Mariana-Yap	145.7410	43.7461	237	25	65.99
kisz-20z	Kamchatka-Kuril-Japan-Izu-Mariana-Yap	146.0470	43.4047	237	25	44.86
kisz-21a	Kamchatka-Kuril-Japan-Izu-Mariana-Yap	145.3331	42.5948	239	25	23.73
kisz-21b	Kamchatka-Kuril-Japan-Izu-Mariana-Yap	145.6163	42.2459	239	22	5
kisz-21y	Kamchatka-Kuril-Japan-Izu-Mariana-Yap	144.7603	43.2927	239	25	65.99
kisz-21z	Kamchatka-Kuril-Japan-Izu-Mariana-Yap	145.0475	42.9438	239	25	44.86
kisz-22a	Kamchatka-Kuril-Japan-Izu-Mariana-Yap	144.3041	42.1631	242	25	23.73
kisz-22b	Kamchatka-Kuril-Japan-Izu-Mariana-Yap	144.5605	41.8037	242	22	5
kisz-22y	Kamchatka-Kuril-Japan-Izu-Mariana-Yap	143.7854	42.8819	242	25	65.99
kisz-22z	Kamchatka-Kuril-Japan-Izu-Mariana-Yap	144.0455	42.5225	242	25	44.86
kisz-23a	Kamchatka-Kuril-Japan-Izu-Mariana-Yap	143.2863	41.3335	202	21	21.28
kisz-23b	Kamchatka-Kuril-Japan-Izu-Mariana-Yap	143.8028	41.1764	202	19	5
kisz-23v	Kamchatka-Kuril-Japan-Izu-Mariana-Yap	140.6816	42.1189	202	21	110.9
kisz-23w	Kamchatka-Kuril-Japan-Izu-Mariana-Yap	141.2050	41.9618	202	21	92.95
kisz-23x	Kamchatka-Kuril-Japan-Izu-Mariana-Yap	141.7273	41.8047	202	21	75.04
kisz-23y	Kamchatka-Kuril-Japan-Izu-Mariana-Yap	142.2482	41.6476	202	21	57.12
kisz-23z	Kamchatka-Kuril-Japan-Izu-Mariana-Yap	142.7679	41.4905	202	21	39.2
kisz-24a	Kamchatka-Kuril-Japan-Izu-Mariana-Yap	142.9795	40.3490	185	21	21.28
kisz-24b	Kamchatka-Kuril-Japan-Izu-Mariana-Yap	143.5273	40.3125	185	19	5
kisz-24x	Kamchatka-Kuril-Japan-Izu-Mariana-Yap	141.3339	40.4587	185	21	75.04
kisz-24y	Kamchatka-Kuril-Japan-Izu-Mariana-Yap	141.8827	40.4221	185	21	57.12
kisz-24z	Kamchatka-Kuril-Japan-Izu-Mariana-Yap	142.4312	40.3856	185	21	39.2
kisz-25a	Kamchatka-Kuril-Japan-Izu-Mariana-Yap	142.8839	39.4541	185	21	21.28
kisz-25b	Kamchatka-Kuril-Japan-Izu-Mariana-Yap	143.4246	39.4176	185	19	5
kisz-25y	Kamchatka-Kuril-Japan-Izu-Mariana-Yap	141.8012	39.5272	185	21	57.12
kisz-25z	Kamchatka-Kuril-Japan-Izu-Mariana-Yap	142.3426	39.4907	185	21	39.2
kisz-26a	Kamchatka-Kuril-Japan-Izu-Mariana-Yap	142.7622	38.5837	188	21	21.28
kisz-26b	Kamchatka-Kuril-Japan-Izu-Mariana-Yap	143.2930	38.5254	188	19	5
kisz-26x	Kamchatka-Kuril-Japan-Izu-Mariana-Yap	141.1667	38.7588	188	21	75.04
kisz-26y	Kamchatka-Kuril-Japan-Izu-Mariana-Yap	141.6990	38.7004	188	21	57.12
kisz-26z	Kamchatka-Kuril-Japan-Izu-Mariana-Yap	142.2308	38.6421	188	21	39.2
kisz-27a	Kamchatka-Kuril-Japan-Izu-Mariana-Yap	142.5320	37.7830	198	21	21.28

Table B5: (continued)

Segment	Description	Longitude (°E)	Latitude (°N)	Strike (°)	Dip (°)	Depth (km)
kisz-27b	Kamchatka-Kuril-Japan-Izu-Mariana-Yap	143.0357	37.6534	198	19	5
kisz-27x	Kamchatka-Kuril-Japan-Izu-Mariana-Yap	141.0142	38.1717	198	21	75.04
kisz-27y	Kamchatka-Kuril-Japan-Izu-Mariana-Yap	141.5210	38.0421	198	21	57.12
kisz-27z	Kamchatka-Kuril-Japan-Izu-Mariana-Yap	142.0269	37.9126	198	21	39.2
kisz-28a	Kamchatka-Kuril-Japan-Izu-Mariana-Yap	142.1315	37.0265	208	21	21.28
kisz-28b	Kamchatka-Kuril-Japan-Izu-Mariana-Yap	142.5941	36.8297	208	19	5
kisz-28x	Kamchatka-Kuril-Japan-Izu-Mariana-Yap	140.7348	37.6171	208	21	75.04
kisz-28y	Kamchatka-Kuril-Japan-Izu-Mariana-Yap	141.2016	37.4202	208	21	57.12
kisz-28z	Kamchatka-Kuril-Japan-Izu-Mariana-Yap	141.6671	37.2234	208	21	39.2
kisz-29a	Kamchatka-Kuril-Japan-Izu-Mariana-Yap	141.5970	36.2640	211	21	21.28
kisz-29b	Kamchatka-Kuril-Japan-Izu-Mariana-Yap	142.0416	36.0481	211	19	5
kisz-29y	Kamchatka-Kuril-Japan-Izu-Mariana-Yap	140.7029	36.6960	211	21	57.12
kisz-29z	Kamchatka-Kuril-Japan-Izu-Mariana-Yap	141.1506	36.4800	211	21	39.2
kisz-30a	Kamchatka-Kuril-Japan-Izu-Mariana-Yap	141.0553	35.4332	205	21	21.28
kisz-30b	Kamchatka-Kuril-Japan-Izu-Mariana-Yap	141.5207	35.2560	205	19	5
kisz-30y	Kamchatka-Kuril-Japan-Izu-Mariana-Yap	140.1204	35.7876	205	21	57.12
kisz-30z	Kamchatka-Kuril-Japan-Izu-Mariana-Yap	140.5883	35.6104	205	21	39.2
kisz-31a	Kamchatka-Kuril-Japan-Izu-Mariana-Yap	140.6956	34.4789	190	22	22.1
kisz-31b	Kamchatka-Kuril-Japan-Izu-Mariana-Yap	141.1927	34.4066	190	20	5
kisz-31v	Kamchatka-Kuril-Japan-Izu-Mariana-Yap	138.2025	34.8405	190	22	115.8
kisz-31w	Kamchatka-Kuril-Japan-Izu-Mariana-Yap	138.7021	34.7682	190	22	97.02
kisz-31x	Kamchatka-Kuril-Japan-Izu-Mariana-Yap	139.2012	34.6958	190	22	78.29
kisz-31y	Kamchatka-Kuril-Japan-Izu-Mariana-Yap	139.6997	34.6235	190	22	59.56
kisz-31z	Kamchatka-Kuril-Japan-Izu-Mariana-Yap	140.1979	34.5512	190	22	40.83
kisz-32a	Kamchatka-Kuril-Japan-Izu-Mariana-Yap	141.0551	33.0921	180	32	23.48
kisz-32b	Kamchatka-Kuril-Japan-Izu-Mariana-Yap	141.5098	33.0921	180	21.69	5
kisz-33a	Kamchatka-Kuril-Japan-Izu-Mariana-Yap	141.0924	32.1047	173.8	27.65	20.67
kisz-33b	Kamchatka-Kuril-Japan-Izu-Mariana-Yap	141.5596	32.1473	173.8	18.27	5
kisz-34a	Kamchatka-Kuril-Japan-Izu-Mariana-Yap	141.1869	31.1851	172.1	25	18.26
kisz-34b	Kamchatka-Kuril-Japan-Izu-Mariana-Yap	141.6585	31.2408	172.1	15.38	5
kisz-35a	Kamchatka-Kuril-Japan-Izu-Mariana-Yap	141.4154	30.1707	163	25	17.12
kisz-35b	Kamchatka-Kuril-Japan-Izu-Mariana-Yap	141.8662	30.2899	163	14.03	5
kisz-36a	Kamchatka-Kuril-Japan-Izu-Mariana-Yap	141.6261	29.2740	161.7	25.73	18.71
kisz-36b	Kamchatka-Kuril-Japan-Izu-Mariana-Yap	142.0670	29.4012	161.7	15.91	5
kisz-37a	Kamchatka-Kuril-Japan-Izu-Mariana-Yap	142.0120	28.3322	154.7	20	14.54
kisz-37b	Kamchatka-Kuril-Japan-Izu-Mariana-Yap	142.4463	28.5124	154.7	11	5
kisz-38a	Kamchatka-Kuril-Japan-Izu-Mariana-Yap	142.2254	27.6946	170.3	20	14.54
kisz-38b	Kamchatka-Kuril-Japan-Izu-Mariana-Yap	142.6955	27.7659	170.3	11	5
kisz-39a	Kamchatka-Kuril-Japan-Izu-Mariana-Yap	142.3085	26.9127	177.2	24.23	17.42

Table B5: (continued)

Segment	Description	Longitude (°E)	Latitude (°N)	Strike (°)	Dip (°)	Depth (km)
kisz-39b	Kamchatka-Kuril-Japan-Izu-Mariana-Yap	142.7674	26.9325	177.2	14.38	5
kisz-40a	Kamchatka-Kuril-Japan-Izu-Mariana-Yap	142.2673	26.1923	189.4	26.49	22.26
kisz-40b	Kamchatka-Kuril-Japan-Izu-Mariana-Yap	142.7090	26.1264	189.4	20.2	5
kisz-41a	Kamchatka-Kuril-Japan-Izu-Mariana-Yap	142.1595	25.0729	173.7	22.07	19.08
kisz-41b	Kamchatka-Kuril-Japan-Izu-Mariana-Yap	142.6165	25.1184	173.7	16.36	5
kisz-42a	Kamchatka-Kuril-Japan-Izu-Mariana-Yap	142.7641	23.8947	143.5	21.54	18.4
kisz-42b	Kamchatka-Kuril-Japan-Izu-Mariana-Yap	143.1321	24.1432	143.5	15.54	5
kisz-43a	Kamchatka-Kuril-Japan-Izu-Mariana-Yap	143.5281	23.0423	129.2	23.02	18.77
kisz-43b	Kamchatka-Kuril-Japan-Izu-Mariana-Yap	143.8128	23.3626	129.2	15.99	5
kisz-44a	Kamchatka-Kuril-Japan-Izu-Mariana-Yap	144.2230	22.5240	134.6	28.24	18.56
kisz-44b	Kamchatka-Kuril-Japan-Izu-Mariana-Yap	144.5246	22.8056	134.6	15.74	5
kisz-45a	Kamchatka-Kuril-Japan-Izu-Mariana-Yap	145.0895	21.8866	125.8	36.73	22.79
kisz-45b	Kamchatka-Kuril-Japan-Izu-Mariana-Yap	145.3171	22.1785	125.8	20.84	5
kisz-46a	Kamchatka-Kuril-Japan-Izu-Mariana-Yap	145.6972	21.3783	135.9	30.75	20.63
kisz-46b	Kamchatka-Kuril-Japan-Izu-Mariana-Yap	145.9954	21.6469	135.9	18.22	5
kisz-47a	Kamchatka-Kuril-Japan-Izu-Mariana-Yap	146.0406	20.9341	160.1	29.87	19.62
kisz-47b	Kamchatka-Kuril-Japan-Izu-Mariana-Yap	146.4330	21.0669	160.1	17	5
kisz-48a	Kamchatka-Kuril-Japan-Izu-Mariana-Yap	146.3836	20.0690	158	32.75	19.68
kisz-48b	Kamchatka-Kuril-Japan-Izu-Mariana-Yap	146.7567	20.2108	158	17.07	5
kisz-49a	Kamchatka-Kuril-Japan-Izu-Mariana-Yap	146.6689	19.3123	164.5	25.07	21.41
kisz-49b	Kamchatka-Kuril-Japan-Izu-Mariana-Yap	147.0846	19.4212	164.5	19.16	5
kisz-50a	Kamchatka-Kuril-Japan-Izu-Mariana-Yap	146.9297	18.5663	172.1	22	22.1
kisz-50b	Kamchatka-Kuril-Japan-Izu-Mariana-Yap	147.3650	18.6238	172.1	20	5
kisz-51a	Kamchatka-Kuril-Japan-Izu-Mariana-Yap	146.9495	17.7148	175.1	22.06	22.04
kisz-51b	Kamchatka-Kuril-Japan-Izu-Mariana-Yap	147.3850	17.7503	175.1	19.93	5
kisz-52a	Kamchatka-Kuril-Japan-Izu-Mariana-Yap	146.9447	16.8869	180	25.51	18.61
kisz-52b	Kamchatka-Kuril-Japan-Izu-Mariana-Yap	147.3683	16.8869	180	15.79	5
kisz-53a	Kamchatka-Kuril-Japan-Izu-Mariana-Yap	146.8626	16.0669	185.2	27.39	18.41
kisz-53b	Kamchatka-Kuril-Japan-Izu-Mariana-Yap	147.2758	16.0309	185.2	15.56	5
kisz-54a	Kamchatka-Kuril-Japan-Izu-Mariana-Yap	146.7068	15.3883	199.1	28.12	20.91
kisz-54b	Kamchatka-Kuril-Japan-Izu-Mariana-Yap	147.0949	15.2590	199.1	18.56	5
kisz-55a	Kamchatka-Kuril-Japan-Izu-Mariana-Yap	146.4717	14.6025	204.3	29.6	26.27
kisz-55b	Kamchatka-Kuril-Japan-Izu-Mariana-Yap	146.8391	14.4415	204.3	25.18	5
kisz-56a	Kamchatka-Kuril-Japan-Izu-Mariana-Yap	146.1678	13.9485	217.4	32.04	26.79
kisz-56b	Kamchatka-Kuril-Japan-Izu-Mariana-Yap	146.4789	13.7170	217.4	25.84	5
kisz-57a	Kamchatka-Kuril-Japan-Izu-Mariana-Yap	145.6515	13.5576	235.8	37	24.54
kisz-57b	Kamchatka-Kuril-Japan-Izu-Mariana-Yap	145.8586	13.2609	235.8	23	5
kisz-58a	Kamchatka-Kuril-Japan-Izu-Mariana-Yap	144.9648	12.9990	237.8	37.72	24.54
kisz-58b	Kamchatka-Kuril-Japan-Izu-Mariana-Yap	145.1589	12.6984	237.8	23	5

Table B5: (continued)

Segment	Description	Longitude (°E)	Latitude (°N)	Strike (°)	Dip (°)	Depth (km)
kisz-59a	Kamchatka-Kuril-Japan-Izu-Mariana-Yap	144.1799	12.6914	242.9	34.33	22.31
kisz-59b	Kamchatka-Kuril-Japan-Izu-Mariana-Yap	144.3531	12.3613	242.9	20.25	5
kisz-60a	Kamchatka-Kuril-Japan-Izu-Mariana-Yap	143.3687	12.3280	244.9	30.9	20.62
kisz-60b	Kamchatka-Kuril-Japan-Izu-Mariana-Yap	143.5355	11.9788	244.9	18.2	5
kisz-61a	Kamchatka-Kuril-Japan-Izu-Mariana-Yap	142.7051	12.1507	261.8	35.41	25.51
kisz-61b	Kamchatka-Kuril-Japan-Izu-Mariana-Yap	142.7582	11.7883	261.8	24.22	5
kisz-62a	Kamchatka-Kuril-Japan-Izu-Mariana-Yap	141.6301	11.8447	245.7	39.86	34.35
kisz-62b	Kamchatka-Kuril-Japan-Izu-Mariana-Yap	141.7750	11.5305	245.7	35.94	5
kisz-63a	Kamchatka-Kuril-Japan-Izu-Mariana-Yap	140.8923	11.5740	256.2	42	38.46
kisz-63b	Kamchatka-Kuril-Japan-Izu-Mariana-Yap	140.9735	11.2498	256.2	42	5
kisz-64a	Kamchatka-Kuril-Japan-Izu-Mariana-Yap	140.1387	11.6028	269.6	42.48	38.77
kisz-64b	Kamchatka-Kuril-Japan-Izu-Mariana-Yap	140.1410	11.2716	269.6	42.48	5
kisz-65a	Kamchatka-Kuril-Japan-Izu-Mariana-Yap	139.4595	11.5883	288.7	44.16	39.83
kisz-65b	Kamchatka-Kuril-Japan-Izu-Mariana-Yap	139.3541	11.2831	288.7	44.16	5
kisz-66a	Kamchatka-Kuril-Japan-Izu-Mariana-Yap	138.1823	11.2648	193.1	45	40.36
kisz-66b	Kamchatka-Kuril-Japan-Izu-Mariana-Yap	138.4977	11.1929	193.1	45	5
kisz-67a	Kamchatka-Kuril-Japan-Izu-Mariana-Yap	137.9923	10.3398	189.8	45	40.36
kisz-67b	Kamchatka-Kuril-Japan-Izu-Mariana-Yap	138.3104	10.2856	189.8	45	5
kisz-68a	Kamchatka-Kuril-Japan-Izu-Mariana-Yap	137.7607	9.6136	201.7	45	40.36
kisz-68b	Kamchatka-Kuril-Japan-Izu-Mariana-Yap	138.0599	9.4963	201.7	45	5
kisz-69a	Kamchatka-Kuril-Japan-Izu-Mariana-Yap	137.4537	8.8996	213.5	45	40.36
kisz-69b	Kamchatka-Kuril-Japan-Izu-Mariana-Yap	137.7215	8.7241	213.5	45	5
kisz-70a	Kamchatka-Kuril-Japan-Izu-Mariana-Yap	137.0191	8.2872	226.5	45	40.36
kisz-70b	Kamchatka-Kuril-Japan-Izu-Mariana-Yap	137.2400	8.0569	226.5	45	5
kisz-71a	Kamchatka-Kuril-Japan-Izu-Mariana-Yap	136.3863	7.9078	263.9	45	40.36
kisz-71b	Kamchatka-Kuril-Japan-Izu-Mariana-Yap	136.4202	7.5920	263.9	45	5
kisz-72a	Kamchatka-Kuril-Japan-Izu-Mariana-Yap	135.6310	7.9130	276.9	45	40.36
kisz-72b	Kamchatka-Kuril-Japan-Izu-Mariana-Yap	135.5926	7.5977	276.9	45	5
kisz-73a	Kamchatka-Kuril-Japan-Izu-Mariana-Yap	134.3296	7.4541	224	45	40.36
kisz-73b	Kamchatka-Kuril-Japan-Izu-Mariana-Yap	134.5600	7.2335	224	45	5
kisz-74a	Kamchatka-Kuril-Japan-Izu-Mariana-Yap	133.7125	6.8621	228.1	45	40.36
kisz-74b	Kamchatka-Kuril-Japan-Izu-Mariana-Yap	133.9263	6.6258	228.1	45	5
kisz-75a	Kamchatka-Kuril-Japan-Izu-Mariana-Yap	133.0224	6.1221	217.7	45	40.36
kisz-75b	Kamchatka-Kuril-Japan-Izu-Mariana-Yap	133.2751	5.9280	217.7	45	5
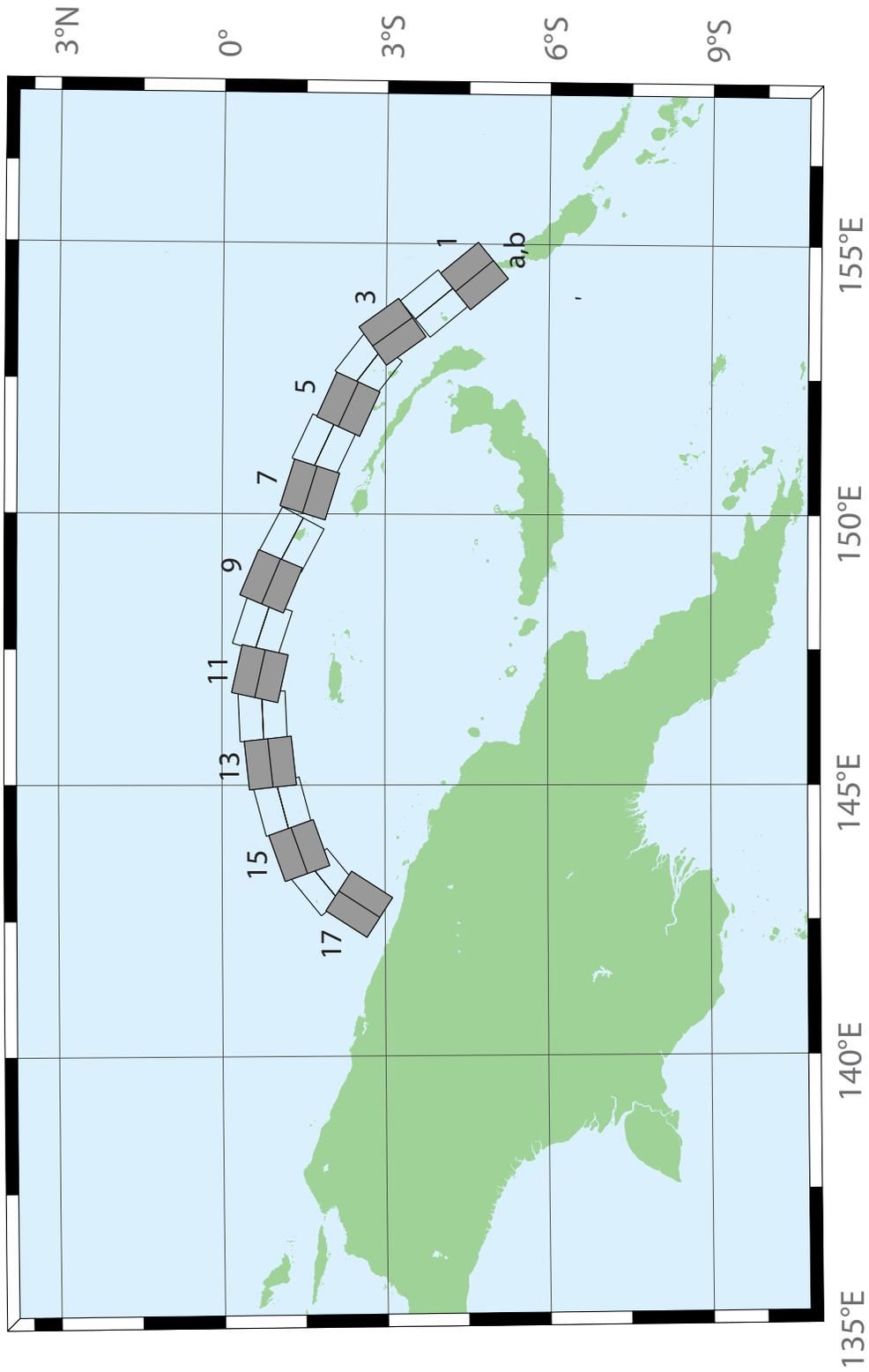
Figure B6: Manus–Oceanic Convergent Boundary Subduction Zone unit sources.

Table B6: Earthquake parameters for Manus–Oceanic Convergent Boundary Subduction Zone unit sources.

Segment	Description	Longitude (°E)	Latitude (°N)	Strike (°)	Dip (°)	Depth (km)
mosz-1a	Manus-Oceanic Convergent Boundary	154.0737	-4.8960	140.2	15	15.88
mosz-1b	Manus-Oceanic Convergent Boundary	154.4082	-4.6185	140.2	15	2.94
mosz-2a	Manus-Oceanic Convergent Boundary	153.5589	-4.1575	140.2	15	15.91
mosz-2b	Manus-Oceanic Convergent Boundary	153.8931	-3.8800	140.2	15	2.97
mosz-3a	Manus-Oceanic Convergent Boundary	153.0151	-3.3716	143.9	15	16.64
mosz-3b	Manus-Oceanic Convergent Boundary	153.3662	-3.1160	143.9	15	3.7
mosz-4a	Manus-Oceanic Convergent Boundary	152.4667	-3.0241	127.7	15	17.32
mosz-4b	Manus-Oceanic Convergent Boundary	152.7321	-2.6806	127.7	15	4.38
mosz-5a	Manus-Oceanic Convergent Boundary	151.8447	-2.7066	114.3	15	17.57
mosz-5b	Manus-Oceanic Convergent Boundary	152.0235	-2.3112	114.3	15	4.63
mosz-6a	Manus-Oceanic Convergent Boundary	151.0679	-2.2550	115	15	17.66
mosz-6b	Manus-Oceanic Convergent Boundary	151.2513	-1.8618	115	15	4.72
mosz-7a	Manus-Oceanic Convergent Boundary	150.3210	-2.0236	107.2	15	17.73
mosz-7b	Manus-Oceanic Convergent Boundary	150.4493	-1.6092	107.2	15	4.79
mosz-8a	Manus-Oceanic Convergent Boundary	149.3226	-1.6666	117.8	15	17.83
mosz-8b	Manus-Oceanic Convergent Boundary	149.5251	-1.2829	117.8	15	4.89
mosz-9a	Manus-Oceanic Convergent Boundary	148.5865	-1.3017	112.7	15	17.84
mosz-9b	Manus-Oceanic Convergent Boundary	148.7540	-0.9015	112.7	15	4.9
mosz-10a	Manus-Oceanic Convergent Boundary	147.7760	-1.1560	108	15	17.78
mosz-10b	Manus-Oceanic Convergent Boundary	147.9102	-0.7434	108	15	4.84
mosz-11a	Manus-Oceanic Convergent Boundary	146.9596	-1.1226	102.5	15	17.54
mosz-11b	Manus-Oceanic Convergent Boundary	147.0531	-0.6990	102.5	15	4.6
mosz-12a	Manus-Oceanic Convergent Boundary	146.2858	-1.1820	87.48	15	17.29
mosz-12b	Manus-Oceanic Convergent Boundary	146.2667	-0.7486	87.48	15	4.35
mosz-13a	Manus-Oceanic Convergent Boundary	145.4540	-1.3214	83.75	15	17.34
mosz-13b	Manus-Oceanic Convergent Boundary	145.4068	-0.8901	83.75	15	4.4
mosz-14a	Manus-Oceanic Convergent Boundary	144.7151	-1.5346	75.09	15	17.21
mosz-14b	Manus-Oceanic Convergent Boundary	144.6035	-1.1154	75.09	15	4.27
mosz-15a	Manus-Oceanic Convergent Boundary	143.9394	-1.8278	70.43	15	16.52
mosz-15b	Manus-Oceanic Convergent Boundary	143.7940	-1.4190	70.43	15	3.58
mosz-16a	Manus-Oceanic Convergent Boundary	143.4850	-2.2118	50.79	15	15.86
mosz-16b	Manus-Oceanic Convergent Boundary	143.2106	-1.8756	50.79	15	2.92
mosz-17a	Manus-Oceanic Convergent Boundary	143.1655	-2.7580	33	15	16.64
mosz-17b	Manus-Oceanic Convergent Boundary	142.8013	-2.5217	33	15	3.7
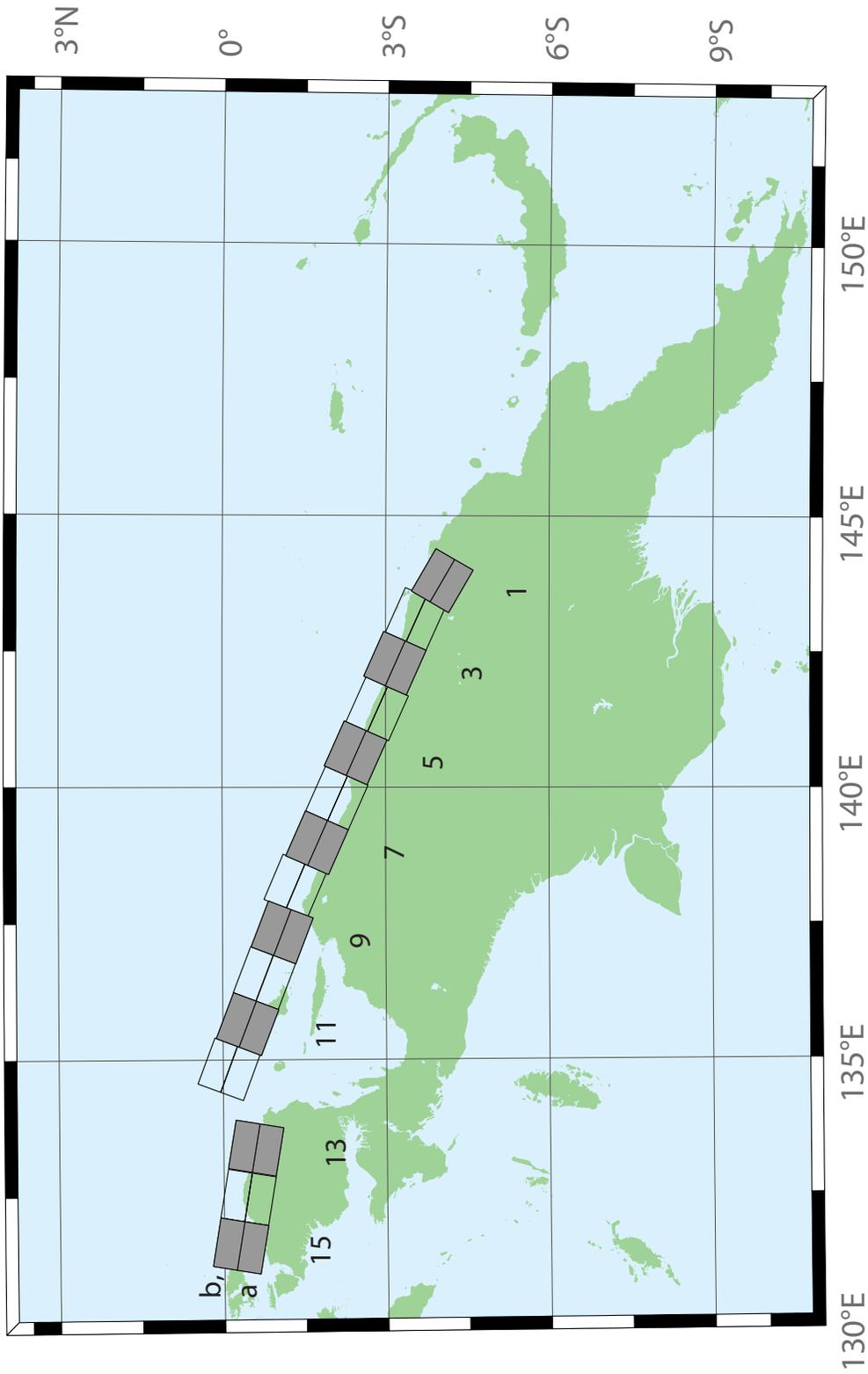
Figure B7: New Guinea Subduction Zone unit sources.

Table B7: Earthquake parameters for New Guinea Subduction Zone unit sources.

Segment	Description	Longitude (°E)	Latitude (°N)	Strike (°)	Dip (°)	Depth (km)
ngsz-1a	New Guinea	143.6063	-4.3804	120	29	25.64
ngsz-1b	New Guinea	143.8032	-4.0402	120	29	1.4
ngsz-2a	New Guinea	142.9310	-3.9263	114	27.63	20.1
ngsz-2b	New Guinea	143.0932	-3.5628	114	21.72	1.6
ngsz-3a	New Guinea	142.1076	-3.5632	114	20.06	18.73
ngsz-3b	New Guinea	142.2795	-3.1778	114	15.94	5
ngsz-4a	New Guinea	141.2681	-3.2376	114	21	17.76
ngsz-4b	New Guinea	141.4389	-2.8545	114	14.79	5
ngsz-5a	New Guinea	140.4592	-2.8429	114	21.26	16.14
ngsz-5b	New Guinea	140.6296	-2.4605	114	12.87	5
ngsz-6a	New Guinea	139.6288	-2.4960	114	22.72	15.4
ngsz-6b	New Guinea	139.7974	-2.1175	114	12	5
ngsz-7a	New Guinea	138.8074	-2.1312	114	21.39	15.4
ngsz-7b	New Guinea	138.9776	-1.7491	114	12	5
ngsz-8a	New Guinea	138.0185	-1.7353	113.1	18.79	15.14
ngsz-8b	New Guinea	138.1853	-1.3441	113.1	11.7	5
ngsz-9a	New Guinea	137.1805	-1.5037	111	15.24	13.23
ngsz-9b	New Guinea	137.3358	-1.0991	111	9.47	5
ngsz-10a	New Guinea	136.3418	-1.1774	111	13.51	11.09
ngsz-10b	New Guinea	136.4983	-0.7697	111	7	5
ngsz-11a	New Guinea	135.4984	-0.8641	111	11.38	12.49
ngsz-11b	New Guinea	135.6562	-0.4530	111	8.62	5
ngsz-12a	New Guinea	134.6759	-0.5216	110.5	10	13.68
ngsz-12b	New Guinea	134.8307	-0.1072	110.5	10	5
ngsz-13a	New Guinea	133.3065	-1.0298	99.5	10	13.68
ngsz-13b	New Guinea	133.3795	-0.5935	99.5	10	5
ngsz-14a	New Guinea	132.4048	-0.8816	99.5	10	13.68
ngsz-14b	New Guinea	132.4778	-0.4453	99.5	10	5
ngsz-15a	New Guinea	131.5141	-0.7353	99.5	10	13.68
ngsz-15b	New Guinea	131.5871	-0.2990	99.5	10	5
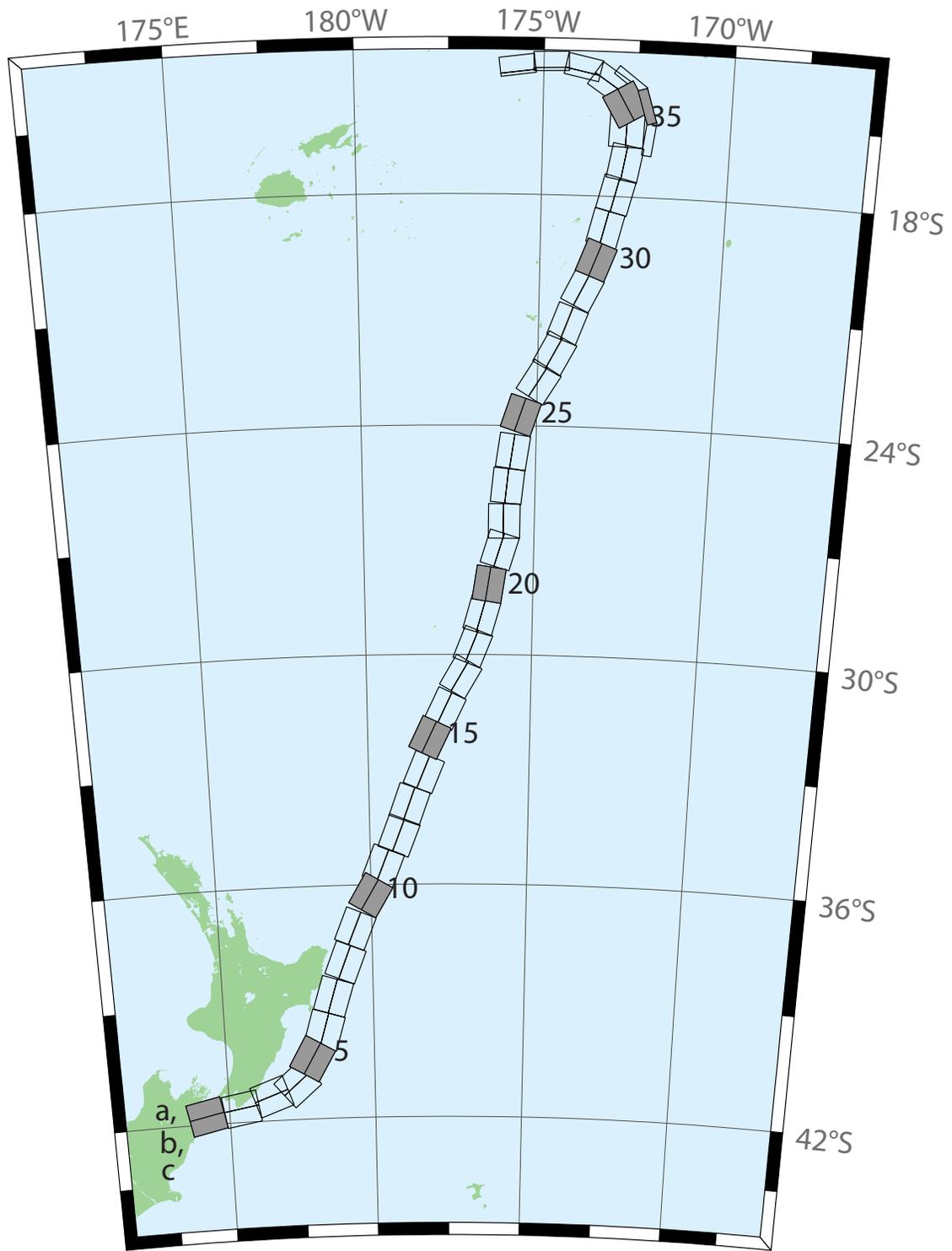
Figure B8: New Zealand–Kermadec–Tonga Subduction Zone unit sources.

Table B8: Earthquake parameters for New Zealand–Kermadec–Tonga Subduction Zone unit sources.

Segment	Description	Longitude (°E)	Latitude (°N)	Strike (°)	Dip (°)	Depth (km)
ntsz-1a	New Zealand–Kermadec–Tonga	174.0985	-41.3951	258.6	24	25.34
ntsz-1b	New Zealand–Kermadec–Tonga	174.2076	-41.7973	258.6	24	5
ntsz-2a	New Zealand–Kermadec–Tonga	175.3289	-41.2592	260.6	29.38	23.17
ntsz-2b	New Zealand–Kermadec–Tonga	175.4142	-41.6454	260.6	21.31	5
ntsz-3a	New Zealand–Kermadec–Tonga	176.2855	-40.9950	250.7	29.54	21.74
ntsz-3b	New Zealand–Kermadec–Tonga	176.4580	-41.3637	250.7	19.56	5
ntsz-4a	New Zealand–Kermadec–Tonga	177.0023	-40.7679	229.4	24.43	18.87
ntsz-4b	New Zealand–Kermadec–Tonga	177.3552	-41.0785	229.4	16.1	5
ntsz-5a	New Zealand–Kermadec–Tonga	177.4114	-40.2396	210	18.8	19.29
ntsz-5b	New Zealand–Kermadec–Tonga	177.8951	-40.4525	210	16.61	5
ntsz-6a	New Zealand–Kermadec–Tonga	177.8036	-39.6085	196.7	18.17	15.8
ntsz-6b	New Zealand–Kermadec–Tonga	178.3352	-39.7310	196.7	12.48	5
ntsz-7a	New Zealand–Kermadec–Tonga	178.1676	-38.7480	197	28.1	17.85
ntsz-7b	New Zealand–Kermadec–Tonga	178.6541	-38.8640	197	14.89	5
ntsz-8a	New Zealand–Kermadec–Tonga	178.6263	-37.8501	201.4	31.47	18.78
ntsz-8b	New Zealand–Kermadec–Tonga	179.0788	-37.9899	201.4	16	5
ntsz-9a	New Zealand–Kermadec–Tonga	178.9833	-36.9770	202.2	29.58	20.02
ntsz-9b	New Zealand–Kermadec–Tonga	179.4369	-37.1245	202.2	17.48	5
ntsz-10a	New Zealand–Kermadec–Tonga	179.5534	-36.0655	210.6	32.1	20.72
ntsz-10b	New Zealand–Kermadec–Tonga	179.9595	-36.2593	210.6	18.32	5
ntsz-11a	New Zealand–Kermadec–Tonga	179.9267	-35.3538	201.7	25	16.09
ntsz-11b	New Zealand–Kermadec–Tonga	180.3915	-35.5040	201.7	12.81	5
ntsz-12a	New Zealand–Kermadec–Tonga	180.4433	-34.5759	201.2	25	15.46
ntsz-12b	New Zealand–Kermadec–Tonga	180.9051	-34.7230	201.2	12.08	5
ntsz-13a	New Zealand–Kermadec–Tonga	180.7990	-33.7707	199.8	25.87	19.06
ntsz-13b	New Zealand–Kermadec–Tonga	181.2573	-33.9073	199.8	16.33	5
ntsz-14a	New Zealand–Kermadec–Tonga	181.2828	-32.9288	202.4	31.28	22.73
ntsz-14b	New Zealand–Kermadec–Tonga	181.7063	-33.0751	202.4	20.77	5
ntsz-15a	New Zealand–Kermadec–Tonga	181.4918	-32.0035	205.4	32.33	22.64
ntsz-15b	New Zealand–Kermadec–Tonga	181.8967	-32.1665	205.4	20.66	5
ntsz-16a	New Zealand–Kermadec–Tonga	181.9781	-31.2535	205.5	34.29	23.59
ntsz-16b	New Zealand–Kermadec–Tonga	182.3706	-31.4131	205.5	21.83	5
ntsz-17a	New Zealand–Kermadec–Tonga	182.4819	-30.3859	210.3	37.6	25.58
ntsz-17b	New Zealand–Kermadec–Tonga	182.8387	-30.5655	210.3	24.3	5
ntsz-18a	New Zealand–Kermadec–Tonga	182.8176	-29.6545	201.6	37.65	26.13
ntsz-18b	New Zealand–Kermadec–Tonga	183.1985	-29.7856	201.6	25	5
ntsz-19a	New Zealand–Kermadec–Tonga	183.0622	-28.8739	195.7	34.41	26.13
ntsz-19b	New Zealand–Kermadec–Tonga	183.4700	-28.9742	195.7	25	5
ntsz-20a	New Zealand–Kermadec–Tonga	183.2724	-28.0967	188.8	38	26.13
ntsz-20b	New Zealand–Kermadec–Tonga	183.6691	-28.1508	188.8	25	5

Table B8: (continued)

Segment	Description	Longitude (°E)	Latitude (°N)	Strike (°)	Dip (°)	Depth (km)
ntsz-21a	New Zealand–Kermadec–Tonga	183.5747	-27.1402	197.1	32.29	24.83
ntsz-21b	New Zealand–Kermadec–Tonga	183.9829	-27.2518	197.1	23.37	5
ntsz-22a	New Zealand–Kermadec–Tonga	183.6608	-26.4975	180	29.56	18.63
ntsz-22b	New Zealand–Kermadec–Tonga	184.0974	-26.4975	180	15.82	5
ntsz-23a	New Zealand–Kermadec–Tonga	183.7599	-25.5371	185.8	32.42	20.56
ntsz-23b	New Zealand–Kermadec–Tonga	184.1781	-25.5752	185.8	18.13	5
ntsz-24a	New Zealand–Kermadec–Tonga	183.9139	-24.6201	188.2	33.31	23.73
ntsz-24b	New Zealand–Kermadec–Tonga	184.3228	-24.6734	188.2	22	5
ntsz-25a	New Zealand–Kermadec–Tonga	184.1266	-23.5922	198.5	29.34	19.64
ntsz-25b	New Zealand–Kermadec–Tonga	184.5322	-23.7163	198.5	17.03	5
ntsz-26a	New Zealand–Kermadec–Tonga	184.6613	-22.6460	211.7	30.26	19.43
ntsz-26b	New Zealand–Kermadec–Tonga	185.0196	-22.8497	211.7	16.78	5
ntsz-27a	New Zealand–Kermadec–Tonga	185.0879	-21.9139	207.9	31.73	20.67
ntsz-27b	New Zealand–Kermadec–Tonga	185.4522	-22.0928	207.9	18.27	5
ntsz-28a	New Zealand–Kermadec–Tonga	185.4037	-21.1758	200.5	32.44	21.76
ntsz-28b	New Zealand–Kermadec–Tonga	185.7849	-21.3084	200.5	19.58	5
ntsz-29a	New Zealand–Kermadec–Tonga	185.8087	-20.2629	206.4	32.47	20.4
ntsz-29b	New Zealand–Kermadec–Tonga	186.1710	-20.4312	206.4	17.94	5
ntsz-30a	New Zealand–Kermadec–Tonga	186.1499	-19.5087	200.9	32.98	22.46
ntsz-30b	New Zealand–Kermadec–Tonga	186.5236	-19.6432	200.9	20.44	5
ntsz-31a	New Zealand–Kermadec–Tonga	186.3538	-18.7332	193.9	34.41	21.19
ntsz-31b	New Zealand–Kermadec–Tonga	186.7339	-18.8221	193.9	18.89	5
ntsz-32a	New Zealand–Kermadec–Tonga	186.5949	-17.8587	194.1	30	19.12
ntsz-32b	New Zealand–Kermadec–Tonga	186.9914	-17.9536	194.1	16.4	5
ntsz-33a	New Zealand–Kermadec–Tonga	186.8172	-17.0581	190	33.15	23.34
ntsz-33b	New Zealand–Kermadec–Tonga	187.2047	-17.1237	190	21.52	5
ntsz-34a	New Zealand–Kermadec–Tonga	186.7814	-16.2598	182.1	15	13.41
ntsz-34b	New Zealand–Kermadec–Tonga	187.2330	-16.2759	182.1	9.68	5
ntsz-34c	New Zealand–Kermadec–Tonga	187.9697	-16.4956	7.62	57.06	6.571
ntsz-35a	New Zealand–Kermadec–Tonga	186.8000	-15.8563	149.8	15	12.17
ntsz-35b	New Zealand–Kermadec–Tonga	187.1896	-15.6384	149.8	8.24	5
ntsz-35c	New Zealand–Kermadec–Tonga	187.8776	-15.6325	342.4	57.06	6.571
ntsz-36a	New Zealand–Kermadec–Tonga	186.5406	-15.3862	123.9	40.44	36.72
ntsz-36b	New Zealand–Kermadec–Tonga	186.7381	-15.1025	123.9	39.38	5
ntsz-36c	New Zealand–Kermadec–Tonga	187.3791	-14.9234	307	57.06	6.571
ntsz-37a	New Zealand–Kermadec–Tonga	185.9883	-14.9861	102	68.94	30.99
ntsz-37b	New Zealand–Kermadec–Tonga	186.0229	-14.8282	102	31.32	5
ntsz-38a	New Zealand–Kermadec–Tonga	185.2067	-14.8259	88.4	80	26.13
ntsz-38b	New Zealand–Kermadec–Tonga	185.2044	-14.7479	88.4	25	5
ntsz-39a	New Zealand–Kermadec–Tonga	184.3412	-14.9409	82.55	80	26.13
ntsz-39b	New Zealand–Kermadec–Tonga	184.3307	-14.8636	82.55	25	5

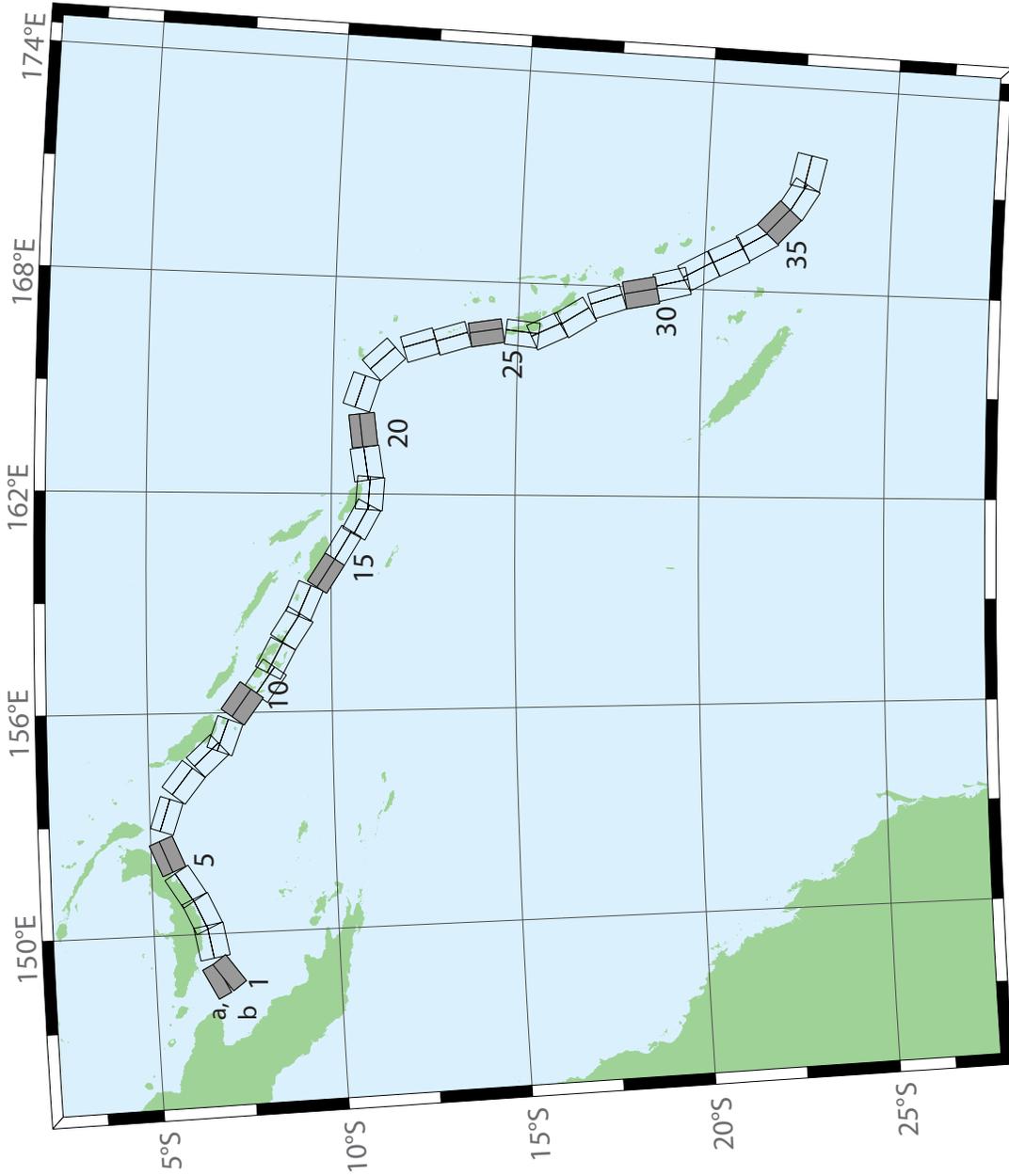**Figure B9**: New Britain–Solomons–Vanuatu Subduction Zone unit sources.

Table B9: Earthquake parameters for New Britain–Solomons–Vanuatu Subduction Zone unit sources.

Segment	Description	Longitude (°E)	Latitude (°N)	Strike (°)	Dip (°)	Depth (km)
nvsz-1a	New Britain–Solomons–Vanuatu	148.6217	-6.4616	243.2	32.34	15.69
nvsz-1b	New Britain–Solomons–Vanuatu	148.7943	-6.8002	234.2	12.34	5
nvsz-2a	New Britain–Solomons–Vanuatu	149.7218	-6.1459	260.1	35.1	16.36
nvsz-2b	New Britain–Solomons–Vanuatu	149.7856	-6.5079	260.1	13.13	5
nvsz-3a	New Britain–Solomons–Vanuatu	150.4075	-5.9659	245.7	42.35	18.59
nvsz-3b	New Britain–Solomons–Vanuatu	150.5450	-6.2684	245.7	15.77	5
nvsz-4a	New Britain–Solomons–Vanuatu	151.1095	-5.5820	238.2	42.41	23.63
nvsz-4b	New Britain–Solomons–Vanuatu	151.2851	-5.8639	238.2	21.88	5
nvsz-5a	New Britain–Solomons–Vanuatu	152.0205	-5.1305	247.7	49.22	32.39
nvsz-5b	New Britain–Solomons–Vanuatu	152.1322	-5.4020	247.7	33.22	5
nvsz-6a	New Britain–Solomons–Vanuatu	153.3450	-5.1558	288.6	53.53	33.59
nvsz-6b	New Britain–Solomons–Vanuatu	153.2595	-5.4089	288.6	34.87	5
nvsz-7a	New Britain–Solomons–Vanuatu	154.3814	-5.6308	308.3	39.72	19.18
nvsz-7b	New Britain–Solomons–Vanuatu	154.1658	-5.9017	308.3	16.48	5
nvsz-8a	New Britain–Solomons–Vanuatu	155.1097	-6.3511	317.2	45.33	22.92
nvsz-8b	New Britain–Solomons–Vanuatu	154.8764	-6.5656	317.2	21	5
nvsz-9a	New Britain–Solomons–Vanuatu	155.5027	-6.7430	290.5	48.75	22.92
nvsz-9b	New Britain–Solomons–Vanuatu	155.3981	-7.0204	290.5	21	5
nvsz-10a	New Britain–Solomons–Vanuatu	156.4742	-7.2515	305.9	36.88	27.62
nvsz-10b	New Britain–Solomons–Vanuatu	156.2619	-7.5427	305.9	26.9	5
nvsz-11a	New Britain–Solomons–Vanuatu	157.0830	-7.8830	305.4	32.97	29.72
nvsz-11b	New Britain–Solomons–Vanuatu	156.8627	-8.1903	305.4	29.63	5
nvsz-12a	New Britain–Solomons–Vanuatu	157.6537	-8.1483	297.9	37.53	28.57
nvsz-12b	New Britain–Solomons–Vanuatu	157.4850	-8.4630	297.9	28.13	5
nvsz-13a	New Britain–Solomons–Vanuatu	158.5089	-8.5953	302.7	33.62	23.02
nvsz-13b	New Britain–Solomons–Vanuatu	158.3042	-8.9099	302.7	21.12	5
nvsz-14a	New Britain–Solomons–Vanuatu	159.1872	-8.9516	293.3	38.44	34.06
nvsz-14b	New Britain–Solomons–Vanuatu	159.0461	-9.2747	293.3	35.54	5
nvsz-15a	New Britain–Solomons–Vanuatu	159.9736	-9.5993	302.8	46.69	41.38
nvsz-15b	New Britain–Solomons–Vanuatu	159.8044	-9.8584	302.8	46.69	5
nvsz-16a	New Britain–Solomons–Vanuatu	160.7343	-10.0574	301	46.05	41
nvsz-16b	New Britain–Solomons–Vanuatu	160.5712	-10.3246	301	46.05	5
nvsz-17a	New Britain–Solomons–Vanuatu	161.4562	-10.5241	298.4	40.12	37.22
nvsz-17b	New Britain–Solomons–Vanuatu	161.2900	-10.8263	298.4	40.12	5
nvsz-18a	New Britain–Solomons–Vanuatu	162.0467	-10.6823	274.1	40.33	29.03
nvsz-18b	New Britain–Solomons–Vanuatu	162.0219	-11.0238	274.1	28.72	5
nvsz-19a	New Britain–Solomons–Vanuatu	162.7818	-10.5645	261.3	34.25	24.14
nvsz-19b	New Britain–Solomons–Vanuatu	162.8392	-10.9315	261.3	22.51	5
nvsz-20a	New Britain–Solomons–Vanuatu	163.7222	-10.5014	262.9	50.35	26.3

Table B9: (continued)

Segment	Description	Longitude (°E)	Latitude (°N)	Strike (°)	Dip (°)	Depth (km)
nvsz-20b	New Britain–Solomons–Vanuatu	163.7581	-10.7858	262.9	25.22	5
nvsz-21a	New Britain–Solomons–Vanuatu	164.9445	-10.4183	287.9	40.31	23.3
nvsz-21b	New Britain–Solomons–Vanuatu	164.8374	-10.7442	287.9	21.47	5
nvsz-22a	New Britain–Solomons–Vanuatu	166.0261	-11.1069	317.1	42.39	20.78
nvsz-22b	New Britain–Solomons–Vanuatu	165.7783	-11.3328	317.1	18.4	5
nvsz-23a	New Britain–Solomons–Vanuatu	166.5179	-12.2260	342.4	47.95	22.43
nvsz-23b	New Britain–Solomons–Vanuatu	166.2244	-12.3171	342.4	20.4	5
nvsz-24a	New Britain–Solomons–Vanuatu	166.7236	-13.1065	342.6	47.13	28.52
nvsz-24b	New Britain–Solomons–Vanuatu	166.4241	-13.1979	342.6	28.06	5
nvsz-25a	New Britain–Solomons–Vanuatu	166.8914	-14.0785	350.3	54.1	31.16
nvsz-25b	New Britain–Solomons–Vanuatu	166.6237	-14.1230	350.3	31.55	5
nvsz-26a	New Britain–Solomons–Vanuatu	166.9200	-15.1450	365.6	50.46	29.05
nvsz-26b	New Britain–Solomons–Vanuatu	166.6252	-15.1170	365.6	28.75	5
nvsz-27a	New Britain–Solomons–Vanuatu	167.0053	-15.6308	334.2	44.74	25.46
nvsz-27b	New Britain–Solomons–Vanuatu	166.7068	-15.7695	334.2	24.15	5
nvsz-28a	New Britain–Solomons–Vanuatu	167.4074	-16.3455	327.5	41.53	22.44
nvsz-28b	New Britain–Solomons–Vanuatu	167.1117	-16.5264	327.5	20.42	5
nvsz-29a	New Britain–Solomons–Vanuatu	167.9145	-17.2807	341.2	49.1	24.12
nvsz-29b	New Britain–Solomons–Vanuatu	167.6229	-17.3757	341.2	22.48	5
nvsz-30a	New Britain–Solomons–Vanuatu	168.2220	-18.2353	348.6	44.19	23.99
nvsz-30b	New Britain–Solomons–Vanuatu	167.8895	-18.2991	348.6	22.32	5
nvsz-31a	New Britain–Solomons–Vanuatu	168.5022	-19.0510	345.6	42.2	22.26
nvsz-31b	New Britain–Solomons–Vanuatu	168.1611	-19.1338	345.6	20.2	5
nvsz-32a	New Britain–Solomons–Vanuatu	168.8775	-19.6724	331.1	42.03	21.68
nvsz-32b	New Britain–Solomons–Vanuatu	168.5671	-19.8338	331.1	19.49	5
nvsz-33a	New Britain–Solomons–Vanuatu	169.3422	-20.4892	332.9	40.25	22.4
nvsz-33b	New Britain–Solomons–Vanuatu	169.0161	-20.6453	332.9	20.37	5
nvsz-34a	New Britain–Solomons–Vanuatu	169.8304	-21.2121	329.1	39	22.73
nvsz-34b	New Britain–Solomons–Vanuatu	169.5086	-21.3911	329.1	20.77	5
nvsz-35a	New Britain–Solomons–Vanuatu	170.3119	-21.6945	311.9	39	22.13
nvsz-35b	New Britain–Solomons–Vanuatu	170.0606	-21.9543	311.9	20.03	5
nvsz-36a	New Britain–Solomons–Vanuatu	170.9487	-22.1585	300.4	39.42	23.5
nvsz-36b	New Britain–Solomons–Vanuatu	170.7585	-22.4577	300.4	21.71	5
nvsz-37a	New Britain–Solomons–Vanuatu	171.6335	-22.3087	281.3	30	22.1
nvsz-37b	New Britain–Solomons–Vanuatu	171.5512	-22.6902	281.3	20	5
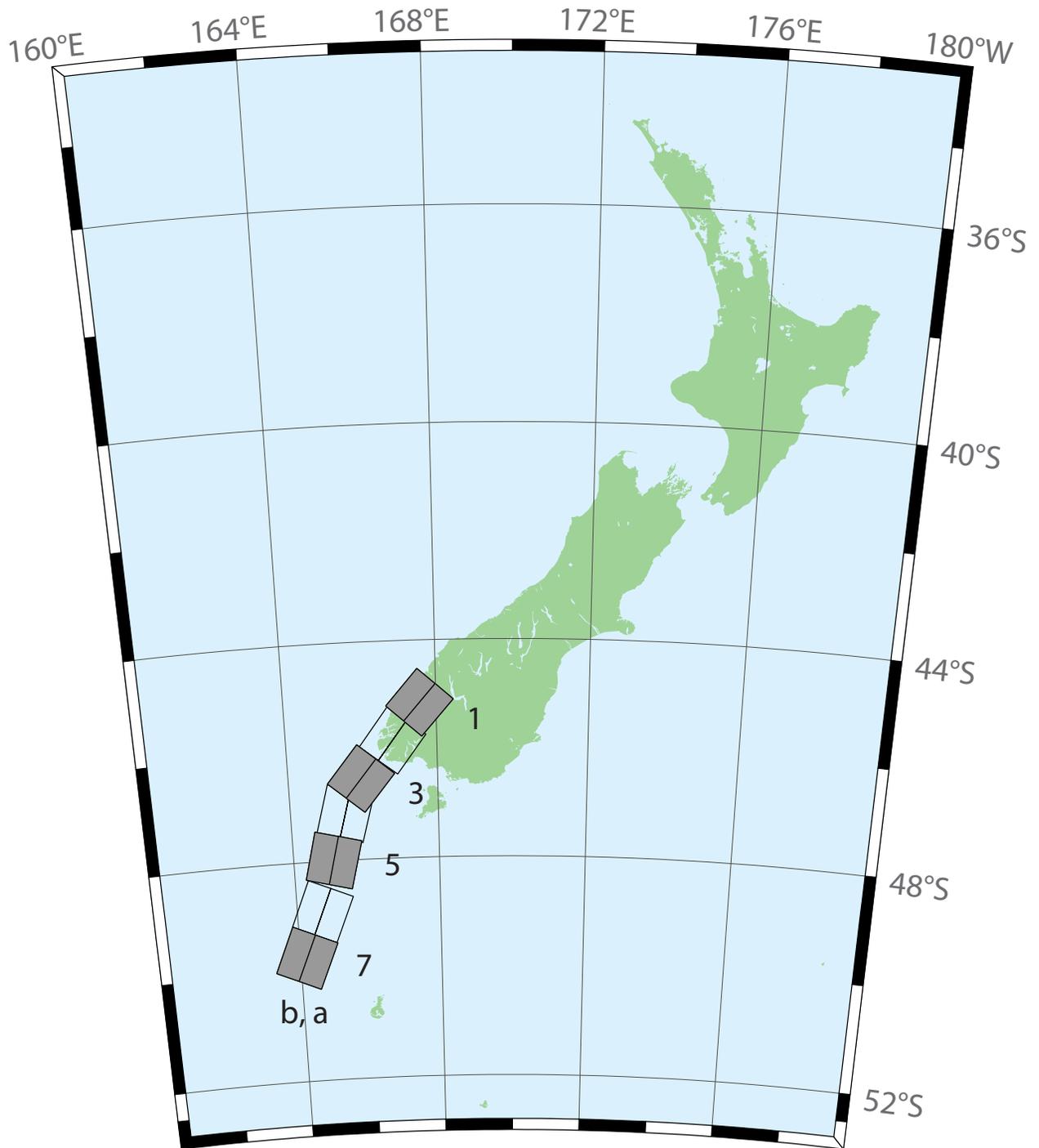
Figure B10: New Zealand–Puysegur Subduction Zone unit sources.

Table B10: Earthquake parameters for New Zealand–Puysegur Subduction Zone unit sources.

Segment	Description	Longitude (°E)	Latitude (°N)	Strike (°)	Dip (°)	Depth (km)
nzsz-1a	New Zealand–Puysegur	168.0294	-45.4368	41.5	15	17.94
nzsz-1b	New Zealand–Puysegur	167.5675	-45.1493	41.5	15	5
nzsz-2a	New Zealand–Puysegur	167.3256	-46.0984	37.14	15	17.94
nzsz-2b	New Zealand–Puysegur	166.8280	-45.8365	37.14	15	5
nzsz-3a	New Zealand–Puysegur	166.4351	-46.7897	39.53	15	17.94
nzsz-3b	New Zealand–Puysegur	165.9476	-46.5136	39.53	15	5
nzsz-4a	New Zealand–Puysegur	166.0968	-47.2583	15.38	15	17.94
nzsz-4b	New Zealand–Puysegur	165.4810	-47.1432	15.38	15	5
nzsz-5a	New Zealand–Puysegur	165.7270	-48.0951	13.94	15	17.94
nzsz-5b	New Zealand–Puysegur	165.0971	-47.9906	13.94	15	5
nzsz-6a	New Zealand–Puysegur	165.3168	-49.0829	22.71	15	17.94
nzsz-6b	New Zealand–Puysegur	164.7067	-48.9154	22.71	15	5
nzsz-7a	New Zealand–Puysegur	164.8017	-49.9193	23.25	15	17.94
nzsz-7b	New Zealand–Puysegur	164.1836	-49.7480	23.25	15	5

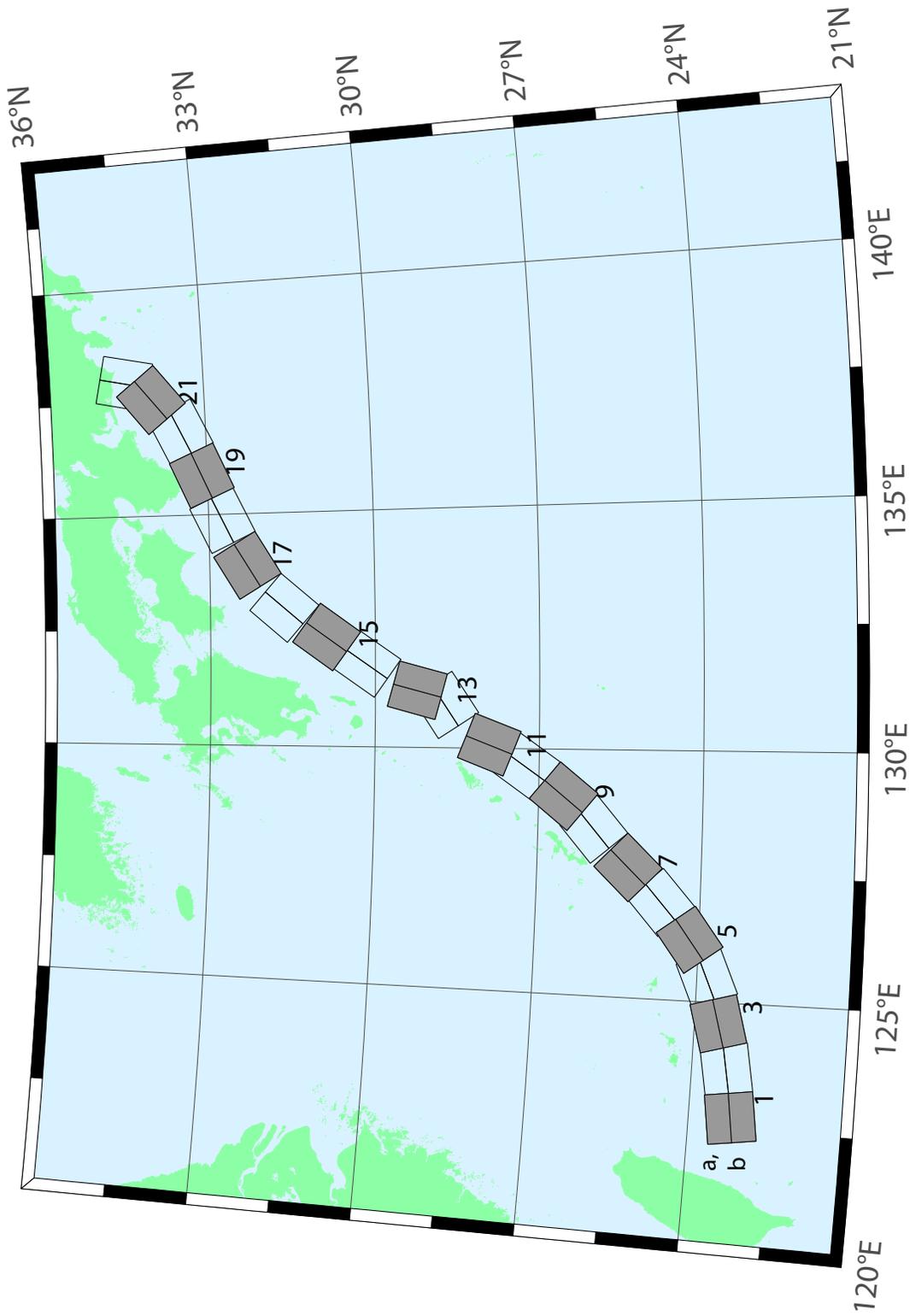**Figure B11**: Ryukyu–Kyushu–Nankai Subduction Zone unit sources.

Table B11: Earthquake parameters for Ryukyu–Kyushu–Nankai Subduction Zone unit sources.

Segment	Description	Longitude (°E)	Latitude (°N)	Strike (°)	Dip (°)	Depth (km)
rnsz-1a	Ryukyu–Kyushu–Nankai	122.6672	23.6696	262	14	11.88
rnsz-1b	Ryukyu–Kyushu–Nankai	122.7332	23.2380	262	10	3.2
rnsz-2a	Ryukyu–Kyushu–Nankai	123.5939	23.7929	259.9	18.11	12.28
rnsz-2b	Ryukyu–Kyushu–Nankai	123.6751	23.3725	259.9	10	3.6
rnsz-3a	Ryukyu–Kyushu–Nankai	124.4604	23.9777	254.6	19.27	14.65
rnsz-3b	Ryukyu–Kyushu–Nankai	124.5830	23.5689	254.6	12.18	4.1
rnsz-4a	Ryukyu–Kyushu–Nankai	125.2720	24.2102	246.8	18	20.38
rnsz-4b	Ryukyu–Kyushu–Nankai	125.4563	23.8177	246.8	16	6.6
rnsz-5a	Ryukyu–Kyushu–Nankai	125.9465	24.5085	233.6	18	20.21
rnsz-5b	Ryukyu–Kyushu–Nankai	126.2241	24.1645	233.6	16	6.43
rnsz-6a	Ryukyu–Kyushu–Nankai	126.6349	25.0402	228.7	17.16	19.55
rnsz-6b	Ryukyu–Kyushu–Nankai	126.9465	24.7176	228.7	15.16	6.47
rnsz-7a	Ryukyu–Kyushu–Nankai	127.2867	25.6343	224	15.85	17.98
rnsz-7b	Ryukyu–Kyushu–Nankai	127.6303	25.3339	224	13.56	6.26
rnsz-8a	Ryukyu–Kyushu–Nankai	128.0725	26.3146	229.7	14.55	14.31
rnsz-8b	Ryukyu–Kyushu–Nankai	128.3854	25.9831	229.7	9.64	5.94
rnsz-9a	Ryukyu–Kyushu–Nankai	128.6642	26.8177	219.2	15.4	12.62
rnsz-9b	Ryukyu–Kyushu–Nankai	129.0391	26.5438	219.2	8	5.66
rnsz-10a	Ryukyu–Kyushu–Nankai	129.2286	27.4879	215.2	17	12.55
rnsz-10b	Ryukyu–Kyushu–Nankai	129.6233	27.2402	215.2	8.16	5.45
rnsz-11a	Ryukyu–Kyushu–Nankai	129.6169	28.0741	201.3	17	12.91
rnsz-11b	Ryukyu–Kyushu–Nankai	130.0698	27.9181	201.3	8.8	5.26
rnsz-12a	Ryukyu–Kyushu–Nankai	130.6175	29.0900	236.7	16.42	13.05
rnsz-12b	Ryukyu–Kyushu–Nankai	130.8873	28.7299	236.7	9.57	4.74
rnsz-13a	Ryukyu–Kyushu–Nankai	130.7223	29.3465	195.2	20.25	15.89
rnsz-13b	Ryukyu–Kyushu–Nankai	131.1884	29.2362	195.2	12.98	4.66
rnsz-14a	Ryukyu–Kyushu–Nankai	131.3467	30.3899	215.1	22.16	19.73
rnsz-14b	Ryukyu–Kyushu–Nankai	131.7402	30.1507	215.1	17.48	4.71
rnsz-15a	Ryukyu–Kyushu–Nankai	131.9149	31.1450	216	15.11	16.12
rnsz-15b	Ryukyu–Kyushu–Nankai	132.3235	30.8899	216	13.46	4.48
rnsz-16a	Ryukyu–Kyushu–Nankai	132.5628	31.9468	220.9	10.81	10.88
rnsz-16b	Ryukyu–Kyushu–Nankai	132.9546	31.6579	220.9	7.19	4.62
rnsz-17a	Ryukyu–Kyushu–Nankai	133.6125	32.6956	239	10.14	12.01
rnsz-17b	Ryukyu–Kyushu–Nankai	133.8823	32.3168	239	8.41	4.7
rnsz-18a	Ryukyu–Kyushu–Nankai	134.6416	33.1488	244.7	10.99	14.21
rnsz-18b	Ryukyu–Kyushu–Nankai	134.8656	32.7502	244.5	10.97	4.7
rnsz-19a	Ryukyu–Kyushu–Nankai	135.6450	33.5008	246.5	14.49	14.72
rnsz-19b	Ryukyu–Kyushu–Nankai	135.8523	33.1021	246.5	11.87	4.44
rnsz-20a	Ryukyu–Kyushu–Nankai	136.5962	33.8506	244.8	15	14.38
rnsz-20b	Ryukyu–Kyushu–Nankai	136.8179	33.4581	244.8	12	3.98
rnsz-21a	Ryukyu–Kyushu–Nankai	137.2252	34.3094	231.9	15	15.4
rnsz-21b	Ryukyu–Kyushu–Nankai	137.5480	33.9680	231.9	12	5
rnsz-22a	Ryukyu–Kyushu–Nankai	137.4161	34.5249	192.3	15	15.4
rnsz-22b	Ryukyu–Kyushu–Nankai	137.9301	34.4327	192.3	12	5

Appendix C.
Synthetic Testing: Elfin Cove, Alaska*

C1. Purpose

Forecast models are tested with synthetic tsunami events covering a range of tsunami source locations and magnitudes ranging from mega-tsunami events to micro-tsunami events. Testing is also done with selected historical tsunami events when available.

The purpose of forecast model testing is three-fold. The first objective is to assure that the results obtained with NOAA's tsunami forecast system, which has been released to the Tsunami Warning Centers for operational use, are consistent with those obtained by the researcher during the development of the forecast model. The second objective is to test the forecast model for consistency, accuracy, time efficiency, and quality of results over a range of possible tsunami locations and magnitudes. The third objective is to identify bugs and issues in need of resolution by the researcher who developed the forecast model or by the forecast software development team before the next version release to NOAA's two Tsunami Warning Centers.

Local hardware and software applications are used with tools familiar to the researcher(s) to run the Method of Splitting Tsunami (MOST) model during the forecast model development. The test results presented in this report lend confidence that the model performs as developed and produces the same results when initiated within the forecast application in an operational setting as those produced by the researcher during the forecast model development. The test results assure those who rely on the tsunami forecast model for Elfin Cove, Alaska, that consistent results are produced irrespective of the system used.

C2. Testing procedure

The general procedure for forecast model testing is to run a set of synthetic tsunami scenarios and a selected set of historical tsunami events through the forecast system application, and compare the results with those obtained by the researcher during the forecast model development (as presented in the Tsunami Forecast Model Report). Specific steps taken to test the model include:

1. Identification of testing scenarios, including the standard set of synthetic events, appropriate historical events, and customized synthetic scenarios that may have been used by the researcher(s) in the development of the forecast model.

2. Creation of new events to represent customized synthetic scenarios used by the researcher(s) in the development of the forecast model, if any.

3. Submission of test model runs with the forecast system, and export of the results from A, B, and C grids, along with time series.

---

* Authors: Mick Spillane, Lindsey Wright

4. Recording applicable metadata, including the specific version of the forecast system used for testing.

5. Examination of forecast system model results for instabilities in both time series and plot results.

6. Comparison of forecast model results obtained through the forecast system with those obtained during the forecast model development.

7. Summarization of results with specific mention of quality, consistency, and time efficiency.

8. Reporting of issues identified to modeler and forecast software development team.

9. Retesting the forecast models in the forecast system when reported issues have been addressed or explained.

Synthetic model runs were tested on a DELL PowerEdge R510 computer equipped with two Xeon E5670 processors at 2.93 GHz, each with 12 MBytes of cache and 32 GB memory. The processors are hex core and support hyperthreading, resulting in the computer performing as a 24 processor core machine. Additionally, the testing computer supports 10 Gigabit Ethernet for fast network connections. This computer configuration is similar or the same as the configurations of the computers installed at the Tsunami Warning Centers so the compute times should only vary slightly.

C3. Results

The Elfin Cove forecast model was tested with NOAA's tsunami forecast system, SIFT (Short-term Inundation Forecasting of Tsunamis). Test results from the forecast system and comparisons with the results obtained during the forecast model development are shown numerically in **Table C1** and graphically in **Figures C1– C5** as described below. The results show that the forecast model is stable and robust, with consistent and high-quality results across geographically distributed tsunami sources and mega-tsunami event magnitudes. The model run (wall-clock) times for all five cases were under 25.88 min for 8 hr of simulation, and under 12.92 min for 4.0 hr. This run time is not within the criterion of 10 min run time per 4 hr of simulation time for operational efficiency.

A suite of four synthetic events and one historical case were run on the Elfin Cove forecast model. The modeled scenarios were stable for all cases tested, with no instabilities or ringing. The largest modeled height (see **Table C1**) was 60 cm, from the Cascadia source ACSZ 56–65. Amplitudes less than 75 cm were recorded for all of the test sources; the smallest signal of 23 cm originated from the far-field South American source CSSZ 89–98. Direct comparisons of output from the forecast tool with results of both the historical event (2011 Tohoku, alternately referred to as 2011 Honshu) and available development synthetic events demonstrated that the wave patterns were similar in shape, pattern, and amplitude. The figure captions in this appendix point to the relevant figures of the main report. The extrema reported in **Table C1** were obtained from the output files produced during model development

Table C1: Maximum and minimum amplitudes (cm) at the Elfin Cove, Alaska, warning point for synthetic and historical events tested using SIFT 3.2 and those obtained during development.

Scenarios	Source Zone	Tsunami Source	α [m]	Maxima (cm)		Minima (cm)	
				SIFT	Development	SIFT	Development
Mega-tsunami Scenarios							
KISZ 22–31	Kamchatka-Kuril-Japan-Izu-Mariana-Yap	A22–31, B22–31	25	42.9	42.90	-35.1	-34.99
ACSZ 56–65	Aleutian-Alaska-Cascadia	A56–65, B56–65	25	59.9	59.60	-70.3	-70.41
CSSZ 89–98	Central and South America	A89–98, B89–98	25	22.9	22.90	-32.9	-32.9
NTSZ 30–39	New Zealand-Kermadec-Tonga	A30–39, B30–39	25	38.2	38.15	-29.5	-29.55
Historical Event							
2011 Tohoku	Kamchatka-Kuril-Japan-Izu-Mariana-Yap	4.66 × B24 + 12.23 × B25 + 26.31 × A26 + 21.27 × B26 + 22.75 × A27 + 4.98 × B27		13.9	13.89	-13.6	-13.59

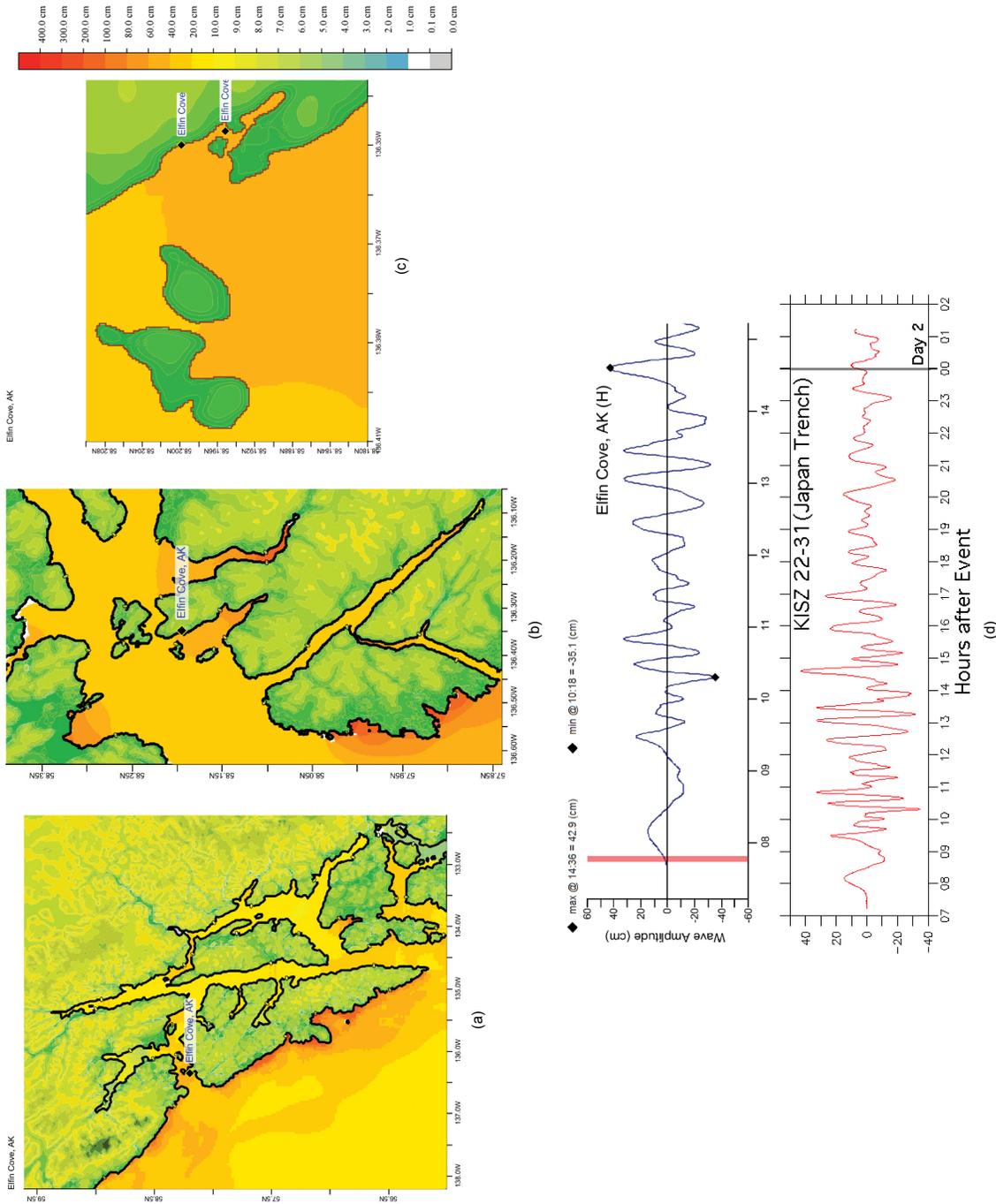**Figure C1**: Response of the Elfin Cove forecast model to synthetic scenario KISZ 22–31 (α=25). Maximum sea surface elevation for (a) A grid, (b) B grid, and (c) C grid. Sea surface elevation time series at the C-grid warning point (d). Panel (d) can be compared to the equivalent results obtained during model development, displayed in **Figure 32a** and **Table C1**.

Figure C2: Response of the Elfin Cove forecast model to synthetic scenario ACSZ 56–65 (α=25). Maximum sea surface elevation for (a) A grid, (b) B grid, and (c) C grid. Sea surface elevation time series at the C-grid warning point (d). For extrema computed during model development, see **Figure 16** and **Table C1**.

Figure C3: Response of the Elfin Cove forecast model to synthetic scenario CSSZ 89–98 (α=25). Maximum sea surface elevation for (a) A grid, (b) B grid, and (c) C grid. Sea surface elevation time series at the C-grid warning point (d). Panel (d) can be compared to the equivalent results obtained during model development, displayed in **Figure 32d** and **Table C1.**
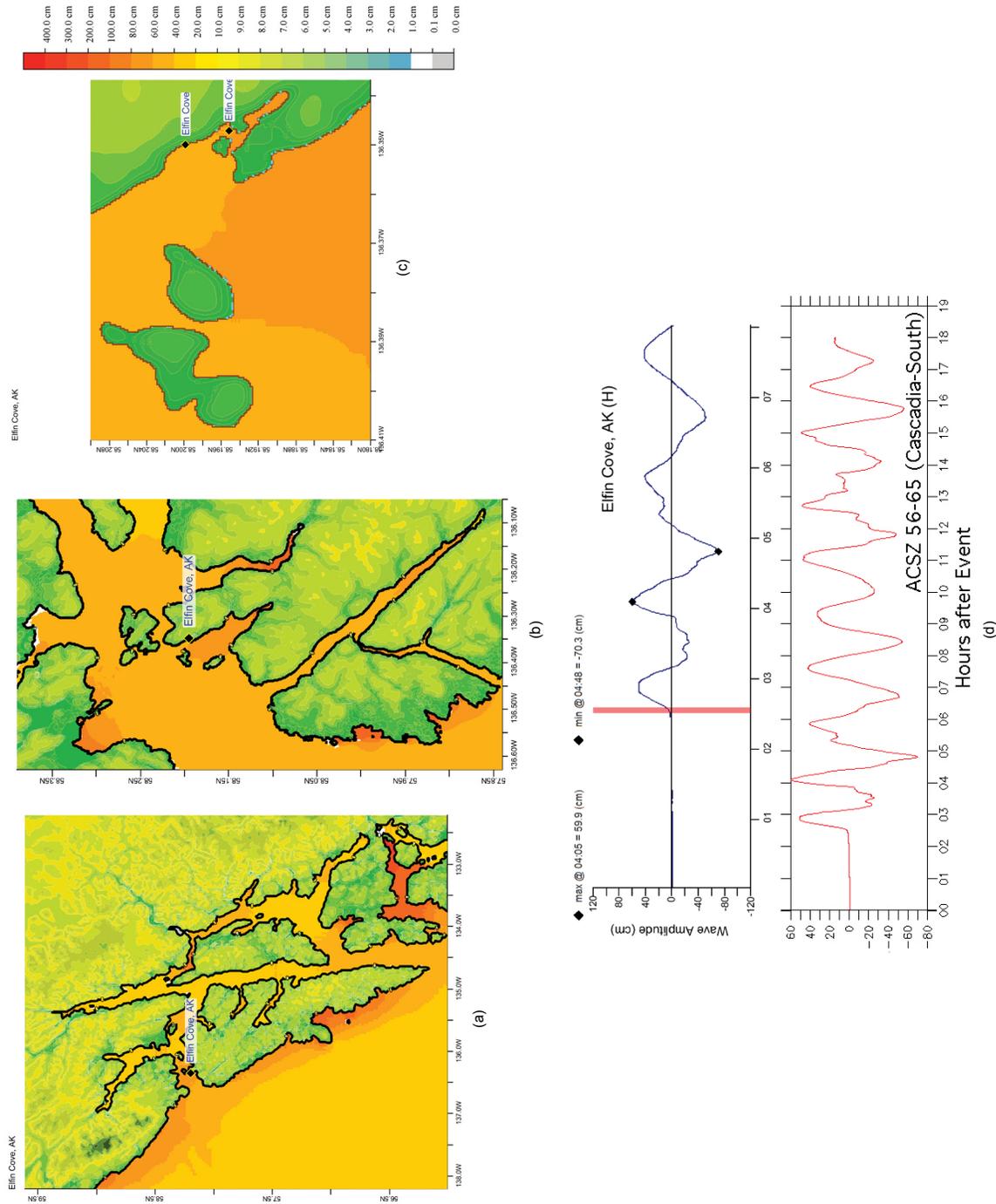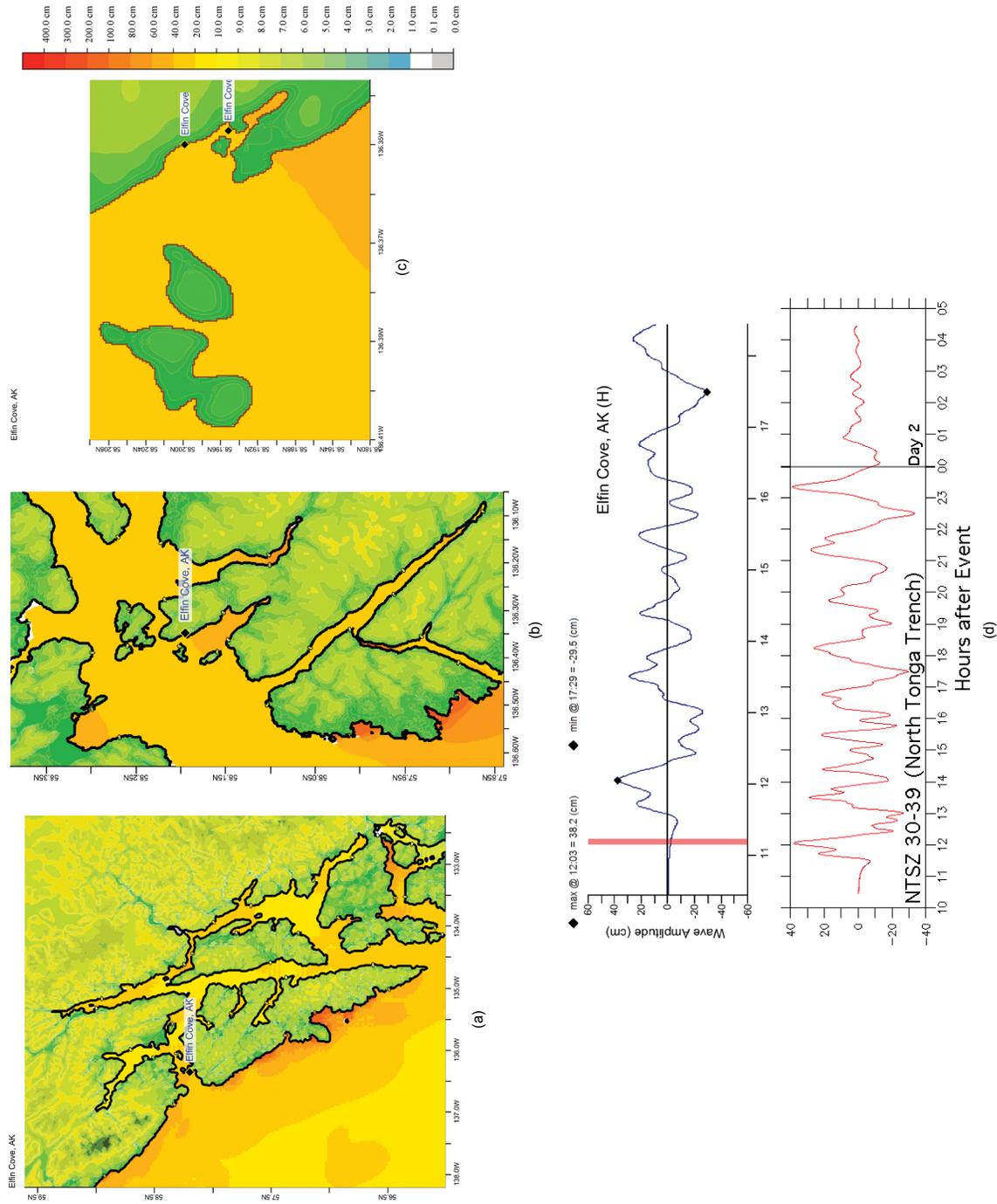
Figure C4: Response of the Elfin Cove forecast model to synthetic scenario NTSZ 30–39 (α=25). Maximum sea surface elevation for (a) A grid, (b) B grid, and (c) C grid. Sea surface elevation time series at the C-grid warning point (d). For extrema computed during model development, see **Figure 32d** and **Table C1**.
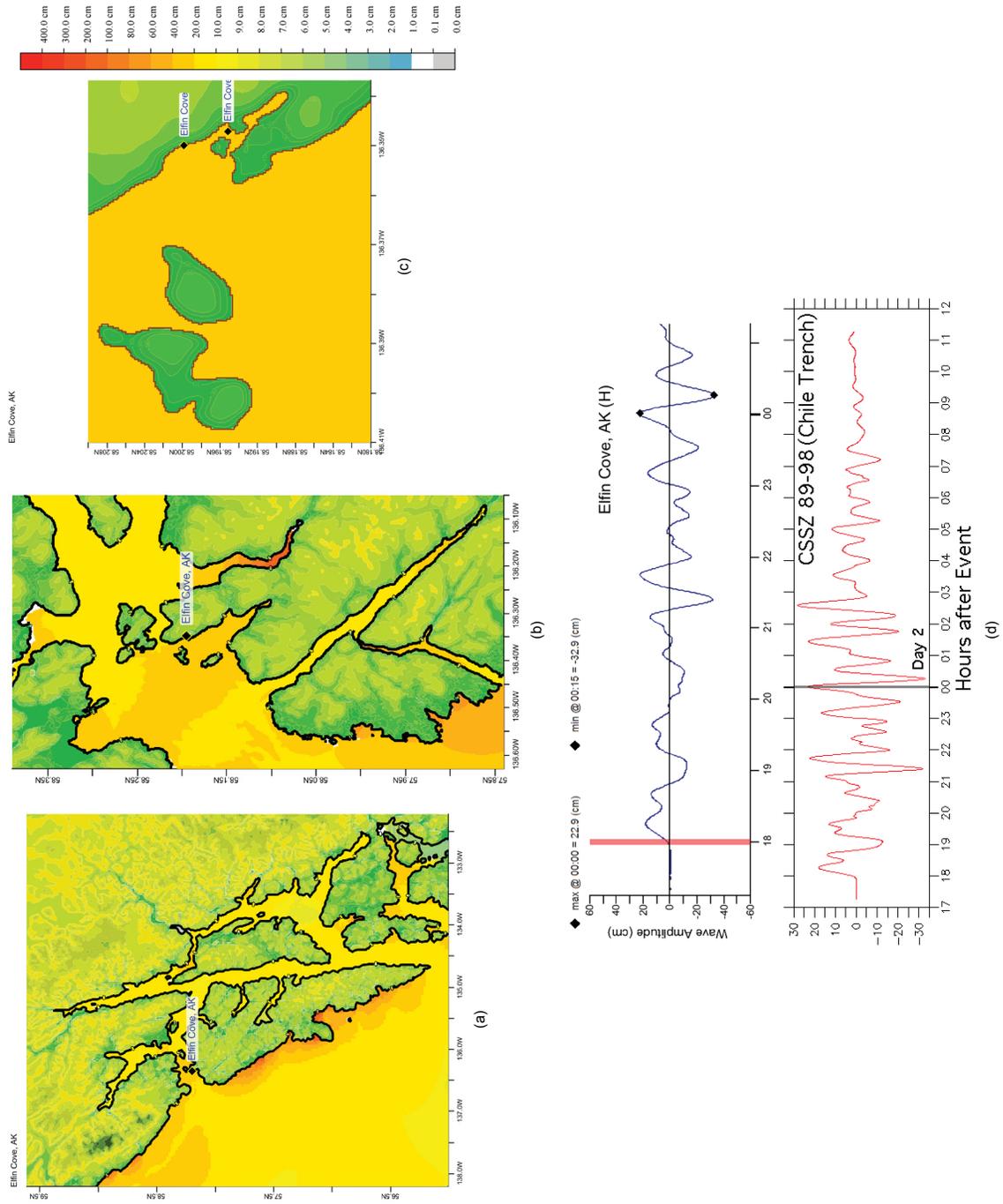
Figure C5: Response of the Elfin Cove forecast model to the 11 March 2011 Tohoku (Honshu) tsunami. Maximum sea surface elevation for (a) A grid, (b) B grid, and (c) C grid. Sea surface elevation time series at the C-grid warning point (d). Panel (d) can be compared to the equivalent results obtained during model development, displayed in **Figure 20** and in **Table C1**.
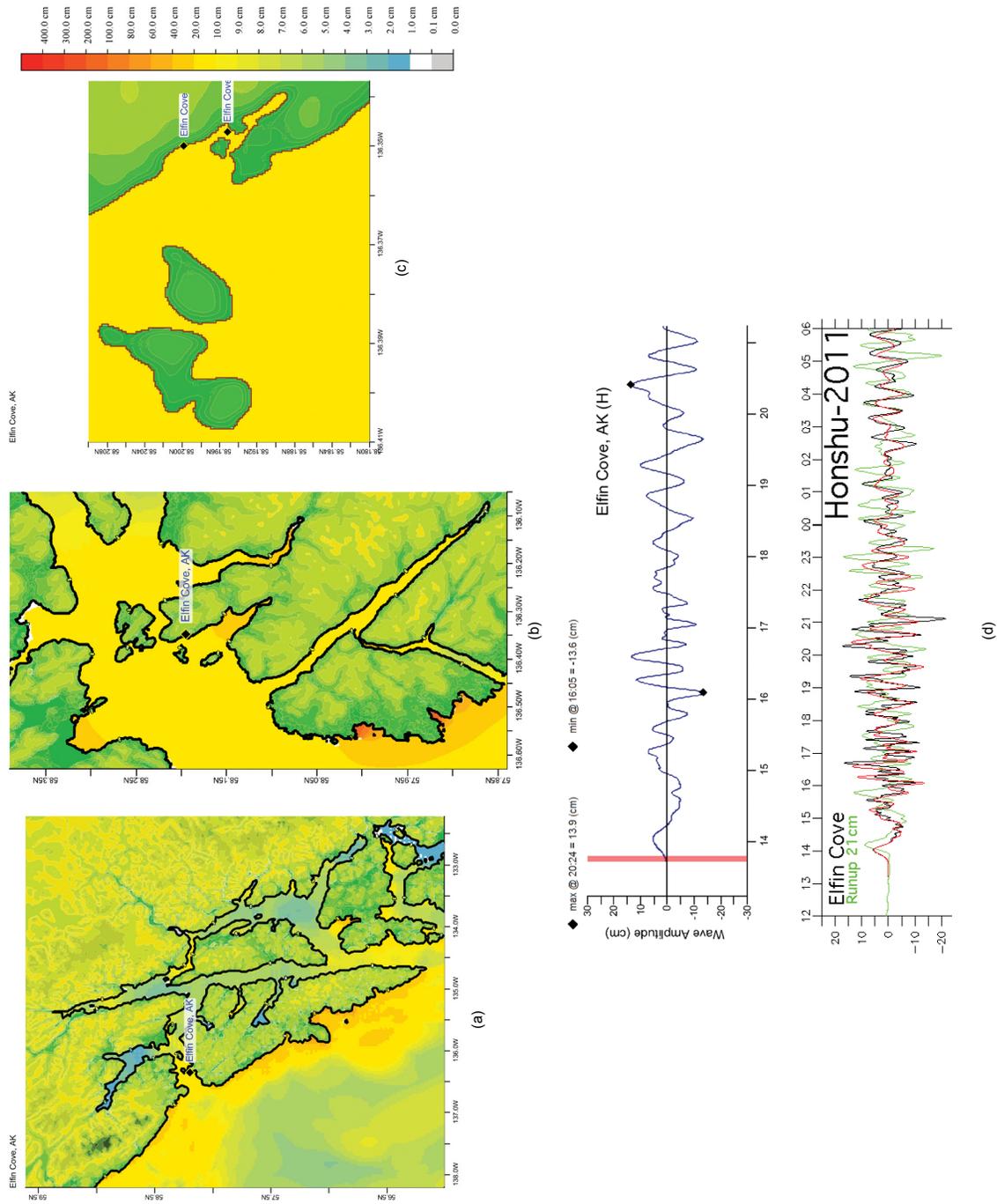
Glossary

Arrival time   The time when the first tsunami wave is observed at a particular location, typically given in local and/or universal time, but also commonly noted in minutes or hours relative to the time of the earthquake.

Bathymetry   The measurement of water depth of an undisturbed body of water.

Cascadia Subduction Zone   Fault that extends from Cape Mendocino in Northern California northward to mid-Vancouver Island, Canada. The fault marks the convergence boundary where the Juan de Fuca tectonic plate is being subducted under the margin of the North America plate.

Current speed   The scalar rate of water motion measured as distance/time.

Current velocity   Movement of water expressed as a vector quantity. Velocity is the distance of movement per time coupled with direction of motion.

Deep-ocean Assessment and Reporting of Tsunamis (DART®)   Tsunami detection and transmission system that measures the pressure of an overlying column of water and detects the passage of a tsunami.

Digital Elevation Model (DEM)   A digital representation of bathymetry or topography based on regional survey data or satellite imagery. Data are arrays of regularly spaced elevations referenced to a map projection of the geographic coordinate system.

Epicenter   The point on the surface of the earth that is directly above the focus of an earthquake.

Far-field   Region outside of the source of a tsunami where no direct observations of the tsunami-generating event are evident, except for the tsunami waves themselves.

Focus   The point beneath the surface of the earth where a rupture or energy release occurs due to a buildup of stress or the movement of Earth's tectonic plates relative to one another.

Inundation   The horizontal inland extent of land that a tsunami penetrates, generally measured perpendicularly to a shoreline.

Marigram   Tide gauge recording of wave level as a function of time at a particular location. The instrument used for recording is termed a marigraph.

Method of Splitting Tsunami (MOST)   A suite of numerical simulation codes used to provide estimates of the three processes of tsunami evolution: tsunami generation, propagation, and inundation.

Moment magnitude (Mw)   The magnitude of an earthquake on a logarithmic scale in terms of the energy released. Moment magnitude is based on the size and characteristics of a fault rupture as determined from long-period seismic waves.

Near–field   Region of primary tsunami impact near the source of a tsunami. The near-field is defined as the region where non-tsunami effects of the tsunami-generating event have been observed, such as earth shaking from the earthquake, visible or measured ground deformation, or other direct (non-tsunami) evidences of the source of the tsunami wave.

Propagation database   A basin-wide database of precomputed water elevations and flow velocities at uniformly spaced grid points throughout the world oceans. Values are computed from tsunamis generated by earthquakes with a fault rupture at any one of discrete 100×50 km unit sources along worldwide subduction zones.

Runup   Vertical difference between the elevation of tsunami inundation and the sea level at the time of a tsunami. Runup is the elevation of the highest point of land inundated by a tsunami as measured relative to a stated datum, such as mean sea level.

Short-term Inundation Forecasting for Tsunamis (SIFT)   A tsunami forecast system that integrates tsunami observations in deep ocean with numerical models to provide an estimate of tsunami wave arrival and amplitude at specific coastal locations while a tsunami propagates across an ocean basin.

Subduction zone   A submarine region of the earth's crust at which two or more tectonic plates converge to cause one plate to sink under another, over-riding plate. Subduction zones are regions of high seismic activity.

Synthetic event   Hypothetical events based on computer simulations or theory of possible or even likely future scenarios.

Tele-tsunami or **distant tsunami** or **far-field tsunami**   Most commonly, a tsunami originating from a source greater than 1000 km away from a particular location. In some contexts, a tele-tsunami is one that propagates through deep ocean before reaching a particular location without regard to distance separation.

Tidal wave   Term frequently used incorrectly as a synonym for tsunami. A tsunami is unrelated to the predictable periodic rise and fall of sea level due to the gravitational attractions of the moon and sun; see **Tide**, below.

Tide   The predictable rise and fall of a body of water (ocean, sea, bay, etc.) due to the gravitational attractions of the moon and sun.

Tide gauge   An instrument for measuring the rise and fall of a column of water over time at a particular location.

Travel time   The time it takes for a tsunami to travel from the generating source to a particular location.

Tsunameter   An oceanographic instrument used to detect and measure tsunamis in the deep ocean. Tsunami measurements are typically transmitted acoustically to a surface buoy that in turn relays them in real time to ground stations via satellite.

Tsunami   A Japanese term that literally translates to "harbor wave." Tsunamis are a series of long-period shallow water waves that are generated by the sudden displacement of water due to subsea disturbances such as earthquakes, submarine landslides, or volcanic eruptions. Less commonly, meteoric impact to the ocean or meteorological forcing can generate a tsunami.

Tsunami hazard assessment   A systematic investigation of seismically active regions of the world oceans to determine their potential tsunami impact at a particular location. Numerical models are typically used to characterize tsunami generation, propagation, and inundation, and to quantify the risk posed to a particular community from tsunamis generated in each source region investigated.

Tsunami propagation   The directional movement of a tsunami wave outward from the source of generation. The speed at which a tsunami propagates depends on the depth of the water column in which the wave is traveling. Tsunamis travel at a speed of 700 km/hr (450 mi/hr) over the average depth of 4000 m in the open deep Pacific Ocean.

Tsunami magnitude   A number that characterizes the strength of a tsunami based on the tsunami wave amplitudes. Several different tsunami magnitude determination methods have been proposed.

Tsunami source   Location of tsunami origin, most typically an underwater earthquake epicenter. Tsunamis are also generated by submarine landslides, underwater volcanic eruptions, or, less commonly, by meteoric impact of the ocean.

Wall-clock time   The time that passes on a common clock or watch between the start and end of a model run, as distinguished from the time needed by a CPU or computer processor to complete the run, typically less than wall-clock time.

Wave amplitude   The maximum vertical rise or drop of a column of water as measured from wave crest (peak) or trough to a defined mean water level state.

Wave crest or peak   The highest part of a wave or maximum rise above a defined mean water level state, such as mean lower low water.

Wave height   The vertical difference between the highest part of a specific wave (crest) and its corresponding lowest point (trough).

Wavelength   The horizontal distance between two successive wave crests or troughs.

Wave period   The length of time between the passage of two successive wave crests or troughs as measured at a fixed location.

Wave trough   The lowest part of a wave or the maximum drop below a defined mean water level state, such as mean lower low water.

PMEL Tsunami Forecast Series Locations

Adak, AK
Apra Harbor, Guam
Arecibo, Puerto Rico
Arena Cove, CA — **Vol. 10**
Atka, AK
Atlantic City, NJ
Bar Harbor, ME
Cape Hatteras, NC
Charlotte Amalie, U.S. Virgin Islands
Chignik, AK
Christiansted, U.S. Virgin Islands
Cordova, AK
Craig, AK
Crescent City, CA — **Vol. 2**
Daytona Beach, FL
Elfin Cove, AK — **Vol. 13**
Eureka, CA
Fajardo, PR
Florence, OR
Garibaldi, OR
Haleiwa, HI
Hilo, HI — **Vol. 1**
Homer, AK
Honolulu, HI
Kahului, HI
Kailua-Kona, HI
Kawaihae, HI
Keauhou, HI
Key West, FL
Kihei, HI — **Vol. 11**
King Cove, AK
Kodiak, AK — **Vol. 4**
Lahaina, HI
La Push, WA
Los Angeles, CA
Mayaguez, PR
Midway Atoll — **Vol. 7**
Montauk, NY

Monterey, CA
Morehead City, NC
Myrtle Beach, SC
Nantucket, MA — **Vol. 8**
Nawiliwili, HI
Neah Bay, WA
Newport, OR — **Vol. 5**
Nikolski, AK
Ocean City, MD
Pago Pago, American Samoa
Palm Beach, FL
Pearl Harbor, HI
Point Reyes, CA — **Vol. 6**
Ponce, PR
Port Alexander, AK
Port Angeles, WA
Port Orford, OR
Port San Luis, CA
Port Townsend, WA
Portland, ME
San Diego, CA
San Francisco, CA — **Vol. 3**
San Juan, Puerto Rico
Sand Point, AK
Santa Barbara, CA — **Vol. 12**
Santa Monica, CA — **Vol. 9**
Savannah, GA
Seaside, OR
Seward, AK
Shemya, AK
Sitka, AK
Toke Point, WA
Unalaska, AK
Virginia Beach, VA
Wake Island, U.S. Territory
Westport, WA
Yakutat, AK

West Coast and Pacific Tsunami Forecast Model Sites

Cordova
Seward
Homer
Yakutat
Elfin Cove
Kodiak
Sitka
Port Alexander
Craig
Chignik
King Cove
Sand Point
Unalaska
Shemya
Atka
Nikolski
Adak

Neah Bay
La Push
Port Angeles
Toke Point
Westport
Garibaldi
Seaside
Newport
Florence
Port Orford
Crescent City
Eureka
Arena Cove
Point Reyes
San Francisco
Monterey
Port San Luis
Santa Barbara
Santa Monica
Los Angeles
San Diego

Wake Island
Apra Harbor
U.S. Territories

Hanalei
Nawiliwili
Haleiwa
Pearl Harbor
Honolulu
Lahaina
Kahului
Kihei
Kawaihae
Kailua
Keauhou
Hilo
Hawaii

Midway Island

Pago Pago
American Samoa

East Coast and Caribbean Tsunami Forecast Model Sites

Bar Harbor
Portland
Montauk
Nantucket
Atlantic City
Ocean City
Virginia Beach
Cape Hatteras
Morehead City
Myrtle Beach
Savannah
Daytona Beach
Palm Beach
Key West

San Juan
Arecibo
Fajardo
Mayaguez
Charlotte Amalie
Ponce
Christiansted
Puerto Rico and U.S. Virgin Islands